# THE KINETICS OF COPPER HYBRID LASERS

Colin Whyte

A Thesis Submitted for the Degree of PhD
at the
University of St Andrews

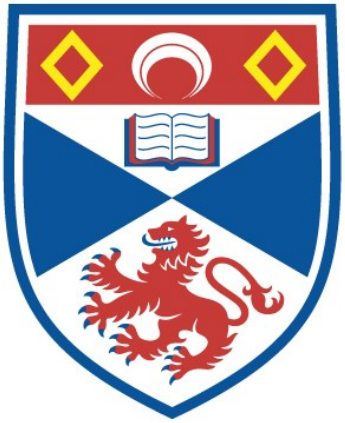

1996

# THE KINETICS OF COPPER HyBrID LASERS

Colin Whyte
University of St.Andrews


Thesis submitted for the degree of
PhD
27th November 1995

Th C16

DECLARATION

I Colin Whyte, hereby certify that this thesis which is approximately 37,000 words in length, has been written by me, that it is the record of work carried out by me and has not been submitted in any previous application for a higher degree.

27/11/95

I was admitted as a research student in October 1991 and as a candidate for the degree of PhD. in October 1992; the higher study for which this is a record was carried out in the University of StAndrews between 1992 and 1995.

27/11/95

I hereby certify that the candidate has fulfilled the conditions of the Resolution and Regulations appropriate for the degree of PhD. in the University of St.Andrews and that the candidate is qualified to submit this thesis in application for that degree.

27/11/95

COPYRIGHT

In submitting this thesis to the University of St.Andrews I understand that I am giving permission for it to be made available for use in accordance with the regulations of the University Library for the time being in force, subject to any copyright vested in the work not being affected thereby. I also understand that the title and abstract will be published, and that a copy of the work may be made and supplied to any bona fide library or research worker.

27/11/95

**ACKOWLEDGEMENTS**

I would like to thank Professor CE Webb & Dr GP Hogan for their assistance without which this project would never have been completed.

I would like to thank Dr DR Jones for much practical help and discussion during various parts of this work.

I would also like to thank Dr RJ Carman & Dr DJW Brown for giving me the benefit of their opinions on my electron density results and, in particular, permission to reproduce one of their diagrams, Figure 6.12 in this thesis.

I would like to thank URENCO Plc. for their financial support of both myself and the project. I would also like to thank the SERC with whose funding I started this project and the EPSRC who funded my final year of work. I would also like to thank the ACCESS fund at the University of StAndrews who funded me over the final weeks of writing.

I would also like to thank the staff in the department workshop and Mr F Akerboom without whom I would have had no laser to study.

I would like to thank my parents who supported me through my undergraduate degree and continue to do so.

Finally I would like to thank all my friends in St.Andrews without whom I would probably have worked a lot more weekends and finished in half the time.

## CONTENTS

## ABSTRACT

THE KINETICS OF COPPER HyBrID LASERS

CG Whyte

University of St.Andrews

Spatially and temporally resolved measurements of many of the parameters of a 25mm bore, 800mm active length copper HyBrID laser have been performed. The laser was operated under excitation conditions for maximum efficiency of light generation at all times.

The hook method has been used to investigate the population densities in the copper ground state, the upper laser levels, the lower laser levels and one of the quartet levels in copper. The population density in one of the neon metastable levels has also been measured. All of these measurements have been performed with 5 ns time resolution and 2 mm spatial resolution. A two wavelength laser interferometric technique has been used to measure the electron density with nanosecond time resolution and 2mm spatial resolution. The waveforms of the voltage across the laser head and current through the laser tube have been measured. The temporally resolved laser pulse radial profile has been investigated.

The results from these investigations have been compared to those for a 42 mm bore CVL previously studied with the same experimental apparatus. Comparison has also been made with a detailed computer model of a 19mm bore CVL. Deductions as to the effect of the remanent electron density prior to the excitation pulse on the current and voltage waveforms have been made. The effect of added HBr has been discussed, relative to the remanent electron density. The laser kinetics are discussed in terms of the electron temperature and the relative rate coefficients of the mechanisms affecting the level populations.

# CHAPTER 1 INTRODUCTION

The copper HyBrID laser has been developed at the University of St. Andrews over the past seven years as an alternative approach to solving the engineering problems presented by the construction of high temperature (~1500 °C) copper vapour lasers (CVLs). In the HyBrID laser the necessary pressure of copper vapour is produced by the reaction of elemental copper pieces with flowing hydrogen bromide gas in the discharge tube, hence the name HyBrID. This approach allows operation over a wide range of tube wall temperatures (500-900 °C). There are additional benefits to this approach; the copper density is decoupled from the wall temperature and the by-product of the reaction between the copper and HBr (hydrogen) is beneficial to the laser performance (Astadjov et al. 1985, 1988). The resulting laser constructed using this technology has superior specific output power, efficiency (Livingstone et al. 1991a; Jones et al. 1992; Jones et al. 1994) and extremely high beam quality output can be more easily achieved than in a similar CVL.

The copper HyBrID laser is a member of the family of self-terminating metal vapour lasers. These lasers operate on a three level system. A term diagram is given in Figure 1.1. The upper laser level is connected to the ground state by a fully allowed transition which has a high oscillator strength. The corresponding transition to the lower laser level is optically forbidden and therefore has a much lower oscillator strength. Under the correct excitation conditions it is possible to pump significant population into the upper laser levels. Whilst it is generally not possible to produce an absolute population inversion, the ratio of the degeneracies of the upper and lower levels allow laser action. The conditions for lasing

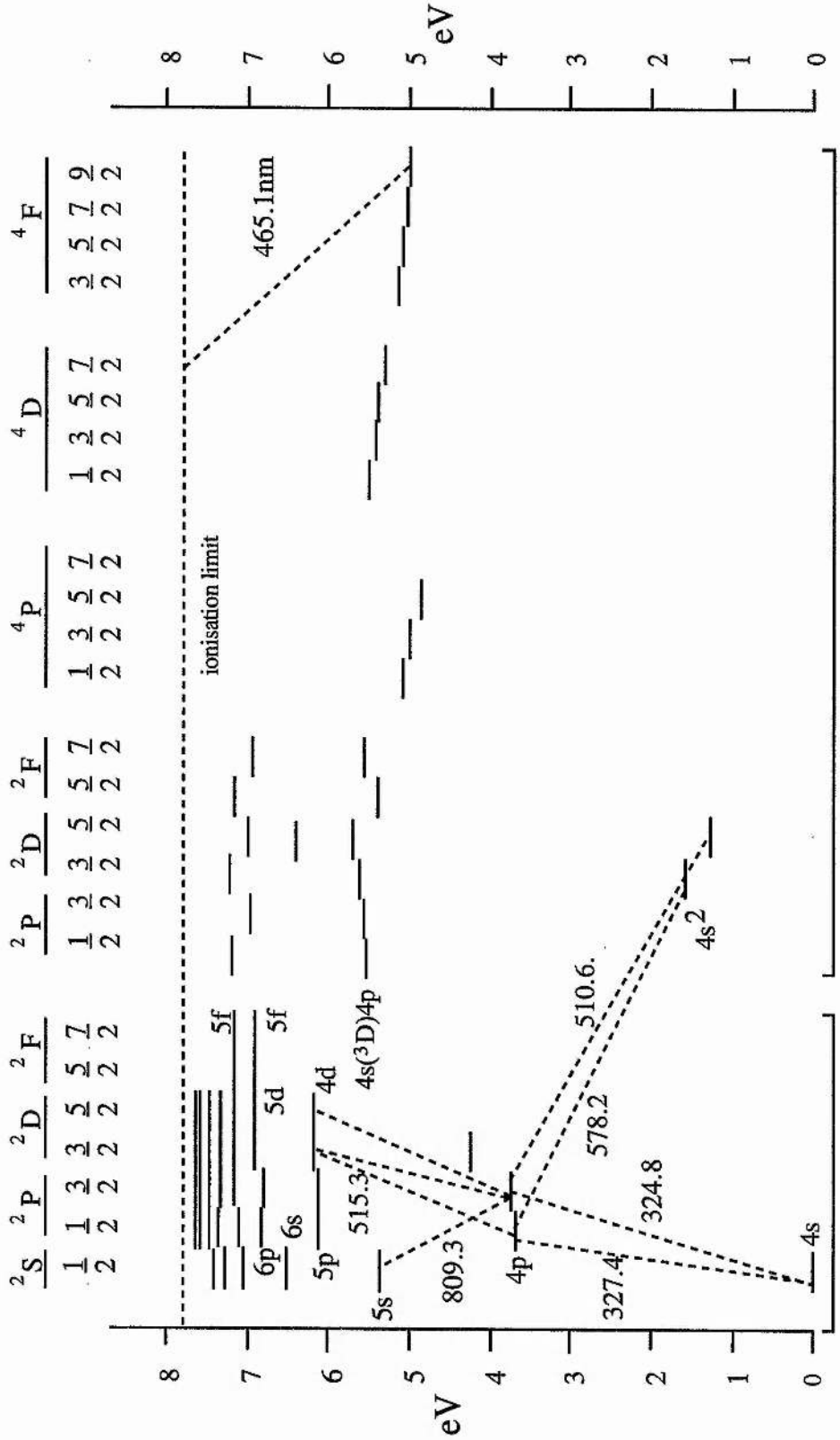


Figure 1.1. Copper Term Diagram

cannot be maintained indefinitely as the lower laser level is metastable and as it's population increases, eventually a point is reached where gain can no longer be maintained. The lasers therefore operate in the pulsed regime.

## 1.1 HISTORY

The first report of lasing in a metal vapour was reported by Fowles & Silfvast in 1965 when they demonstrated gain in lead vapour. This was the start of a period of rapid development of metal vapour lasers as lasing was next demonstrated in manganese (Piltch et al. 1965) and then in copper (Walter et al. 1966a, 1966b). Further developments of the copper system were reported in 1967 & 1968 (Walter 1967; Walter et al. 1968; Leonard 1967). Copper had at this time established itself as the most promising metal vapour laser, principally because of the high efficiency and power obtainable. After this initial period of activity, publications on the subject of copper vapour lasers ceased, partly due to the engineering difficulties researchers encountered in the construction of high temperature ovens and vacuum systems. Two approaches were taken to the solution of these problems. In 1972 Isaev et al. published a description of a copper vapour laser system where no ovens were used and the required copper vapour density was produced by discharge heating. In 1973 Liu et al. reported superradiance from a copper iodide at 600 $^{o}$C, and later the same year Chen et al. reported laser action using CuCl with a double pulse excitation circuit. In this system the first pulse was used to dissociate the molecules and the second to excite the atoms produced. These discoveries prompted a great deal of research into copper halide systems and repetitively pulsed systems were reported by Lieberman et al. 1975 and Chen et al. 1975. Lasing using CuBr was reported in 1975 by Akirtava et al. & Shtukin et al. Development

of copper halide systems continued along both double pulse and repetitively pulsed routes (Nerheim et al. 1978, Chen et al. 1978) until problems in scaling to large diameters resulted in a decline in interest. The use of copper halides was not the only technique used to achieve lasing on copper lines at low temperature. There were numerous other approaches including exploding copper wires (Asmus & Moncur 1968) and supersonic flows of heated copper in an argon and helium gas jet (Russell et al. 1972). There have also been reports of very low temperature (20 $^{o}$C) lasing using copper acetylacetonate as the donor molecule (Andrews et al. 1977).

During this period research into CVLs proceeded, principally in the USSR. The problem of high output beam divergence was addressed with the use of unstable resonators (Zemskov et al. 1974, Isaev et al. 1977). Laser lifetime was also a major consideration and two long-lifetime sealed tubes were reported by Bokhan et al. 1975 and Burmakin 1978. The initial work done by Walter et al. (1968) had demonstrated that volume scaling of copper lasers might be a productive route towards increased power output. This was demonstrated in 1977 by Isaev & Lemmerman. In 1979 an efficiency of 2.9% was reported by Bokan & Gerasimov, this efficiency was only recently bettered, by a so-called copper HyBrID laser (Jones et al. 1994).

This early work in the USSR provided the lead for a large part of copper vapour laser research worldwide. Volume scaling proved to be the subject of many papers, there were two reports of laser scaling experiments from Israel (Smilanski et al. 1978 & 1979). In 1982 interest in this field of research increased dramatically as the Lawrence Livermore National Laboratory (LLNL) instigated an Atomic Vapour Laser Isotope Separation (AVLIS) programme (Grove 1982) which demanded focusable high average power and high reliability. It had been realised in 1975 (Anderson et al.

1975) that the copper vapour laser operated at maximum efficiency when used as an amplifier. High power, low divergence output could be produced by amplifying the output from a low divergence source, the master oscillator (MO) in one or more power amplifiers (PA) in the so-called MOPA scheme. After experiments with alternative laser tube geometries proved unsatisfactory (Kan et al. 1979), interest switched to the development of systems based on the geometries used in the USSR and Israel, to improve both output power and reliability.

Considerable effort was invested in the development of low divergence oscillators, resulting in the development of the injection controlled oscillator (ICO) This systems uses two coupled unstable resonators to produce low divergence output. (Naylor et al. 1986; Warner 1986) Small scale, single oscillator systems with near diffraction limited performance have also been developed (Pini et al. 1991).

A number of attempts have been made to model the kinetic processes in a CVL using computers. The first appeared in 1967 (Leonard 1967). The difficulties involved in modelling the copper system; such as longitudinal and radial inhomogeneity, the importance and interaction of the excitation circuit including, in particular, the switch, and the complex nature of the electron energy distribution function (EEDF) prevented further development until much later. The first paper to address these difficulties was that by Kushner (1981). This paper was followed by further publications which gave more detail of the model's predictions and comparison with measurement (Warner & Kushner 1981). The final paper incorporating radial dependence was published in 1983 (Kushner & Warner 1983). The latest model, and most powerful to date, is that by Carman (Carman 1994) which sucessfully addresses the EEDF problem as well as the others

mentioned above. This model is still undergoing further development to incorporate further refinements to the radial dependence and also consider the effects of added hydrogen on the system.

The HyBrID laser was developed from an initial device which employed the halogens $Br_2$, $Cl_2$ or HBr in the buffer gas and internal tube walls made of copper tubing at low (~500°C) temperature (Livingstone & Maitland, 1989; 1991a). HBr was found to be the most effective additive. The copper tube walls led to instabilities and caused the laser to fail within hours. The operating regime was not well understood. This unstable, short lifetime device subsequently underwent further development. Amongst other improvements the metal tubing was replaced by a single alumina or quartz tube into which the metal lasant was placed as small pieces. In this way, stable reliable operation was attained in the HyBrID laser for the first time using bismuth (Jones & Little 1991; Jones & Little 1992a) and then in lead (Jones & Little 1992b). In subsequent experiments reliable operation was achieved using copper (Livingstone et al. 1991a), iron (Jones & Little 1992d) and finally manganese (Jones & Little 1992c).

## 1.2 OBJECTIVES

The purpose of the present study is to provide as complete a survey as possible of the operating parameters of a copper HyBrID laser. To this end temporally and spatially resolved measurements of the population density in six fundamental levels in copper and one in neon have been made. These levels are: the copper ground state, the two upper laser levels, the two lower laser levels and one of the high lying quartet levels in copper and the first metastable level in neon. Temporally and spatially resolved measurements of the free electron density have also been made.

It is expected that the data collected may be of use in any future computer models of the system as well as providing some data to compare with the wealth of information already collected for various different high temperature CVLs. It is hoped that this may lead to greater understanding of the processes which lead to the differences observed in operating characteristics of CVLs, HyBrID lasers and copper halide lasers.

## 1.3 THE LASER UNDER INVESTIGATION

### 1.3.1 LASER DESIGN

The layout and laser end flange design of the laser used in these experimental studies is shown in Figures 1.2 & 1.3. The laser has an active region of 25mm bore, 800mm long. The plasma is confined by an alumina tube supported inside a quartz vacuum envelope. The stainless steel laser end flanges are sealed to the quartz vacuum jacket and end window extensions using Viton™ 'O'rings. The laser end flanges are water cooled to prevent overheating of the 'O'rings and to cool the copper electrodes. The end window extensions are 350mm and 250mm long, the longer extension is at the gas inlet end because of the increased CuBr particle flux caused by the turbulent flow of HBr over the hot copper electrode. Copper was introduced to the system as a series of 1cm x 1cm square pieces, bent to sit on the bottom of the curved tube without protruding into the discharge region. Approximately 7-8 pieces were used at 10cm intervals along the length of the tube. Two pieces were placed together nearest the anode end as the piece nearest the gas inlet suffered the greatest erosion.

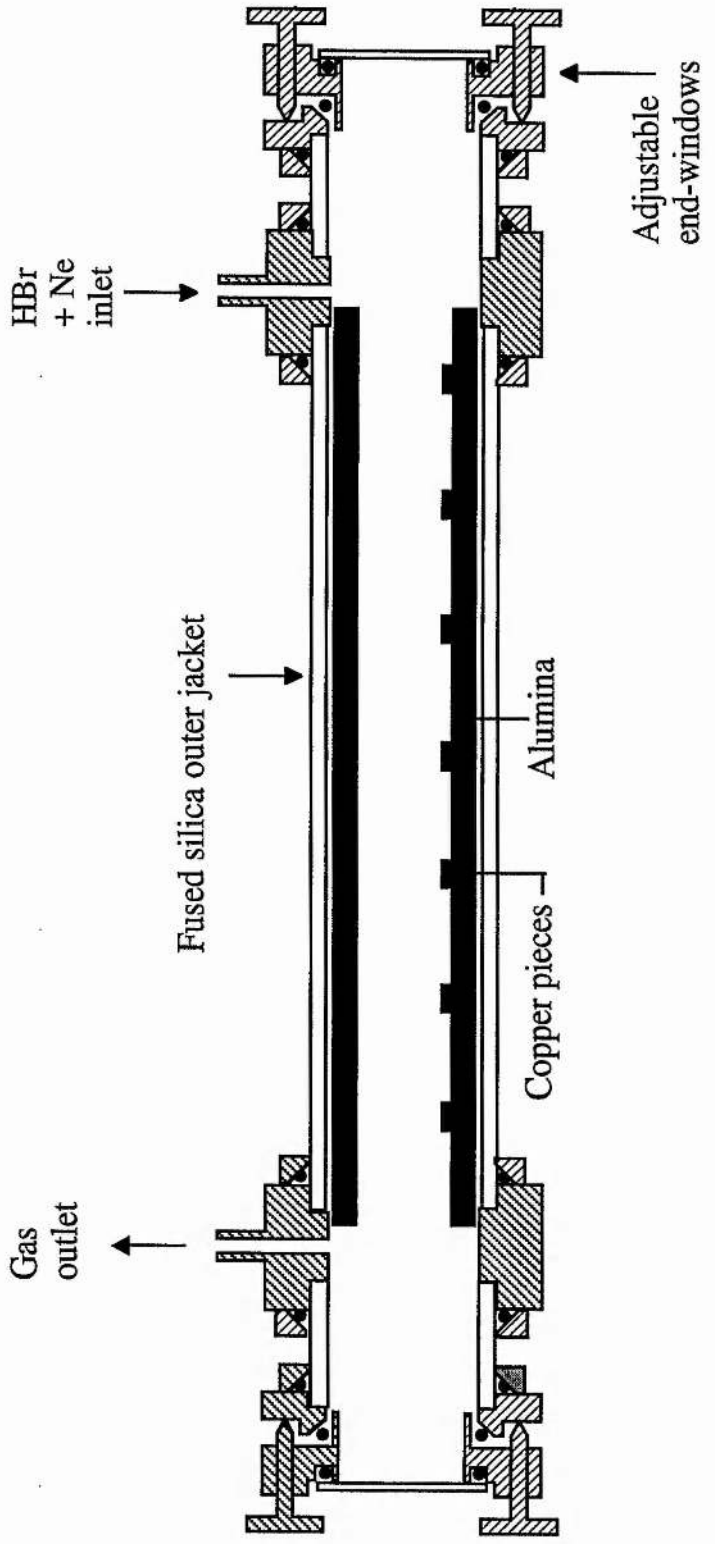


Figure 1.2. Schematic view of Copper HyBrID laser

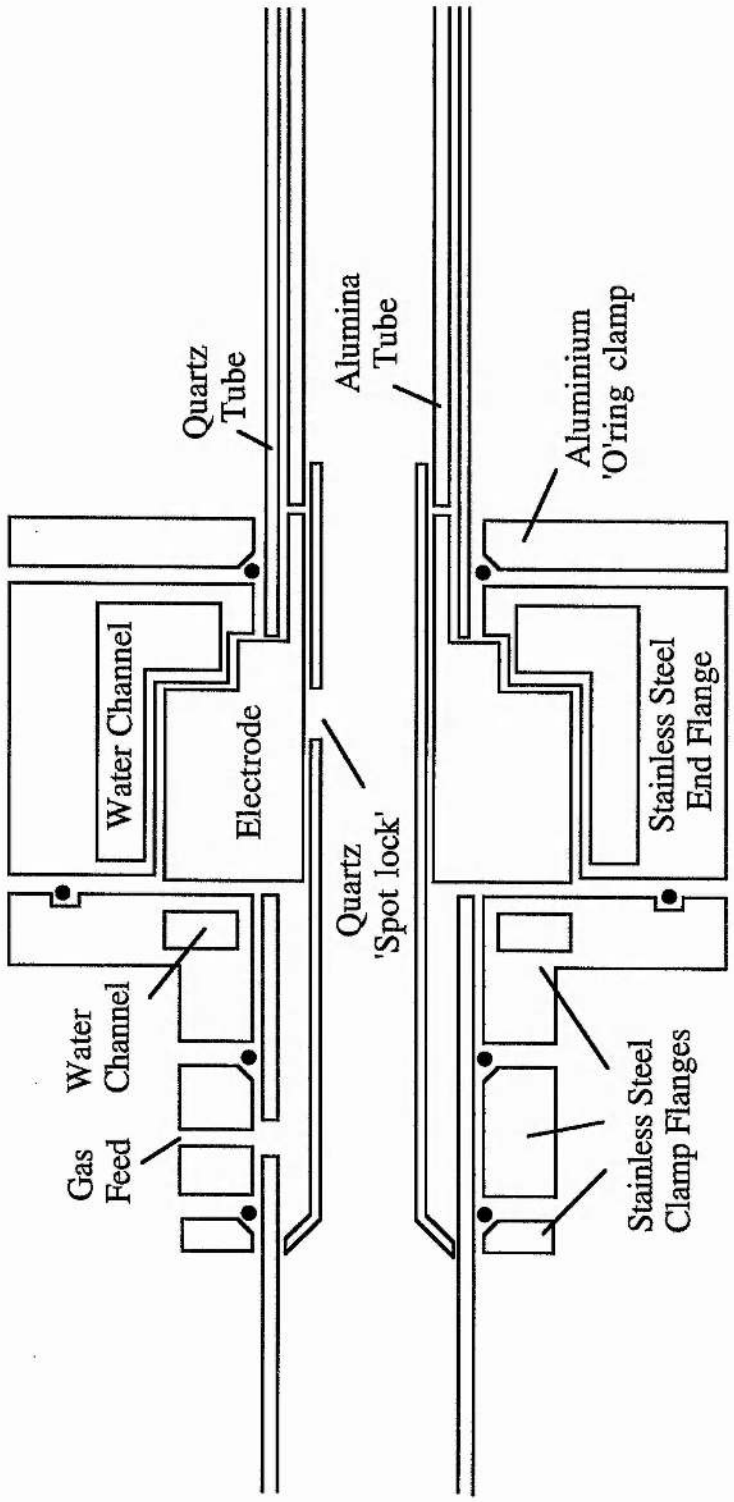


Figure 1.3. Laser end flange design for 25mm bore HyBrID laser

The neon and HBr flow rates were controlled by separate fine metering valves. The gases were mixed immediately after the valves to allow mixing before the gases entered the laser volume at the anode end. The gases were removed from the laser via a single line from the cathode end which was connected to a rotary vacuum pump (Edwards EM12) via a coarse flow adjustment valve. The total gas flow was in the range 1-2 litre atm/hr.

The cavity was formed between the vacuum enclosure windows, one of which had a multi-layer dielectric coating with high reflectance at the laser wavelengths. The coating was on the back surface of the window to prevent coating degradation by the reactive gases in the vacuum enclosure. The output coupler was an uncoated quartz flat. The cavity mirrors were mounted on 2-axis adjustable mounts.

A standard charge transfer (CT) circuit was used for excitation (see Figure 2.5). The operating storage capacitance was 1.15nF and the peaking capacitance was 0.4nF. The excitation circuit is discussed in more detail in Chapter 2.1.

### 1.3.2 LASER POWER AND EFFICIENCY

The laser power for various storage capacitances is shown in Figure 1.4. Whilst over 30W of output power was obtainable at high input powers (32W at 25kHz, 30W at 17kV), the efficiency was poor (~1%). As one of the more interesting characteristics of the HyBrID laser is the high efficiency obtainable, the laser was optimised with this in mind. Maximum efficiency operation is obtained for a charging voltage of 13kV and PRF of 17kHz. See Figures 1.5 & 1.6. The maximum efficiency which could be reliably and repeatedly achieved for this laser was 1.5% based on stored energy.

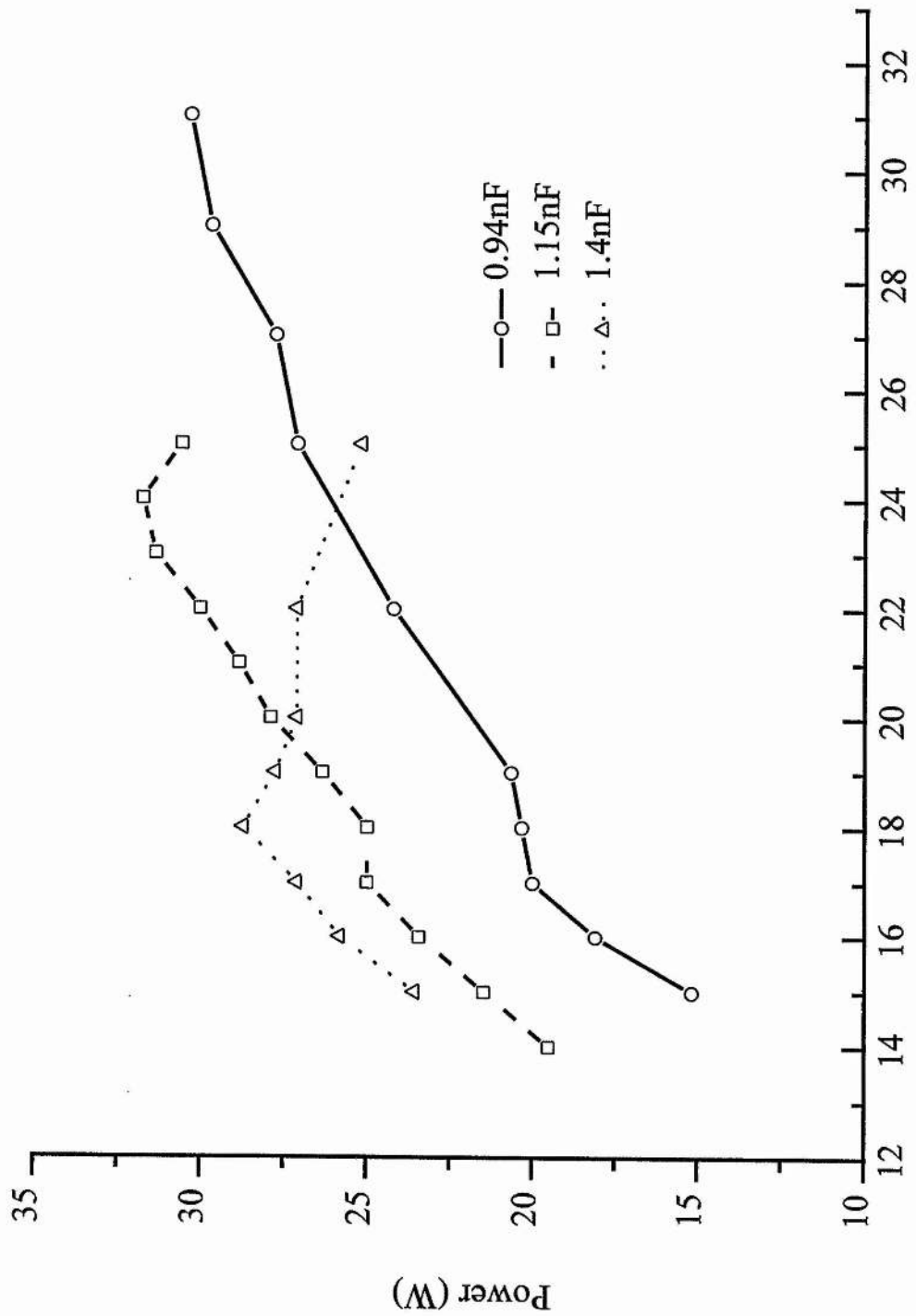


Figure 1.4. Laser output power as a function of PRF for various storage capacitances

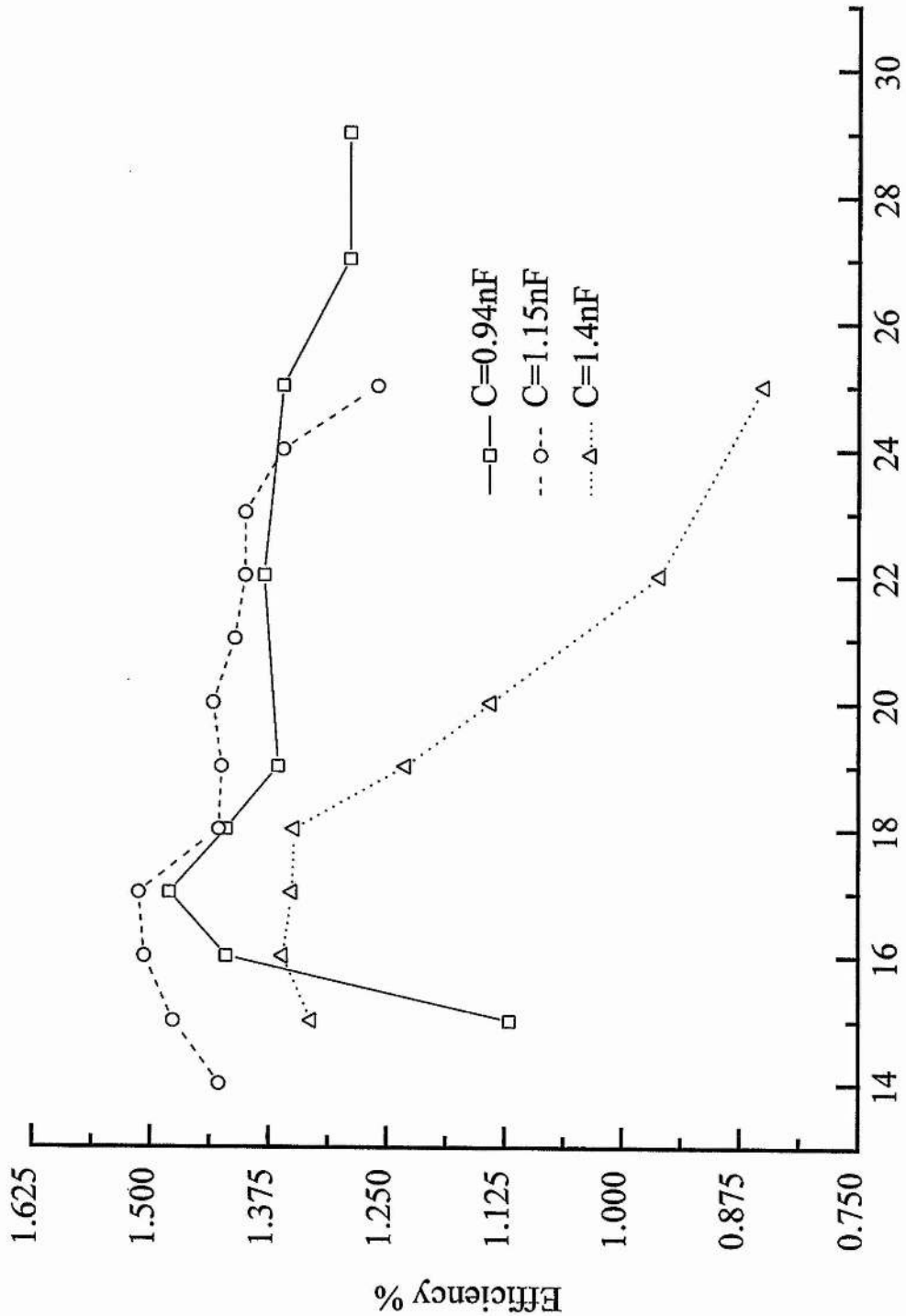


Figure 1.5. Laser efficiency as a function of PRF for various storag capacitances

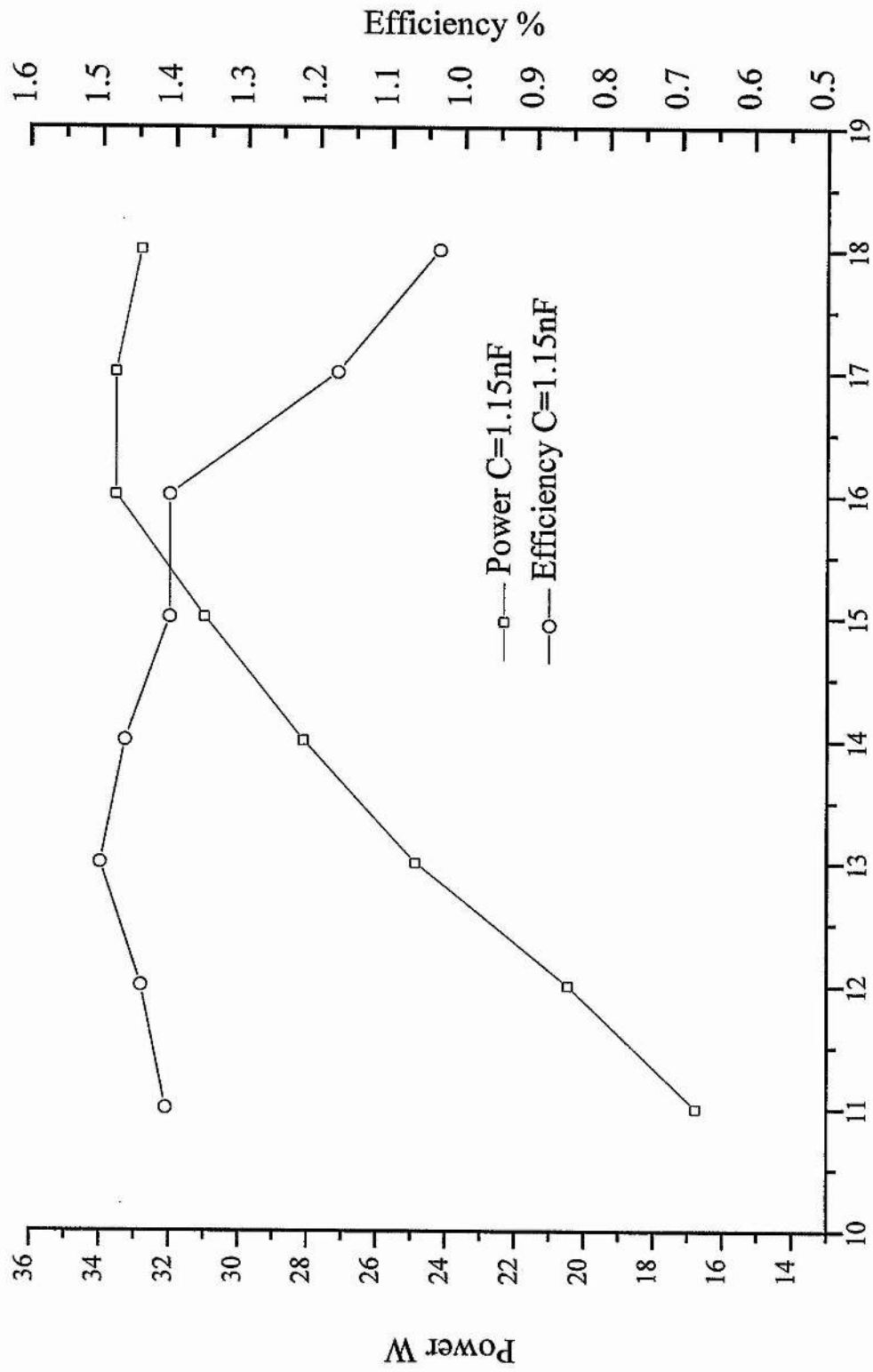


Figure 1.6. Laser power and efficiency as a function of voltage.

### 1.3.3 THE STANDARD OPERATING CONDITION

It is of vital importance in this study that the laser should be operating under identical conditions for each measurement. To facilitate this a set of standard operating conditions was chosen.

The conditions were:

| | |
|---|---|
| Storage capacitance | 1.15nF |
| Peaking capacitance | 0.4nF |
| PRF | 17kHz |
| Charging voltage | 13kV |
| Peak tube voltage | 14kV |
| Peak tube current | 130A |

Using these standard conditions the proportion of HBr ( which must be reset each time the laser is switched off and restarted ) could be reliably returned to the same level. The laser output power could then be used as a check to ensure the laser performance was consistant.

# CHAPTER 2. ELECTRICAL CHARACTERISTICS

## 2.1 INTRODUCTION

The electrical characteristics of the HyBrID laser system are significantly different from those of the typical CVL. This is important in that the laser excitation circuit must be matched to the discharge conditions. The excitation circuit will influence all of the laser parameters and in most systems there will be a trade off between ultimate laser performance and longevity. This trade-off usually occurs because of the need to conserve expensive circuit components such as the switch, usually a hydrogen-filled thyratron.

The most significant difference between HyBrID and CVL systems is the relatively high efficiency of the HyBrID laser, typically 1-3% compared to 0.5-1% for a CVL. The HyBrID laser discharge also has a much higher pre-pulse impedance and breakdown voltage, leading to better and easier circuit to discharge matching. Finally, HyBrID lasers typically run at significantly higher PRFs than CVLs for tubes of comparable bore and may be scaled to larger tube diameters without associated laser pulse timing delays between axis and tube edge.

A typical excitation circuit is shown in Figure 2.1. This is a charge transfer or CT circuit. In this circuit a storage capacitor C1 is resonantly charged through inductor L1 to twice the supply voltage, the diodes D1 preventing discharge to the reservoir capacitor $C_r$. When the switch is triggered the potential of the left hand plate of C1 drops rapidly to ground. This causes the right hand plate of C1 to swing negative, transferring charge to the top plate of C2 until the breakdown voltage of the laser tube is reached and both capacitors discharge into the active medium. The maximum voltage to which C2 may be charged (and hence the maximum breakdown voltage which can be reached) will depend on the circuit stray inductance and

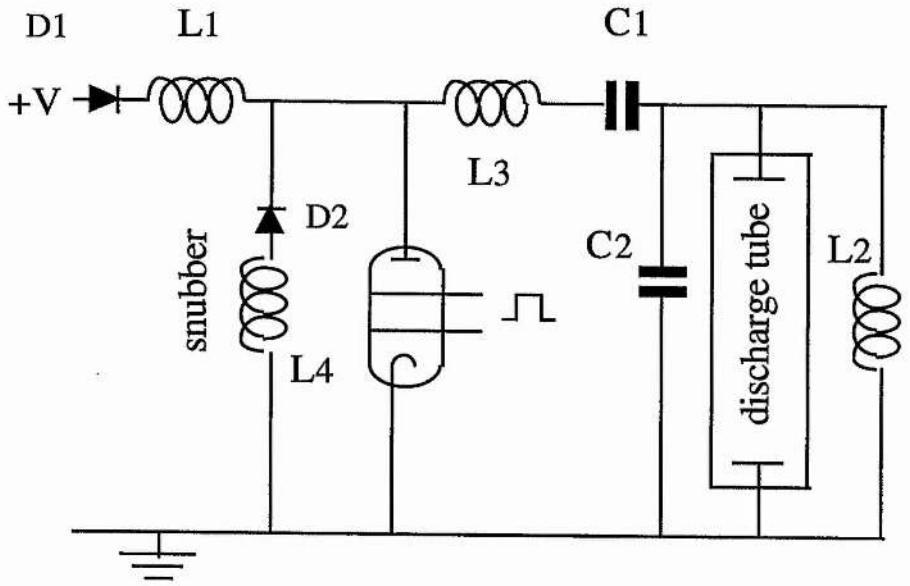


Figure 1. Charge Transfer Circuit

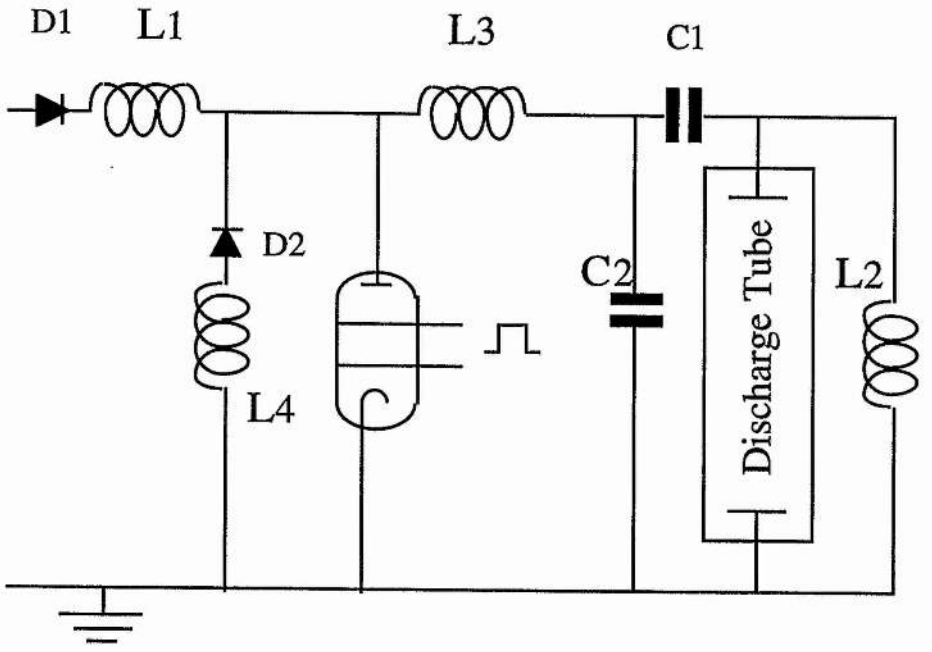


Figure 2.2 Blumlein Circuit

resistance, it is often possible to reach voltages significantly above the switched voltage when exciting a HyBrID laser. This is not the case with a CVL where it is frequently impossible to develop the switched voltage on the tube due to the low tube breakdown voltage. The ratio of the capacitances C1:C2 can be varied to change the risetime of the current pulse, reducing C2 will sharpen the leading edge. Inductor L2 has a high impedance at the frequency corresponding to the current pulse preventing current flow through the inductor. On the longer timescale of the inter-pulse period the inductor has a low impedance and allows the right hand plate of C1 to be grounded.

Numerous other circuits can be used such as the modified Blumlein circuit shown in Figure 2.2 or the interacting circuit (Vuchkov et al. 1991) shown in Figure 2.3.

## 2.2 THYRATRON LIFETIME

Poor laser efficiency has important implications for the laser power supply. To generate a given laser output power a CVL will typically require two to three times the input power that would be required for a HyBrID laser. This situation is exacerbated by the relatively low PRF operation which combines with the high average input power to demand very high excitation pulse energies and peak powers. The excitation circuit for a CVL is therefore required to deliver high peak currents (~1kA) with correspondingly high $\partial i/\partial t$ (~5kA/μs). There are few switches available which are capable of fulfilling these requirements. Hydrogen thyratrons will work but only at the cost of reduced lifetime. High power CVLs often use more than one thyratron to reduce the current loading on each. As thyratrons are expensive devices their replacement can be a major part of the laser's operating costs. This problem led to the introduction of magnetic assistance and saturable

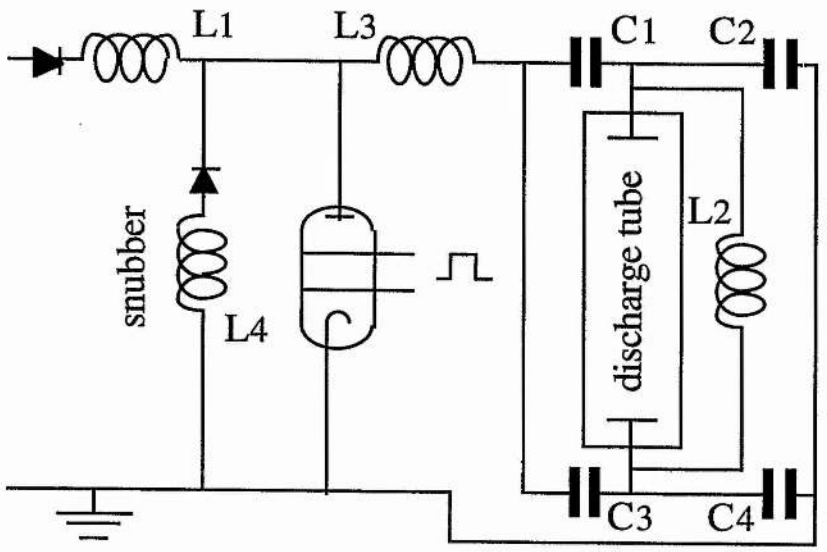


Figure 3. Interacting peaking capacitor circuit

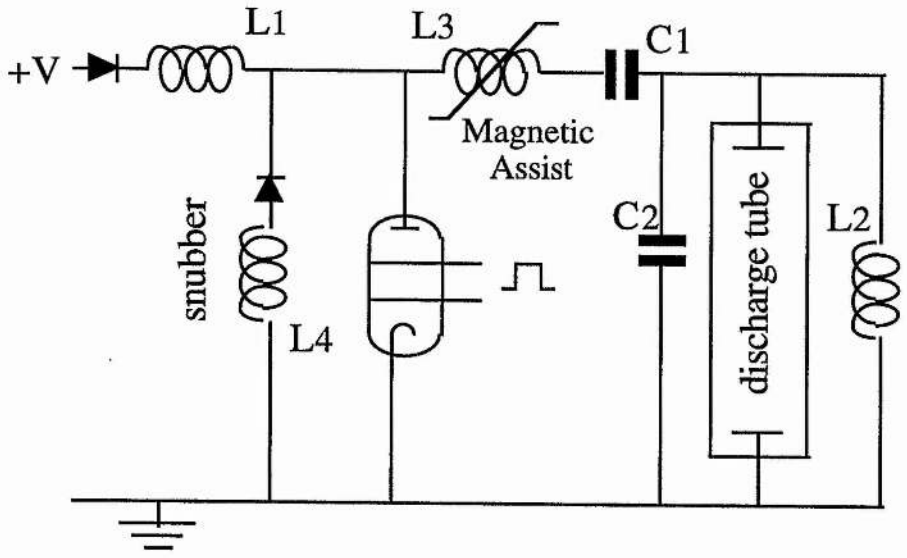


Figure 4. Charge-transfer circuit with magnetic assist

charging inductors to the excitation circuit. A major cause of reduced lifetime in the thyratron is anode heating caused by high current demand before the anode voltage has collapsed after triggering. Heating may be reduced by fitting a small saturable inductor or 'magnetic assist' (Figure 2.4) on the thyratron anode to provide suitable delay between thyratron triggering and high current flow. This technique can significantly reduce thyratron heating but at the cost of additional inductance in the discharge circuit.

High $\partial i/\partial t$ operation will also reduce thyratron lifetime. This can be alleviated with the use of magnetic pulse sharpening techniques (Figure 2.5). In these circuits the thyratron circuit is slowed by the use of large capacitors (at lower voltage if the input power is to remain constant), the slow current pulse is then sharpened by a (usually multi-stage) magnetic switch to achieve the required excitation pulse at the laser head. Using these techniques the thyratron lifetime can be greatly increased (to ~$10^{11}$ shots) and with the use of new ferrite materials the energy loss in the magnetic circuit may be as low as 12% (Deguishi et al. 1994). The penalty to be paid is increased complexity, reduced efficiency and higher initial expense.

HyBrID systems have lower current demands than CVLs, partly due to their higher PRF operation. High PRF operation also has it's disadvantages. If we can expect $10^{11}$ shots from a given thyratron then we can operate for fewer hours with a HyBrID laser than with a CVL. Anode heating is proportional to PRF as a certain amount of power is dissipated in the thyratron per switching operation.

Thyratron lifetime is shortened when power reflected from the load appears on the anode of the thyratron forcing the anode voltage to become negative. This causes sputtering of material from the thyratron anode onto

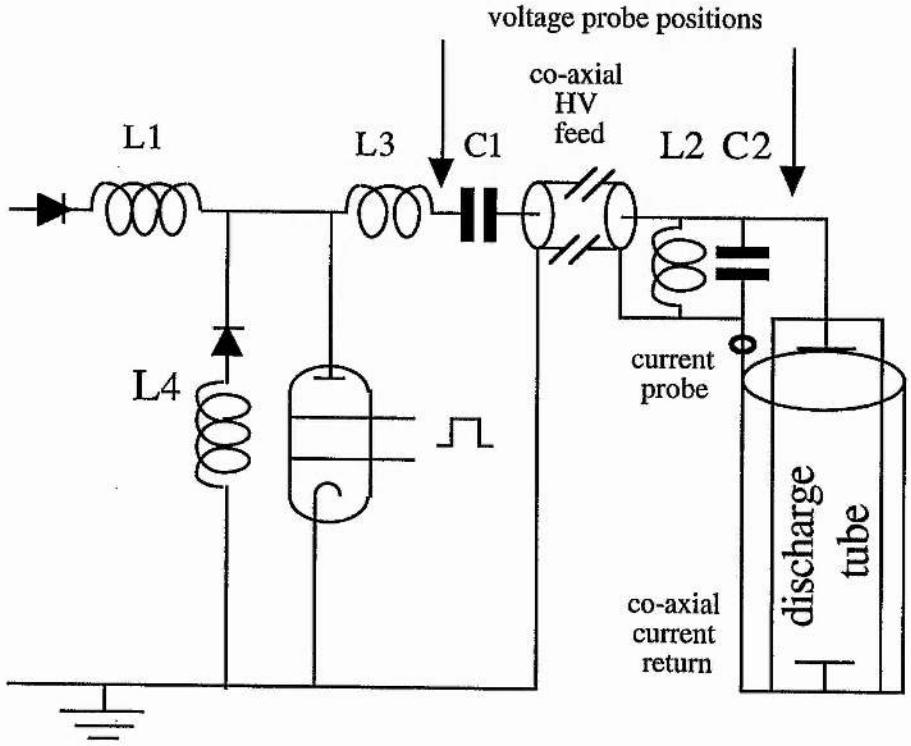


Figure 2.5 Excitation circuit showing measurement points

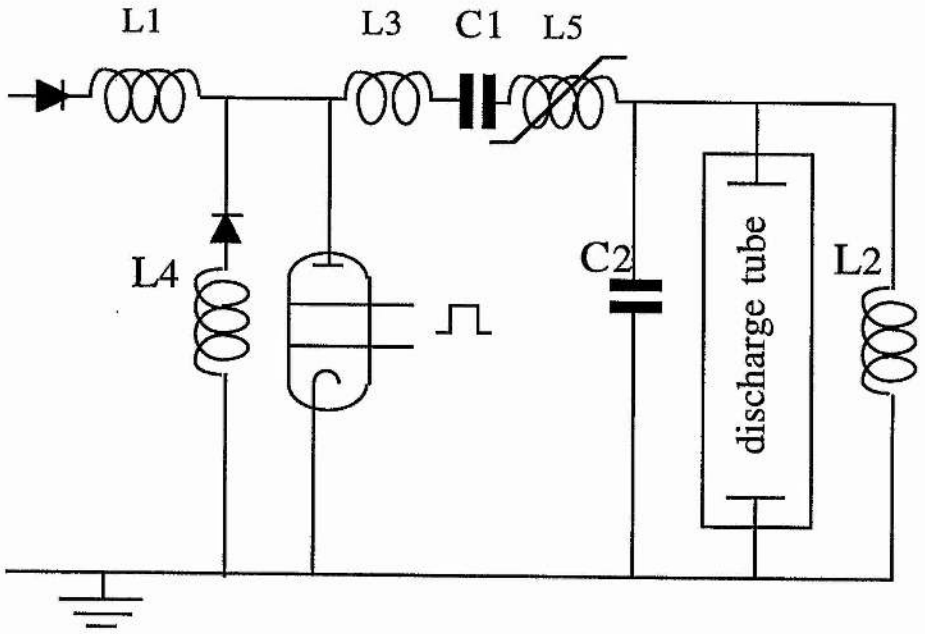


Figure 2.6 Circuit with magnetic pulse compression

the grids. The thyratron will eventually fail due to reduced inter-electrode hold-off.

Negative over-swing on the thyratron anode also causes the storage capacitance to be charged from below zero and the peak voltage reached will be greater than twice the charging voltage. This can lead to instability in the storage capacitor voltage as the thyratron overswing can vary significantly for small changes in discharge conditions. To alleviate this, a snubber network consisting of a diode chain and either a resistor or inductor to ground may be connected to the thyratron anode to quickly remove the negative voltage from the thyratron anode. This allows the storage capacitor to be charged consistently from ground, independent of thyratron overswing.

The CVL has a lower pre-pulse impedance and carries a larger current, therefore more energy is stored in the laser head inductance. This energy is not absorbed and must return to the excitation circuit where it charges the storage and peaking capacitors and produces negative voltage on the thyratron anode. This mechanism can be a major source of thyratron failure in CVLs. HyBrID lasers, by virtue of their higher pre-pulse plasma resistance have better matching to the circuit output impedance and generally produce less over-swing at the thyratron anode. It should be noted that some thyratrons require a small amount of negative over-swing on the anode to aid recovery to the non-conducting state, especially when operating at high PRF. Thyratrons will not conduct appreciable negative current, therefore a negative voltage holds the switch off and allows time for remanent carriers to be removed from the holdoff region.

## 2.3 CURRENT AND VOLTAGE WAVEFORMS

The HyBrID laser's performance was monitored during operation by measurement of the laser tube voltage and laser tube current, the storage capacitor charging voltage was also measured to allow calculation of the input power. The voltages were measured using Tektronix P6015A high voltage probes and the current was monitored using a Stangenes 0.1V/A current transformer. The voltage probes had a bandwidth of 75MHz, giving a corresponding risetime of approximately 4.5ns, the current transformer risetime was quoted at 10 ns. The measurement points are shown in Figure 2.6 which details the laser excitation circuit and laser head layout.

The current, voltage and light traces for the HyBrID laser running under optimal excitation conditions for maximum efficiency of light generation are shown in Figure 2.7. The laser was run under these conditions for all measurements because investigation of the laser at high efficiency was considered to be more important than say, at the maximum power. The laser was also less stable under operating conditions for maximum power.

Initially, the voltage on the tube increases with no effect on tube current (the initial dip in tube current is believed to be a measurement artefact). As the voltage increases the tube current increases slowly, but only to approximately 10A. The current remains at this level until the tube voltage has peaked at approximately 13kV. At this point the tube current starts to increase rapidly and simultaneously (to within 10 ns) laser action commences. The laser tube has broken down at this time. Laser action ceases when the tube voltage reaches zero and the current peaks. The current now falls, slightly more rapidly than it rose, before rising again to produce a second peak.

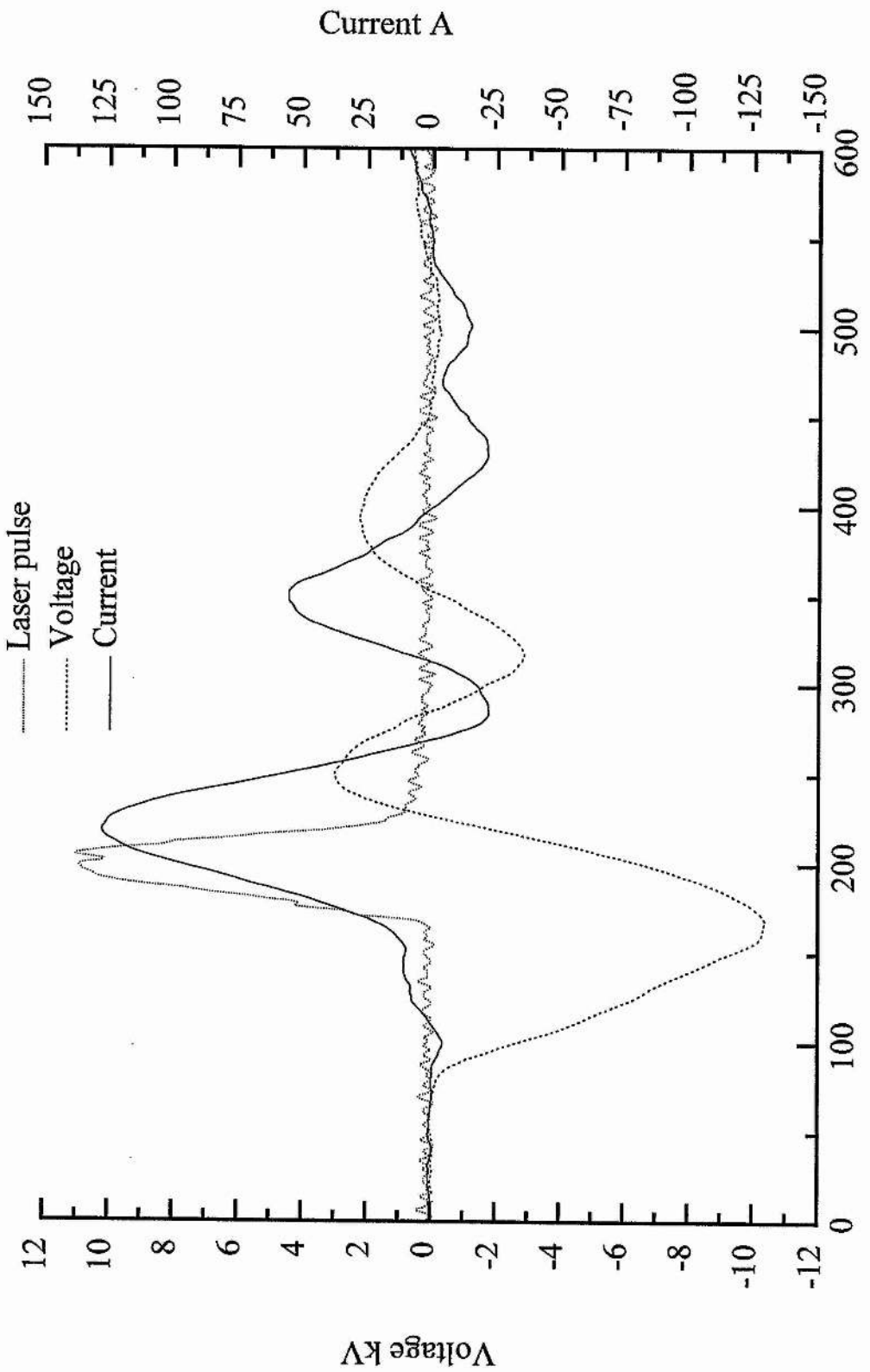


Figure 2.7 Tube voltage, tube current and laser pulse waveforms

### 2.3.1 CIRCUIT INDUCTANCE AND PLASMA RESISTANCE

The traces in Figure 2.7 are of the measured voltage across the tube and will therefore include an inductive component. It is possible to calculate the circuit inductance and resistance from the current and voltage waveforms using Equation [2.1] below.

$$V = IR + L\frac{\partial i}{\partial t}. \qquad [2.1]$$

At times where the current is zero we may evaluate the inductance from

$$L = \frac{V}{\partial i / \partial t}, \qquad [2.2]$$

and when the rate of change of current is zero.

$$V=IR \qquad [2.3]$$

using these equations we can calculate the tube inductance at each zero of the current and the tube resistance at each turning point. As the current passes through zero several times each current pulse we can calculate the temporal evolution of the circuit inductance. The calculated laser head circuit inductance is plotted in Figure 2.8 with the calculated resistance shown in Figure 2.9. The calculated circuit inductance is initially very high, this is intuitively correct as Figure 2.7 shows the voltage phase leading that of the current by roughly $\pi/2$. The current and voltage waveforms in Figure 2.7 are strongly damped, there must therefore be a significant resistive component to the load. Figure 2.9 shows that the plasma resistance is high before the pulse but falls to a low level during the first half of the current pulse.

These deductions about load impedance can be supported by consideration of a sinusoidal electric field applied to an electron gas. If the electron momentum transfer collision frequency ($\nu$) is lower than the frequency of the applied field ($\omega$) the force on the electrons is in phase with

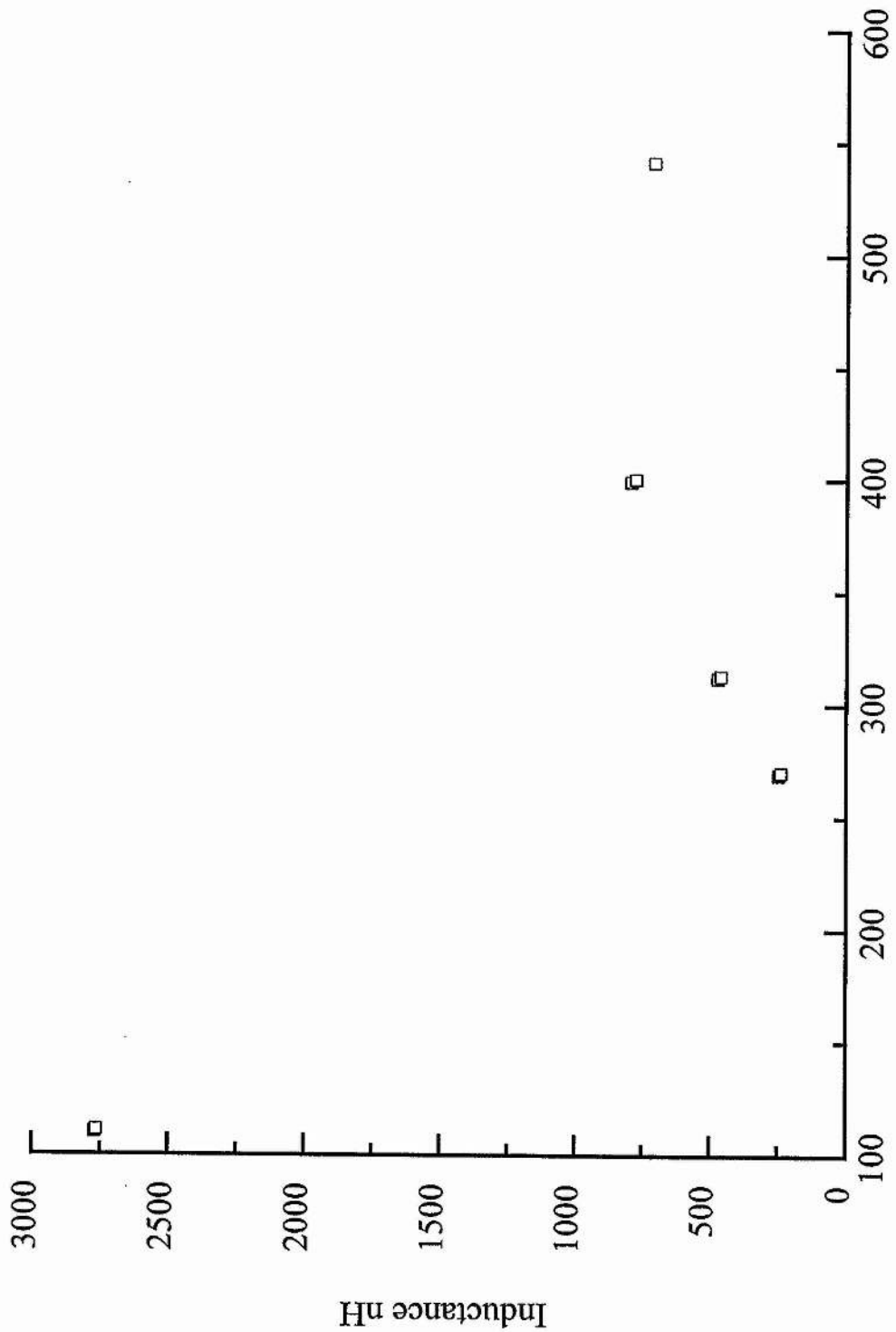


Figure 2.8 Calculated laser head inductance

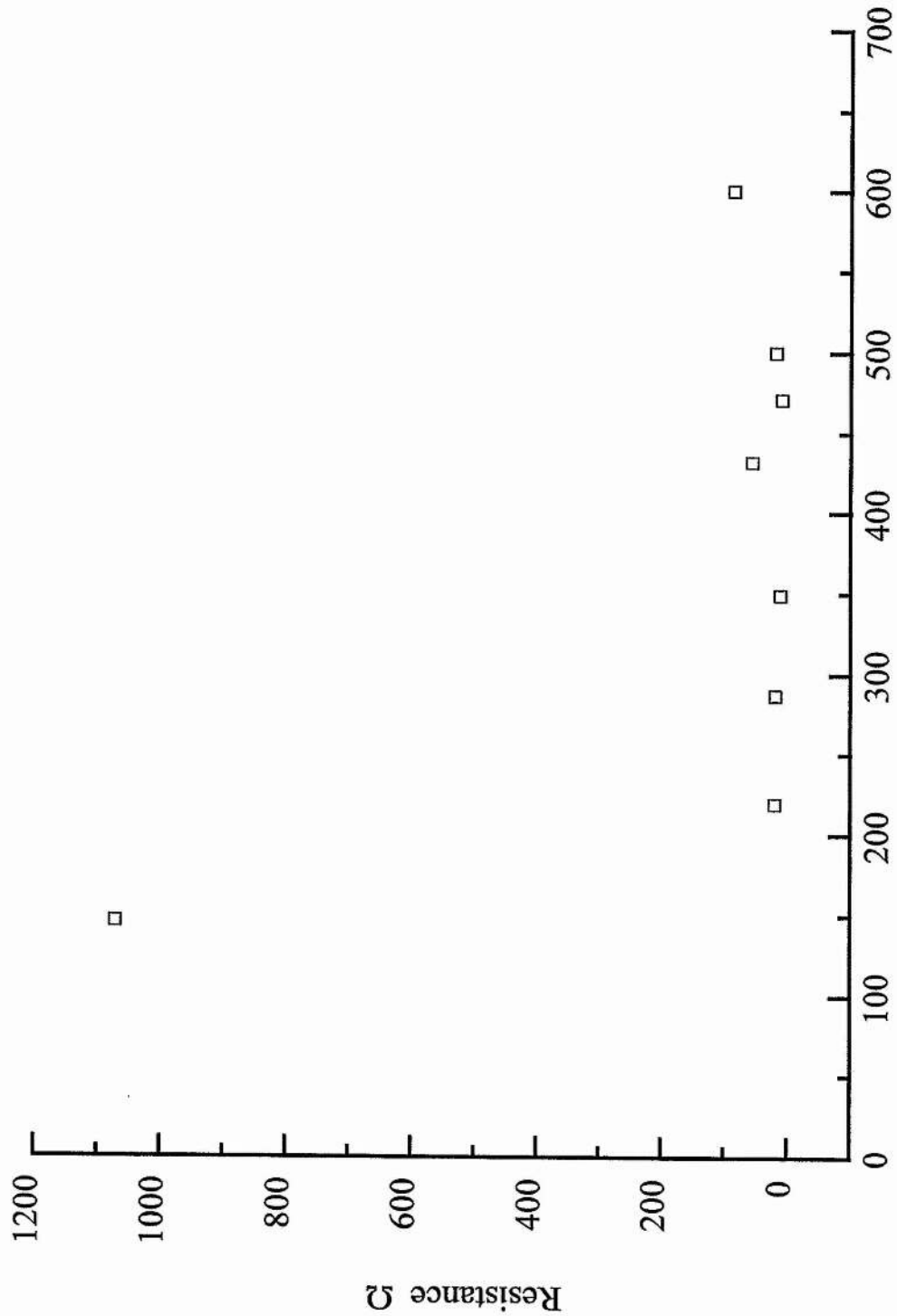


Figure 2.9 Calculated plasma resistance

the field. The current, which is proportional to the electron velocity, will therefore be $\pi/2$ out of phase and the plasma will be inductive. Initially the electron density is very low and the electron momentum transfer collision frequency will be correspondingly low. At the very beginning of the pulse, the plasma will be inductive. As the electron density increases so must the electron momentum transfer collision frequency ($\nu$) and the plasma will become more resistive according to the relation

$$\tan\phi = \frac{\nu}{\omega} \qquad [2.4]$$

where $\phi$ is the phase angle between the current and voltage and $\omega$ is the frequency of the applied field. $L_1$ will decrease and R will increase in this case. This explains the switch in impedance from inductive to resistive during the current pulse.

The load across which we measured the voltage would then be represented as in Figure 2.10:

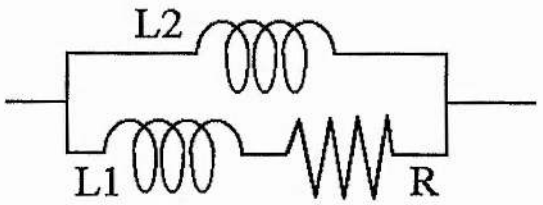


Figure 2.10

If we apply conventional circuit theory to this problem and consider the impedances of the plasma and bypass inductor in parallel we have;

$$\frac{1}{Z} = \frac{1}{R + j\omega L_1} + \frac{1}{j\omega L_2}. \qquad [2.5]$$

This may be simplified as

$$Z = \frac{j\omega L_2\left[R^2 + \omega^2 L_1\left(L_1 + L_2\right) + j\omega R L_2\right]}{R^2 + \omega^2\left(L_1 + L_2\right)^2}. \qquad [2.6]$$

For $L_1 << L_2$ we may simplify [2.6]

$$Z \approx \frac{j\omega L_2\left[R^2 + \omega^2 L_1 L_2 + j\omega R L_2\right]}{R^2 + \omega^2 L_2^2}. \qquad [2.7]$$

If $\omega L_1 << R$, then

$$Z \approx \frac{j\omega L_2 R\left[R + j\omega L_2\right]}{R^2 + \omega^2 L_2^2}. \qquad [2.8]$$

If $R << \omega L_1$, Equation [2.6] becomes

$$Z = \frac{j\omega L_2 L_1 (L_1 + L_2)}{(L_1 + L_2)^2} = \frac{j\omega L_1 L_2}{(L_1 + L_2)}. \qquad [2.9]$$

The load is mostly inductive for large R and mostly resistive for large $L_2$. Note that $L_1$ contains contributions from both the laser head geometrical inductance and the plasma inductance. In practice the impedance of the bypass inductor at the dominant frequency of the applied field is of the order of 1MΩ, and may be neglected. The load impedance in this case is determined by the plasma impedance in series with the laser head inductance.

### 2.3.2 DISCHARGE EVOLUTION

During the first 80 ns of the excitation pulse only a very small current flows through the laser tube despite the high field across the laser head. The plasma must therefore have high impedance due to the low number of charge carriers present and/or the low mobility of the charge carriers. A low electron density as indicated by our measurements would result in a low electron momentum transfer collision frequency, and the plasma would be inductive. The calculated tube resistance during this time is also very high as shown in Figure 2.10. As the plasma has not 'broken down' at this point, additional charge carriers are not being created therefore the electron energy must be

too low to cause ionisation. There is no laser action at this time either. As the copper HyBrID laser system has very high gain significant light output is observed soon after gain is established. This implies that the electron temperature must be too low to produce any appreciable inversion density. Upon first inspection this indicates that the electron energy does not follow the tube voltage during the initial part of the excitation pulse (-100 to 0 ns). This behaviour is not what one would expect as most successful computer models calculate electron temperature and plasma voltage temporal dependences which are very similar. (Carman et al. 1994, Kushner & Warner 1983, Carman 1990).

It is important to consider what is represented by the tube voltage measurement. The voltage measured by the probe placed on the laser head is the summation of the voltage across the laser head inductance and the discharge voltage, as discussed below. The discharge voltage itself comprises the cathode fall, the positive glow and the anode fall regions as well as the dark spaces. The majority of the discharge region is occupied by the positive glow, but it cannot be inferred that the majority of the voltage is dropped across the positive column. There will be significant voltage developed across the cathode fall region. The anode fall will be smaller than the cathode fall, but this may still be non-negligible. (See Luck et al. 1994 for discussion of experimental investigation of cathode fall). The positive column of the discharge cannot be considered to be uniform either as there are regions at each end of the tube where there is a lower density of copper due to the falling gas temperature. These regions will have a relatively high voltage drop across them as electrons must be generated by ionisation of neon. The above discussion illustrates that the tube voltage measured is not the same as the voltage drop across the active region. The voltage on the

active region may display markedly different temporal behaviour to the measured voltage. This is illustrated by Carman (Carman et al. 1994). In his calculation of the voltage on the active region Carman finds it necessary to assume an exponentially falling resistance at the cathode to reflect the formation time of the cathode sheath. Carman uses a formation time for the cathode sheath of 50-100 ns. Using this approximation the calculated voltage on the active medium starts to rise some 100ns later than the laser head voltage and it is this voltage which the electron temperature in the active region follows closely. The voltage on the active medium peaks slightly later than the laser head voltage and the period of highest voltage (and hence highest electron energy) matches the period of laser action.

When the plasma 'breaks down' three things happen; the tube voltage peaks, the current starts to rise rapidly and laser action commences. All three of these changes can be explained by a sharp rise in electron temperature at this time. The current starts to rise quickly as the electron energy is now sufficient to ionise copper and an avalanche of electrons is produced. Due to the high gain of the system, laser action commences shortly after the electron energy becomes high enough to produce a population inversion. The sudden increase in charge carriers at breakdown causes the plasma resistance to drop and the external circuit is no longer able to maintain the tube voltage as the storage and peaking capacitors are discharged.

The tube voltage continues to fall, when it reaches zero the current peaks and laser action ceases. The electron temperature has started to fall by this point as the electrons are cooled by collisions and the lost energy cannot be replaced by the falling electric field. The fact that a high current continues to flow after the tube voltage has fallen to zero shows that the load is strongly inductive at this time. At this point the calculated tube resistance is

very low and the circuit impedance is now largely contributed by the laser head inductance as it is much smaller than $L_2$ (Equation [2.9]). The calculated inductance is now much lower, as seen in Figure 2.8, and is close to the value we would expect for the co-axial laser head geometry. (The inductance associated with the co-axial laser head geometry can be calculated as between 300 and 600nH depending on discharge constriction.) The calculated tube resistance has also collapsed, ( Figure 2.9 ).

The voltage and current waveforms continue to oscillate about zero after this as energy rings between the inductive laser head and the peaking capacitor. This continues until the remaining energy is absorbed in the various circuit and plasma resistances. The calculated inductance during this period increases by a considerable amount. As the plasma resistance is still low this must be due to constriction of the discharge acting to increase the laser head inductance.

During the first peak in the current pulse the plasma resistance collapses. At the same time the inductance due to the plasma itself has reduced due to the increase in electron collision frequency for momentum transfer (increased electron density). The load can now be considered as a low resistance due to the plasma and the distributed laser head geometrical inductance. At this time a significant proportion of the work done by the voltage across the tube goes into changing the stored energy in the electric and magnetic fields between the plasma column and the co-axial current return. At this time very little power is dissipated in the plasma because the resistance is so small.

## 2.4 WAVEFORM DEPENDENCE ON HBr CONCENTRATION

The evolution of the current and voltage waveforms as the percentage of HBr in the neon buffer gas is increased from zero to optimum is shown in Figures 2.11, 2.12, 2.13 & 2.14.

In Figure 2.12 the current and voltage waveforms are shown for a discharge in pure neon. The current rises at the same time as the voltage and the two traces are nominally in phase throughout the excitation period. There is a dip in the peak of both the current and voltage waveforms. It is again important to consider the differences between the laser head voltage and the voltage across the active medium. In the case for a discharge in pure neon, the voltage across the active medium will be very similar to that on the cold end regions of the plasma of a CVL (where there is a negligible density of copper and hence the discharge is supported by the neon buffer gas). This has been calculated by Carman (Carman et al. 1994) and is quite different from the laser head voltage, see above. The leading edge of the current pulse is therefore carried by low energy electrons which are slowly accelerated down the tube by the low voltage on the active medium. A high current can be carried because there are a large number of electrons remaining from the preceding pulse. 'Breakdown' has not occurred at this time.

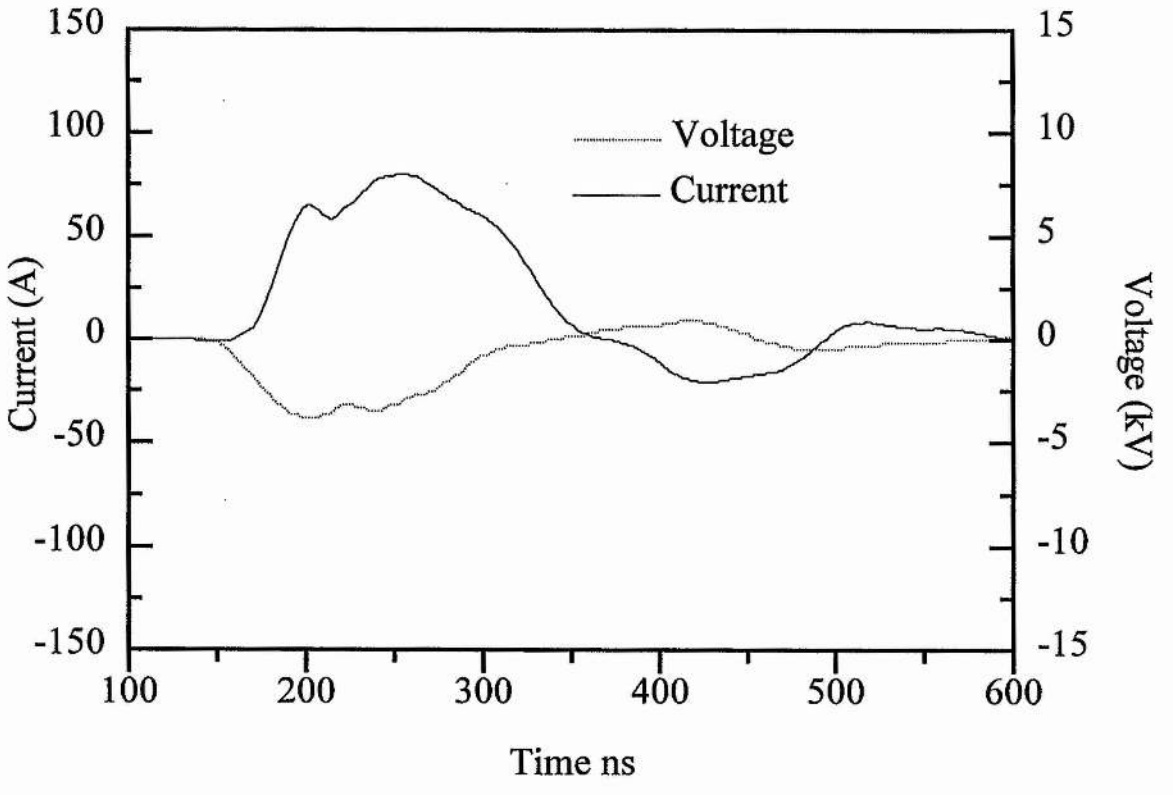


Figure 2.12 Current and voltage waveforms, pure neon

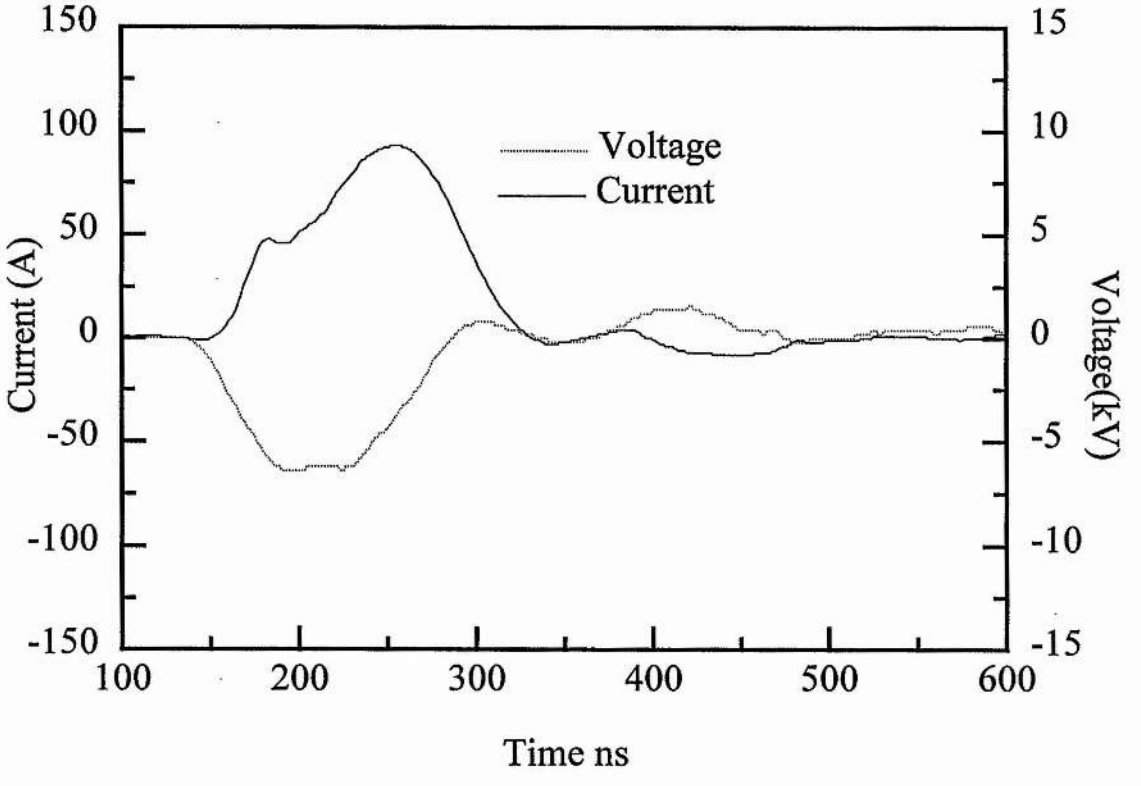


Figure 2.13 Voltage and current waveforms, low HBr

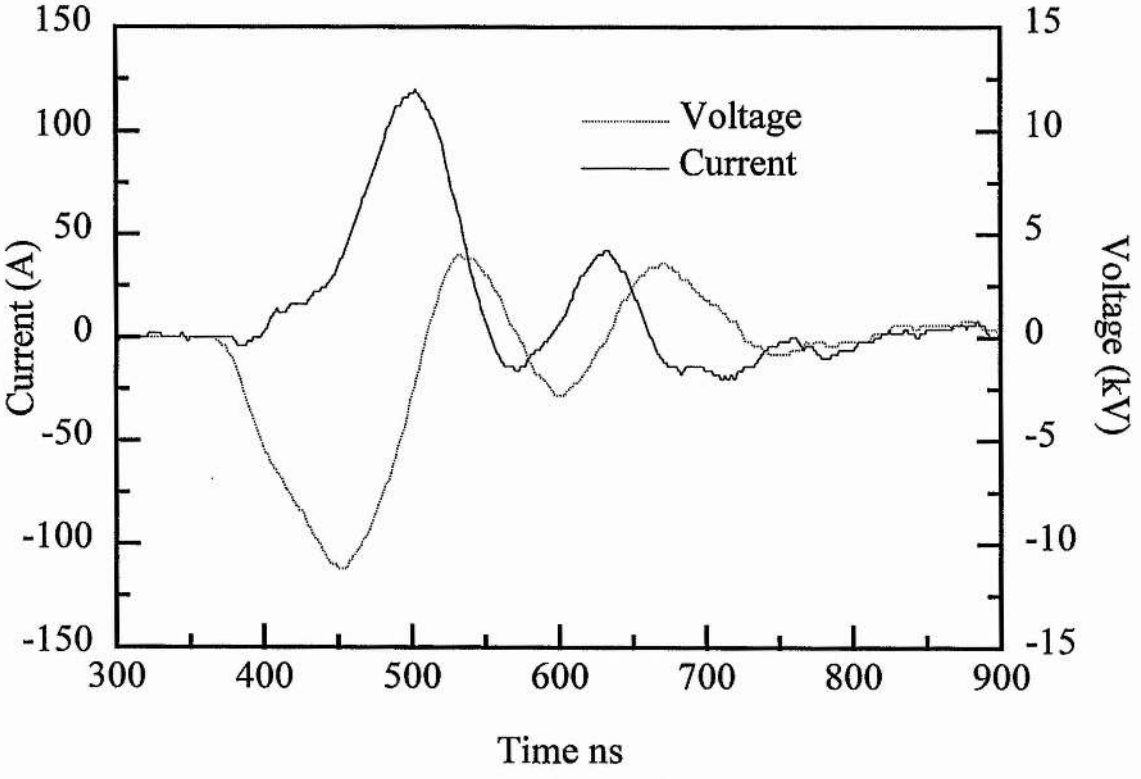


Figure 2.14 Voltage and current waveforms, near optimum HBr

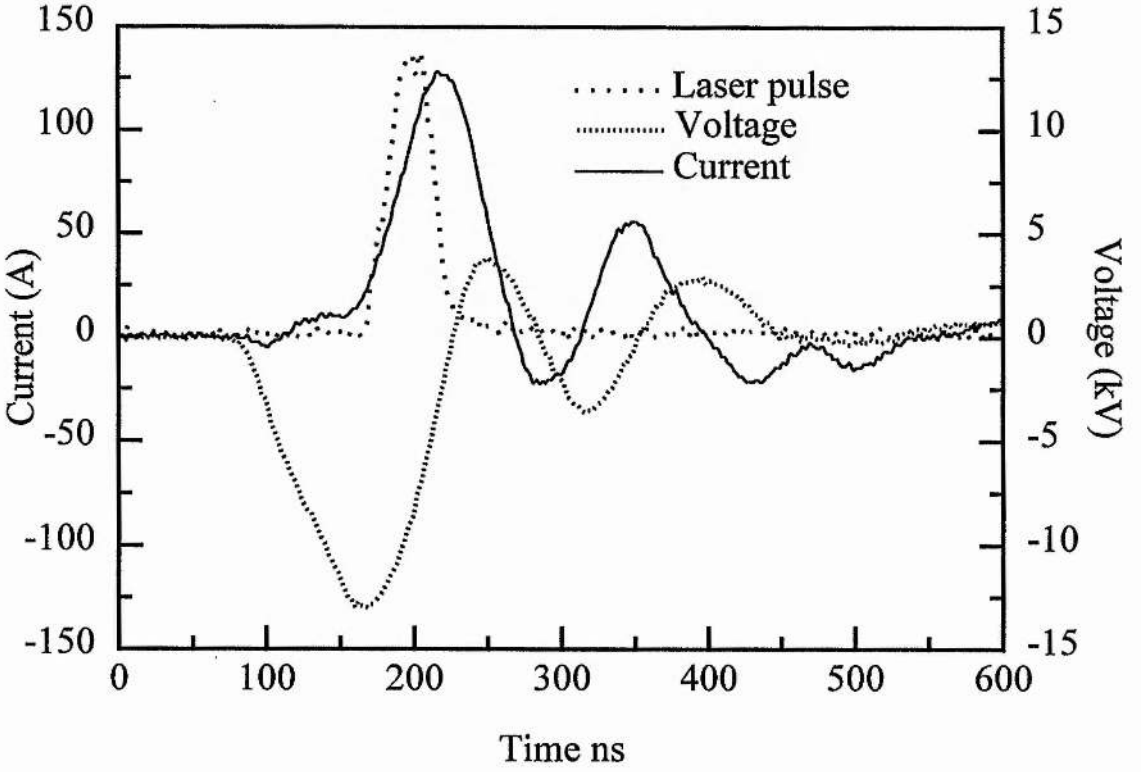


Figure 2.15 Voltage, current and laser pulse waveforms, optimum HBr.

Unless there is an unforeseen shielding effect operating in the active medium to reduce the field acting on the electrons, it must be the case that the voltage measured is not that across the active medium. If this were not so each electron would experience strong acceleration and the electron energy must rise. This would rapidly lead to ionisation, electron avalanche, tube breakdown and lasing.

When the voltage on the active medium does increase some 100 ns after the laser head voltage, due to the formation time of the cathode fall, the electron energy increases rapidly, ionisation occurs and there is an electron avalanche. This point is called 'tube breakdown' and at this time neon emission is seen. The period of conduction before tube breakdown can play an important part in the laser kinetics of both CVLs and HyBrID lasers as power is deposited in the discharge volume during this period.

In Figure 2.13 a small amount of HBr has been added to the discharge volume. The main difference between the waveforms of Figure 2.12 & 2.13 is that the peak current has increased, the peak voltage has increased and the step in the current leading edge has fallen. The decrease in the magnitude of the step in the current pulse is due to a decrease in pre-pulse electron density (Jones et al. 1994) caused by the addition of hydrogen which cools the electrons and allows faster three body recombination in the afterglow. Also electro-negative species have been introduced which may attach free electrons in the afterglow period. The reduced pre-pulse electron density is able to carry less current and as the voltage on the active medium is believed to be low at this time, no additional charge carriers can be produced. The height of the step in the leading edge of the current pulse is therefore a guide as to the pre-pulse electron density.

The tube breakdown voltage is increased due to the lower pre-pulse electron density, this leads to increased charging of the peaking capacitor. When breakdown does occur the increased energy stored on the peaking capacitor allows the external circuit to maintain the electron energy for a longer period and drive a larger current through the tube.

Figure 2.14 shows the current and voltage waveforms when the proportion of HBr added has been increased to 75% of the optimum. The step in the leading edge of the current pulse has now fallen further, the peak current and voltage are increased and there is significant ringing of both the current and voltage waveforms. This behaviour is that which would be expected if there has been a further reduction in pre-pulse electron density and a consequent increase in breakdown voltage.

The current and voltage waveforms with HBr concentration optimised for maximum efficiency operation are shown in Figure 2.15. The laser pulse shape is also shown. The above explanation of the waveforms is supported by observations of the waveforms as the HBr concentration is varied over a limited range. HBr concentration controls the pre-pulse electron density and the step in the current waveform leading edge changes in magnitude. The step magnitude increases for decreased HBr content and vice versa, as we would predict (Jones et al. 1994).

It is interesting to note that, in experiments performed to investigate the effects of hydrogen addition to CuBr laser, on addition of hydrogen it was found that the current rise was delayed with respect to the voltage rise (Astadjov et al. 1985; 1988). The delay between the rise of the current and the start of the laser pulse was also found to decrease with added $H_2$. This supports the argument that the hydrogen plays an important part in controlling the pre-pulse electron density. The resolution of the current,

voltage and laser waveforms in these papers is not sufficiently high to determine if there is a step in the leading edge of the current pulse which changes height with hydrogen concentration. There is an increase in pulse width with increased hydrogen concentration. This indicates that the electron energy is maintained at a high level for a longer period when hydrogen is added. This may be due to the observed increase in breakdown voltage resulting in increased energy storage on the peaking capacitor, as described above.

Further corroboration is provided from an investigation performed by Hogan on the CVL (Hogan 1994). In this study the excitation was gated off for several hundred milliseconds and the waveforms of first and second subsequent pulses were recorded. This allowed Hogan to look at the waveforms when the pre-pulse electron density was much lower than the equilibrium value. The second excitation pulse after gating off showed a step in the leading edge of the current pulse similar to that seen in the HyBrID and subsequent pulses had steps at increasing heights on the leading edge. Observation of the spontaneous neon emission at tube temperatures below lasing showed no emission until the tube voltage had peaked. It was suggested that the step was due to conduction by the pre-pulse electrons and under equilibrium conditions the pre-pulse electron density was sufficient to support almost the entire peak current. Current through a plasma may be considered as the net flux of charge carriers passing through the cross section of the plasma per second. There is therefore an inverse relationship between charge carrier density and charge carrier velocity, a high density of charge carriers need only move relatively slowly in order that a large current be passed. Calculations showed that only at a current of 1250A would the electron drift velocity exceed the mean thermal velocity at 2000K.

In the case of the CVL, because the pre-pulse electron density is much higher there is a much higher current carried before the tube breaks down and much more power is deposited in the tube. The electron energy during this time is low because the voltage on the active medium is low. The laser pulse is delayed relative to the current rising edge due to this delay in voltage rise. (The delay between the rise of the tube voltage and the start of the laser pulse is not changed appreciably). When lasing does commence it is clear from the form of the laser pulse leading edge that the gain has switched on very quickly and there is very high gain early in the pulse. This is not the case in the HyBrID where the rising and falling edges of the laser pulse are of equal length and the laser pulse is much more temporally symmetric. This indicates that the temporal evolution of the gain in the HyBrID laser is different to that in the CVL.

# CHAPTER 3 REFRACTIVE INDEX MEASUREMENT OF ELECTRON DENSITY

## 3.1 INTRODUCTION

The electron density of a plasma may be determined by a number of different techniques. The methods most commonly used are; 1. measurement of the linewidth of one or more of the lines in the Balmer series of hydrogen. (Trace amounts of hydrogen are present in most laser systems.); or 2. Investigation of the contribution to the refractive index due to free electrons.

In the calculation of the contribution to the hydrogen linewidth of natural, pressure, instrumental and self-absorption broadening as well as fine structure splitting allows the investigator to derive the theoretical Doppler and Stark broadened lineshape from the complex lineshape measured.

This technique has several disadvantages. It requires detailed knowledge of all of the relevant line broadening mechanisms and due to the low concentrations of hydrogen in most of the systems to be investigated, the spontaneous emission signal is of very low intensity. In many cases the contributions to the measured linewidth will not be known to the accuracy desirable. This situation is exacerbated by the fact that the contributions may often be of similar magnitude. Acquisition of the lineshapes of several lines on which the different line broadening processes have different relative effects can help to assess the relative magnitudes of the components, but high accuracy is still not possible (Blau et al. 1992).

The low intensity of the signal necessitates the use of high sensitivity photomultiplier tubes and long exposure times. In this case the result is a measure of the average electron density over the integration time. If spatial resolution is also required then an appropriate cylindrical imaging technique must be chosen. This has the effect of reducing the intensity incident at the detector by a significant factor and the integration time must be increased to

compensate for this, further compromising the time resolution of the measurement.

It is also possible to calculate the electron density from the time dependant resistance of the discharge gap. This technique only yields results for the period of the excitation pulse and will not be further considered.

In comparison the refractive index measurement technique suffers from relatively few constraints. There are few assumptions necessary and fast detectors are available. The disadvantages of this method are;

1. relatively low sensitivity and;

2. the fact that it gives only a measure of relative electron density, the initial electron density must be determined by measurement of the refractive index as the electron density is allowed to fall to zero, or by another independent technique.

## 3.2 HISTORY

The application of interferrometry to the measurement of the electron density in a plasma is a well established technique. It was initially employed with a probe source operating in the microwave region ( Biondi 1949; Varnerin 1951; Whitmer 1956) but was later extended to the visible (Alpher et al. 1959; Wright et al. 1961; Ramsden et al. 1962). The technique has been applied to the study of many different types of plasma including RF discharges (Ascoli-Bartoli et al. 1960) and plasma torus discharges such as that in Sceptre IV ( Dyson et al. 1962).

Lasers were applied to the technique as probe sources by Ashby et al. (Ashby et al. 1963, 1965) using a novel interferometer arrangement in which the phase shifted beam was fed back into the laser cavity and the electron density was calculated from measurement of the laser output power. This

system was used, slightly modified for improved sensitivity, in other investigations (Gerardo et al. 1963).

The technique has recently been applied in modified form to the study of electron densities in He-Sr recombination lasers ( Loveland et al. 1992) and CVLs (Hogan 1993).

Alternative techniques used for electron density measurement in the literature have included calculation of the electron density from the measured resistance of the discharge gap. (Batenin et al. 1977) and measurement of the hydrogen linewidth (Blau et al. 1992)

## 3.3 THEORY

### 3.3.1 ELECTRON - PROBE INTERACTION

We wish to model the interaction of free electrons in the discharge region with the probe beam. Free electrons generate a space charge when displaced from their equilibrium positions, this produces an electric field exerting a restoring force on the electrons. In combination with the oscillating electric field due to the probe beam this effect causes a net electric field $E$ to act upon the electron. If the electrons' interaction with atoms and ions is modelled by the inclusion of a viscous damping term ($\nu$), then the electrons' motion can be described by the following equation where $x$ is the electrons' position.

$$\ddot{x} + \nu\dot{x} + \omega^2 x = -\frac{e}{m}E\,. \qquad [3.1]$$

The steady state solution to this equation is

$$x = \frac{e}{m\omega(\omega - i\nu)}E\,. \qquad [3.2]$$

From the identities

$$J = -ne\dot{x}\,, \qquad [3.3]$$

$$\bar{n}^2 = 1 - i\sigma/\varepsilon_0\omega \,, \qquad [3.4]$$

we can write the complex refractive index as

$$\bar{n}^2 = 1 - \frac{\omega_p^2}{\omega}\left(\frac{\omega + j\nu}{\omega^2 + \nu^2}\right), \qquad [3.5]$$

where

$$_p^2 \approx \frac{ne^2}{\varepsilon_0 m} \,. \qquad [3.6]$$

In the case where the collision frequency is much less than the plasma frequency and the probe beam frequency is much greater than the plasma frequency (i.e. $\nu << \omega_p << \omega$) this can be simplified to

$$\bar{n}^2 \approx 1 - \frac{\omega_p^2}{\omega^2} \,, \qquad [3.7]$$

in which case the refractive index is fully real, (i.e. the absorption is negligible.) This result enables us to calculate the change in plasma frequency from a measured change in refractive index. Using [7] we can then derive the change in electron density.

## 3.2 THE TWO WAVELENGTH EXPERIMENT

The experiment was performed at two different wavelengths to allow us to assess the relative contributions to the refractive index due to atom & ion densities and that which we wish to measure, the contribution due to free electrons. The fringe shift due to a change in free electron density is linearly dependant on the probe wavelength (Chapter 5.1) while that due to atom and ion densities is wavelength independant provided the wavelength range of interest is not near a transition. If there were a transition in the region of interest fringes would be produced, this was not the case, therefore we were able to separate the two contributions by performing the experiment at two wavelengths, one in the infra-red at 10.6 μm and one in the red spectral

region at 670 nm. A fringe shift at 670nm due to a change in atom and ion density are relatively 15.8 times smaller at 10.6μm and so the two contributions could be separated.

## 3.4 EXPERIMENTAL METHOD

### 3.4.1 INTERFEROMETRY

To measure the change in refractive index of the plasma a Mach-Zehnder interferometer was set up with the HyBrID laser in one arm, as shown in Figure 3.1. The interferometer was aligned to give uniform illumination at the detectors.

A change in the refractive index in the laser will cause a change in path length in that arm of the interferometer which will result in a change in intensity at the detectors. The change in intensity will depend on the real refractive index, $n$, according to the relation

$$I = \frac{I_0}{2}\left(1 + \cos\left(\frac{2\pi l(n-1)}{\lambda_0}\right)\right), \qquad [3.8]$$

Using a CW laser as the probe beam source, the variation in electron density may be observed and measured in real time, by viewing the detector output on a fast oscilloscope. In this experiment a second wavelength was used to assess the effect of changing atom and ion densities on the refractive index, as explained in Chapter 2.2. No measurable effect due to atoms and ions was found. One advantage the visible laser did provide however, was that once aligned with the beam from the $CO_2$ laser, using the beam combining optics BS1 & HR1, the red beam greatly aids alignment of the interferometer. The probe beams were aligned using iris apertures to define a path through the laser parallel to the axis, though the ultimate spatial resolution was defined by the sizes of the active elements of the detectors.

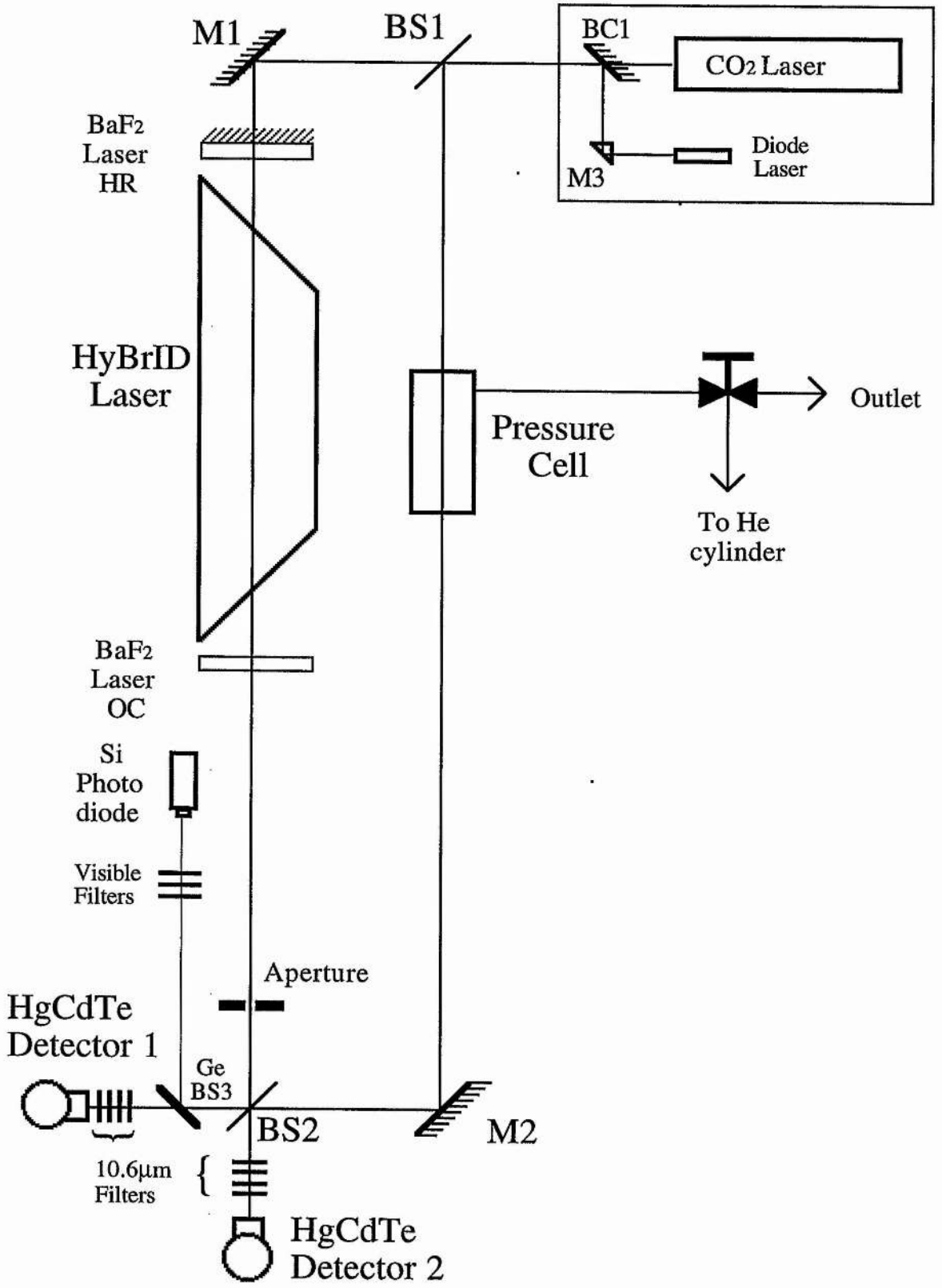


Fig 3.1. Electron density measurement experimental layout

### 3.4.2 DETECTION

The detectors used for the infra-red laser are liquid $N_2$ cooled, HgCdTe photovoltaic detectors with matched preamplifiers. These devices had 100μm x 100μm elements with a specified bandwidth of DC to 100MHz. The pre-amplifiers matched to the detectors had a lower bandwidth and the system was thus limited to a maximum of 75MHz.

Appropriate filtering was placed before the detectors to remove any blackbody emission from the HyBrID laser or surroundings and to reduce the incident signal intensity to the required level.

Provision was also made to observe the visible radiation using a fast photodiode. Attenuators of the HyBrID laser emission were placed before the photodiode, though it was possible to observe the HyBrID laser pulse if desired in order to give absolute verification of timing accuracy. Residual $CO_2$ laser emission was filtered out of the beam before the photodiode.

### 3.4.3 STARTING PHASE ADJUSTMENT

In the reference arm of the interferometer there was a compensation cell to allow the introduction of an additional fringe shift of more than $\pi$ radians, for calibration purposes. This was effected by increasing or decreasing the pressure of He in a 50cm tube sealed with $BaF_2$ windows. This facility also allowed us to adjust the starting phase of any measurement.

### 3.4.4 TIMING

Output from the detectors was monitored on a $500MSs^{-1}$ digital oscilloscope, Tektronix model 2440. This device was connected to the control computer via a GPIB link to allow downloading of traces to a computer hard disc for subsequent manipulation and analysis. The

oscilloscope was triggered from the master oscillator which also controlled the HyBrID laser timing to ensure low jitter and good timing accuracy. This could be verified by observing the laser output pulse on the photodetector as mentioned above.

### 3.4.5 PRE-PULSE ELECTRON DENSITY MEASUREMENT

To allow measurement of the pre-pulse electron density, a momentary action switch with bounce suppression was connected to the inhibit socket of the master oscillator to gate the laser off for a short period to allow the electron density to fall to zero.

## 3.5 ACCURACY

The overall accuracy of this technique depends on several factors. The minimum fringe shift which can be detected determines the sensitivity of the experiment. The short term, pulse to pulse, laser stability must be good in order to provide a stable reading while measurements are taken. Longer term stability is also important as the measurements are relative and a calibration measurement of refractive index change as the electron density falls from the pre-pulse level to zero is required. In the case where less than half a fringe shift is observed, a calibrating measurement of full fring shift will also be necessary.

### 3.5.1 SENSITIVITY

We can calculate the fringe shift $\Delta m$ due to a change in electron density $\Delta n_e$ from Equations [3.6] &[3.7]

$$\Delta m = -l\frac{\omega_p \Delta\omega_p \lambda_0}{4\pi^2 c^2} \qquad [3.9]$$

From this equation we can see that the sensitivity of this measurement will be determined by two factors over which we have control, the path length $l$ and the probe wavelength $\lambda_o$ .

The path length $l$ corresponds to the length of the active region, though the effective path length may be increased by passing the probe beam through the active region multiple times. The accuracy with which this dimension is known may be a significant source of error.

The interferometric technique measures the electron density integrated over the path length; measurement of the contribution to the total due to a particular section of the discharge plasma was not possible with the equipment used in this investigation..

Illustrative of this problem is the situation in the high temperature CVL where the discharge region must be partitioned to allow explanation of the observed phenomena. In the case of the CVL it is convenient to consider the discharge region as partitioned into a central 'hot' region with a 'cool' region at either end. This approximation allows us to postulate a credible explanation for electron density behaviour in the high temperature laser. This is obviously a simplification and determination of the length of the 'hot' region is not accurate.

The situation in the much cooler HyBrID will be complicated further by chemical reactions and the hot discharge attachment points on the electrodes. The length of plasma column interogated can be estimated to within +/-2%.

The second parameter over which we have control is the wavelength $\lambda_o$ of the probe laser, which is important in determining the experiment's sensitivity. In practice this variable is heavily influenced by practical issues such as availability and cost of suitable sources, optics and detectors, as well

as the wavelength necessary to provide adequate sensitivity at the electron densities encountered in the plasma to be investigated. In certain situations where either very high sensitivity is required or low electron densities must be measured, it is necessary to go to very long wavelengths, such as the millimeter systems used to interogate the plasmas of fusion tori.

In the lasers under investigation the change in electron density is of the order of $1 \times 10^{14} cm^{-3}$, this will give a fringe shift of 0.35 for a probe beam at 10.6μm, giving a change in intensity of approximately 70%. This is quite measurable and well developed technology exists in the $CO_2$ laser industry to produce and handle laser radiation at 10.6μm. Sources and detectors at significantly longer wavelengths are more expensive, less well supported and in the electron density range of interest offer little benefit for significantly increased cost.

### 3.5.2 STABILITY

Laser stability is an important consideration when evaluating the measurement accuracy. If multiple acquisitions are made, averaged and the background noise subtracted the pulse to pulse variation in output will result in a broadening of the trace which will translate into a scatter of results, this may compromise the accuracy with which the turning points in the result can be determined, and thus the accuracy of determination of the fractional fringe shift. If laser stability is very poor, averaging of acquisitions may not be possible as a large proportion of the data detail will be lost in the averaging process. This was not the case in our system where the only limitation on the number of acquisitions averaged was the time taken for the oscilloscope to perform the averaging and consequently the response time of the system to adjustments. The number of acquisitions was kept low for this reason as the

traces were highly reproducible even for single shot acquisitions. It should be noted that pulse to pulse instability as measured at the detectors may be due to factors other than the laser itself. Effects such as air currents in the reference arm or vibration in the table or optical mounts will also affect the result.

### 3.5.3 CALIBRATION

The accuracy of the measurement will also be affected by the magnitude of the observed fringe shift. If the observed fringe shift is greater than one half fringe, then with suitable adjustment of the initial phase, the investigator can assess the magnitude of a full fringe shift from the trace. Such a measurement is called self-calibrating. If this is not the case then a separate measurement of a full fringe shift must be made to calibrate the system. Clearly self-calibrating measurements will be more accurate as there is no possibility for change in any of the system parameters between result and calibration measurements.

The precision with which the full fringe shift is measured is of great importance as the data manipulation required to give an electron density trace includes a cosine function (Equation [3.7]) which is sensitive to accurate calibration. Because of this cosine dependence, errors and inaccuracies will be disproportionately magnified at the extrema. (See Figure 3.2). This mitigates against arranging the system to give either maximum or minimum intensity at the initial position, as the starting point of the measurement would then have maximum error. However, the extrema are by far the easiest points at which to reliably and repeatedly set the initial intensity. In addition, starting at the maximum or minimum intensity gives us the best chance of observing a full fringe shift and hence achieving a self-

calibrating measurement. For these reasons, all measurements were started from either maximum or minimum intensity.

The measurement of the full fringe shift for non-self-calibrated results will be of inferior accuracy as the full fringe shift can only be introduced by means of the compensation pressure cell which is unable to react quickly enough to allow capture of a full fringe shift on the oscilloscope screen. The extrema of the fringe shift can only be measured by cursor placement or by using measurement functions on the oscilloscope; this is not as accurate as the analysis of stored data containing information over the full fringe shift.

It is possible that the full fringe shift will vary in time during the laser pulse cycle due to absorption, scattering or beam steering effects in the laser itself. For this reason two identical fast detectors were used to look simultaneously at the two outputs from the interferometer. As the two outputs are 180° out of phase, the sum of the two measurements gives a measure of the change in full fringe shift during the pulse inter-pulse period. This allows correction of the trace for amplitude effects. See Figures 3.2 & 3.3.

### 3.5.4 DETECTION LIMITATIONS

The ultimate limit to the accuracy of the measurement, when all other contributions are minimised, will be the signal to noise ratio (*S/N*) of the detectors and their pre-amplifiers. This may be calculated from the detectivity $D^*$ specified by the detector manufacturers, the power $W$ incident on the detector of area $A$ and the amplifier bandwidth $\Delta f$, using the following relation

$$D^* = \frac{(S/N)(A\Delta f)^{1/2}}{W} \qquad [3.10]$$

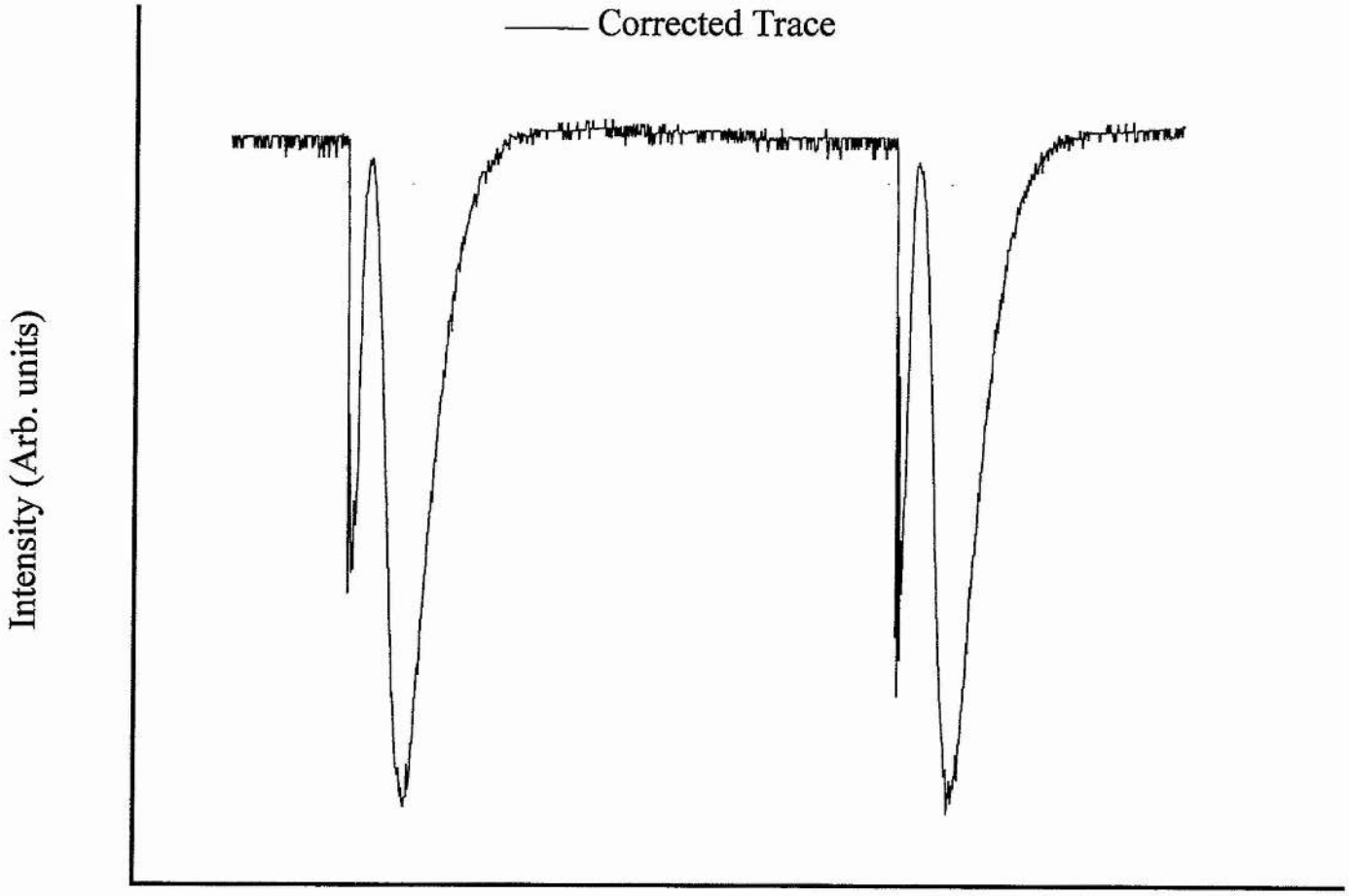


Fig 3.2 Detector output showing increased result scatter at extrema

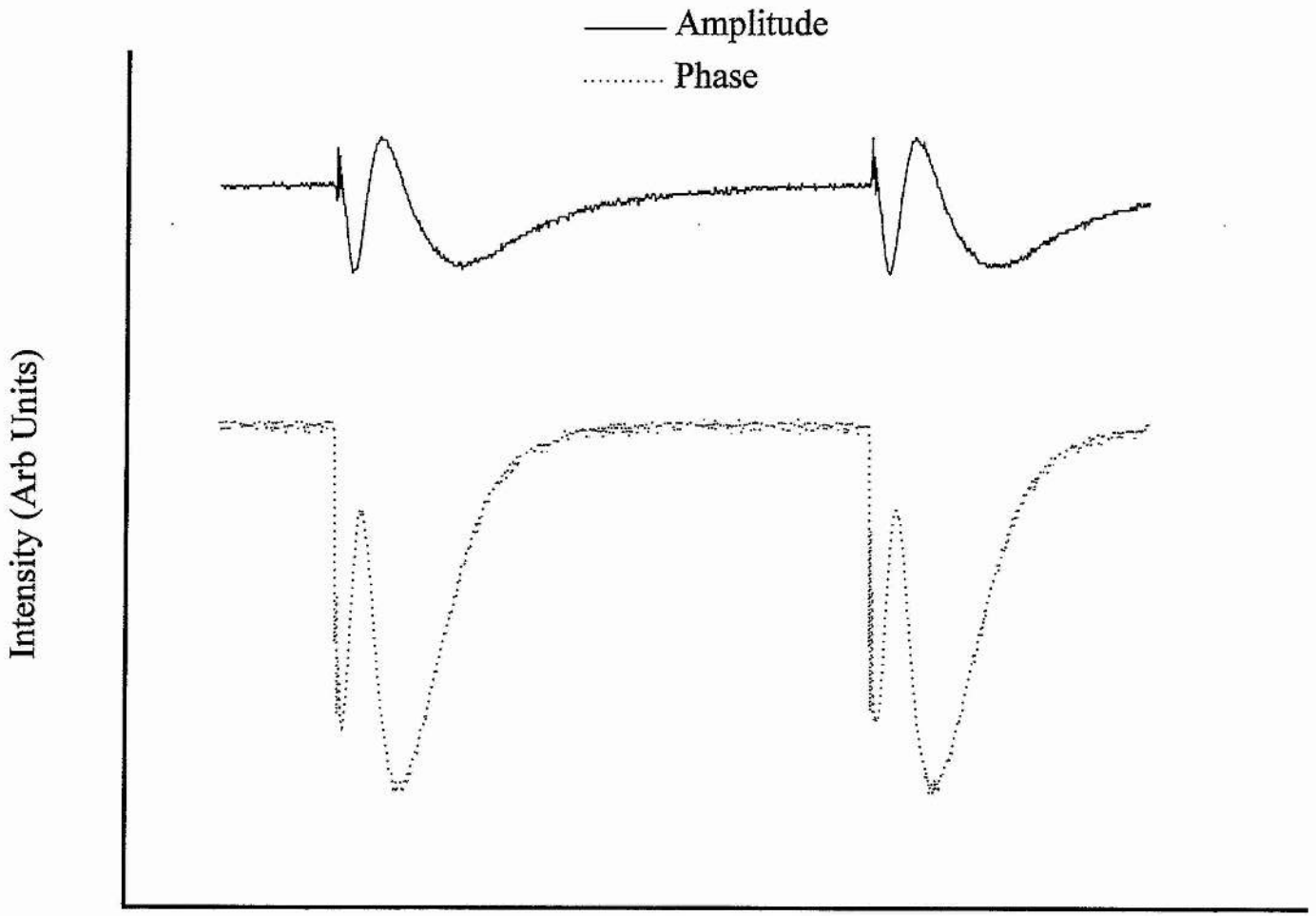


Fig 3.3 Amplitude and phase effects at interferometer outputs

As the laboratory in which the experiments were performed is a hostile environment in terms of radiated electromagnetic interference, the signal may be corrupted between the detector elements and the oscilloscope by electromagnetic pick-up, and precautions must be taken to minimise such interference. Proper grounding and shielding techniques must be employed and short, good quality cables used in all signal paths. To maximise the signal to noise ratio it would be preferable to maximise the available signal level from the detector preamplifiers in order to minimise the importance of noise pick-up. In earlier work with this experimental arrangement it was found that at high incident laser intensities the detectors were limited to a much smaller frequency range than that specified by the manufacturers. If we reduce the incident laser intensities at the detectors to that specified by the manufacturers for full bandwidth operation, additional amplification is needed due to the limited sensitivity of the oscilloscope. We were unable to achieve suitable low noise amplification, as the devices available to us introduced unacceptable levels of noise to the experiment, negating any advantage gained due to increased bandwidth from the detectors. It was therefore necessary to operate in the regime where the detection system's bandwidth was reduced to a maximum frequency of less than 10MHz.

It is good practice to record a background noise measurement. This was easily done by simply blanking off the $CO_2$ laser output. To ensure that the noise signature was not altered, as the detectors would now be operating in their full bandwidth state, it was verified that the noise signal was generated by pick up on the co-axial cable between the detector preamplifier and the oscilloscope. No change in noise pick-up was observed. Noise traces were then acquired and subtracted from the fringe shift signal to give the signal trace with reduced noise.

# CHAPTER 4 ELECTRON DENSITY MEASUREMENTS

## 4.1 SOURCE OF ELECTRONS

### 4.1.1 CONVENTIONAL CVLs

In the conventional CVL there are two sources of electrons, copper and neon atoms. The number of recombination processes is similarly limited, and three body recombination of copper ions is held to be the dominant process in the active region (Carman et al. 1994). Singly charged copper ions will also be accompanied by smaller populations of doubly charged copper ions and singly charged neon ions. In the CVL there will be a more significant population of neon ions in the end regions where the temperature is insufficient to support a high copper density and neon must provide the charge carriers. As the measurements are of the electron density integrated over the probe beam path, by the nature of the experiment the effects due to neon ions will be included in the result and must be allowed for, i.e. three body recombination of neon ions will be a significant process at particular times and radial positions (Carman 1994; Hogan 1993).

### 4.1.2 HyBrID LASERS

In the HyBrID laser system, there are two additional elements present which are not found in conventional CVLs, hydrogen and bromine. Therefore there will be alternative sources of electrons in addition to the two mentioned above. It may be argued that unless particular care has been taken there will be trace amounts of hydrogen present in most CVL systems. This is undoubtedly the case and small amounts of hydrogen have been shown to have considerable effect on the performance of CVLs and CuBr lasers, (Astadjov et al. 1985; 1988; Withford et al. 1994). HyBrID lasers typically

operate with hydrogen concentrations up to twice the maximum amount for conventional CVLs.

Due to their relatively high ionisation energies compared to copper, hydrogen and bromine are unlikely to be important electron donors in the active region.

## 4.2 END REGION EFFECTS

Analogous to the situation in the CVL, there will be a region at each end of the discharge where the temperature is too low to support an equilibrium concentration of CuBr sufficient for the discharge current to be provided entirely by ionisation of copper. Estimation of the size of these regions is complicated by the fact that HBr entrained in the neon buffer gas flow passes over the anode of the laser and reacts with the hot copper at the discharge contact spot, producing CuBr in the cool region. At the cathode copper bromide will be entrained in the gas flow and carried into the cool end region. Both of these effects were observed to have occurred when the laser tube was dismantled and inspected after many hours of use. There is noticeable erosion of the anode electrode and both water-cooled laser end flanges could have deposits of copper bromide on the exposed surfaces.

The best method of estimating the length of the cool regions is to look at the quartz 'spot-lock' (the 'spot-lock' is a quartz tube passing through the electrode from the end window region into the plasma tube. The tube has a 10 mm hole in one side which acts to restrict the area of electrode exposed to the discharge. The 'spot-lock' design may be seen in Figure 1.3) The end of the 'spot-lock' facing the hot zone has elemental copper driven into the flaws in the quartz and no CuBr deposits, showing that it was hot (>600 $^{o}$C). At the point where the spot-lock passes through the water-cooled electrode there is

evidence of CuBr build-up showing that the region is too cool to support the high vapour pressure of CuBr found in the central region. The cool region corresponding to the volume where the discharge is not supported by copper is therefore only the distance from the end of the electrode to the hole in the spot lock, approximately 1cm at each end, or a total of 2 cm, less than 3% of the discharge length. In these regions the electrons that carry the discharge current must be contributed by other species. Neon and hydrogen will both strongly influence the discharge kinetics in this region. Hydrogen has a lower ionisation energy than neon and so may be expected to contribute a large proportion of its electrons directly to the discharge in the cool regions. However, the number of electrons donated by hydrogen will be limited due to the low hydrogen concentration compared to neon. The first excited state of neon is metastable. This increases the rate at which stepwise excitation can occur, and will result in increased neon ionisation. Due to its high ionisation potential it is unlikely that significant amounts of bromine are ionised, even in the end regions.

Recombination in these regions may occur by several processes, three body recombination with neon or hydrogen ions, two body attachment to electronegative species such as bromine and perhaps hydrogen and dissociative attachment to molecular species such as $H_2$ and HBr.

Two body processes would be expected to proceed at much higher rates than the three body ones. However, the density of electronegative species for two body processes will be much less than the density of neon and the electronegative species must be recycled by recombination of the negative ion formed with a positive ion before the process can continue, otherwise the low density of electronegative species will slow the reaction to a very low rate.

Three body processes in the end regions may be relatively fast due to the low gas temperature and an electron temperature cooled by hydrogen.

## 4.3 ON AXIS MEASUREMENTS

### 4.3.1 GENERAL REMARKS

The temporal behaviour of the on axis electron density for laser operation at the maximum efficiency condition can be seen in Figures 4.1 & 4.2. The corresponding result for the conventional CVL investigated previously by Hogan is shown on the same scale for comparison. It should be noted that the HyBrID laser data given in these figures show information only on the pre-pulse electron density and the period of falling electron density. This is due to the bandwidth limits of the detectors as discussed in Chapter 3.5.4 above. The fast rising edge of the electron density corresponds to a frequency of the order of 1 MHz. Due to the reduced gain available from the detector system at this frequency and significant noise pick-up on the low level signal it was not possible to obtain accurate measurements of the rising electron density. The results as shown therefore represent the pre-pulse electron density and the falling edge of the electron density, the two sections of data being connected by a straight line. The results for the conventional CVL suffer from similar restrictions although the problem is less severe due to the slower rate of rise of electron density in the CVL.

The results for the HyBrID laser shown in Figures 4.1 & 4.2 have a number of interesting features including;

1. The pre-pulse electron density is very small compared to that in the CVL.

2. The peak electron density is very high.

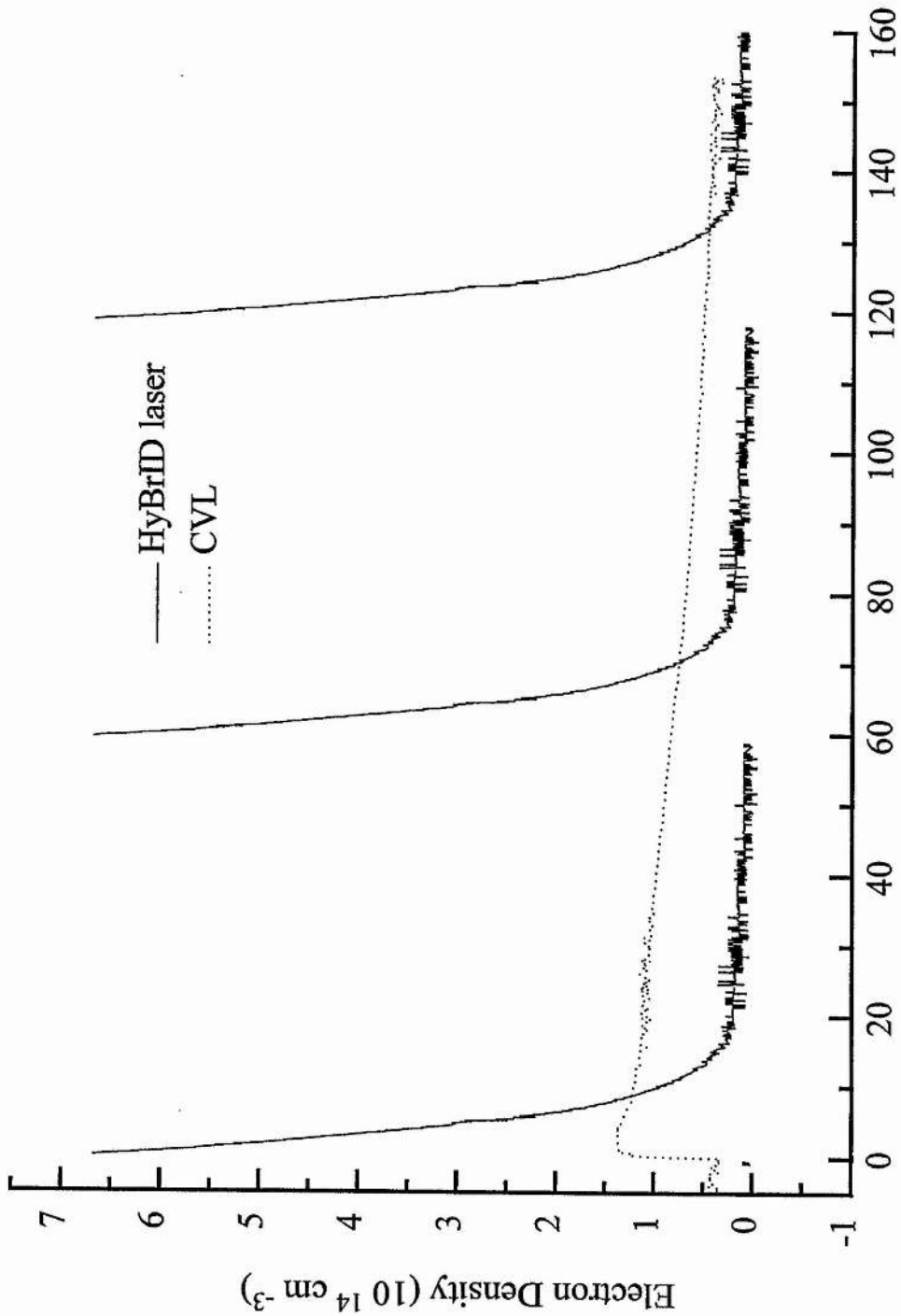


Figure 4.2 Electron density, HyBrID laser and CVL. Short time scale

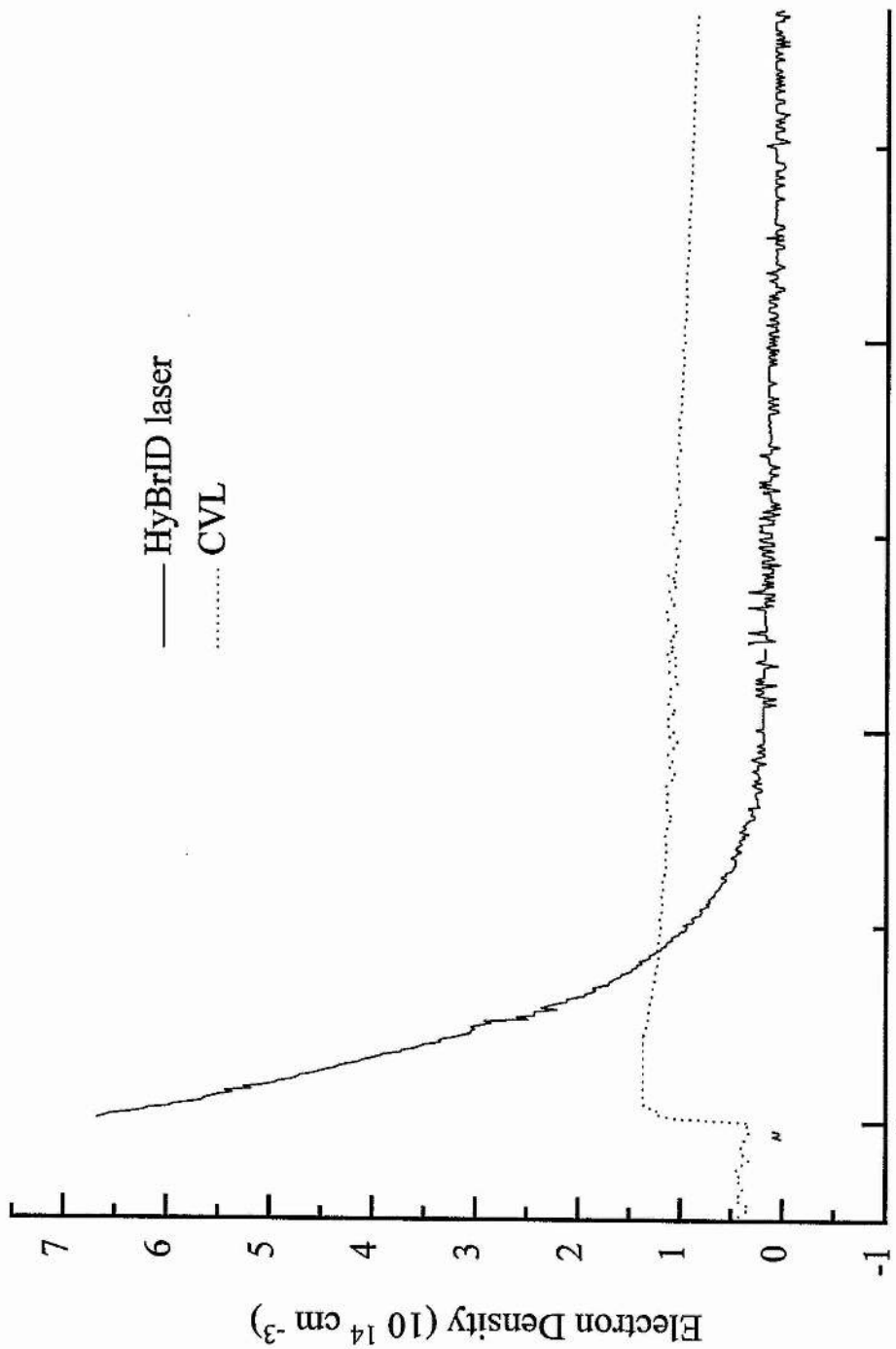


Figure 4.2 Electron density, HyBrID laser and CVL. Short time scale

3. The initial decay of electron density is very fast, this period of fast electron removal is then followed by a period of much slower decrease in electron density which continues until the onset of the next excitation pulse. If we plot the on-axis electron density on a log scale, Figure 4.3, we can clearly see this change in decay rate at time ~15 μs.

### 4.3.2 PRE-PULSE ELECTRON DENSITY

Possibly the most significant characteristic of this data is the very low pre-pulse electron density. In the high temperature CVL investigated previously by Hogan (1993), the electron density was seen to fall only to approximately 25% of its peak value before the subsequent excitation pulse was applied. In the HyBrID laser the electron density has collapsed to a very low fraction of its peak level after only 15 μs. In measurements to determine the absolute value of the electron density, where the laser was gated off for several ms, no further fringe shift was seen after one interpulse period. This shows that the pre-pulse electron density in the HyBrID system is at or below the noise level of our apparatus (~ $2 \times 10^{13}$ $cm^{-3}$) and is less than 2% of the peak electron density. As was discussed previously, for reasons of reproducibility and to maximise the possibility of observing a full fringe shift, all measurements were made with a starting point at the extremum of the output range. For measurement of the pre-pulse density this is unfortunate as it means we have minimum sensitivity to small changes in refractive index, and maximum error. It is therefore unreasonable to interpret the data as showing the electron density arriving conveniently at zero immediately pre-pulse, allowance must be made for the increased percentage error at this point. This error is approximately $2 \times 10^{13}$ $cm^{-3}$ which is a small

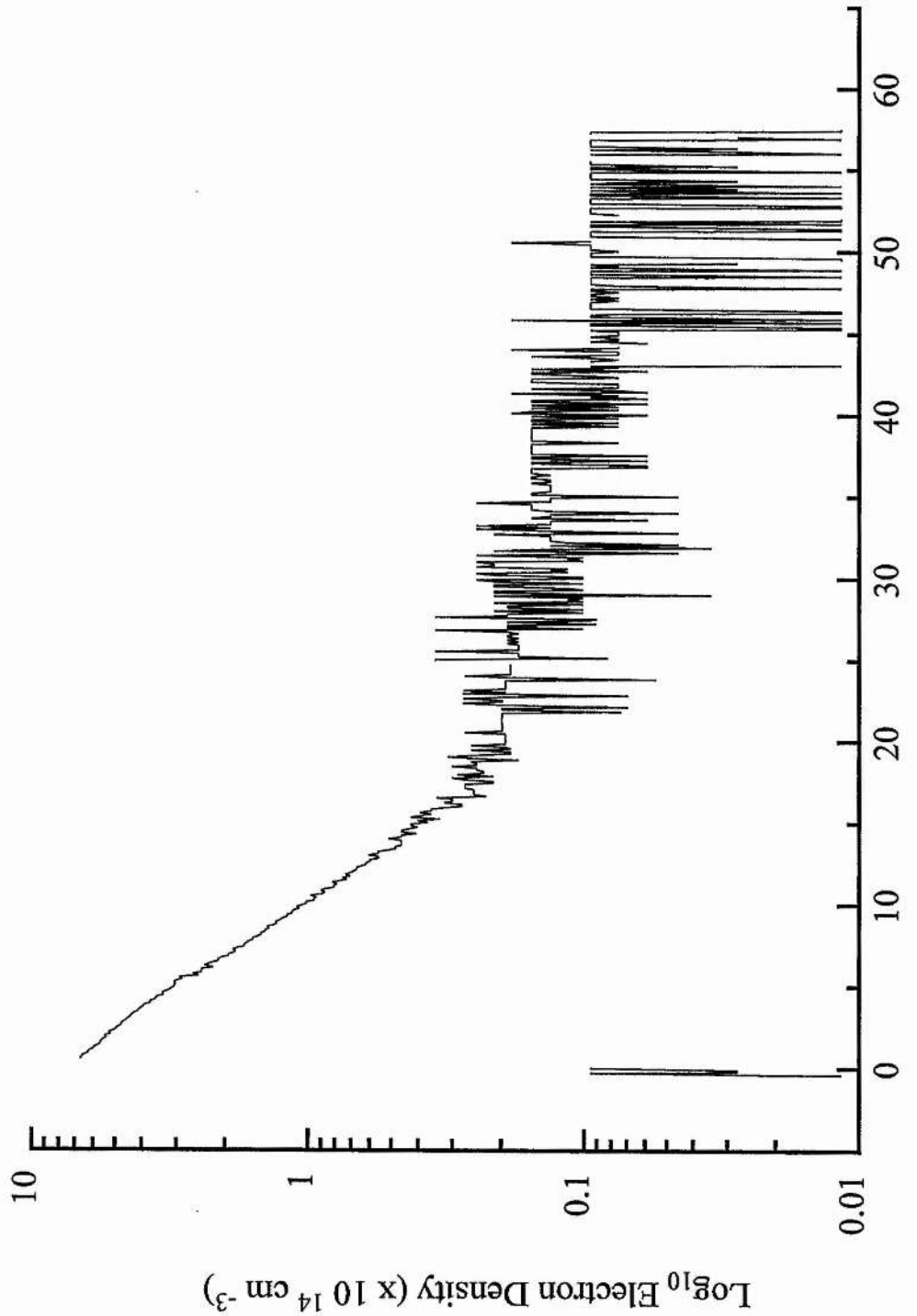


Fig 4.3 Electron density, log scale

fraction (< 10 %) of the total electron density in the early afterglow and is only significant at time points after 20 μs.

A plasma with a very low pre-pulse electron density will have a high impedance before the excitation pulse and the plasma breakdown voltage will be high. This is exactly as observed in the HyBrID system and many of the laser's desirable characteristics are associated with this property. For instance, in the HyBrID laser energy is transferred more efficiently from the power supply to the discharge than is the case in conventional CVLs. This is largely due to the low pre-pulse electron density allowing a high field to be developed across the laser tube before breakdown occurs and the correspondingly high impedance of the tube upon breakdown. The high impedance discharge demands a lower peak current and a slower rate of rise of the current. This allows the impedance of the thyratron to fall to a lower value before high current is demanded and so less power is deposited in the thyratron. The high discharge impedance also causes less power to be reflected back to the thyratron in the form of negative voltage overswing on the thyratron anode due to better matching between circuit and load impedances. The high discharge impedance also allows better matching of small capacitors to the discharge, which favours high PRF, low peak current operation.

### 4.3.3 THE PERIOD OF 'MISSING' DATA

As discussed earlier there is a period of 'missing' data due to experimental limitations. This period of 'missing' data is 400 ns long and covers the period from the start of the current pulse to a time about 100-150 ns after the last oscillation of the current pulse has ended. From Figures 4.1 & 4.2 we conclude that during this period the electron density has reached its

maximum value and has started to decrease. From the calculations of the time dependence of the power input to the plasma discussed earlier we have seen that although the majority of the power is deposited in the plasma during the first positive excursion of the current pulse, there remains some 25% which is not fully absorbed until almost 300 ns after the onset of lasing. We must therefore conclude that the electron density ceases to rise when the power input to the tube stops, or even before while current is still flowing in the tube.

This is in stark contrast to the situation in the elemental copper vapour laser where the electron density is seen to increase monotonically for the full 1 μs duration of the current pulse and is not seen to reduce for a further 3 μs. Indeed Hogan's explanation of the form of the decay of the electron density argues that recombination does not start in the hot part of the tube until some 25 μs after the start of the laser pulse.

### 4.3.4 PEAK ELECTRON DENSITY

The peak measured value of the electron density in the HyBrID system (as opposed to the actual peak value which we do not know as the electron density is already decreasing at the first data point) is seen to be some 5 to 6 times the peak value measured in the CVL. The CVL however is of 42mm bore compared to the HyBrID's 25 mm. If we assume uniform power deposition into the laser plasma, the energy deposited per pulse per unit volume in the CVL is 429 $\mu J/cm^{-3}$ compared to 247 $\mu J/cm^{-3}$ in the HyBrID. These figures are calculated on the assumption of 100% efficiency in energy transfer from storage capacitors to the discharge volume, this is not the case. Neither may we assume that the fraction of power lost in the two excitation circuits is similar as the HyBrID laser has much higher pre-pulse impedance

and hence will have much better circuit to discharge matching. A reasonable estimate of power lost in the thyratron in a typical CVL excitation circuit is 30% (Hogan 1993, Carman et al. 1994, Nehmadi et al. 1989). In his thesis Hogan estimates that the amount of energy deposited in the lasing region of the discharge is further reduced to approximately 50% of the stored energy because of the increased power per unit length deposited in the cold end regions where neon is the dominant electron source (Carman et al. 1994). In this case however we are considering the electron density integrated over the entire probe beam path length, including the end regions. In a HyBrID system thyratron losses have been measured to be in the 10-15% range (Jones 1995). Using these estimates, the energy deposited per pulse per unit volume is 300 $\mu J/cm^{-3}$ in the CVL and 223 $\mu J/cm^{-3}$ in the HyBrID.

Examination of the radial profiles of the electron densities of the two systems (see Chapter 4.4) shows that the discharge in the HyBrID system is significantly constricted at this power loading. This is not so in the CVL, though electron density is by no means uniform across the bore. This suggests that the current density on axis in the HyBrID laser, as compared to that in the CVL, is appreciably higher than the power loading per unit volume would suggest. More than 90% of the discharge electrons are produced inside the central 12 mm of the cross section of the bore of the HyBrID laser. Using this figure the power loading per pulse per unit volume is approximately 890 $\mu J/cm^{-3}$, three times that in the CVL.

Note, 12 mm is an estimate of the diameter inside which the majority of the electrons are created, this is not identical to the diameter of the laser beam. The discharge constricts during the current pulse, this may be seen from the increase in the tube inductance as calculated from the current and voltage waveforms Chapter 2.3.1. Due to this constriction the increase in

electron density near the axis will be greater towards the end of the current pulse than will be the case for positions further from the axis. As the laser pulse occurs in the early part of the current pulse, it is the electron density radial profile up to the end of laser action that influences the radial laser intensity. To further investigate this effect it is necessary to resolve the period of increasing electron density which proved impossible with the equipment available to us at the time.

The energy required to ionise 6.8 x $10^{14}$ $cm^{-3}$ copper atoms in the ground state is 835 $\mu J/cm^{-3}$. The only other significant population measured at this time resides in the metastable levels. These populations peak at 1 x $10^{14}$ $cm^{-3}$ in the green lower laser level and 5 x $10^{13}$ $cm^{-3}$ for the yellow lower laser level. The energy required to produce these populations is approximately 50 $\mu J/cm^{-3}$. The total energy transferred to excited states in the active volume of the HyBrID laser is the sum of these, i.e. 885 $\mu J/cm^{-3}$, this agrees well with the amount of energy deposited in the HyBrID calculated above. In the CVL only 1.0 x $10^{14}$ $cm^{-3}$ electrons are produced each pulse. The energy required for this is approximately 125 $\mu J/ cm^{-3}$. We calculate a value of approximately 300 $\mu J/cm^{-3}$ deposited. If we accept the explanation that the plasma may be divided into hot and cool regions and make adjustments to allow for a proportion (in the region of 30% on axis) of the electrons resulting from neon ion production then the energy required jumps to approximately 200 $\mu J/cm^{-3}$. There is still a significant discrepancy between the two values. A possible explanation is that the large remanent electron density from the previous pulse results in a period of 'ohmic' conduction at the start of the pulse during which no ions are produced but energy is deposited in the plasma and stored in the tube inductance. Energy stored in the tube inductance will be deposited in the plasma later in the

pulse and will mostly contribute to gas heating and not ionisation. This explanation is consistent with the earlier discussion of current and voltage waveforms.

To assess whether the high peak electron density can be attributed to tube bore differences it is instructive to examine the specific input powers per pulse of other HyBrID laser of different bore, constructed in the JF Allen Research Laboratories. HyBrID lasers of bore 13 mm (Livingstone et al. 1991), 45 mm (Jones et al. 1992) and 60 mm (Jones et al. 1994) as well as the 25 mm one currently under investigation have been constructed, their characteristics are detailed in Table 1 below. All values are calculated for maximum efficiency operation.

| Tube Bore | Volume, V | Input Energy per Pulse | Specific Input Energy per Pulse |
|---|---|---|---|
| 13 mm | 40 $cm^{-3}$ | 24.4 μJ | 610 $\mu J/cm^{-3}$ |
| 25 mm | 393 $cm^{-3}$ | 97.2 μJ | 250 $\mu J/cm^{-3}$ |
| 45 mm | 1908 $cm^{-3}$ | 152.3 μJ | 80 $\mu J/cm^{-3}$ |
| 60 mm | 5654 $cm^{-3}$ | 294.4 μJ | 52 $\mu J/cm^{-3}$ |

Table 4.1

From Table 4.1 we can see that the specific input power per pulse decreases with increasing tube bore and the 45 mm bore tube has a specific input energy per pulse which is a factor of three less than the 25 mm bore tube. If electron density scales linearly with specific input energy per pulse (and it is common in electrical discharges for > 90% of the input energy to be transferred into ionisation) then this accounts for a large fraction of the difference between the CVL and HyBrID measurements. The remaining difference is only a factor of two and this is easily accounted for by the

discharge constriction observed in the HyBrID laser system, but not in the CVL, as discussed above.

The results of Carman's modelling work on an 18 mm bore CVL (Carman et al. 1994) give an peak axial electron density of 3.5 x $10^{14}$ $cm^{-3}$ which is less than a factor of two less than in the HyBrID laser. It is interesting to note that this peak electron density is dependent on PRF and the peak electron density may be increased to a level comparable with that seen in the HyBrID laser by decreasing the PRF (Carman 1995). This shows that the peak electron density is dependent on the pre-pulse electron density in the CVL. The increased peak electron density may be due to increased breakdown voltage which results in increased energy storage on the peaking capacitor and enables the external circuit to maintain the electron energy at a higher level later in the pulse and so ionise more copper. Also the fraction of the stored energy deposited in the tube as gas heating prior to the rise in electron temperature will be reduced due to the lower pre-pulse electron density.

### 4.3.5 THE PERIOD OF FAST FALLING ELECTRON DENSITY

The electron density in the HyBrID laser is seen to be falling from the first post-pulse data points. It decreases rapidly for a period of about 20 μs after which it has recovered to about 3% of its peak value. It then decreases at a slower rate until the onset of the next excitation pulse. It is this period of fast decay which now concerns us.

There are several methods available for the removal of electrons from the plasma of the HyBrID laser. These processes will be considered in two groups;

1. three body recombination with positive ions, and

2. other processes such as two body electron attachment to electronegative species and dissociative attachment to molecular species.

### 4.3.5(i) THREE BODY RECOMBINATION

Three body recombination is very sensitive to electron temperature. In his computer model of the CVL system Carman models the rate as:

$$\frac{dn_e}{dt} = -4.0\times10^{-19} n_e^2 N_i T_e^{-5} \qquad [4.1]$$

where $n_e$ is the electron density and $N_i$ is the ion density. This $T_e^{-5}$ dependence prevents any significant recombination by this process until the electron temperature has fallen below 1eV. Once three body recombination has started it will act to raise the temperature of the electron gas as the second electron must carry away additional momentum and hence will have increased energy. In addition the neutral atom formed in the recombination will be in a high lying excited state, relaxation towards the ground state will be mostly by super-elastic collisions which will cause further heating of the electrons. The combination of these two effects is known as recombination heating. It has been shown in models of both the strontium recombination laser (Carman 1990 & 1991) and the CVL (Carman et al. 1994) that recombination heating is the dominant mechanism maintaining the electron temperature above the gas temperature at all times during the inter-pulse period. Strong support is given to this prediction by the good agreement found between the model's predicted values and measured values of the lower laser level population densities. Models such as that of Kushner and Warner which predicted that the electron temperature should fall to the gas temperature after 50 μs, were not able to correctly predict the $^2D_{5/2}$ & $^2D_{3/2}$ populations.

### 4.3.5(ii) ELECTRON COOLING

From the fast initial decay we can therefore conclude that if three body recombination is the dominant effect there must be a mechanism for strongly cooling the electrons. This process must not only cool the electrons initially to allow fast three body recombination, but must also maintain the electron temperature at a low level counteracting the strong recombination heating. This implies that the cooling effect must be relatively persistent, at least 15μs, and the species involved must be similarly long lived.

In the high temperature CVL, models have shown that the dominant mechanism of cooling the electrons in the early afterglow is inelastic collisions with copper atoms and ions. This effect dominates because the copper has low lying energy levels, much lower than those in neon, the other main species present. In the HyBrID laser, results detailed in Chapter 6.1. show a copper density of approximately twice that found in Hogan's CVL. Such a high density of copper would certainly strongly cool the electrons. However, once the electron energy has dropped below a couple of electron volts this process can no longer continue unless there is significant population in the higher lying levels. In the HyBrID laser this is not the case as there is negligible upper state population density after 1μs. Inelastic collisions with copper atoms and ions could therefore be an important process cooling the electrons in the early afterglow (up to 1μs) but only when the electron temperature is quite high. Therefore inelastic collisions cannot cause the strong cooling below a few eV seen in the afterglow at times after 1 μs. The dominant cooling mechanism must therefore be elastic collisions.

There are several possible elastic collision partners in the HyBrID system; hydrogen, copper, neon and bromine are all present in appreciable

densities. All of these species and possibly several types of molecules are expected to exist in the discharge at all time points during the interpulse period.

Hydrogen has the highest collision cross-section for momentum transfer, due to its low mass and so may be expected to have an important role. Neon is the next lightest atom present. As neon is present in the CVL system, if elastic neon collisions were the dominant electron cooling mechanism at work in the HyBrID laser, we would expect to see similarly strong electron cooling and fast three body recombination in the CVL. This is clearly not the case as the electron removal rates in the two lasers are quite different. As all the other species present in the HyBrID system are heavier than neon we conclude that hydrogen will be the dominant source of electron cooling by elastic collisions.

Studies investigating the effects of hydrogen on CVLs (Withford et al. 1994) have shown increased breakdown voltage and higher PRF operation. A possibly explanation for these characteristics is that they result from a decreased pre-pulse electron density. This is supported by the fact that models of the CVL predict that higher PRF operation would be possible with a reduced pre-pulse electron density due to decreased skin effects and lower pre-pulse metastable density (metastable decay rate in the mid to late afterglow is slowed due to an electron temperature buoyed by recombination heating in the CVL without hydrogen).

If the addition of hydrogen increases electron cooling then the electron temperature will be able to fall past the previous limit imposed by recombination heating, until it reaches the gas temperature, at which point it can fall no further. The benefit available from increased electron cooling in the CVL in this case is limited by the significantly higher gas temperature at

which the electron temperature stabilises. The electron removal rate in the CVL will never reach that seen in the HyBrID laser for this reason, and there will be a point where increased hydrogen and therefore increased cooling of the electrons has no beneficial effect on the pre-pulse electron density as three body recombination at a rate limited by the gas temperature occurs from early in the afterglow. In practice this limit may not be reached due to other deleterious effects due to hydrogen and there will be an optimum concentration of hydrogen for a given CVL operating under particular conditions. One kinetic effect in the CVL caused by addition of hydrogen which may be detrimental to laser operation is increased inelastic losses as energy is stored in vibrational and rotational states. Hydrogen may also slow the rate of rise of the electron temperature and so increase pumping of the lower laser levels from the ground state. For these and other reasons the optimum amount of hydrogen added to the CVL is less than that in the cooler HyBrID system, typically 0.5-3% $H_2$ for maximum power gain in a CVL, compared to 7-8% HBr in the HyBrID.

### 4.3.5(iii) ELECTRON TEMPERATURE

If we assume that electron removal is effected entirely by three body recombination, (a large assumption but useful for illustrative calculations) then, using Equation [4.1] it is possible to calculate the electron temperature as a function of time from the electron density measurements. The results are shown in Figure 4.4. These results have been calculated for the period of fast falling electron density only.

The peak electron temperature calculated is approximately 6500K. This is an appreciable fraction of an electron volt (1eV=11500K) and is considerably higher than the corresponding value calculated for the CVL,

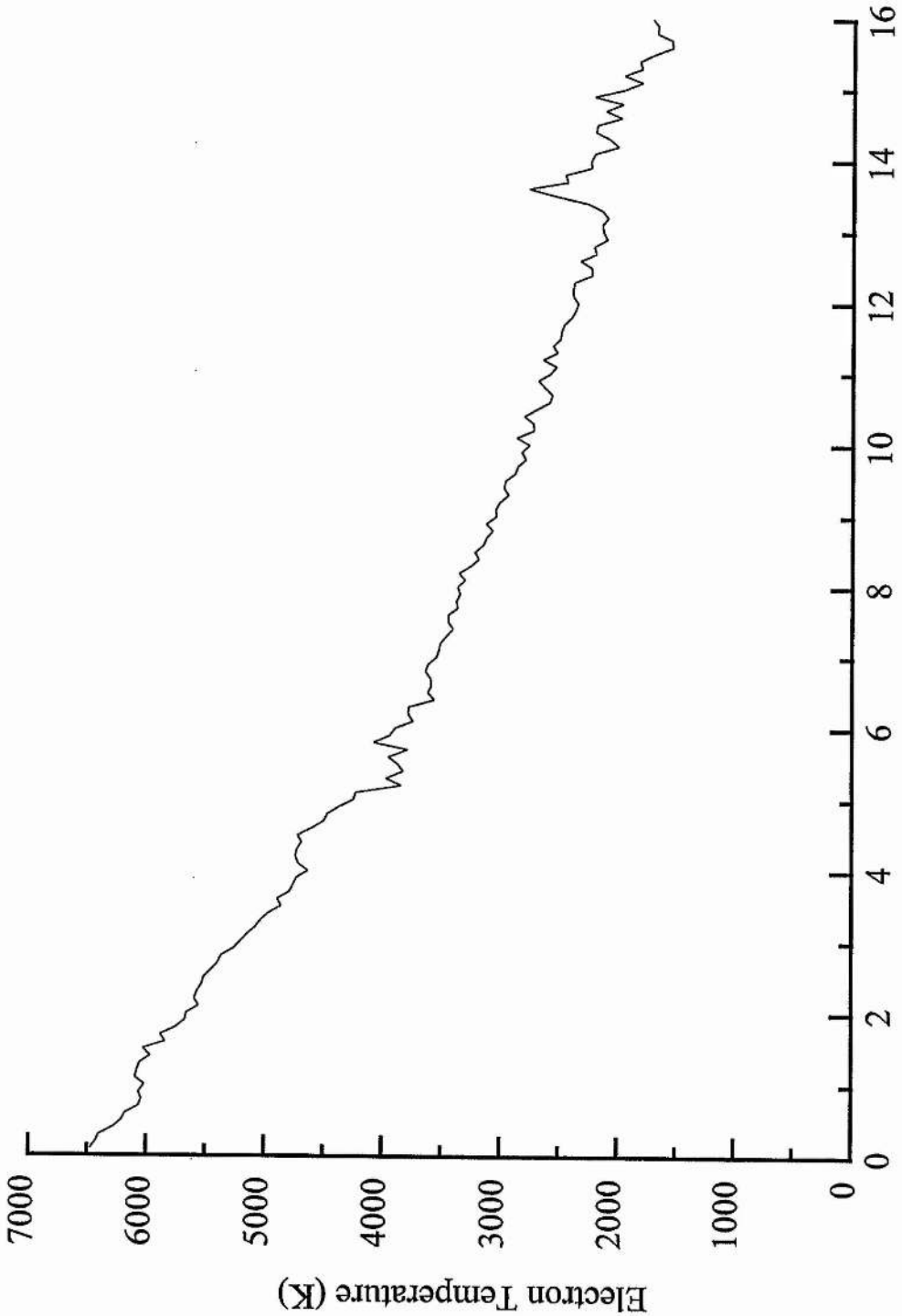


Figure 4.4 Calculated electron temperature

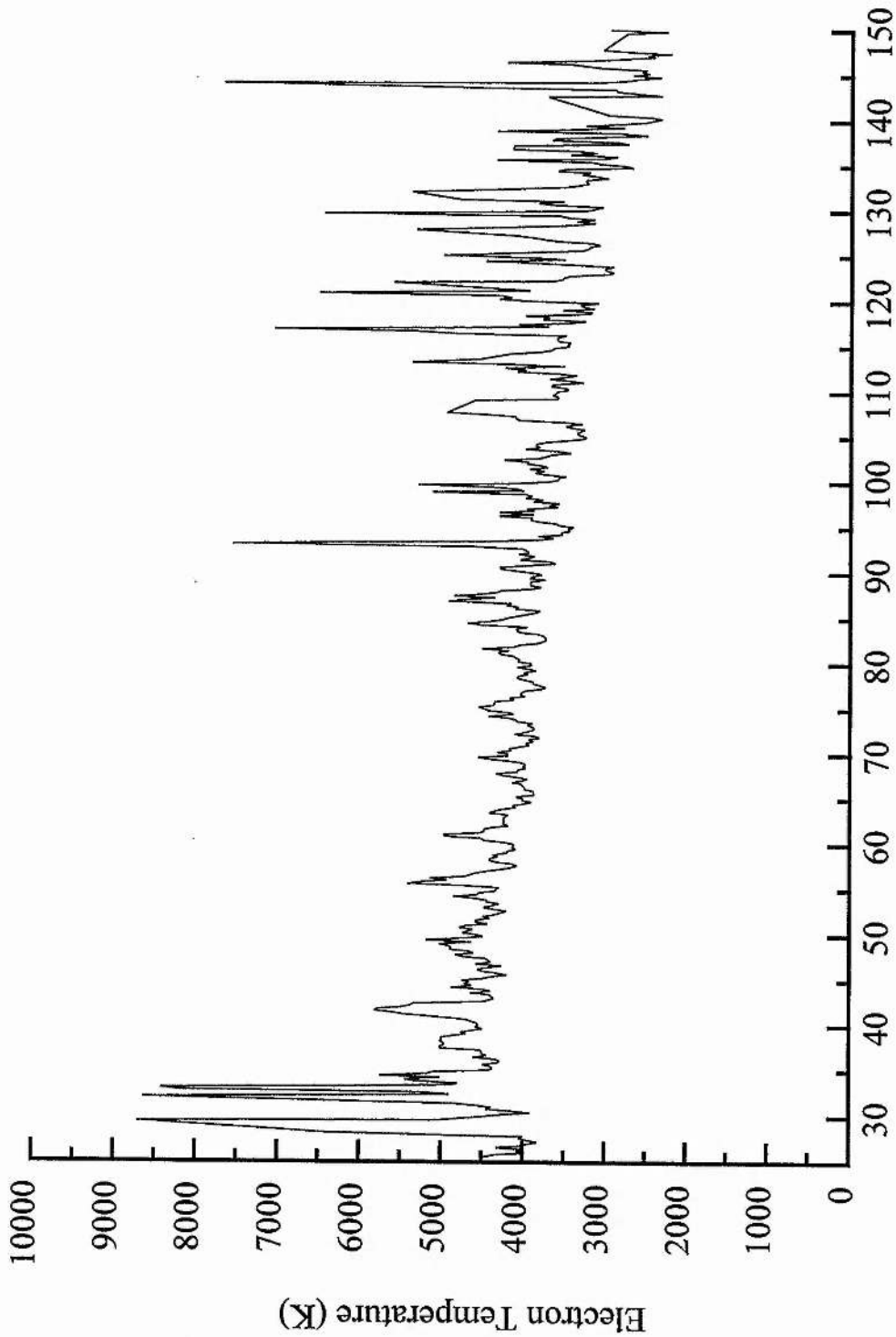


Figure 4.5 Calculated electron temperature (CVL)

Figure 4.5, which gives an electron temperature at the start of recombination of approximately 4500K. It should be noted that these calculations are performed on the data from the point where recombination in the main body of the plasma ( i.e. not the cool end zones ) starts. This time is determined for the CVL using the assumption that the initial period of electron density decay results entirely from recombination taking place in the cool end zones. The starting point for recombination in the main body of the plasma is determined as the time when the second period of decreasing electron density begins. The starting time for the HyBrID laser is the first data point as the electron density decays with a single time constant. The starting point for Figures 4.4 & 4.5 therefore differ by approximately 25μs, the CVL trace, Figure 4.5, beginning later.

From these calculations we can see that fast three body recombination in the HyBrID would occur even at electron temperatures usually considered to be rather too high to allow fast recombination. This is due to the very high electron and ion densities, the recombination rate being dependent on the square of the electron density and linearly dependent on the ion density. The electron temperature decreases rapidly, this enables the recombination rate to be sustained as the electron and ion densities decrease until eventually the electron temperature is stabilised when it reaches the gas temperature. The electron and ion densities are then so low that further recombination is very slow. At this point the calculated value of the electron temperature (~1700K ) shows good agreement with the estimated axial gas temperature of 1900K. This is a possible explanation for the change in decay rate as the rate of electron removal due to three body recombination should now have no electron temperature dependence. (The gas temperature will be constant to a good approximation as the energy deposited per pulse is small when the

large thermal mass of the active medium is considered.) Calculating a curve fit for the three body recombination rate from the electron density with an electron temperature fixed at the gas temperature yields little useful information as the electron density is very close to the noise level. In this regime the error in the determination of the absolute value of the electron density is a significant fraction of the measurement, (as discussed Chapter 4.3.2) and calculations based on the absolute value of these measurements would be unreliable. It is possible to calculate order of magnitude figures at particular times. Taking a time after the change in decay rate and calculating the decay rate for an electron temperature fixed at the gas temperature an electron removal rate of $2x10^{11}cm^{-3}\mu s^{-1}$ at time 17 μs is calculated. Considering the errors in absolute value of the electron density, this is in good agreement with the measured decay rate of $3x10^{11}cm^{3}\mu s^{-1}$.

### 4.3.5(iv) ELECTRON ATTACHMENT

As mentioned previously, in the HyBrID laser system three body recombination is not the only process by which free electrons may be removed from the discharge. Due to the presence of bromine and hydrogen in the discharge region it is possible for free electrons to be removed by attachment to one or other of these species, either by direct attachment to the free atom, or dissociative attachment to a molecular species.

In considering the effects of hydrogen and bromine it is important to realise that they may not be totally dissociated by the discharge and a significant molecular concentration may be present. Early indications from attempts at modelling the effect of hydrogen in a CVL show only 20% dissociation of hydrogen (Carman 1995). In this case there will be a significant concentration of vibrationally excited hydrogen molecules.

Dissociative electron attachment will therefore be an important process to investigate as it may have a large effect on the discharge kinetics.

In the HyBrID laser, matters are further complicated by the presence of bromine which will allow the formation of HBr as well as molecular hydrogen. The HyBrID laser however operates at much higher PRFs than the CVL, and with twice the input power density per pulse so we would expect a higher proportion of the molecules to be dissociated. The degree of dissociation and recombination of these molecular species will be important in any modelling of the HyBrID laser, as dissociative attachment may be an important process. In other pulsed discharges such as those in XeCl excimer lasers, dissociative attachment is seen to be considerable, with the vibrational state of the molecule strongly influencing the attachment rate (Luck et al. 1994). Unfortunately the models for these systems do not consider the interpulse recombination period as the systems generally operate at low PRF. There is therefore little information to be gleaned from these models about electron attachment rates for low electron energies.

The CuBr laser is an interesting system to consider with regard to electron attachment. In investigations of the effect of hydrogen addition on CuBr lasers (Astadjov et al. 1985, 1988) the current and voltage waveforms were considered. As discussed in chapter vil the waveforms indicate that in a CuBr laser system with a pure neon buffer gas, there is an appreciable pre-pulse electron density. On addition of 0.3 torr of hydrogen the waveforms indicate that the pre-pulse electron density falls significantly. This is strong evidence to suggest that electron attachment to bromine is not an important process in reducing the pre-pulse electron density. This may be because $Br_2$ is not a particularly stable molecule, whereas the more stable HBr molecule may create negative ions by dissociative attachment.

Simple modelling of electron attachment is not possible as we must consider the proportion of molecules dissociated, the vibrational distribution of the molecules remaining, the recombination rate of the free atoms and the attachment rates for all the vibrational levels and free atoms. This is best left to a dedicated study as it is too complicated to examine fully in this discussion.

[Some basic information about electron attachment may be derived from consideration of the radial electron density distribution; this will be dealt with later in this chapter.]

## 4.6 SUMMARY

We have measured the temporal evolution of the electron density on axis in the HyBrID laser. The pre-pulse electron density is very low and this gives rise to many of the desirable characteristics associated with HyBrID lasers such as high pre-pulse impedance and efficient energy transfer from excitation circuit to active volume. The low pre-pulse electron density may be attributed partly to fast three body recombination as a result of strong electron cooling by hydrogen. Electron temperatures have been calculated from the data which support this argument. We were unable to model possible effects due to electron attachment processes because of the complexity and the high number of variables involved in these reactions. The peak electron density in the HyBrID laser is at least five times that found in a CVL laser previously investigated using the same experimental equipment. This difference may be mostly accounted for by the geometric differences between the two laser heads and the slight discharge constriction typically seen in the HyBrID system.

## 4.4 RADIAL DEPENDENCE OF ELECTRON DENSITY

### 4.4.1 GENERAL REMARKS

The radial profile of the electron density is shown in Figures 4.6 & 4.7. These graphs, and all other radially resolved measurements presented in this thesis represent data collected in a single scan from the centre to the edge of the tube. Assuming left right symmetry about the tube axis, this data has been plotted to represent the results across the diameter of the tube. For comparison the corresponding graphs for the CVL are shown. Several fundamental differences in the radial structures are evident. The HyBrID laser has a much more constricted beam, not only is the electron density much more strongly peaked on axis, it also fails to fill the bore of the laser. This is in contrast to the situation in the CVL where the discharge diameter is nearly equal to the tube bore and there is a significant electron density close to the tube wall.

The transverse profile of the pre-pulse electron density is difficult to assess as the electron density is very low at all radial positions. The sensitivity of the equipment and the error in determination of the zero is not sufficient for us to assign anything other than an upper limit to the pre-pulse electron density.

The peak electron density in the HyBrID is strongly dependant on radial position, the majority of electrons being produced inside the central 12 mm. In fact the electron density is only 3% of the peak value at 8.75 mm from the axis, this is only 70% of the distance to the tube wall. The recombination rate in the first 20 μs is not constant across the tube diameter. After 20 μs the electron density is very small and changes relatively slowly for all radial positions.

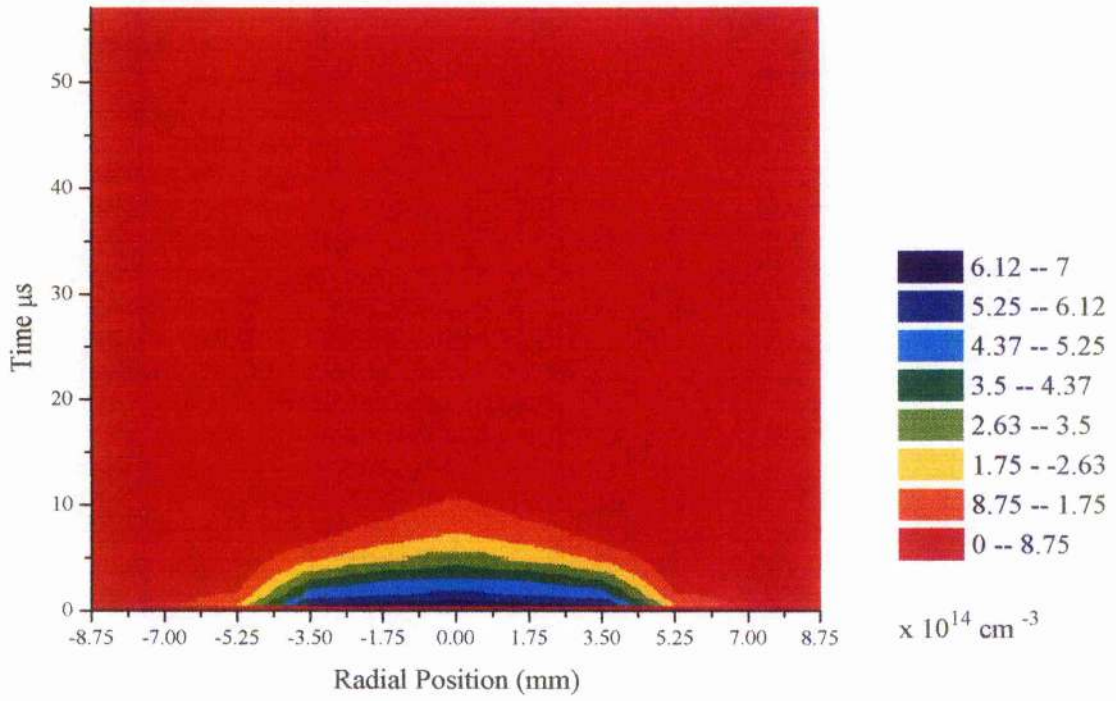


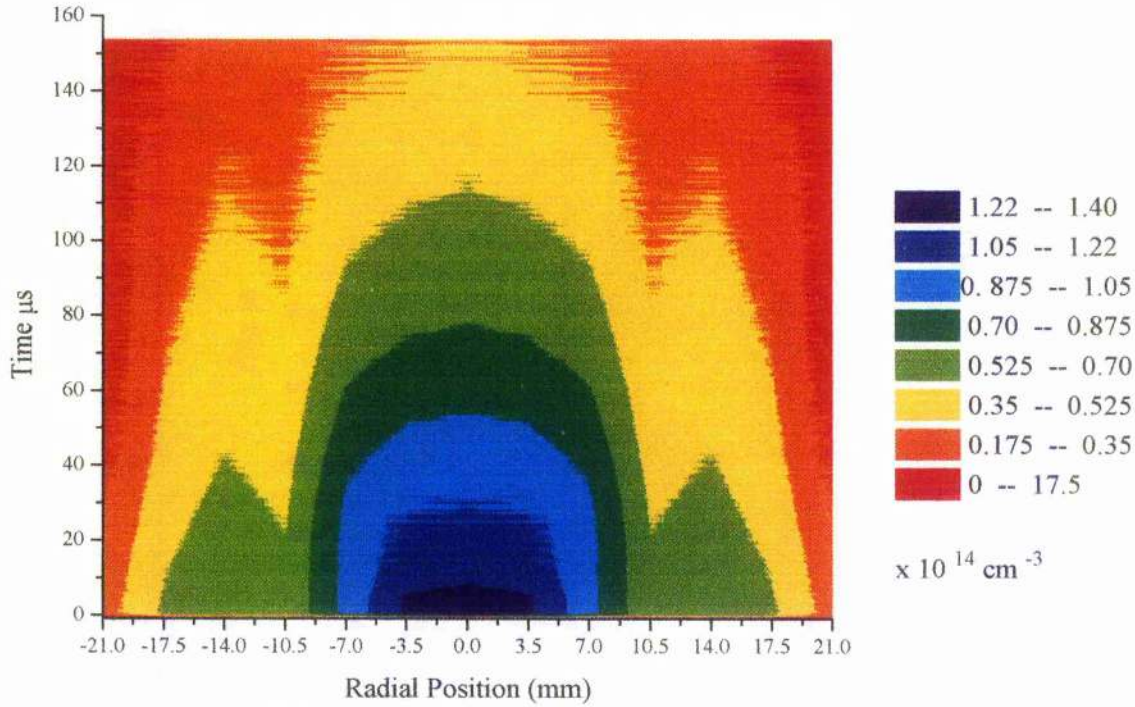


Figure 4.6 Radial dependance of electron density
in HyBrID laser (top) and CVL (bottom)

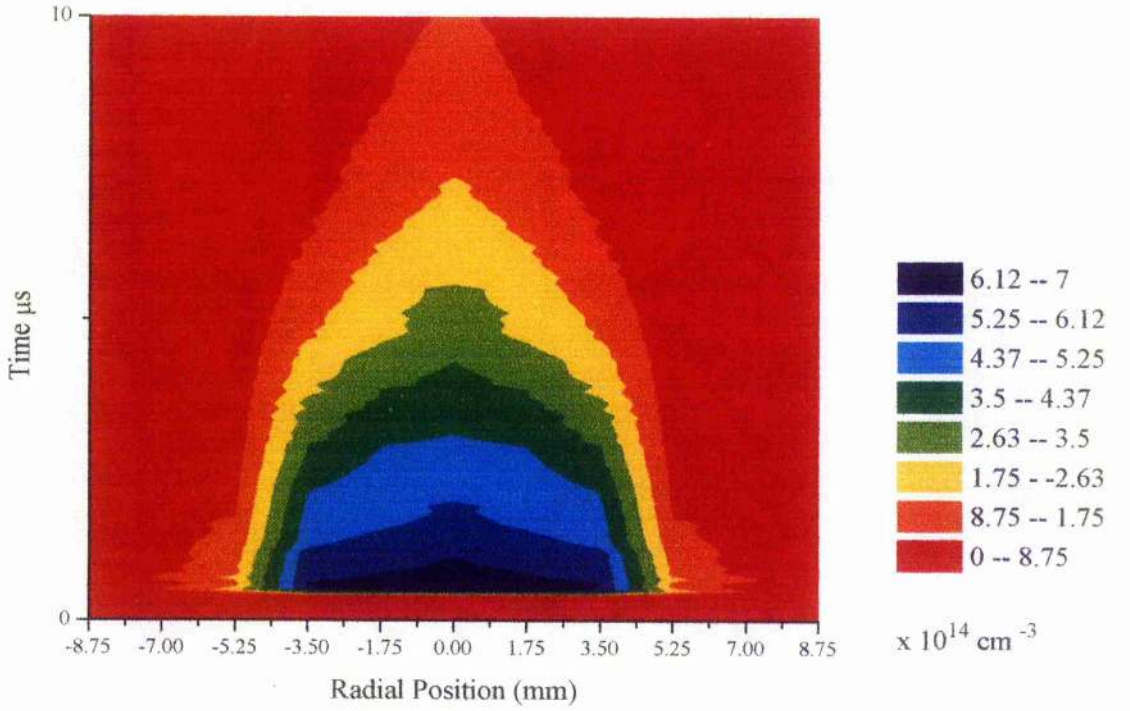


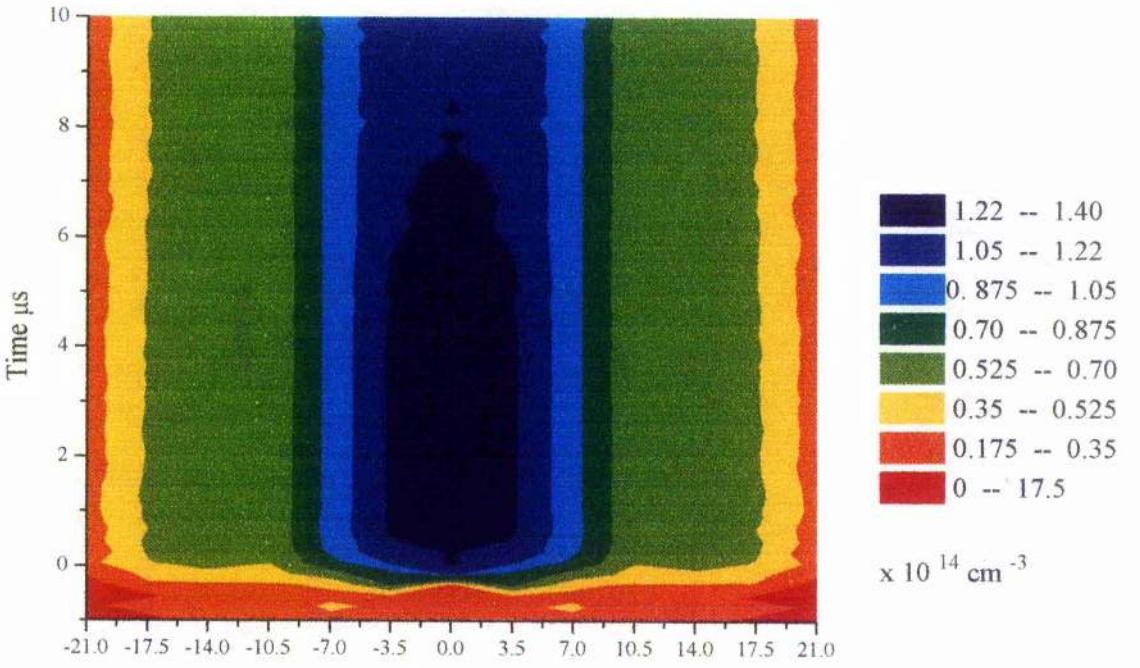


Figure 4.7 Radial dependance of electron density
in HyBrID laser (top) and CVL (bottom) first 10µs

### 4.4.2 PRE-PULSE ELECTRON DENSITY

The pre-pulse electron density is close to the noise level of the equipment for all radial positions, we can however set an upper limit to the electron density. A reasonable estimate of the minimum observable change in intensity is approximately 5%. This corresponds to a minimum observable fringe shift of approximately 0.05, or a change in electron density of $\sim 1.3*10^{13}cm^{-3}$, about 2% of the peak electron density measured on axis. At all radial positions the electron density has reached this level by 20 μs after the laser pulse. In Chapter 4.3.5(iii) it was suggested that on-axis at this time the electron temperature had fallen to the gas temperature. An order of magnitude electron removal rate for three body recombination at an electron temperature equal to the gas temperature was then calculated as $\sim 2x10^{11}cm^{-3}\mu s^{-1}$. The gas temperature is highest on axis, therefore electron removal will be slowest on axis. Electron removal will not continue at this rate throughout the remainder of the inter-pulse period as the electron and ion densities will be falling, but as a first estimate we may say that approximately half the electrons remaining after 20 μs will be removed by the end of the inter-pulse period leaving a density of approximately $6x10^{12}cm^{-3}$ pre-pulse.

At this point it is interesting to consider the radial electron temperature profile in the afterglow. It has been suggested ( Carman 1994; Kushner 1981) that, in the CVL, the electron to electron coupling is much stronger than the electron to atom coupling due to the difference in masses and that this leads to a radial electron temperature profile which is much flatter than the radial gas temperature profile. The results of Hogan (Hogan 1993) contradict this as he calculates a centrally peaked electron temperature from his electron density measurements. In the HyBrID system we have already established that the electron density after 20 μs is much lower than in the CVL. The

system is complicated by the presence of additional species such as hydrogen which may be expected to alter both the radial gas temperature due to its high thermal conductivity and the radial electron temperature as its high collision cross section for momentum transfer will increase the electron to gas energy transfer. This may lead to a substantially different radial electron temperature dependence.

## 4.3 PEAK ELECTRON DENSITY

The radial dependence of the peak electron density is shown in figure 4.8. The density is almost flat across the central 7 mm, and then drops sharply, falling to the noise level at 8.75 mm from axis. This is particularly interesting when we compare this to the radial light output dependence, Figure 4.9. where we see that a high percentage of the light is generated in the central 16 mm section of the tube. From this evidence, the centrally peaked light output intensity of the HyBrID laser would seem to be largely due to the strong radial dependence of the electron density. There is, however, significant light output at radial positions close to the edge of the electron density distribution and the light output radial dependence is seen to be generally less strong than that of the electron density. This may be due to broadening of the laser profile due to highly divergent output reaching the detector. Also calculations of the laser head inductance , Chapter 2.3.1, show that the discharge constricts during the excitation pulse. The central peaking of the electron density may therefore not be as pronounced during the laser pulse as it is 400 ns after the onset of lasing.

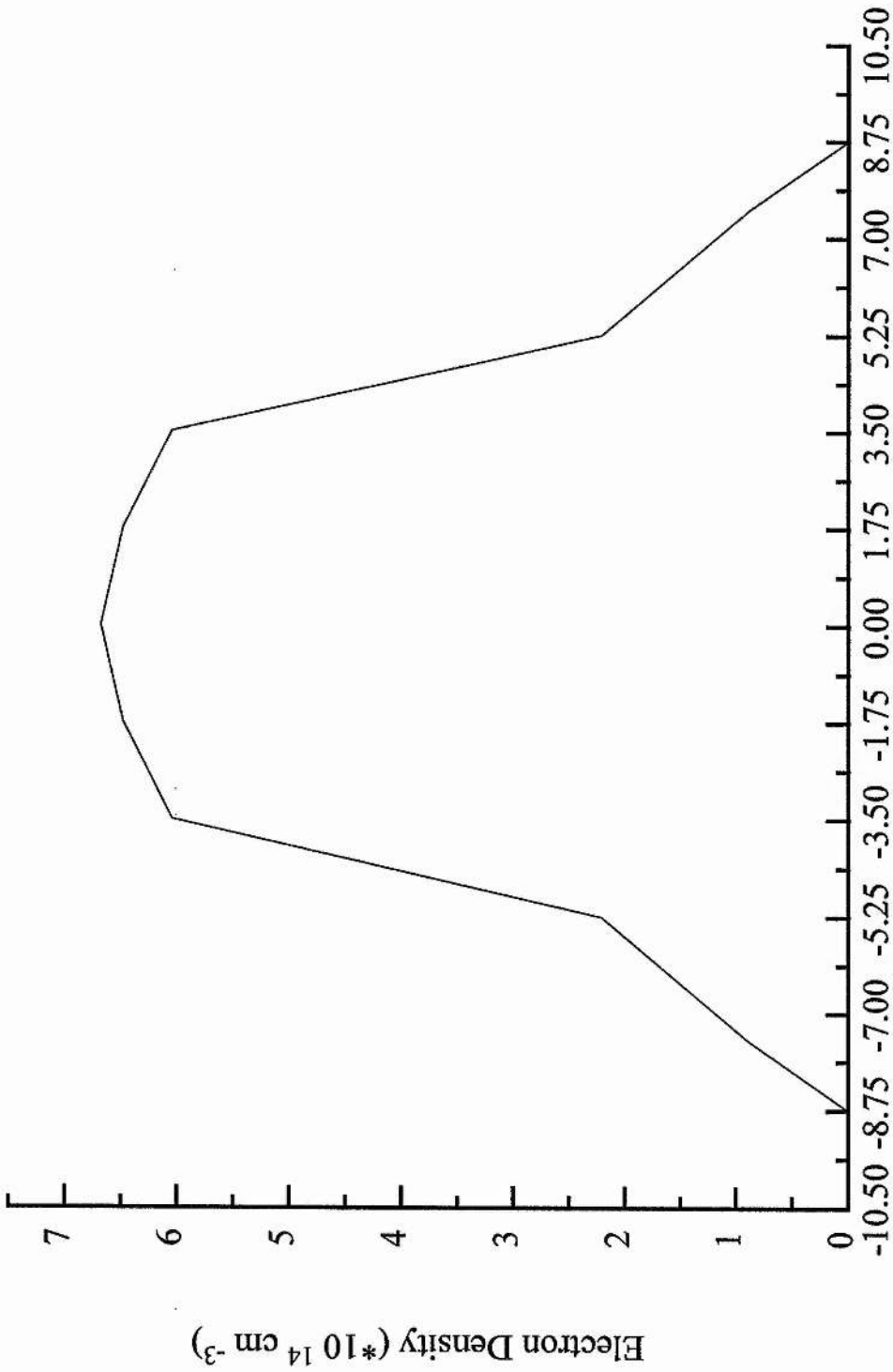


Figure 4.8 Peak electron density as a function of radial position

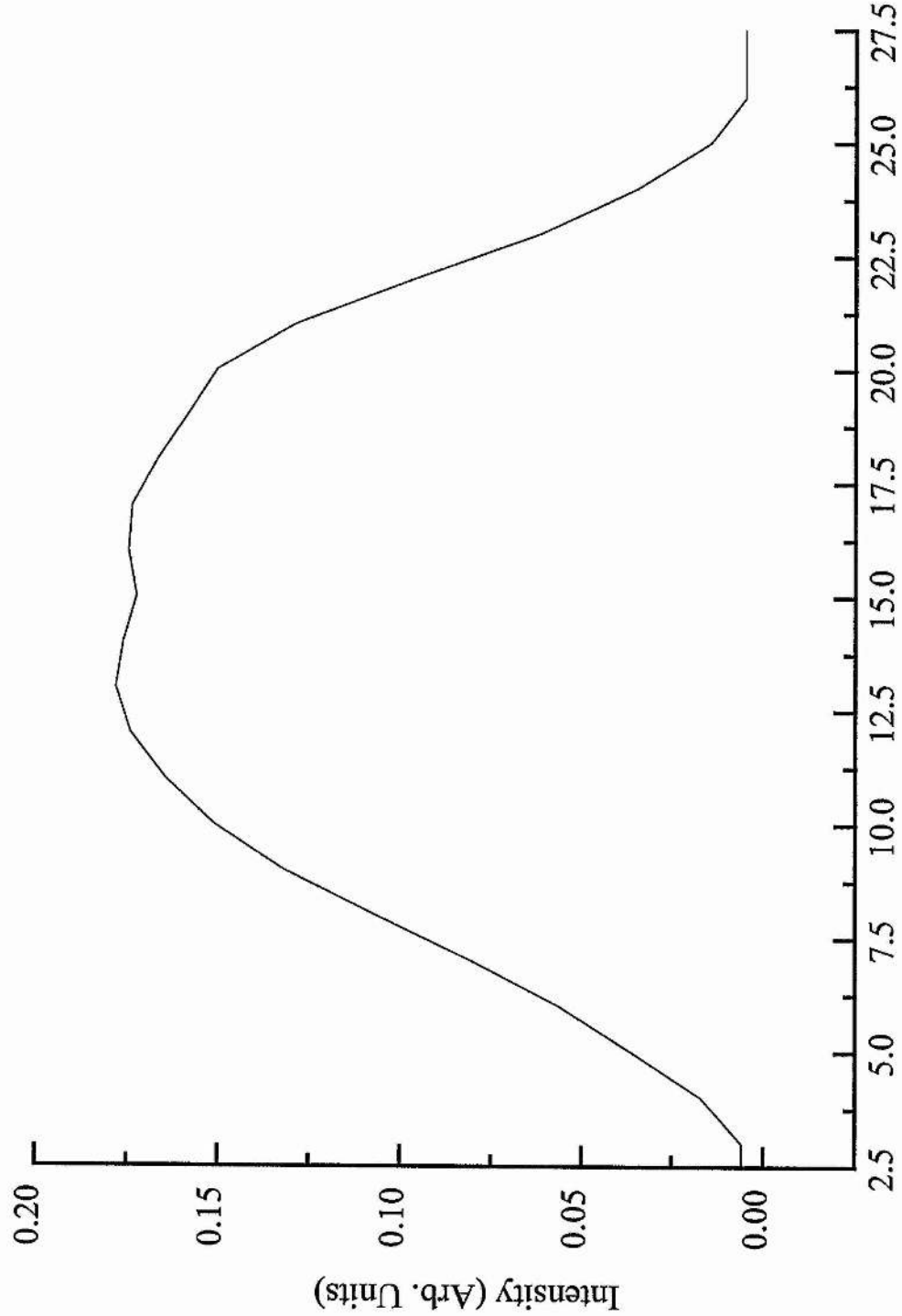


Figure 4.9 Laser pulse radial profile

### 4.4.4 ELECTRON DENSITY DECAY

The radial dependence of the decay in electron density can be seen from Figures 4.6, 4.7 & 4.10. The rate of electron removal is slowest on axis and increases with distance off axis. This is consistent with three body recombination limited by an electron temperature which is highest on axis and falls rapidly to the gas temperature. Using Equation [4.1] it is possible to calculate the electron temperature for the first two radial positions as well as on axis (the electron density at radial positions beyond 5 mm is too low for meaningful calculations to be performed) The results are shown in Figure 4.11. The calculated electron temperature peaks on axis. Off axis, the electron temperature starts from a lower value and falls to the gas temperature faster. The final electron temperature has reasonable agreement with the calculated gas temperature.

In the CVL the electron temperature has an on axis peak during the excitation pulse because the dominant cooling mechanism is inelastic collisions with Cu atoms and the Cu atom density is highest at the tube walls. The radial dependence of the electron temperature reduces after the excitation pulse and the radial profile becomes essentially flat by 1 μs. This change occurs because inelastic collisions can no longer dominate because the electron temperature is too low. Elastic collisions must now dominate and the momentum transfer between electrons will be greater than that between electrons and atoms since the former will have a zero mass difference between collision partners. The radial electron temperature profile will therefore become flatter than the gas temperature profile. In larger bore devices it is possible for the electron density to fall such that the electron to electron coupling is no longer dominant and the electron temperature profile

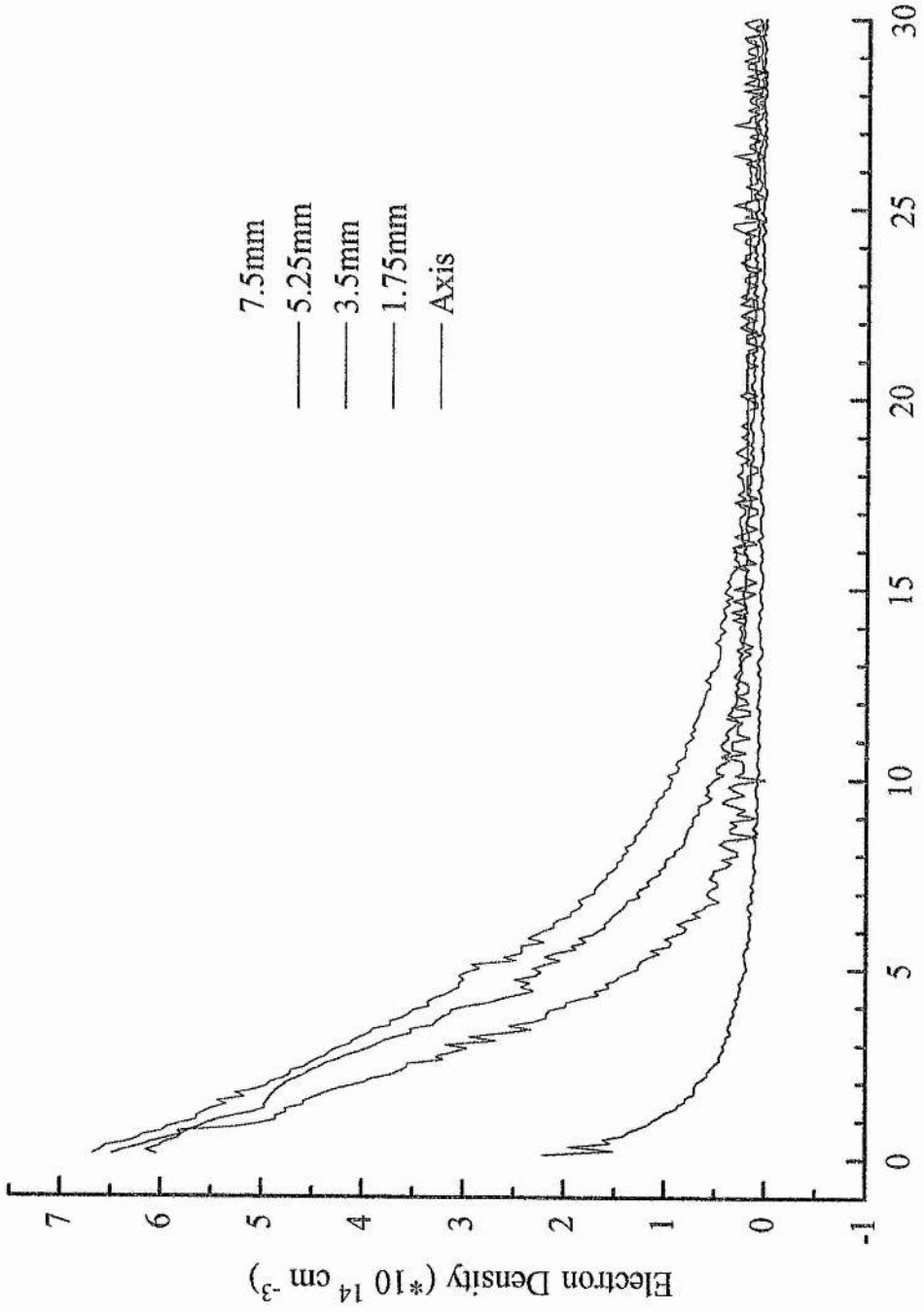


Figure 4.10 Electron density as a function of time for various radial positions

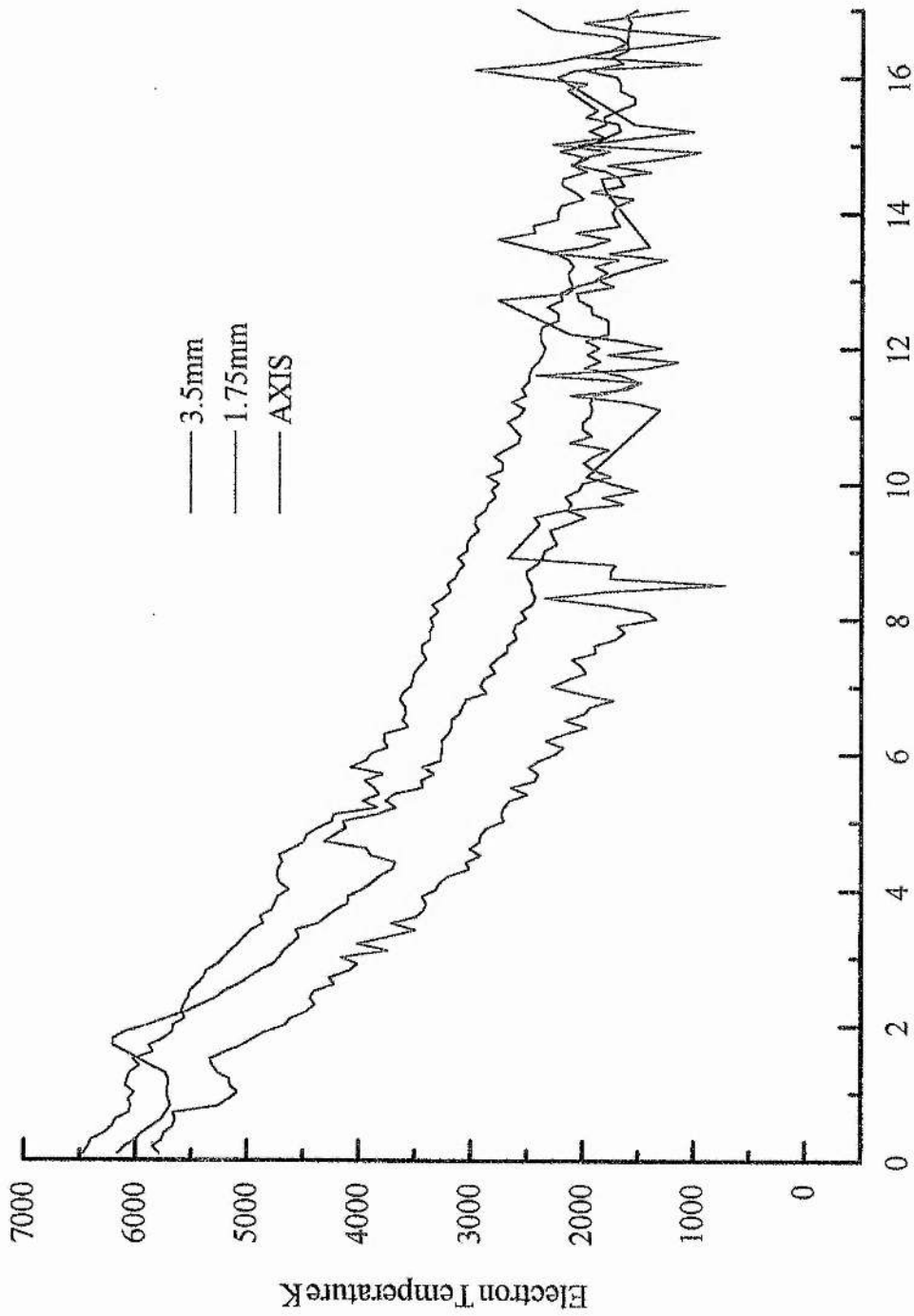


Figure 4.11 Calculated electron temperature as a function of time for various radial positions

tends to that of the gas. This electron temperature behaviour is observed in the late afterglow in larger bore CVLs where the ratios of the ground state to metastable densities indicate a centrally peaked electron temperature.

In the HyBrID system we expect there to be a strong radial dependence of electron temperature during the pulse due to the discharge constriction and the centrally dipped copper concentration. In the late afterglow the electron temperature will be equal to the gas temperature and will therefore have a similar radial dependence.

The degree of momentum coupling between electrons will be directly proportional to the number of electrons and inversely proportional to the electron-atom collision frequency. In the early afterglow the electron density is high and momentum coupling between electrons will be very strong leading to a flat radial electron temperature profile. In the high temperature CVL this effect leads to the flat electron temperature radial profile calculated for times after 1 μs (Carman 1994). In the HyBrID laser the situation is complicated by the presence of hydrogen which will increase the momentum transfer from the electrons to the gas atoms and will strongly cool the electrons. However the electron density is initially very high, leading to very strong inter-electron momentum transfer.

Momentum coupling between electrons and atoms will be dependent on the local gas and electron temperatures and will therefore act to produce a radial electron temperature profile similar to the gas temperature profile. There are therefore two processes operating in opposition during the early afterglow, inter-electron coupling will tend to produce a flat radial electron temperature while electron cooling by hydrogen will produce a radial profile similar to the gas temperature profile.

In the earlier discussion on the temporal behaviour of the electron density on axis Chapter 4.3.5(ii) it was suggested that hydrogen strongly influenced the electron temperature, cooling the electrons by increasing momentum transfer from the electrons to the gas atoms. This process was the most important factor in determining the electron density temporal evolution. Electron cooling by hydrogen must be a strong effect as there will be considerable electron heating due to recombination yet the electron temperature (Figure 4.11) falls monotonically. This characteristic indicates that the electron temperature is controlled to a large degree by hydrogen. As the hydrogen distribution is closely linked to the gas temperature this theory predicts that the radial electron density profile is always peaked on axis, but is flattened to some degree during periods where a high electron density exists and electron to electron momentum transfer is high.

Additional credence is given to this explanation by the radial dependence of the trend in electron temperature. The difference between the electron temperature on and off axis is seen to increase with time and increasing distance from the axis, during the period of fast electron removal. This indicates that the electron temperature radial profile is not tending towards a flat distribution, indeed during its fall to the gas temperature the radial dependence is becoming stronger. This is as we would expect if the effect of electron cooling due to hydrogen and the effect of electron to electron momentum transfer were competing and cooling due to hydrogen was becoming increasingly dominant as the electron density fell.

It is difficult to assess the expected radial dependence of electron attachment. As mentioned in Chapter 4.3.5(iv) above, electrons may attach directly to hydrogen or bromine atoms, and via dissociative attachment of the molecules $H_2$ and HBr.

Considering atomic interactions first, dissociation of hydrogen will be greatest on axis and hence the hydrogen and bromine atomic concentrations should be greatest on axis. However the gas temperature is peaked on axis and if a significant proportion of the hydrogen or bromine remains in the atomic state at the start of the subsequent excitation pulse, then the atomic hydrogen and bromine concentrations may tend towards the gas density profile. Preliminary model calculations have shown that only approximately 20% of the hydrogen is dissociated in a CVL with 2% added hydrogen (Carman 1995). The HyBrID laser operates at higher PRF and hence there will be less time for recombination to the molecular state and the total percentage dissociated may be greater. Electron attachment will also be electron temperature dependent. It is unknown which of the aforementioned effects will dominate. The radial dependence of attachment to atoms is therefore unknown.

The electron attachment rate to a molecule will depend on the molecule's vibrational state which will be changing during the afterglow period. The vibrational state of the molecules will be radially dependant due to the axially concentrated excitation. Whether this dependence is axially peaked or dipped will be determined by the proportion dissociated and the amount of molecular reassociation in the afterglow. The radial dependence of attachment to molecules is therefore unknown. An electron may alter a molecules vibrational state with a single collisions, whereas many, even hundreds of collisions may be required to alter the rotational state of the molecule. This further complicates the rate at which these interactions proceed.

It should be noted at this point that an investigation (Astadjov et al. 1985, 1988) of the effects of addition of hydrogen to CuBr lasers showed

that bromine is unlikely to be important in determining the pre-pulse electron density, see Chapter 4.3.5(iv).

If we assume that the electron temperature is radially flat (a view not held by the author) then we must conclude that three body recombination proceeds at a uniform rate across the bore of the tube. The radial position at which the slowest electron density decay is observed therefore allows us to calculate an upper bound for the three body recombination rate at all radial positions. This in turn gives us the minimum electron temperature. At any radial position where the electron density decay is faster there must be an additional process acting in parallel with three body recombination to remove the additional population. The most likely candidate for this process is electron attachment. The electron density decays most slowly on axis. Under the above assumption we would conclude that electron attachment is fastest off axis.

## 4.5 SUMMARY

The electron density shows a strong radial dependence with the majority of electrons being generated in the central 14 mm.

The calculated electron temperature is also peaked on axis. This is explained by the dominant influence of hydrogen on the electron cooling which links the electron and gas temperatures. This is in contrast to the situation in the CVL where the electron to electron coupling is the dominant factor affecting the electron temperature radial profile, leading to a flat radial profile.

If a flat electron temperature profile is assumed, then electron attachment is significant and occurs fastest off axis.

# CHAPTER 5 THE HOOK METHOD

## 5.1INTRODUCTION

The hook method is a technique which enables the investigator to measure the product of the oscillator strength and the population density in the lower level for a given transition, integrated over a given path length. This is achieved by evaluating the frequency dependence of the change in refractive index due to dispersion in the neighbourhood of a transition.

Relative refractive index measurement is achieved by placing the medium to be interrogated in one arm of a Mach-Zehnder interferometer and passing a probe beam through the interferometer. The probe beam will encounter a path difference between the arm containing the medium to be interrogated (the measurement arm) and the reference arm, due to the difference in refractive indices. The interferometer is usually arranged such that the beams from the two arms meet at a slight angle such that a series of fringes are formed at the output. If the output of the interferometer is then spectrally dispersed in a stigmatic spectrograph orthogonal to the fringes, the wavelength dependence of the path difference and hence the difference in refractive indices can be recorded.

In the absence of dispersion the fringes will appear as sloping lines on the detector, the effect of dispersion in the neighbourhood of a transition is to bend the fringes over into hook shapes on either side of the absorption line. The spacing of these hooks is related to the product of the oscillator strength and the difference in number density between the upper and lower states of the transition, integrated over the probe beam path length.

## 5.2 HISTORY

The hook method, originally proposed by Rozhdestvenskii in 1912, is a powerful technique for measurement of either population density or oscillator strengths. It was initially applied to the measurement of oscillator strengths in spectral doublets (Prokofiev, 1924; 1927) and then, in conjunction with emission techniques, to the measurements of oscillator strengths (Ladenburg 1933). These studies were applied to steady state plasmas only, because of limitations in both the light source and the recording equipment. Subsequent development of the probe light sources available revolutionised the hook technique by offering time resolution, as first flash tubes with pulse lengths of a few μs (Tumakaev & Lazovskaya 1965; Shtukin et al. 1975a & b) and then dye lasers with pulse lengths of a few ns (Miyazaki et al. 1975; Miyazaki & Fukuda 1977) were applied to the technique. Spatial resolution was soon demonstrated (Sandeman & Ebrahim 1977; Neger & Jager 1984) and the technique became the subject of numerous reviews (Penkin 1964; Marlow 1967; Huber 1971; Huber & Sandeman 1986). Since the early eighties the hook technique has been increasingly widely used in the field of metal vapour lasers (Smilanski 1979; Smilanski et al. 1980; Smilanski et al. 1981; Tenenbaum et al. 1981a & b; Warner & Kushner 1981; Warner & Seeley 1983; Kunnemeyer et al. 1987; Molander 1989; Brown 1988; Brown et al. 1989 & 1990).

## 5.3 SUITABILITY

The hook method has many desirable characteristics which make it a good choice for the interrogation of metal vapour laser plasmas.

The hook method uses a pulsed probe beam of low spectral intensity (due to its quasi-broadband nature) which reduces probe induced perturbations and if a suitably sensitive detector is used a hook pattern may be obtained from a single shot, giving time resolution equal to the pulse length of the probe laser.

There are few assumptions made in the hook method theory, as the method utilises dispersion in a region of the spectrum relatively far from the absorption line. This means that detailed knowledge of the line shape and line broadening mechanisms is not necessary, provided the homogeneously broadened linewidth is not more than 10% of the hook separation.

The hook method is an effective technique to use for investigation of plasmas with a high optical density. This characteristic gives dispersion a significant advantage over emission spectroscopy as many of the transitions in the HyBrID system are optically thick (emission spectroscopy demands that the line must be optically thin). Indeed, high optical density is an advantage as it increases the hook separation and allows more accurate determination of the hook separation.

The method is also relatively insensitive to broadband absorption losses in the measurement beam (due to contaminated windows etc.) as this only effects the fringe contrast and can be

redressed by suitable attenuation of the reference beam. This can be a major problem in an absorption measurement.

There are no optical delays associated with the hook method, in contrast to the situation when using the absorption technique in a plasma of high optical thickness (Huber & Sandeman 1986).

The hook method can be applied to spectral regions where multiple absorption lines exist by using the hook vernier method (Sandeman 1979). Absorption spectroscopy measurements are possible but subject to large errors in such situations. Although there are no lines of interest in the HyBrID laser which require the use of the hook vernier method (the ground state resonance transitions are sufficiently separated for conventional hook work) there are other metal vapours which require its use.

The technique has a high dynamic range due to the $\Delta^2$ dependence of the population density, which may be extended further if necessary by adjustment of the interferometer alignment and recalibration.

The one major disadvantage of the hook method is its relatively low sensitivity. In situations where a low population density with a weak oscillator strength must be measured (such as the copper lower laser levels in the late afterglow), it may not be possible to obtain sufficient sensitivity using the hook method and the absorption technique may be more appropriate due to its large dynamic range and higher sensitivity. The absorption technique has been successfully applied in the past to the measurement of populations in the CVL (Isaev et al. 1986).

## 5.4 THEORY

Dispersion may be understood by considering the dispersive medium as a distribution of damped classical electron oscillators. If the incident photon is considered as a time varying external electric field of the form $E(t) = E_0 e^{i\omega t}$, then the differential equation describing the motion of a damped classical electron oscillator in this field is

$$\ddot{x} + \gamma\dot{x} + \omega_0^2 x = \frac{e}{m} E_o e^{i\omega t} . \qquad [5.1]$$

Solving [1] for $x$ we have:

$$x = \frac{e}{m} \frac{1}{\left(\omega_0^2 - \omega^2 + i\omega\gamma\right)} E . \qquad [5.2]$$

The polarisation of the medium is given by the relation

$$P = \mathrm{N}e\,x \qquad \textbf{[5.3]}$$

where N is the number of electrons in a given volume and $e$ is the electronic charge. From this we can calculate the susceptibility $\chi = P/E$, and using the relation $\varepsilon = \varepsilon_0 + \chi$, derive the refractive index $\bar{n} = \sqrt{\varepsilon/\varepsilon_0}$.

$$\bar{n}^2 = 1 + \frac{Ne^2}{\varepsilon_0 m} \left( \frac{1}{\left(\omega^2 - \omega_0^2\right) + i\omega\gamma} \right) \qquad [5.4]$$

If we are dealing with a gas with refractive index $n \sim 1$ and we restrict our investigation to regions relatively close to the absorption line, such that $|\omega - \omega_0| << \omega_0$, Equation [4] may be simplified:

$$\bar{n}^2 = 1 + \frac{Ne^2}{2\varepsilon_0 m \omega_0} \left( \frac{1}{\left(\omega - \omega_0\right) + i\frac{1}{2}\gamma} \right) \qquad [5.5]$$

The real part of the complex refractive index $\bar{n}^2$ is the dispersion of the plasma, the complex part is the absorption coefficient. Thus we

see that the processes of absorption and dispersion (hook) spectroscopy can both be used to measure the change in refractive index in the region of a transition. The difference between the two processes is that one measures the contribution to the real part (n-1); the other measures the contribution to the imaginary part, $k_\nu$ (see Figure. 5.1)

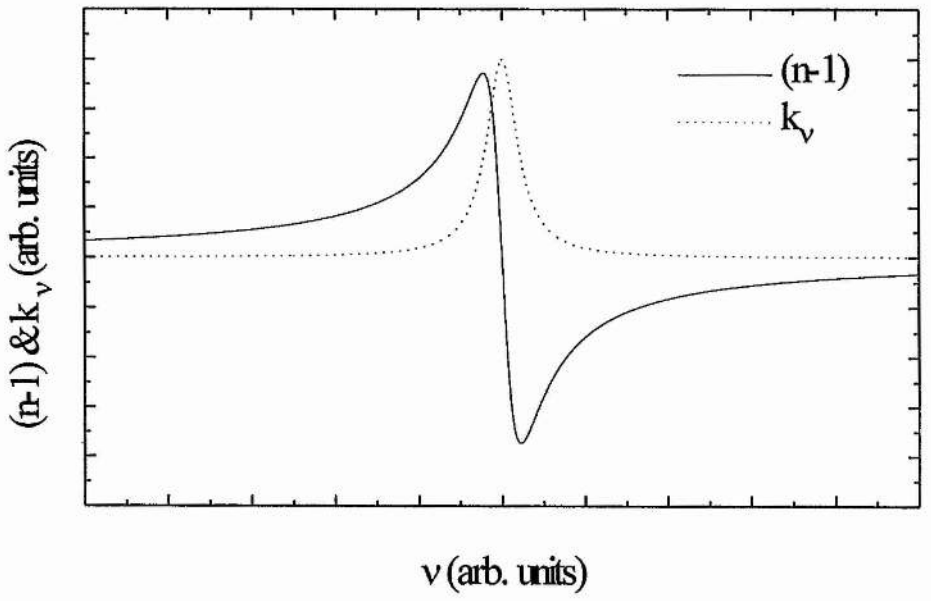


Figure 5.1. Absorption and Dispersion in the Neighbourhood of a Transition.

If the refractive index is measured sufficiently far from the line centre, such that broadening may be neglected, i.e. where $(\omega-\omega_0)^2 >> (\frac{1}{2}\gamma)^2$, then the real part of Equation [5.5] may be expressed as

$$n-1=\frac{Ne^2}{4\varepsilon_0 m\omega_0}\left(\frac{1}{(\omega-\omega_0)}\right) \qquad [5.6]$$

For population densities $N_i$ and $N_j$ in the ith and jth states we can define a parameter $F_s$ such that,

$$F_s = N_i f_{ij} + N_j f_{ji}, \qquad [5.7]$$

where by definition,

$$f_{ji} = -\frac{g_i}{g_j} f_{ij} \qquad [5.8]$$

then,

$$F_s = N_i f_{ij}\left(1 - \frac{g_i N_j}{g_j N_i}\right) = N_i^* f_{ij} \qquad [5.9]$$

where $N_i^*$ is the effective population density. If we now set N in Equation [5.6] equal to $F_s$ we can calculate the contribution to the refractive index due to the effective population density $N_i^*$ in the jth state. Making this substitution and substituting for $\omega$ in terms of λ, we have,

$$n-1=\frac{r_0}{4\pi} N_i^* f_{ij} \frac{\lambda_{ij}^3}{\lambda-\lambda_{ij}} \qquad [5.10]$$

where $r_0$ is the classical electron radius. This is the classical Sellmeier approximation for the refractivity of a plasma in the vicinity of an isolated absorption line. In the presence of multiple absorption lines this formula may be revised to take account of all the contributions;

$$n-1=\frac{r_0}{4\pi}\sum_{i,j} N_i^* f_{ij} \frac{\lambda_{ij}^3}{\lambda-\lambda_{ij}} \qquad [5.11]$$

The lines investigated in this work were all sufficiently widely separated for us to use Equation [5.10] and to ignore the contribution due to neighbouring transitions.

We wish to investigate parameter $N_i^*$. Absolute measurement of the refractive index or wavelength is non-trivial. If instead we investigate n as a function of $\lambda$ and determine $dn/d\lambda$ we will no longer need to perform absolute measurements.

Differentiating Equation [5.10] we get;

$$\frac{dn}{d\lambda} = \frac{-r_0}{4\pi} N_i^* f_{ij} \frac{\lambda_{ij}^3}{\left(\lambda - \lambda_{ij}\right)^2} \qquad [5.12]$$

Our requirement is now reduced to determining a change in refractive index $dn$ and a change in wavelength $d\lambda$. (The wavelength $\lambda_{ij}$ corresponds to the wavelength of the transition ($\lambda_0$ henceforth), which is known.

Measurement of a change in refractive index is easily performed using an interferometer to observe the phase shift between two beams, one being a probe beam passed through the plasma and the other a reference beam.

The remaining requirement is a means of measuring the spectral dispersion to allow absolute measurement of the change in wavelength. A stigmatic spectrograph fulfils these requirements.

The condition for maximum intensity at the output of an interferometer is that the path difference between the two arms is a whole number of wavelengths:

$$\Delta l = m\lambda \qquad [5.13]$$

The path difference $\Delta l$ can be divided into two contributions, that due to the plasma and an additional shift due to the windows etc. The shift due to the laser windows may be compensated for by placing another pair of windows, known as compensation plates, in the reference arm. This has the advantage of allowing the path length in

the reference arm to be increased slightly by rotating these two compensation plates from normal incidence. If the two plates are rotated in opposite senses then beam steering effects may be eliminated. Using the convention that path lengths added to the probe arm are negative and those added to the reference arm are positive, the path difference $\Delta l$ can be written;

$$\Delta l = (n-1)l - (n'-1)l' \qquad [5.14]$$

where $n$ is the refractive index of the plasma, $l$ is the path length in the plasma, $n'$ is the refractive index of the compensation plates and $l'$ is the net path length through the compensation plates and the windows.

If we skew the alignment of the interferometer slightly such that the beams from the two arms meet at a small angle at the entrance slit of the spectrograph, then we can produce a set of fringes at the image plane of the spectrograph. The condition for maximum intensity for two beams meeting at the half angle $\phi$ is,

$$y - (n-1)l + (n'-1)l' = m\lambda \qquad [5.15]$$

where $y$ is the vertical distance at the output plane and $m$ is the order of the interference, an integer. This is known as the fringe equation and gives the vertical position y of the mth fringe.

Differentiating [5.14] we get:

$$\phi\frac{dy}{d\lambda} - l\frac{dn}{d\lambda} = m - l'\frac{dn'}{d\lambda} \qquad [5.16]$$

if we consider the case where the measurement arm of the interferometer is empty, i.e. $dn/d\lambda = 0$, Equation [5.16] becomes

$$\frac{dy}{d\lambda} = \frac{1}{\phi}\left(m - l'\frac{dn'}{d\lambda}\right) \qquad [5.17]$$

as $dn'/d\lambda$ is approximately constant over the restricted range of wavelengths of interest, Equation. [5.16] describes a set of parallel

straight fringes. We can use Equation. [5.16] to define a constant $K$ for the measurement system:

$$K = m - l'\frac{dn'}{d\lambda} = \phi\frac{dy}{d\lambda} \qquad [5.18]$$

Using the fringe Equation [5.14] but rearranging to give $\phi y$ and considering maxima on two fringes, $m$ and $m+\Delta m$, separated by $\Delta\lambda$ we can write:

$$y = m\lambda + (n-1)l - (n'-1)l' \qquad [5.19]$$

$$y = (m+\Delta m)(\lambda+\Delta\lambda) + (n-1)l - (n'-1)l' \qquad [5.20]$$

If we consider points on these fringes at the same vertical height then we may equate the left hand sides of these equations and rearrange to give

$$m = \frac{\Delta\lambda}{\Delta m}(\lambda+\Delta\lambda) \qquad [5.21]$$

substitution for m in Equation [17] gives the following relation for K

$$K = \frac{\Delta\lambda}{\Delta m}(\lambda+\Delta\lambda) - \frac{dn'}{d\lambda}l' \qquad [5.22]$$

This constant may be measured by turning off the laser discharge, evacuating the test cell and measuring the fringe gradient. In practice this is unnecessary because the $dn/d\lambda$ term may be disregarded as it is insignificant in comparison to $m$. $K$ may therefore be evaluated by simply moving the spectrograph a suitable distance either side of line centre such that the fringes are unperturbed by dispersion effects. The hook constant K can then be measured directly.

Combining Equations [5.16],[5.18] and the Sellmeier approximation, Equation [5.12], we have

$$\frac{dy}{d\lambda} = \frac{K}{\phi}\left(1 - \frac{lr_0}{4\pi K}N_i^* f_{ij}\frac{\lambda_0^3}{(\lambda-\lambda_0)^2}\right) \qquad [5.23]$$

we can see by inspection that this equation has a discontinuity at $\lambda = \lambda_0$, this is to be expected as we have made the approximation that we are sufficiently far from line centre to ignore line broadening. The general form of this equation is plotted for several values of m in Figure 5.2.

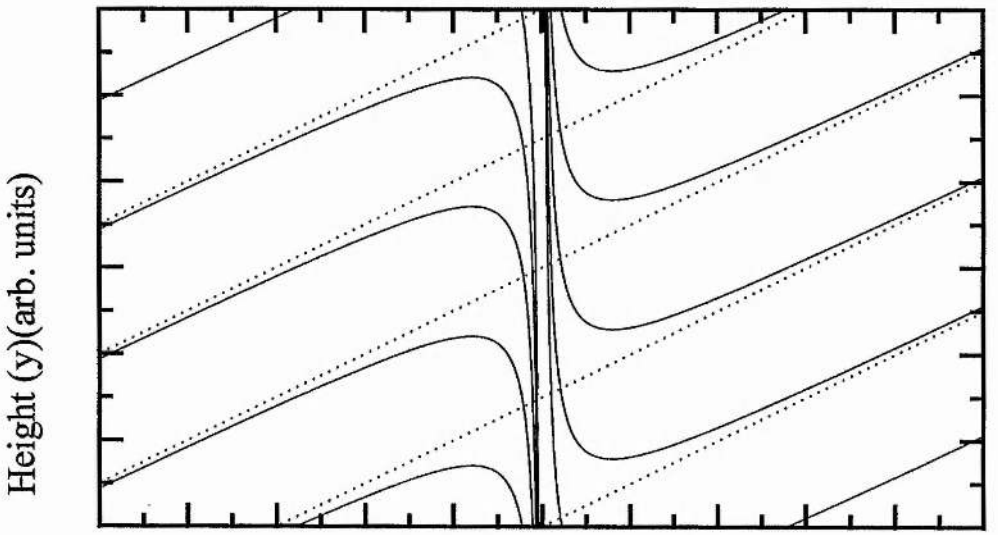


Figure 5.2. A typical hook pattern. Dotted lines indicate position of fringes in absence of anomalous dispersion

The position of the turning points can be calculated by setting $dy/d\lambda = 0$, giving

$$\lambda = \lambda_0 \pm \sqrt{\frac{lr_0 N_i^* \lambda_0^3 f_{ij}}{4\pi K}} \qquad [5.24]$$

We now define a parameter $\Delta$ equal to the separation between the two turning points:

$$\Delta^2 = \frac{lr_0 N_i^* \lambda_0^3 f_{ij}}{\pi K} \qquad [5.25]$$

Rearranging to give $N$ explicitly we have

$$N_i^* = \frac{\pi K}{lr_0 \lambda_0^3 f_{ij}} \Delta^2 \qquad [5.26]$$

Equation [5.26] gives $N_i^*$ in terms of known or measurable quantities.

## 5.5 EXPERIMENTAL METHOD

The experimental layout is shown in Figure 5.3. The system can be divided into 4 major component parts:

1. pump laser
2. interferometer
3. spectrograph and detector
4. timing electronics and image storage apparatus.

All components of the interferometer as well as the pump lasers the spectrometer and the HyBrID laser were mounted on two optical tables for maximum stability and minimum drift during the experiment. The tables were surrounded by laser screens and covered with tinted perspex covers to protect against stray laser radiation and to reduce air currents in the interferometer arms.

### 5.5.1 PUMP LASER

The hook method can be performed using either a genuinely broadband light source such as a flashlamp to cover the whole area of the spectrum in which there are lines of interest, or a quasi-broadband lightsource which may be tuned over the spectral region to be investigated. The light source should offer sufficiently short pulses to allow resolution of the effects to be studied and high enough intensity at the detector to permit single shot capture of images. It is desirable

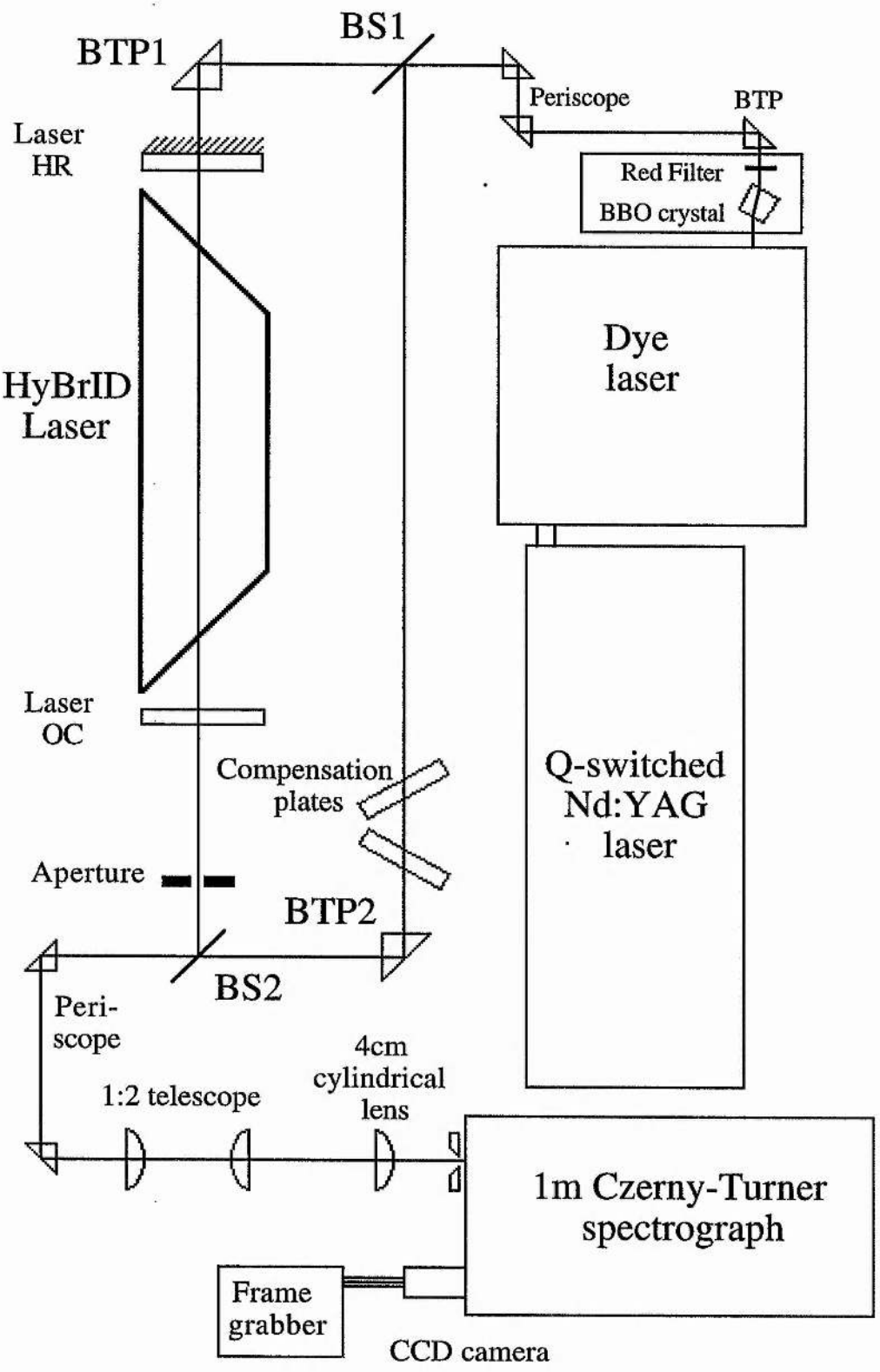


Fig 5.1 Electron density measurement experimental layout

that the probe laser intensity should be variable to allow optimisation for the detector dynamic range and sensitivity.

The flashlamp option is low cost but also low time resolution. With such systems there may be problems associated with insufficient transverse coherence at the detector if it is necessary to use a large interferometer. In addition, achieving good spatial resolution with a flashlamp source is non-trivial and the apertures required for good discrimination may reduce the incident intensity at the detector to an unacceptably low level.

Quasi-broadband emission can be obtained from a modified dye laser pumped by a high energy light source. Using a suitable range of dyes the entire visible spectrum can be covered as well as significant parts of the infra-red and near UV. Dye laser systems have the advantages of short pulse length (~ 5 ns), high intensity and good beam quality (~ 0.5 mrad divergence). These characteristics allow good time resolution and good spatial resolution without undue loss of signal on beam defining apertures resulting in efficient intensity transfer to the detector.

In this study a dye laser pumped by a Q-switched oscillator amplifier configuration Nd:YAG laser was used. This configuration gave maximum flexibility in the pump laser as the oscillator was arranged to give optimum output beam quality, the voltage on the amplifier pump flashlamps was then be varied according to the requirements at the detector. This allowed the pump power to be adjusted to compensate for changes in dye efficiency and dye degradation over its lifetime, beam defining aperture size and spectrograph entrance slit size. The pump laser output could be either

frequency doubled to 532 nm for pumping in the green or frequency tripled to 355 nm to pump in the UV, both of which were suitable for dye pumping. The pump laser output harmonics were separated using Brewster angle prisms, this has important implications for optic specifications, as light generated using the second harmonic pump was orthogonally polarised with respect to light generated using the third harmonic. The beam splitters in the interferometer were specified appropriately as the reflectivities for s and p polarisations were different at 45° incidence.

The dye laser was a standard commercial oscillator amplifier dye laser type arranged by the manufacturers to give narrow-band output. The frequency selection mechanism of the oscillator was modified to give broadband operation- this was achieved by removing the grazing incidence diffraction grating and replacing it with a fused silica prism giving an output bandwidth of 2.8 nm FWHM. The original tuning mechanism for the oscillator consisted of a high reflector on a translation stage driven around the frequency selective element by a precision stepper motor. This system was retained and used to tune the broadband output.

The modified laser system was thus able to produce quasi-broadband tuneable output in pulses of ~ 5 ns duration, at 10 Hz PRF and controllable output energy of up to 100 mJ when using a 532 nm pump wavelength.

There remains one problem regarding the probe laser: the generation of quasi-broadband output at 324.8 & 327.4 nm for investigation of the copper ground state resonance transitions. It is possible to generate these wavelengths using the present laser system

by either pumping a UV dye with the fourth harmonic of the Nd:YAG output, or by frequency doubling red output from the dye laser. As dyes which operate at such short wavelengths are generally of poor stability and poor efficiency it was decided to frequency double the output of the dye laser. This approach has the additional advantage that the power density in the doubling beam is higher due to the smaller diameter of the dye laser output, but there is one notable disadvantage. This is the problem of generating a sufficiently broadband second harmonic. For maximum efficiency of second harmonic generation with type I phase matching the condition

$$n_{2\omega}^{e}(\theta_m) = n_{\omega}^{0} \qquad [5.27]$$

must be satisfied, where $n_{2\omega}^{e}$ is the refractive index for the frequency doubled extraordinary wave travelling at matching angle $\theta_m$ and $n_{\omega}^{0}$ is the refractive index for the fundamental ordinary wave. This condition can only be satisfied for one wavelength. The result is that for a uniform spectral intensity entering the crystal, the second harmonic generated will have a peak at the phase matched frequency with decreasing intensity on either side. This problem is most pronounced when long lengths of doubling crystal are used as the phase difference between waves at the extremes of the frequency range and the fundamental increases with path length until power is no longer coupled from fundamental to second harmonic, but instead in the opposite direction. This is exacerbated by the fact that frequency doubling efficiency is intensity dependant so any variation in intensity across the spectral profile of the dye laser output will be exaggerated in the doubled component. These two effects combine to make wide bandwidth, second harmonic generation problematic, the second

harmonic generally having an intensity profile with a strong spectral dependence.

Nevertheless it was possible to produce sufficiently wide bandwidth output ( estimated at 1 nm FWHM ) at acceptable intensity using a 5 mm cube of BBO with type I phase matching.

To improve on the performance of the present system it may be advantageous to use a shorter crystal to decrease the effects of beam walk off at the cost of decreased conversion efficiency. LBO may be used as an alternative non-linear crystal with lower beam walk off.

### 5.5.2 INTERFEROMETER

The interferometer proper consists of two 50/50 beamsplitters, and two fused silica right angle turning prisms, see Figure 3. There were two sets of laser quality beamsplitters used in the experiment, one set coated for broadband visible use with horizontal polarisation and another set coated for UV use with vertical polarisation. The beamsplitters work at different polarisations because the harmonic separation in the Nd:YAG pump laser is by Brewster angle prisms, which results in orthogonal polarisation of the harmonics. Prisms were used for beam turning because of their high damage threshold.

The portion of the medium being interrogated was defined by two apertures. Scanning of the probe beam across the active medium was achieved by mounting the HyBrID laser on a translation stage moving perpendicular to the measurement arm of the interferometer. Two compensation plates were placed in the reference arm of the interferometer to offset the optical thickness of the laser windows. Adjustment of the unperturbed fringe gradient at the detector without

beam steering could be achieved by counter rotating the two compensation plates.

Beam height adjustment was provided by a pair of right angle prism periscopes to allow coupling of the probe laser beam into the interferometer on the HyBrID laser axis, and relay of the two output beams from the interferometer such that they produced the desired interference pattern at the entrance slit of the spectrograph.

### 5.5.3 SPECTROGRAPH AND DETECTOR

The output from the interferometer was dispersed in a 1m Czerny-Turner spectrograph with a 256 x 256 element CCD detector of 4 mm square area. A 2X magnification telescope was placed before the spectrograph to increase the beam size so that it filled the detector element. An f = 40 mm cylindrical lens was used to focus the beam through the spectrograph entrance slit such that it filled the 102 x 102 mm square high reflector of the spectrograph to maximise image brightness and spectral resolution.

### 5.5.4 TIMING AND IMAGE STORAGE

We require to scan the timing of the probe laser pulse with respect to the HyBrID laser pulse, through a full pulse inter-pulse period. This is achieved by computer control of a precision digital delay generator (DDG) (type Stanford Research Systems DG535). The DDG provides trigger signals to the HyBrID laser, the pump laser and the frame grabbing equipment which captures the detector image.

In order to realise the best time resolution available from the dye laser, it is necessary to have accurate knowledge of the HyBrID laser

timing relative to the probe laser timing. It is essential that the HyBrID laser operates under unperturbed optimum conditions. The first trigger from the DDG is therefore a free running trigger pulse at 17 kHz, used to trigger the HyBrID laser. This trigger remains unaltered unless the DDG is either switched off or reprogrammed, neither of which happens during the experiment. We monitor the temporal dependence of the storage capacitor voltage, the tube voltage, the tube current and the laser pulse during the experiment. For accurate assessment of the HyBrID laser timing we use the rising edge of the laser pulse as a reference as this is the fastest rising edge and is therefore the easiest to accurately assess it's position. All timings are referenced to the HyBrID laser pulse.

The probe laser timing is controlled by the computer which increments the delay of the probe laser trigger and the frame grabber trigger relative to the HyBrID laser trigger by a pre-programmed sequence of increments. The computer is also programmed to download to disc the data from the frame grabber and assign it a sequential file name.

In practice the system is complicated by the needs of the pump laser which is limited to a maximum PRF of 10 Hz, this must be maintained to ensure stable output. The rate at which results can be recorded will be further limited by the data transfer rate from the frame grabber to the computer hard disc. These limitations were overcome using additional delays generated by the DDG and the computer. For full details of the automated acquisition system ( see Hogan et al. 1993).

### 5.5.5 ACCURACY

The population density is calculated from Equation [5.9], given below

$$N_i^* = \frac{\pi K}{l r_0 \lambda^3{}_0 f_{ij}} \Delta^2 \qquad [5.9]$$

The wavelength of the transition $\lambda$ and the classical electron radius $r_0$ are well known. The remaining sources of error are the hook separation $\Delta$, the hook constant $K$, the oscillator strength $f_{ij}$ and the path length $l$. The accuracy with which $K$ can be determined is typically better than 1%, while the error in the hook separation will depend on the detector system used and the accuracy of calibration of the spectrograph. The dispersion of the spectrograph is specified to better than 1% for all the wavelengths of interest. This leaves the hook separation, the length of plasma being interrogated and the oscillator strength of the transition as the major sources of error.

Estimation of the length of the plasma column over which the measurement is made is non-trivial. The ends of the active region are not well defined, indeed the definition of the 'end' of the plasma column is not clear as the density of species will gradually fall off as we move from the hot discharge region towards the cool electrodes. In practise the best estimate of the active region length is that between the points on the electrode 'spot-locks', which define the length of the discharge, less approximately 1 cm at each end, where CuBr is deposited. The length is estimated as 78+/-1 cm, this length is used for calculation of all the copper level population densities.

The electrode to electrode separation is 80 cm. The difference between this and the length of the hot region, 2 cm, is that where neon

is presumed to provide the majority of the charge carriers to sustain the discharge. For this reason, 2 cm is the length used in the calculation of the neon level population density.

Oscillator strengths for the transitions of interest have been investigated by several authors (e.g. Allen et al. 1957; Meggers et al; Kock et al. 1968; & Corliss 1970) A number of these studies investigated only relative oscillator strengths, while others measured absolute values. An excellent review and survey of the available data was performed by Bielski (1975). All the values for copper were taken from that study. The oscillator strengths for neon were those tabulated by the American National Bureau of Standards (Weise et al. 1966). Table 5.1 gives a summary of the transitions studied and the oscillator strengths, with their estimated errors, as used in the data reduction.

| **Lower Level** | **Upper level** | **Wavelength** | **Osc. strength** | **Dye** |
|---|---|---|---|---|
| $3d^{10}4s\ ^2S_{1/2}$ | $3d^{10}4p\ ^2P_{3/2}$ | 324.75nm | 0.433 +/-5% | DODCI (doubled) |
| $3d^{10}4s\ ^2S_{1/2}$ | $3d^{10}4p\ ^2P_{1/2}$ | 327.40nm | 0.218 +/-5% | DODCI (doubled) |
| $3d^{9}4s\ ^2D_{3/2}$ | $3d^{10}4p\ ^2P_{1/2}$ | 578.21nm | 0.0048+/- 10% | Rh 6G |
| $3d^{10}4s\ ^2D_{1/2}$ | $3d^{10}4p\ ^2P_{3/2}$ | 510.55nm | 0.0051+/- 10% | Coumarin 485 |
| $3d^{10}4p\ ^2P_{1/2}$ | $3d^{10}4d\ ^2D_{3/2}$ | 515.32nm | 0.820 +/-10% | Coumarin 503 |
| $3d^{10}4p\ ^2P_{3/2}$ | $3d^{10}5s\ ^2S_{1/2}$ | 809.26nm | 0.255 +/-10% | LDS821 |
| $3d^{9}4s4p\ ^4F_{9/2}$ | $3d^{9}4s5s\ ^4D_{7/2}$ | 465.11nm | 0.109 +/-20% | LD466 |
| $2p^{5}3s\ ^3P_0$(Ne) | $2p^{5}3p\ ^1D_1$(Ne) | 626.65nm | 0.394 +/-10% | DODCI |

Table 5.1

The hook separation was determined from the 256 x 256 element detector image by a procedure involving both computer manipulation of the data and operator input to avoid misidentification.

### 5.5.6 HOOK SEPARATION MEASUREMENT

Our requirement is to identify the vertical columns (and hence the wavelengths) in the fringe spectra where the fringe gradient is zero. The variation in intensity in each column is sinusoidal with a superimposed noise signal. We can determine the phase of this column by taking the FFT (fast fourier transform). We can then identify the hook position by looking for the column where the phase is constant from one column to the next. To guard against misidentification of the turning point caused by noise corruption, instead of recording the phase, the sine and cosine of the phase were written to file. In areas of the spectrum free from dispersion the phase will vary linearly with wavelength and the sine and cosine of the phase will be $\pi/2$ out of phase. The column where the sine and cosine both show a turning point is the hook position.

### 5.5.7 RESOLUTION

The wavelength resolution, $\varepsilon$, of the hook method is limited by the pixel size of the detector, $\Delta x$, in combination with the dispersion of the spectrograph, d, according to the relation $\varepsilon = \Delta x d^{-1}$ . In the present system $\varepsilon \sim 3.5$ pm for second order diffraction. For a system of similar resolution a minimum resolvable hook separation of about 0.02 nm is estimated by Bachor and Kock (1980) for the standard hook. This error will be significant where the populations to be measured start from and

return to values close to zero. This is the case in all the populations of interest here except of the copper ground state.

### 5.5.8 COMPLICATIONS OF HOOK INTERPRETATION

There are three assumptions made in the theoretical derivation of the hook formulae which must be satisfied. These are; that the upper level population should be negligible; that the transitions are isolated and that the linewidth is a small fraction of the hook spacing.

The first of these conditions is clearly violated in the case of the laser lower levels. It must be remembered that the term $N_i^*$ was defined as

$$N_i^* = N_i\left(1 - \frac{g_i N_j}{g_j N_i}\right) \qquad [5.9]$$

When inversion does not occur, we can correct measurements using Equation [5.9] if we have the relevant information on the upper level population density. We can therefore obtain results for the lower laser levels for all of the pulse-interpulse period except the period of laser gain.

When inversion occurs on a transition, $N_i^*$ is negative and the fringes 'bend' in the opposite direction and no hook is formed. It is possible under these conditions to produce 'inverse' hooks by changing the interferometer alignment such that the fringes in an unperturbed region of the spectrum slope in the opposite direction. With this alignment it is possible to measure the difference between the upper and lower laser levels during inversion. Due to the small number of points involved (6 points) and the limited time available for completion of the study, this measurement was not made.

The condition that the transitions be isolated is fulfilled in all cases. The two resonance transitions used for measuring the ground state density are, however, sufficiently close together to preclude the measurement of undisturbed fringe slope between the lines. The calibrations for these measurements were therefore only performed on one side of the line.

The final condition that the line be thin compared to the hook spacing is considered by both Marlow (1967) and Huber (1971). The conclusion of both investigations is that the effect of line broadening is to cause a second set of hooks to be produced, unless the broadening is so great that no hooks are formed at all. Of the two sets of hooks the outer set will be more easily seen, the innner set generally being very close to the absorption line. For line widths up to 10% of the undisturbed hook spacing the effect is a 1-2% change in measured hook spacing. Fortuitously the effects of Lorentzian and Doppler broadening act in opposition, such that the effect of both mechanisms combined results in a change in hook width smaller than would be the case for either mechanism acting alone.

The Doppler width of the lines studied is in all cases less than 10% of the unperturbed hook spacing.

The most significant source of Lorentzian broadening is pressure broadening, which will have most effect on the measurement of the yellow lower laser level population. This transition has a line-width of 0.0099 nm due to the hyperfine structure of the line. For this line hooks will not be formed until the unperturbed separation reaches 0.025 nm, at which point the measured separation is 50% of the unperturbed separation. This is below the resolution limit of our system for the

standard hook method, though the hook vernier method may allow measurements of such small separations. In practice, the low oscillator strength of this transition in combination with the low population density led to a wide scatter in the results, and determination of the population in the mid to late afterglow was not reliable. It is suggested that this level is a suitable candidate for investigation using absorption spectroscopy where the high sensitivity possible with this technique may prove beneficial.

Of the errors discussed above, the error in determination of the plasma length is systematic, that is it's effect is the same for all time points, for all population densities and for all transitions (except neon). This means that the relative magnitude of the results is more accurately known than the absolute value of the population density.

The error in oscillator strength is common to each time point, so we may compare results within a level and analyse trends in population with more confidence than we may compare results between levels.

# CHAPTER 6 POPULATION DENSITY RESULTS

## 6.1.THE COPPER GROUND STATE DENSITY

### 6.1.1 INTRODUCTION

There are several important differences between the HyBrID and CVL systems which we would expect to have a significant effect on the axial copper ground state density.

In the HyBrID laser the copper vapour density is decoupled from the tube wall temperature over a wide range of tube wall temperatures (500-900 $^{o}$C), the copper density is instead controlled by the concentration of HBr entrained in the buffer gas flow.

We may expect there to be some removal of copper from the discharge by formation of CuBr. This effect is likely to be most pronounced near the tube wall and may result in a change in ground state recovery.

### 6.1.2 LIMITATIONS TO GROUND STATE MEASUREMENTS

The measurement of the ground state density is one of the most difficult measurements to make. The only transitions which have an oscillator strength sufficiently high to allow measurement by the hook technique are the resonance transitions to the upper laser levels. These transitions are in the UV at 327.4 nm and 324.8 nm. To produce probe radiation at this wavelength the output of the dye laser was doubled in a BBO crystal. This technique produces output which is limited in bandwidth. This proved to be detrimental to measurement accuracy. In the case of the CVL previously investigated with this apparatus the ground state density was considerably lower than in the HyBrID laser.

Although the plasma length in the CVL was greater by a factor of two, the hook separation was considerably less. Measurements of the CVL ground state density could therefore be performed with a probe beam of significantly lower bandwidth. To achieve the increased bandwidth required for measurement of the HyBrID ground state density it was necessary to increase the pump laser power, this leads to a shortening of the laser dye lifetime and may cause degradation in probe laser performance during an experiment. This technique is an incomplete solution to the problem as the spectral intensity profile of the doubled beam will not be changed, the overall intensity will simply be increased. This may lead to limitation due to the finite dynamic range of the detector elements, with little improvement in fringe visibility at the extrema of the frequency range. At time points where the population density is lower the central portion of the detector may saturate obscuring the hooks. When the population density is high there will be strong absorption in the central portion of the interferogram which will allow the use of high probe beam intensities in order to increase the bandwidth. When the population density is lower and the hook separation is smaller, the probe beam intensity must be reduced to avoid detector saturation near line centre. The ground state density measurements were therefore performed twice, first using a high probe beam intensity and then repeated manually at lower probe intensity to allow investigation of the time points when the population was lower.

It is possible to measure the hook separation using a single hook on one side of the absorption line if the position of line centre can be determined. This was necessary in some cases when the probe

bandwidth did not allow both hooks to be resolved. Such measurements will have increased error due to uncertainty in the determination of the position of the line centre.

The hook technique is limited to populations which are uniform across the diameter of the probe beam. If the population varies significantly across the interrogated area then blurred fringes will be produced as different parts of the probe beam experience different phase delays. From the electron density results detailed in Chapter 4.4 we know that the discharge is constricted and there will be a strong radial dependence of population density at some radial positions across the tube. This effect is seen at radial positions near the tube walls and measurements made off axis are generally less complete than those nearer the tube axis.

Due to these additional error sources it was decided to perform ground state density measurements using both of the resonance transitions to provide additional data. This allowed us to compare two independent measurements of the same population density and thus we were able to assess the accuracy of the results.

### 6.1.3 GENERAL REMARKS ON THE GROUND STATE DENSITY

The temporal dependence of the copper ground state density during the inter-pulse period as measured using the 324.8 nm transition and the 327.4 are shown in Figures 6.1 & 6.2 respectively. The corresponding result for the CVL is given for comparison. The general trend in ground state density is a fast depletion during the excitation pulse followed by a slower recovery.

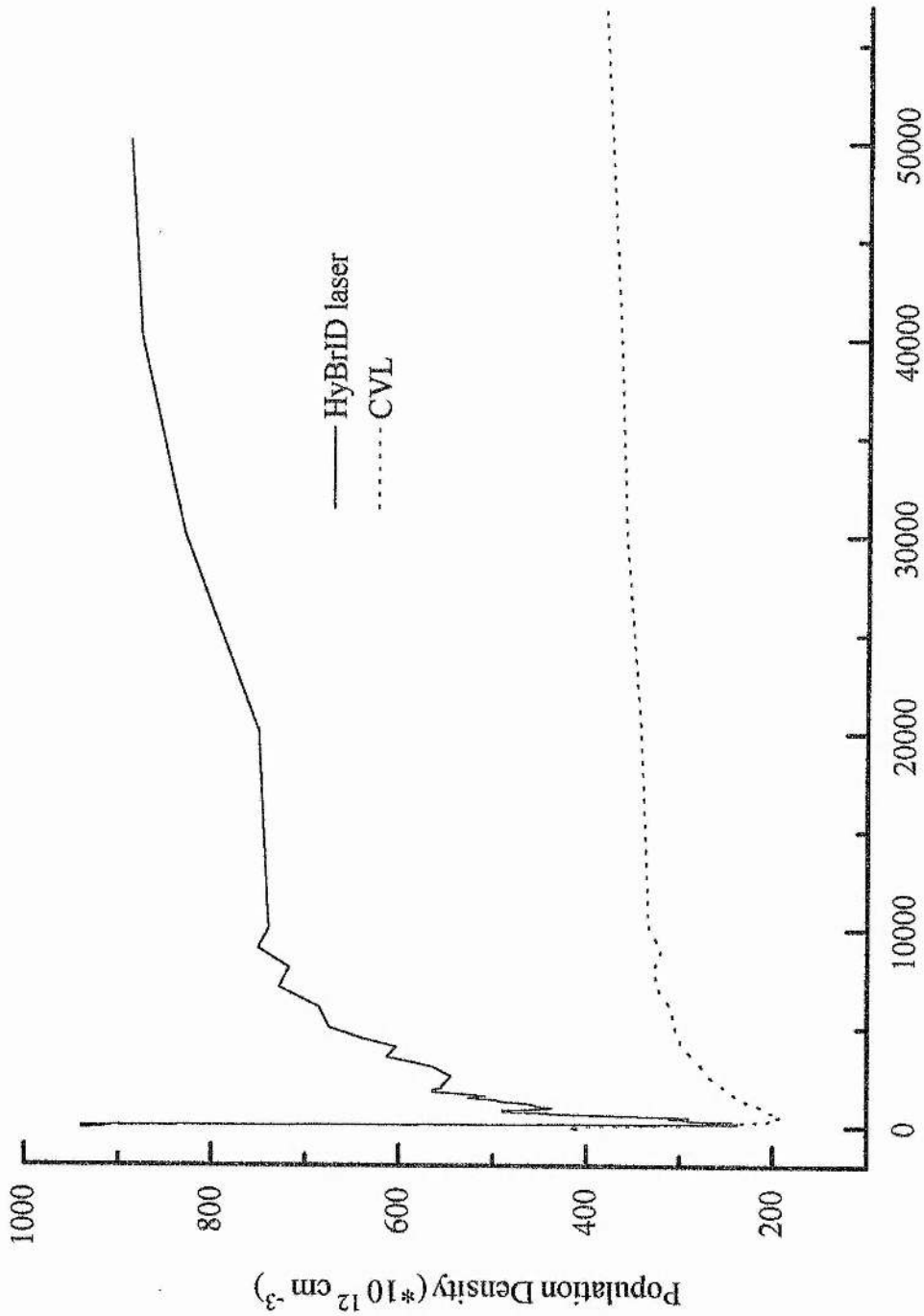


Figure 6.1 Ground state density measured using 324.8nm transition, first 1μs

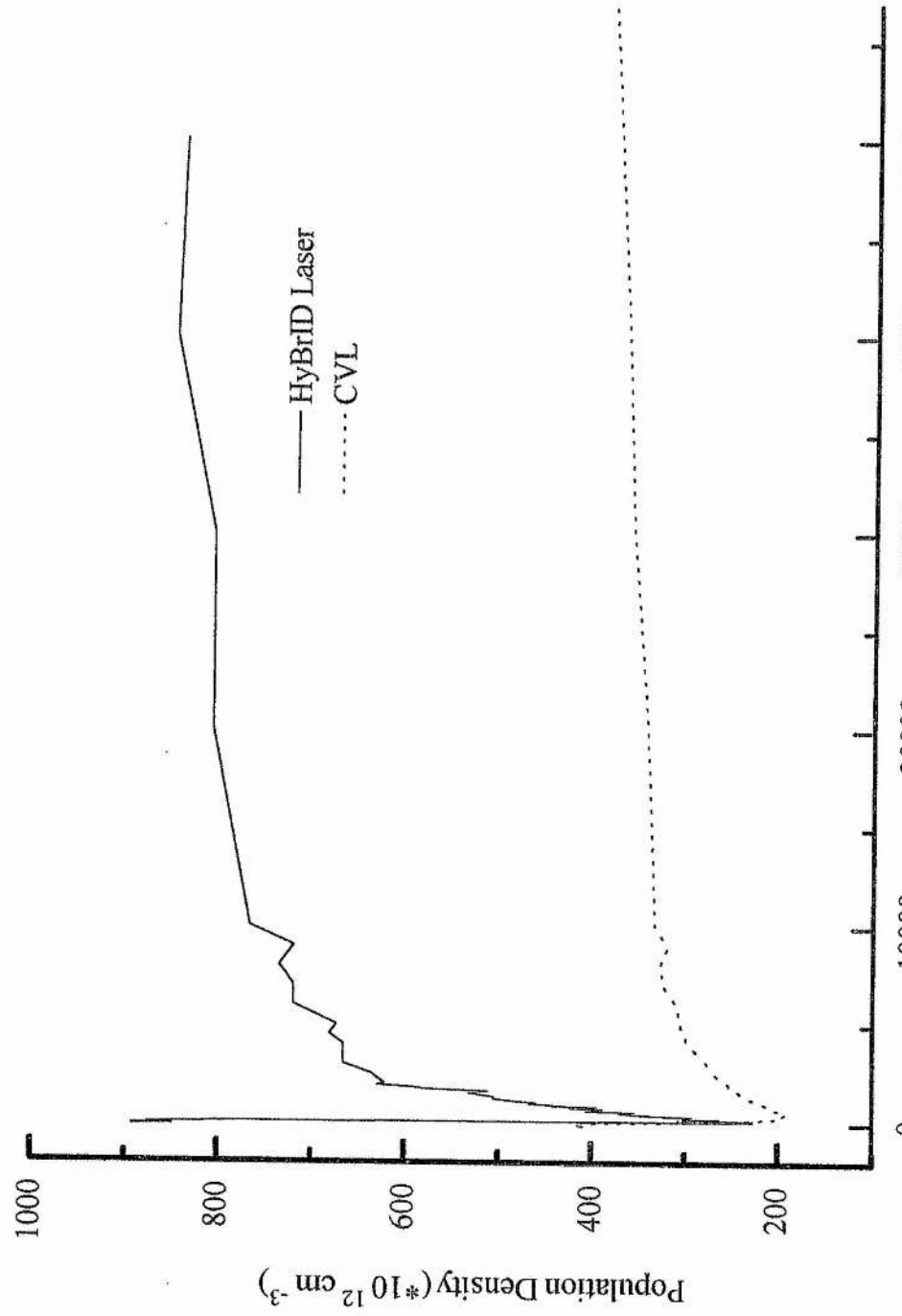


Figure 6.2 Ground state density measured using 327.4nm transition, first 1μs

### 6.1.4 POPULATION DEPLETION

The behaviour of the ground state density during the excitation pulse and immediately afterwards are shown in Figures 6.3 & 6.4. The behaviour of the tube current, tube voltage and laser light output are shown on the same figure.

The first point of interest is the very high initial ground state density in the HyBrID. Prior to the pulse the population density is more than twice that in the CVL on-axis. The ground state in the HyBrID is also depleted to a much greater extent than in the CVL. The minimum population density in the HyBrID is only ~25% of the peak, a depletion of ~75%, in comparison the CVL ground state density is only depleted by a maximum of ~55%. This may be due to the difference in tube bores and the slight discharge constriction in the HyBrID laser.

The ground state depletion before the tube current starts its period of fast rise is less than 5%. There is little if any depletion during the preceding 80-90 ns during which time the tube voltage has risen to its maximum value of 13.5 kV. This behaviour indicates that during this period the electron energy is below 2.1 eV as the electrons are unable to excite copper atoms. Therefore the electron temperature during this period does not follow the tube voltage, but remains low or some mechanism acts to severely impede any rise in electron density from its initial level. If there is a high field in the active medium then an accelerating force must be applied to the electrons in this region and the electron energy must increase. The observed behaviour contradicts this. It is interesting to note that similar behaviour was observed in the CVL previously investigated, where the ground state

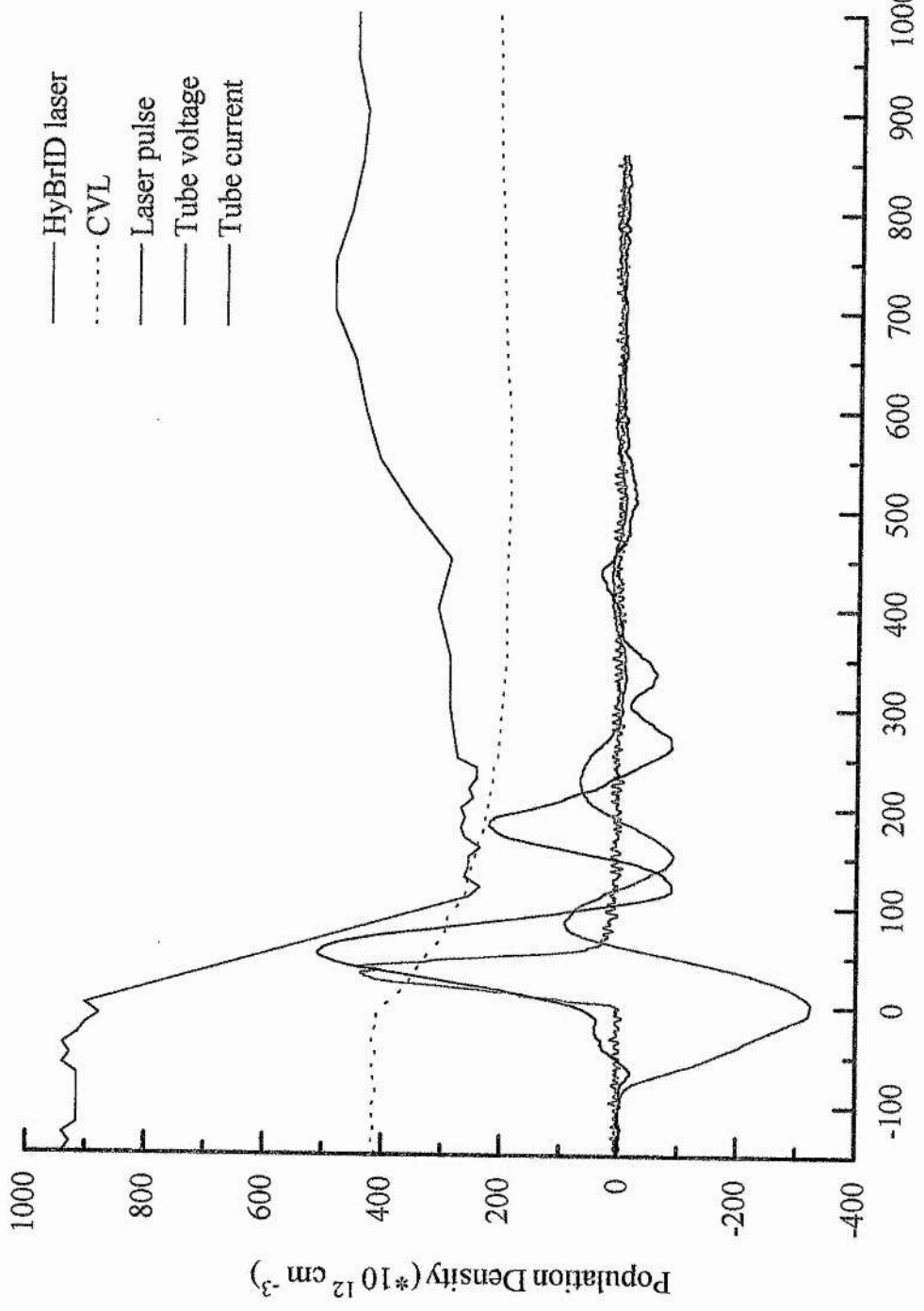


Figure 6.3 Ground state density measured using 324.8nm transition, first 1μs

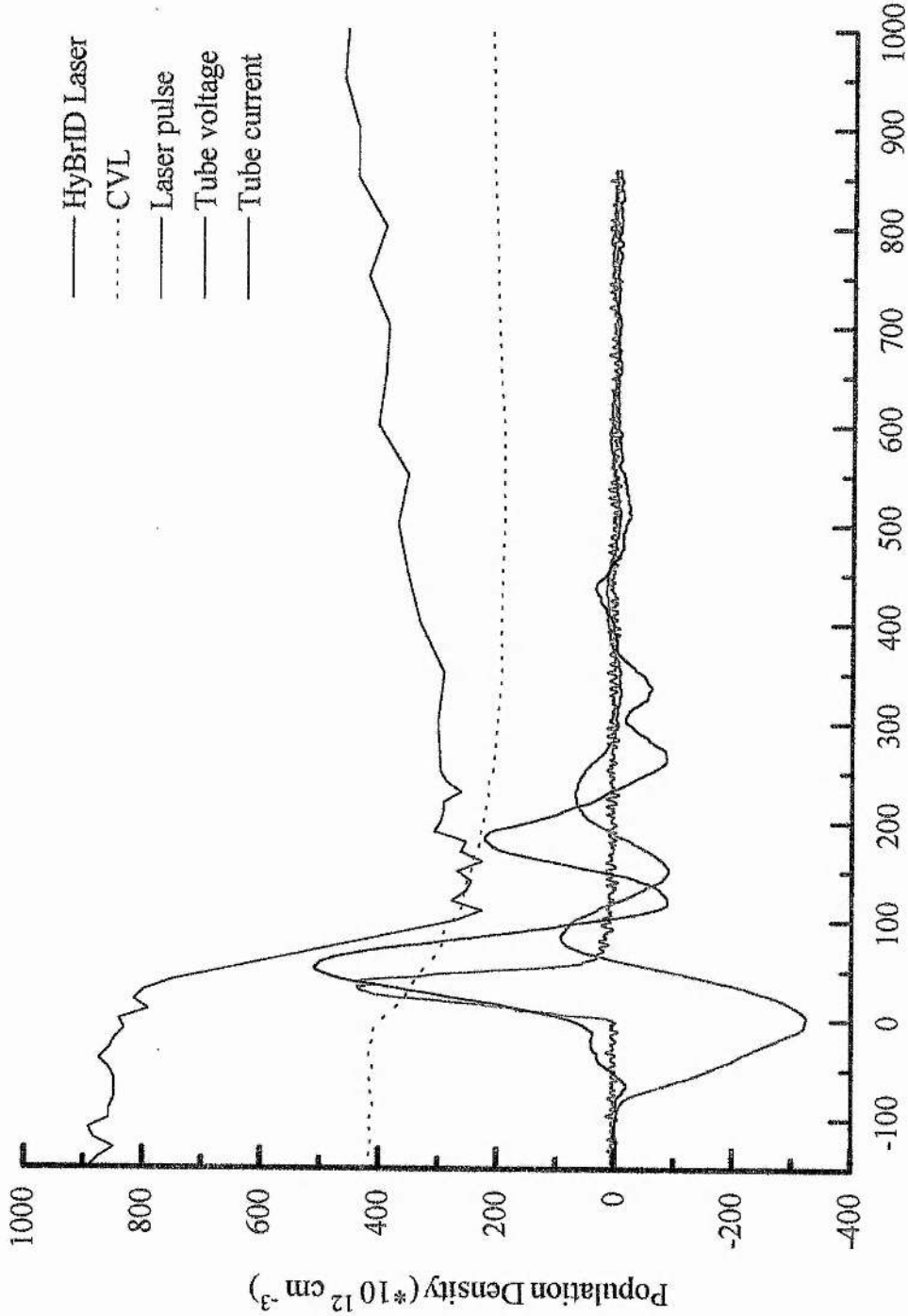


Figure 6.4 Ground state density measured using 327.4nm transition, first 1μs

was not depleted until 20 ns before the onset of laser action despite the large current flowing in the tube for fully 100 ns prior to this.

In their paper on CVL modelling Carman et al. (1994) calculate the voltage on the central, hot part of the active medium. This voltage behaves quite differently to the voltage applied to the laser head as the voltages across the anode and cathode fall regions and the cool end regions must be considered. The voltage across the hot part of the active medium does not rise at the same time as the tube voltage, but is delayed by some 100 ns. The calculated electron temperature in the hot region follows the voltage on the hot region very closely. This explanation can be applied to the case of the HyBrID laser and the observed delay in electron temperature rise may be attributed to the fact that we have not measured the voltage across the active medium. Were we able to do so we would see different behaviour, with a delayed onset of voltage and a faster rate of rise.

The ground state depletion is completed by the end of the first maximum of the current. There is little or no depletion of the ground state population caused by the second peak of the current pulse, in fact the ground state density has started to recover before the second current pulse peak. This is consistent with the discussion in Chapter 2.3.2 where it was argued that the electron temperature had fallen considerably (to ~0.5 eV) by this time and would no longer be sufficient to cause ionisation. The plasma resistance at this time is very low (calculated as ~ 10Ω) and so little power is deposited during the second excursion of the current pulse. What little power is deposited will mostly contribute to ionisation from high lying copper levels as there are low energy transitions from these levels and the rate

coefficients for these transitions remain high at low electron energies, see Figure 6.12. There are significant populations in these levels at this time, as can be seen from the measurements of the 4s 4p $^4F_{9/2}$ level population density.

The behaviour of the ground state depletion therefore supports the argument made in Chapter 2.3.2, that the electron temperature is held at a low level initially and subsequently undergoes a very rapid increase at the time that laser action commences.

### 6.1.5 THE PERIOD OF POPULATION RECOVERY

The ground state population density rises to ~75% of the pre-pulse value after only 2 μs. The recovery rate then slows.

These results have a relatively large error spread and in the late afterglow period there are significant differences between the measurements using the different resonance transitions. It is clear that there is a major discrepancy between the two measurements at time 20 μs. This point may be due to a 'rogue' measurement in the 324.8 nm results caused by a timing glitch or vibrational instability in the system causing a momentary change in interferometer alignment and hence system calibration. If this is the case then the differences between the two results are reduced though there is still a systematic difference of 5% between the two. This discrepancy may be due to variation in the laser operational parameters as the measurements were made on different days.

Because of these problems it is difficult to assess the ground state recovery in anything other than a qualitative fashion. The recovery is much faster in the HyBrID than in the CVL. The majority

of the copper atoms pumped from the ground state are ionised. The rate of ground state recovery is therefore dependent to a large degree on recombination of the copper ions. This process will be relatively rapid in the HyBrID laser compared to the CVL due to the higher ion and electron densities and the electron temperature which falls quickly. The recombined atoms are unlikely to be in the ground state, but will be in high lying levels. In the early afterglow there will be fast de-excitation of copper atoms by inelastic collision with electrons. This process will continue throughout the afterglow limited only by the falling densities of the collision partners.

### 6.1.6 RADIAL DEPENDENCE

The radially resolved results for the copper ground state density are shown in Figures 6.5 & 6.6. Figure 6.5 shows the measured population density for the full bore of the laser tube, over the full interpulse period. The same data are represented in Figure 6.6 as a series of curves each corresponding to a particular radial position.

The ground state population density is lowest on axis and highest at the wall. Measurements of the population density during the excitation pulse and in the early afterglow are poor for radial positions further from the axis. This may be due to populations which are not constant over the entire cross-section of the probe beam. Due to time constraints it was not possible to repeat the experiments with a smaller probe beam diameter in order to obtain measurements at problem positions and times (this process is not simple as one must ensure that sufficient intensity is maintained at the detector, telescopes used to match the beam size to the grating size must also be optimised.) There

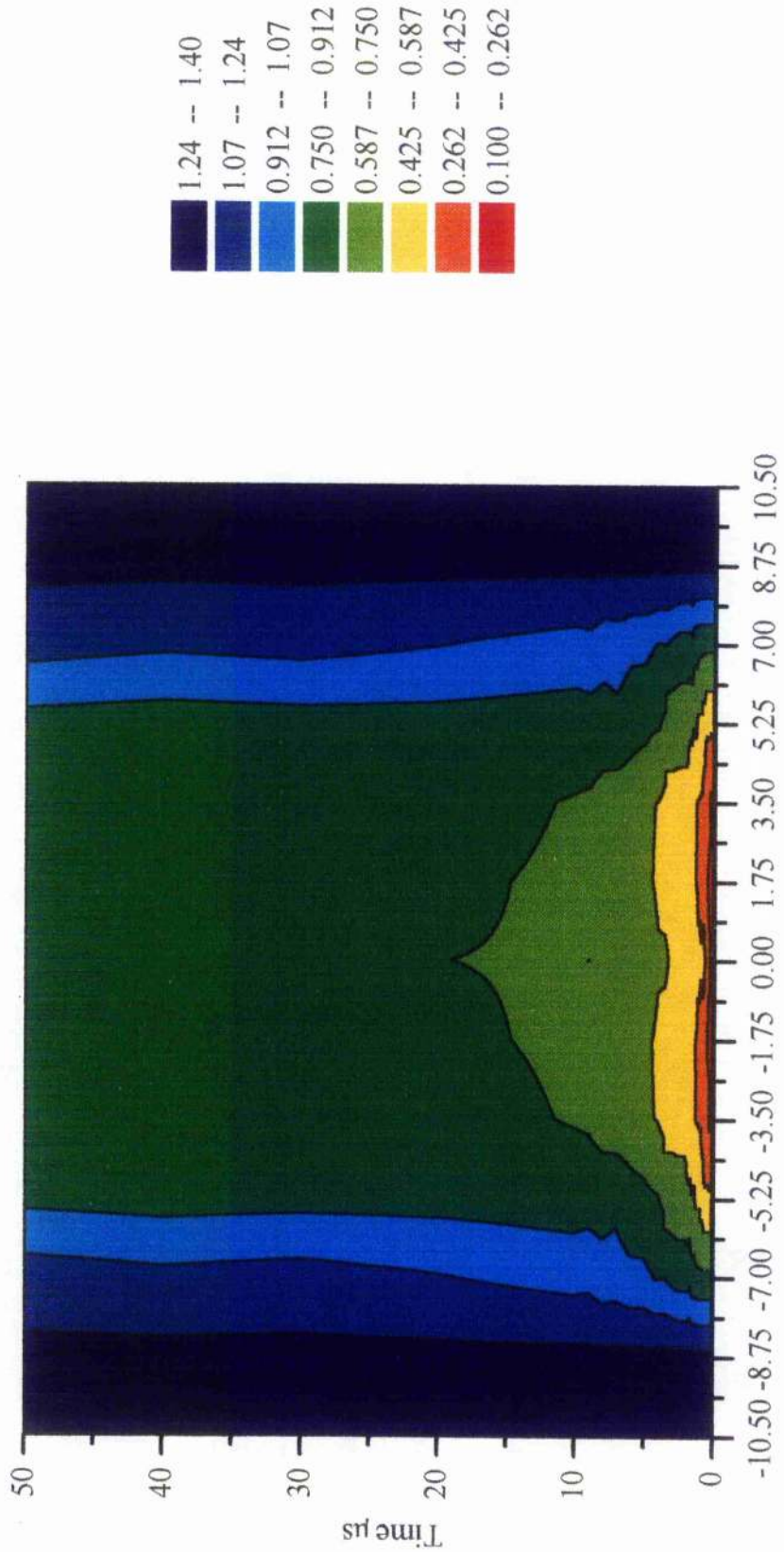


Figure 6.5. Ground state density measured using 324.8nm transition

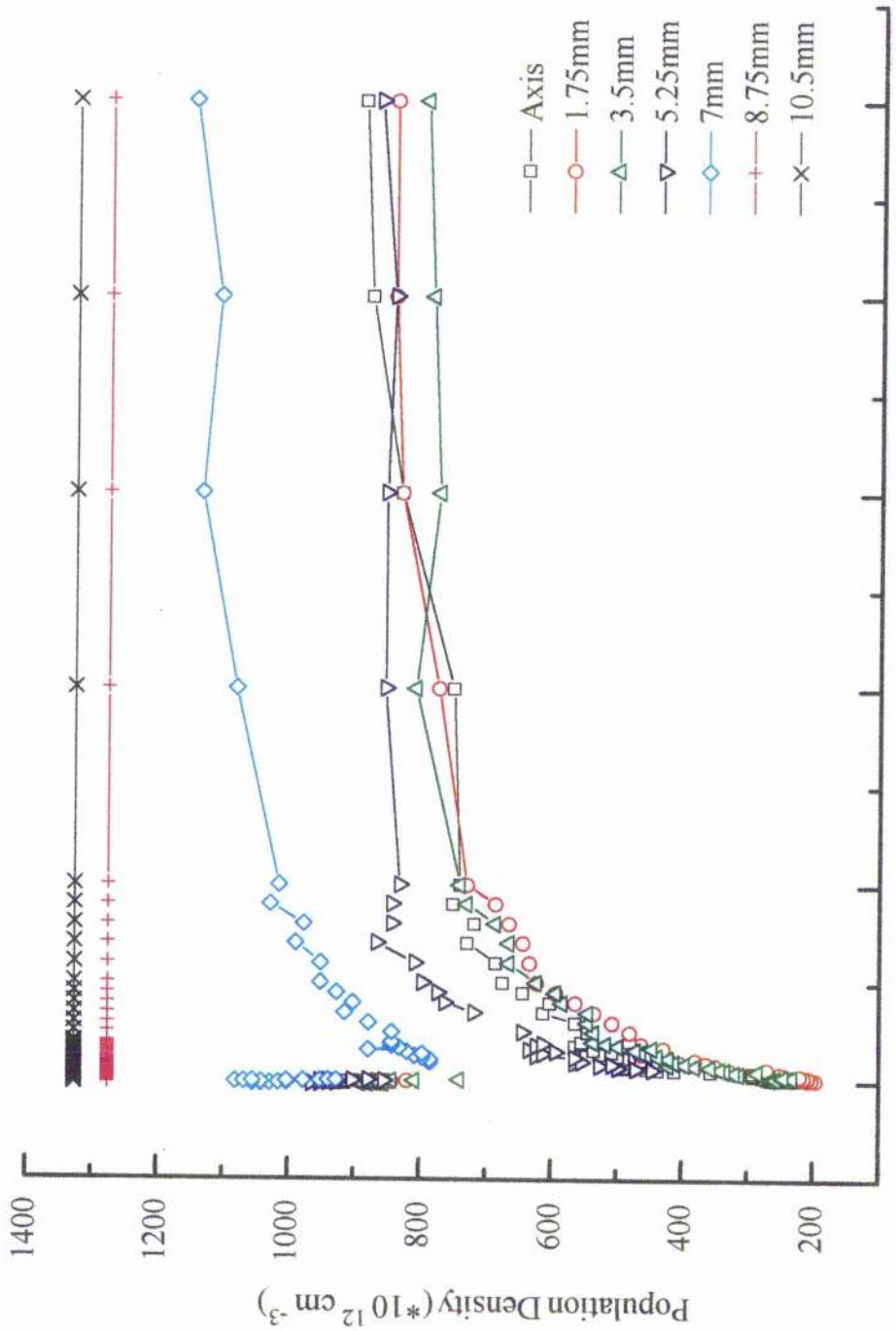


Figure 6.6 Ground state density measured using 324.7nm transition, for various radial positions

is therefore progressively less information at each radial position as distance from the tube axis is increased until, at 8.75 mm from the axis, only the pre-pulse density is known.

## 1.6(i) PRE-PULSE POPULATION DENSITY

The pre-pulse ground state density is decoupled from the wall temperature over a wide range of operating temperatures because the copper density is not controlled by the temperature of a copper reservoir. The population density is instead controlled by the reaction of HBr entrained in the buffer gas with copper pieces placed on the floor of the tube. The ground state density in the temperature range of interest (500-900 °C) is therefore controlled by the HBr concentration in the buffer gas. The radial dependence of the copper density distribution is dependent on the radial temperature profile because the gas density is dependent on the local temperature. The 'average' copper density is dictated by the HBr concentration, but the radial distribution is still temperature dependant. For this reason the gas temperature profile is important and will influence the radial dependence of many of the population densities of interest.

## 6.1.6(ii) GAS TEMPERATURE PROFLIE

The equation governing the conduction of heat through a body with power $P$ per unit volume deposited uniformly throughout the medium is (Carslaw & Jaeger 1959)

$$\nabla \cdot \left(\kappa \nabla T_g\right) + \rho C \frac{\partial T_g}{\partial t} = -P \qquad [1]$$

where $\rho$ is the density, $\kappa$ is the thermal conductivity and $C$ is the thermal capacity. If the thermal conductivity $\kappa$ varies with temperature as

$$\kappa = \kappa_o T_g^p \qquad [2]$$

then [1] may be solved for a cylindrical volume to give the gas temperature $T_g$ as a function of radial position with the boundary condition that the wall temperature $T_w$ is fixed and $T_w = T_g(R)$:

$$T_g(r) = \left[ T_w^{(p+1)} + \frac{P(p+1)}{4\kappa}\left(R^2 - r^2\right)\right]^{\frac{1}{(p+1)}}. \qquad [3]$$

Using published values of $\kappa$ and $p$ for neon (Lewis 1985) and the following physical tube parameters; tube diameter 25 mm, tube wall temperature 850 K, specific input power 4.2 x $10^6$ $Wm^{-3}$, we can calculate an axial gas temperature of 2045K. This figure is calculated from the energy stored on the switched capacitor and assumes all the energy is deposited in the active medium, this is clearly not the case as in the HyBrID system, approximately 10-15% of the energy switched is lost in the thyratron circuit (Jones 1995). Using this approximation we can calculate an axial gas temperature of 1900K. The radial gas temperature profile for the simple case is plotted in Figure 6.7.

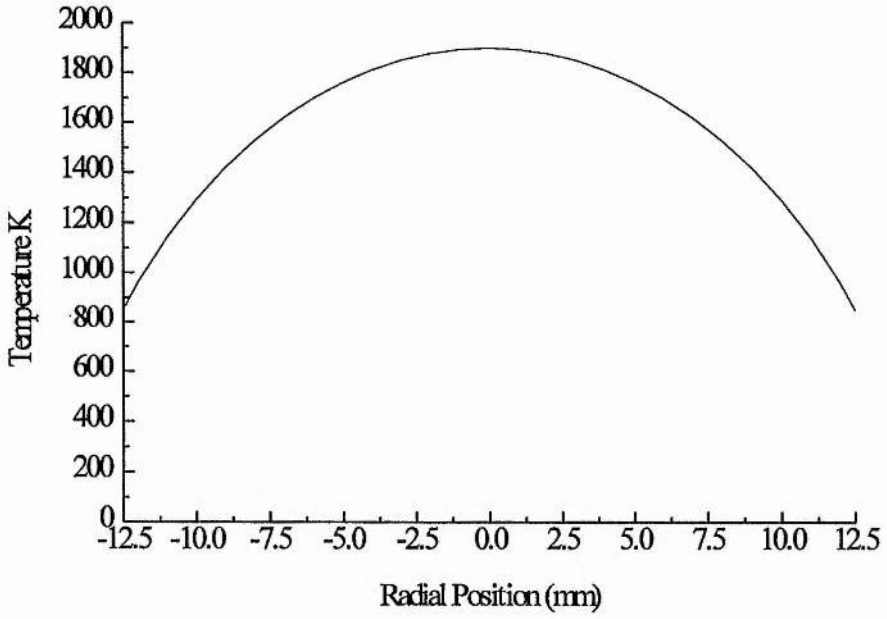


Fig 6.7. Gas temperature radial profile for uniform power deposition

These values must be regarded as a rough guide only as the energy deposition in the active volume is far from uniform due to discharge constriction, and end region effects. Also the buffer gas is not pure neon but contains hydrogen bromide. As power is coupled from the external circuit to the active medium by means of the electrons, it is reasonable to assume that energy is deposited in the tube with a distribution similar to that of the peak electron density which is strongly peaked on axis (Chapter 4.4). This will lead to a proportionately higher axial gas temperature as more power is deposited towards the centre of the tube.

The cool regions at the ends of the discharge region have too low a copper density for copper to provide all the electrons necessary to sustain the discharge current. Additional electrons must therefore be sourced from neon. Because of neon's higher ionisation energy additional specific energy is deposited in these cool regions. The

specific energy deposited elsewhere in the tube must therefore be correspondingly reduced. This will reduce the radial dependence of the gas temperature. The HyBrID system has a significant concentration of hydrogen in the active region. The hydrogen's high thermal conductivity will increase the thermal conductivity of the gas and produce a flatter radial gas temperature profile, with a lower gas temperature on axis.

The pre-pulse population density is shown as a function of radial position in Figure 6.8. The calculated gas temperature profile is also shown. The ground state population density is lowest on axis and highest at the wall. The population density does not show as strong a radial dependence as the calculated gas temperature. This may be due to the assumptions made in the calculation of the gas temperature as discussed above. Also the ground state population density measurement is an integration over the probe beam path length. In the end regions the vapour pressure of copper drops as the gas temperature falls. Due to the radial temperature gradient, the copper density will extend furthest into the end regions on axis. The path length interrogated on axis will therefore be greater than that off axis. This will lead to a systematically higher measured value of population density at positions nearer the tube axis as this variation in path length is not allowed for in the calculations (allowance for radial effects is not justified as it is difficult to assess the position where the population falls at the wall, using CuBr deposits as a guide. There is no such way to estimate the point where the population falls on axis). The results may therefore show a slightly flatter radial distribution than is really the case.

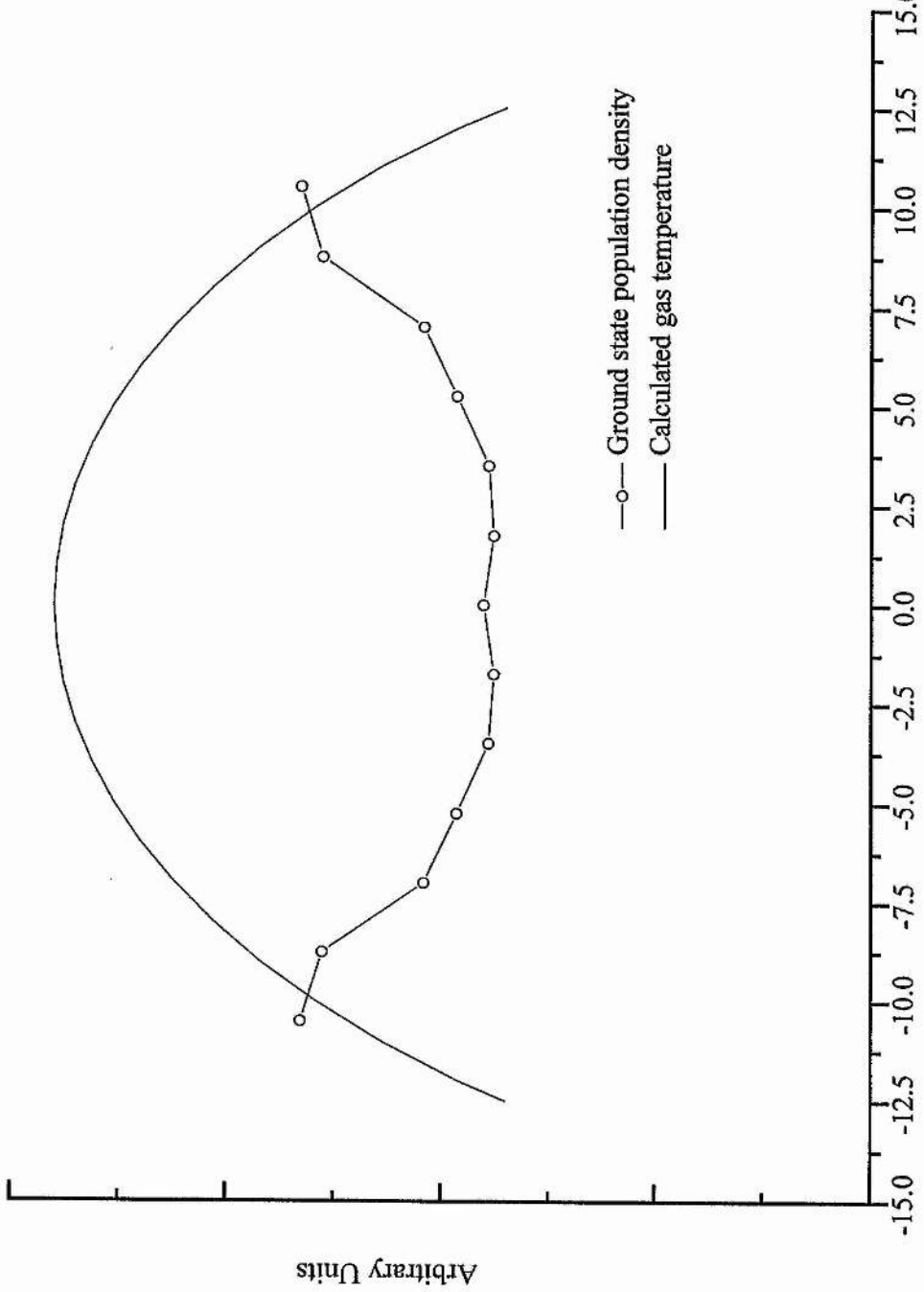


Figure 6.8 Pre-pulse ground state density and calculated gas temperature radial profiles

Figures 6.5 & 6.6 show that the ground state behaviour for the first two radial positions is very similar to the behaviour on axis. The ground state depletion and recovery are very similar to the axial case for these two positions. The differences in behaviour are not significant and may be accounted for by the scatter of the results caused by measurement inaccuracy and error. The recovery rates are similar to those seen on axis indicating that the mechanisms repopulating the ground state are most probably the same for these radial positions.

Further off axis the maximum depletion decreases with increasing distance from the axis. At 5.25 mm and 7 mm from the axis, the results are incomplete but the maximum depletions are only 50% and 30% respectively. The recovery rates after the periods of missing data are again very similar to the rates on axis.

The results for 8.75 mm & 10.5 mm from the axis contain only information on the pre-pulse population density as many of the hook interferograms for these positions were too blurred for analysis. No ground state depletion was seen at these positions, and the axially concentrated nature of the electron density suggests that there is little or no excitation of the gas so close to the tube wall.

The ground state depletion is highest on axis and at the first two radial positions, the central 7 mm of the discharge region. There is significant depletion across the central 17.5 mm of the tube. Comparison with laser pulse radial profiles (Figure 6.9) shows that the light output intensity has a similar radial dependence, the intensity is approximately constant over the central 8-9 mm and then decreases. Light output is recorded at radial positions where no ground state

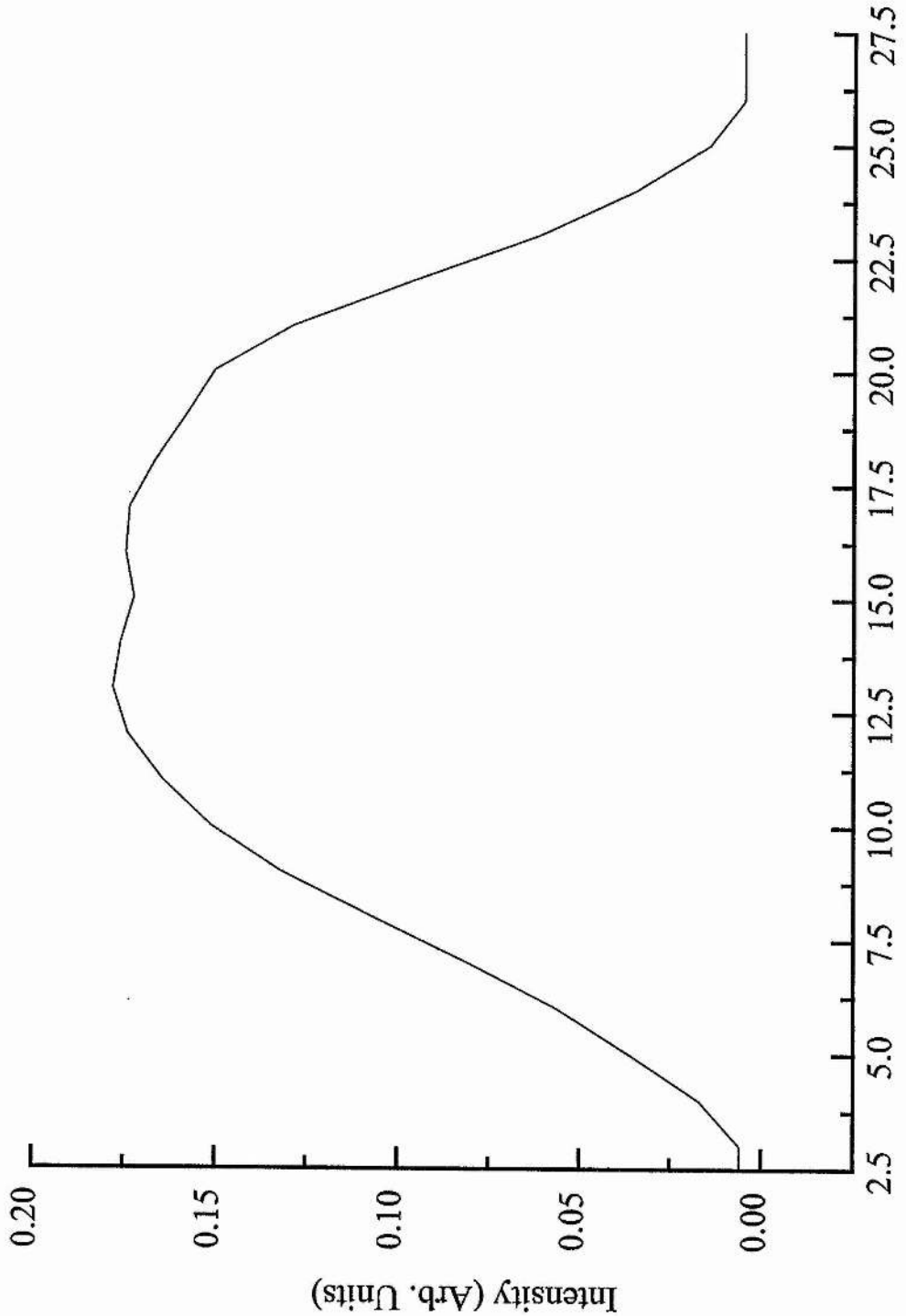


Figure 6.9 Laser pulse radial profile

depletion is seen, this may be due to ASE and highly divergent output. The light output has a bell shaped radial profile.

The radial dependence of the ground state population density shows that the active region of the gas does not extend all the way to the discharge tube walls and the full volume of the available active medium is not used. This contrasts with the results for the CVL (Hogan 1993) where excited populations are created across the entire tube bore and the light output has a 'top hat' radial distribution.

## 6.2 THE UPPER LASER LEVELS

### 6.2.1 INTRODUCTION

The results for the $4p^2P_{3/2}$ (green upper laser level) and the $4p^2P_{1/2}$ (yellow upper laser level) are shown in Figures 6.10 & 6.11, repectively, together with the HyBrID laser pulse and the results for the CVL. The general form of the results is a fast rising population which peaks after laser action has ceased. The population then falls rapidly to approximately 10% of the peak value when a period of slower fall starts. The populations have returned to ~1% of their peak value by 1 μs after the start of lasing.

### 6.2.2 THE PERIOD OF RISING POPULATION DENSITY

The population in the upper laser levels starts to rise 30-40 ns before the onset of lasing. The rise is at first relatively slow and only reaches its maximum rate of rise at the start of the laser pulse. This indicates that the pumping rate to the upper laser levels is at first quite slow and then increases to a maximum during the laser pulse. This behaviour is explained by a relatively slowly rising electron temperature and/or density. By comparison the population density in the CVL does not rise until only 10-20 ns before the onset of lasing, its initial rate of rise is then much faster than in the HyBrID laser. This indicates that it takes longer after the start of upper laser level pumping to establish inversion in the HyBrID laser.

The population density in the HyBrID laser at the start of lasing ($\sim 5 \times 10^{12} cm^{-3}$) is higher than in the CVL ($\sim 3 \times 10^{12} cm^{-3}$), indicating a higher lower laser level population density. The relatively high lower laser level population densities may be due to an increased pre-

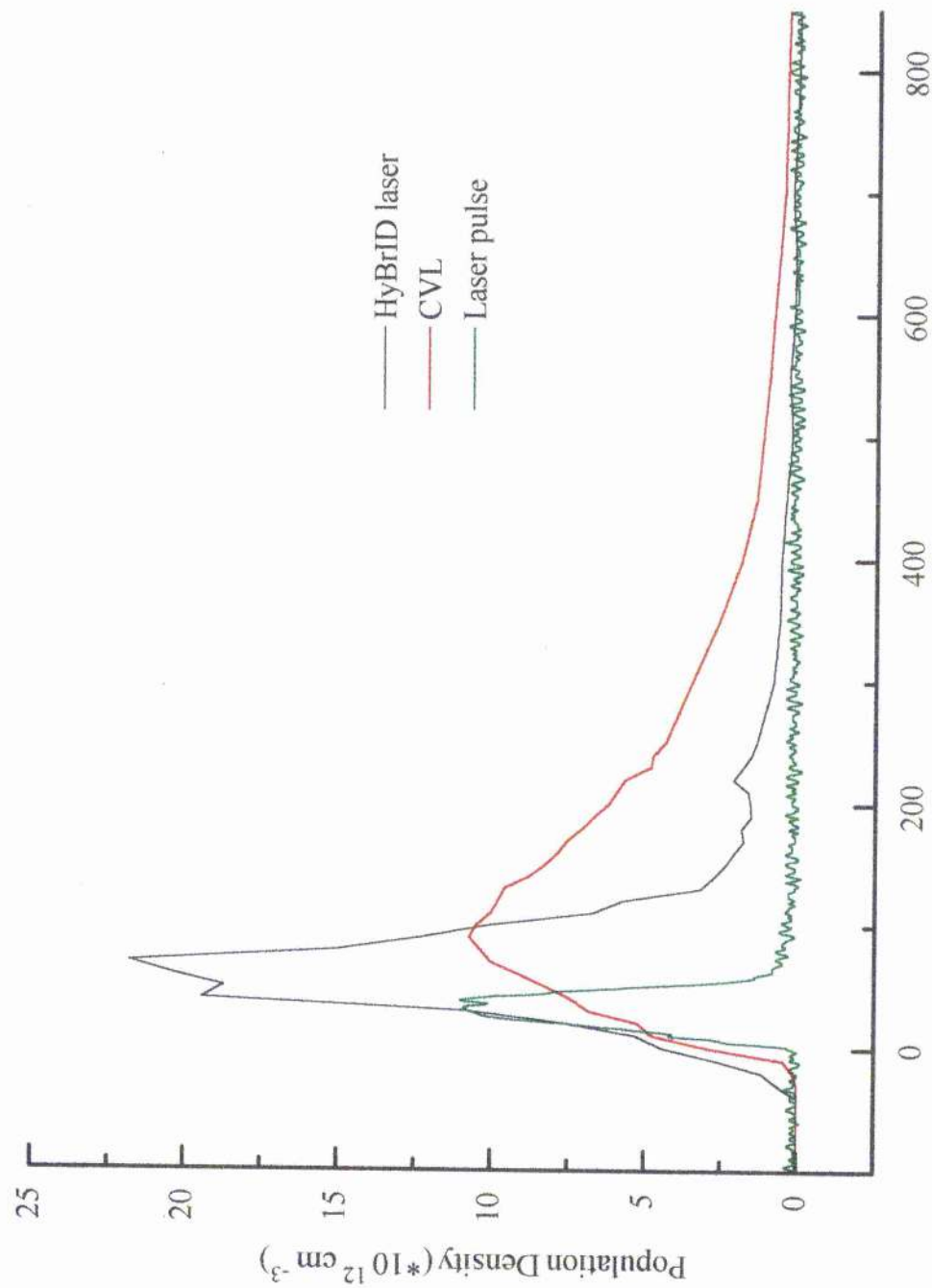


Figure 6.10 Green upper laser level population density

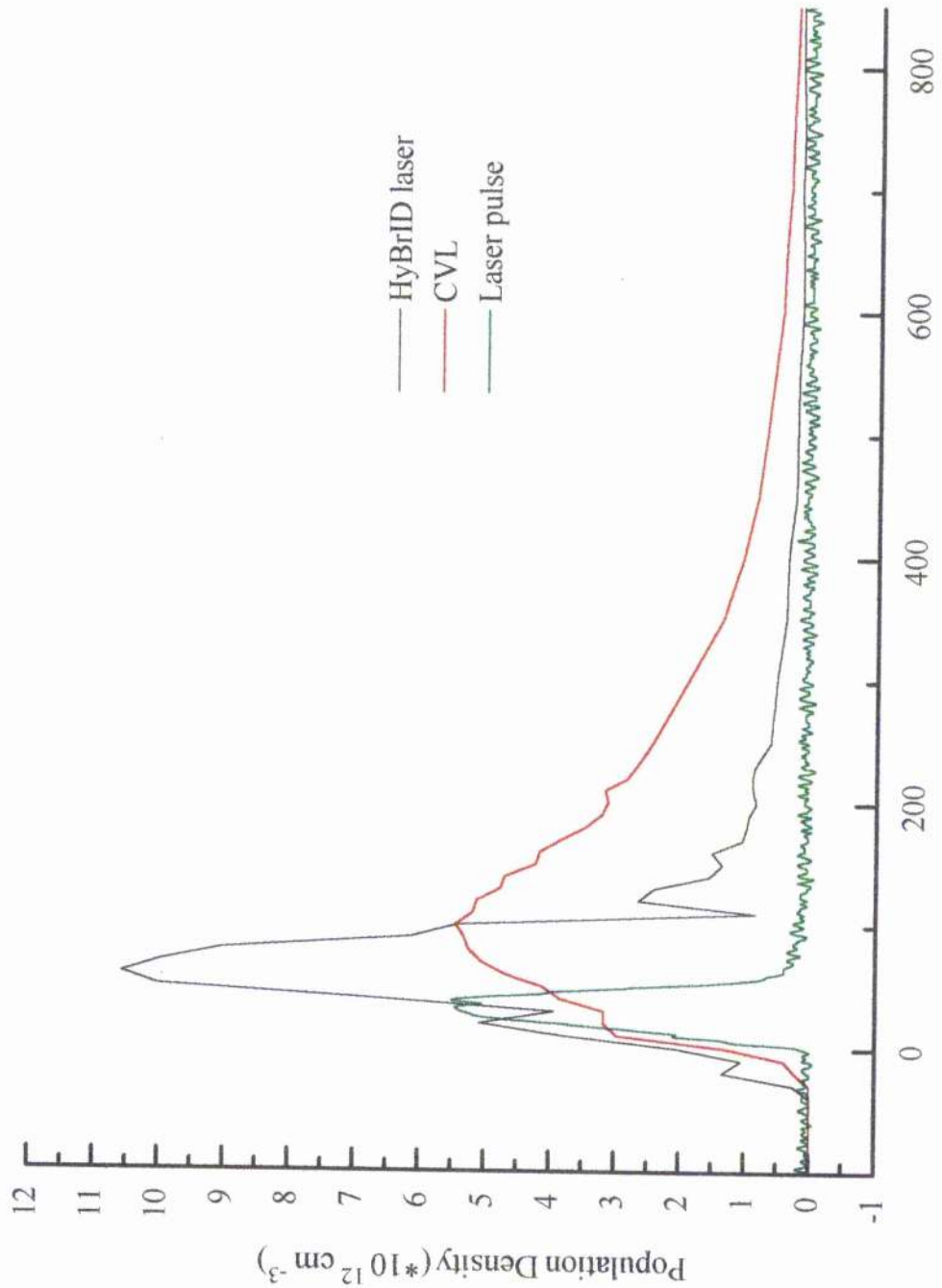


Figure 6.11 Yellow upper laser level population density

pulse population density. In the CVL the pre-pulse metastable density is dictated by the electron temperature. Models of the CVL system (Carman et al. 1994) show the metastable density at times after 10 μs is close to that calculated assuming Boltzmann equilibrium at the electron temperature. The decay rate is then limited by the electron temperature which is itself maintained at a relatively high level by recombination heating. In the HyBrID system the electron temperature falls much more quickly, but the PRF is approximately three times that in the CVL. The metastable population density in the HyBrID may therefore not have fallen to the Boltzmann equilibrium value before the next pulse. Experiments in double pulse CuCl systems indicated lasing extinguished at low pulse pair separations due to excessive metastable population densities. (Isaev et al. 1986b)

The rate coefficients for several transitions are shown in Figure 6.12, this figure is reproduced by kind permission of Dr RJ Carman from his paper (Carman et al. 1994).

An alternative explanation to that given above is that there will be a period at the start of the excitation pulse when pumping from the ground state to the lower laser levels by electron impact occurs preferentially. This happens when the average electron energy is in the range 0.25 - 1.5 eV (curve 1 is above curve 2 in Figure 6.12). The lower laser level population density increase in this period will depend on the rate at which the electron temperature rises.

Both the upper laser level population densities exhibit some structure on the leading edge. After the period of initial slow increase in population density discussed above, there is a period of fast increase in population density. This period of fast increase is not

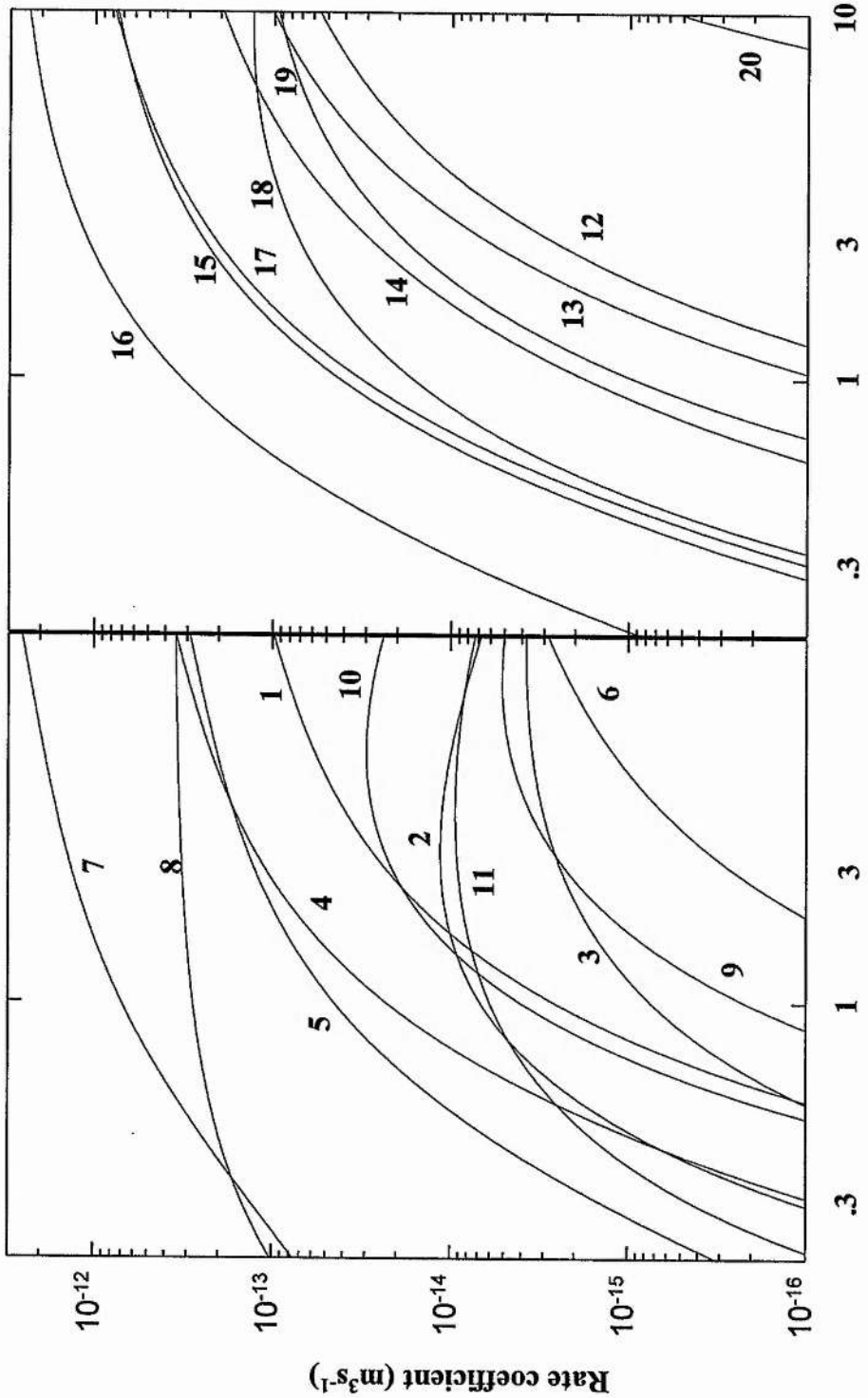


Figure 6.12 Rate coefficients for various transitions in copper

| Curve | Initial level | Final level |
|---|---|---|
| 1 | $3d^{10}\ 4s\ ^2S_{1/2}$ | $3d^{10}\ 4p\ ^2P_{3/2}$ |
| 2 | $3d^{10}\ 4s\ ^2S_{1/2}$ | $3d^9\ 4s^2\ ^2D_{5/2}$ |
| 3 | $3d^9\ 4s^2\ ^2D_{5/2}$ | $3d^{10}\ 4p\ ^2P_{3/2}$ |
| 4 | $3d^{10}\ 4p\ ^2P_{3/2}$ | $3d^9\ 4s^2\ ^2D_{5/2}$ |
| 5 | $3d^{10}\ 4p\ ^2P_{3/2}$ | $3d^{10}\ 5s\ ^2S_{1/2}$ |
| 6 | $3d^9\ 4s^2\ ^2D_{5/2}$ | $3d^{10}\ 5p\ ^2P_{3/2}$ |
| 7 | $3d^{10}\ 5s\ ^2S_{1/2}$ | $3d^{10}\ 5p\ ^2P_{3/2}$ |
| 8 | $3d^9\ 4s^2\ ^2D_{5/2}$ | $3d^9\ 4s^2\ ^2D_{5/2}$ |
| 9 | $3d^{10}\ 4s\ ^2S_{1/2}$ | $3d^9\ 4s(^3D)\ 4p\ ^4P,\ ^4D,\ ^4F$ |
| 10 | $3d^9\ 4s^2\ ^2D_{5/2}$ | $3d^9\ 4s(^3D)\ 4p\ ^4P,\ ^4D,\ ^4F$ |
| 11 | $3d^{10}\ 4p\ ^2P_{3/2}$ | $3d^9\ 4s(^3D)\ 4p\ ^4P,\ ^4D,\ ^4F$ |
| 12 | $3d^{10}\ 4s\ ^2S_{1/2}$ | $3d^{10}\ ^1S_0 + e^-$ |
| 13 | $3d^9\ 4s^2\ ^2D_{5/2}$ | $3d^{10}\ ^1S_0 + e^-$ |
| 14 | $3d^{10}\ 4p\ ^2P_{3/2}$ | $3d^{10}\ ^1S_0 + e^-$ |
| 15 | $3d^{10}\ 5s\ ^2S_{1/2}$ | $3d^{10}\ ^1S_0 + e^-$ |
| 16 | Excited copper pseudo-state | $3d^{10}\ ^1S_0 + e^-$ |
| 17 | $3d^9\ 4s(^3D)\ 4p\ ^4P,\ ^4D,\ ^4F$ | $3d^{10}\ ^1S_0 + e^-$ |
| 18 | $3d^{10}\ ^1S_0$ | Excited ion pseudo-state |
| 19 | Excited ion pseudo-state | Doubly excited ion pseudo-state |

Table 6.12 Designation of curves in Figure 6.12

continuous however and there are time points on each trace where the population density decreases only to increase again. In the case of the yellow upper laser level the dip coincides with the peak in laser emission. (The laser pulse shown on these traces is the combined green and yellow output)

The dip in the population of the green upper laser level may be explained by examination of the data before averaging of the two measurements made at each time point, Figure 6.13. The scatter of the points is large compared to that at other time points and a smooth peak may be drawn through the data points. If we disregard a single measurement, either at time 40 ns or 50 ns, then the plot would show no dip in the peak. It is likely that error caused by either timing jitter or vibrational instability in the apparatus is the source of the dip in the peak and no such feature exists in the true population density.

The above explanation may not be applied to the description of the yellow upper laser level population. Examination of the non-averaged data (Figure 6.14) shows that while the dip in population may not be quite as pronounced as the averaged results indicate, the population density rate of rise definitely reduces and then increases at this time.

This feature may be due to de-population of the upper laser level by radiative de-excitation to the lower laser levels. This mechanism will vary in time due to changes in the stimulating radiation flux.

In the copper vapour laser inversion is never established in the sense that the upper laser level population never exceeds that in the lower laser level. Lasing occurs as a result of the ratio of the

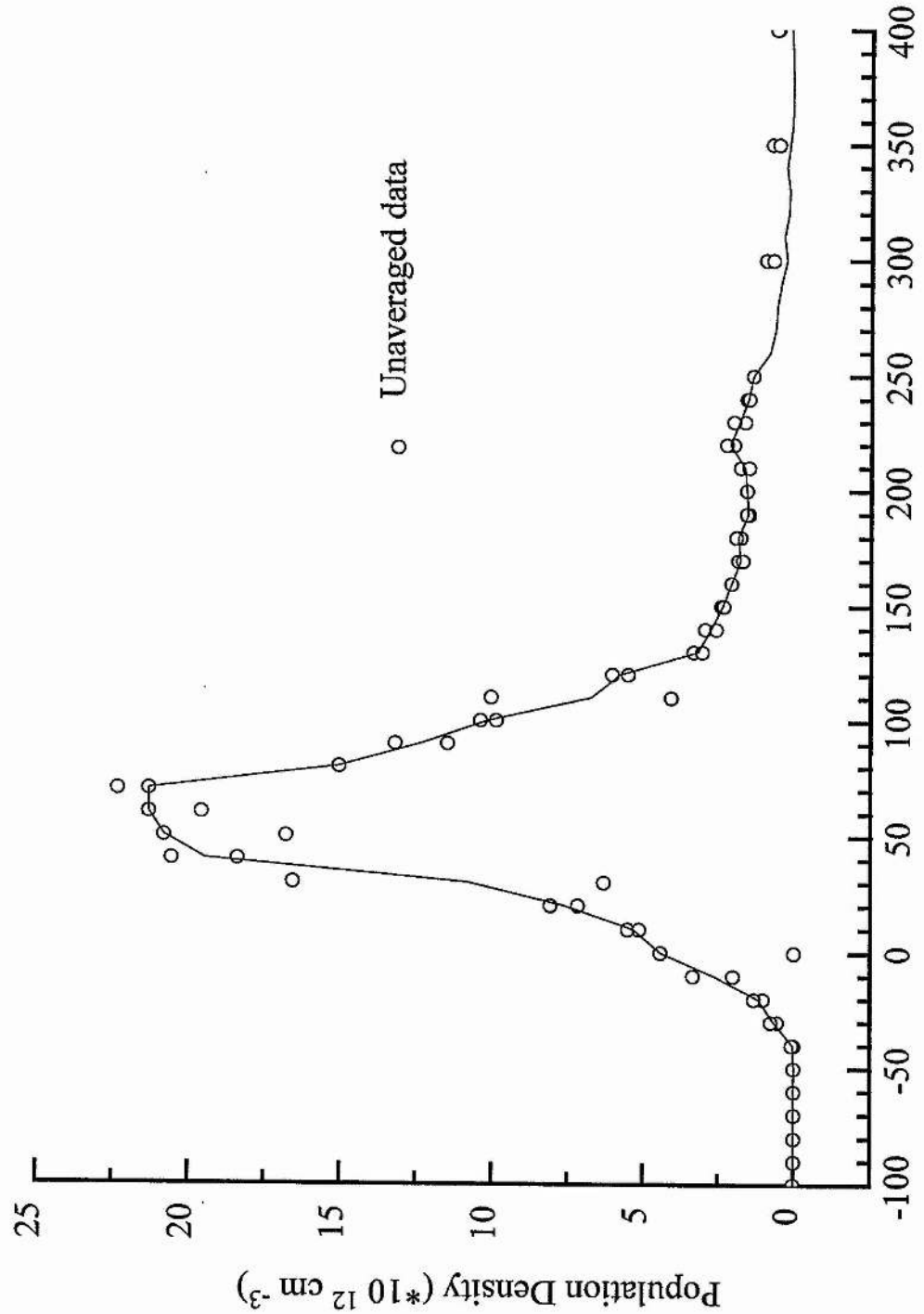


Figure 6.13 Unaveraged green upper laser level data

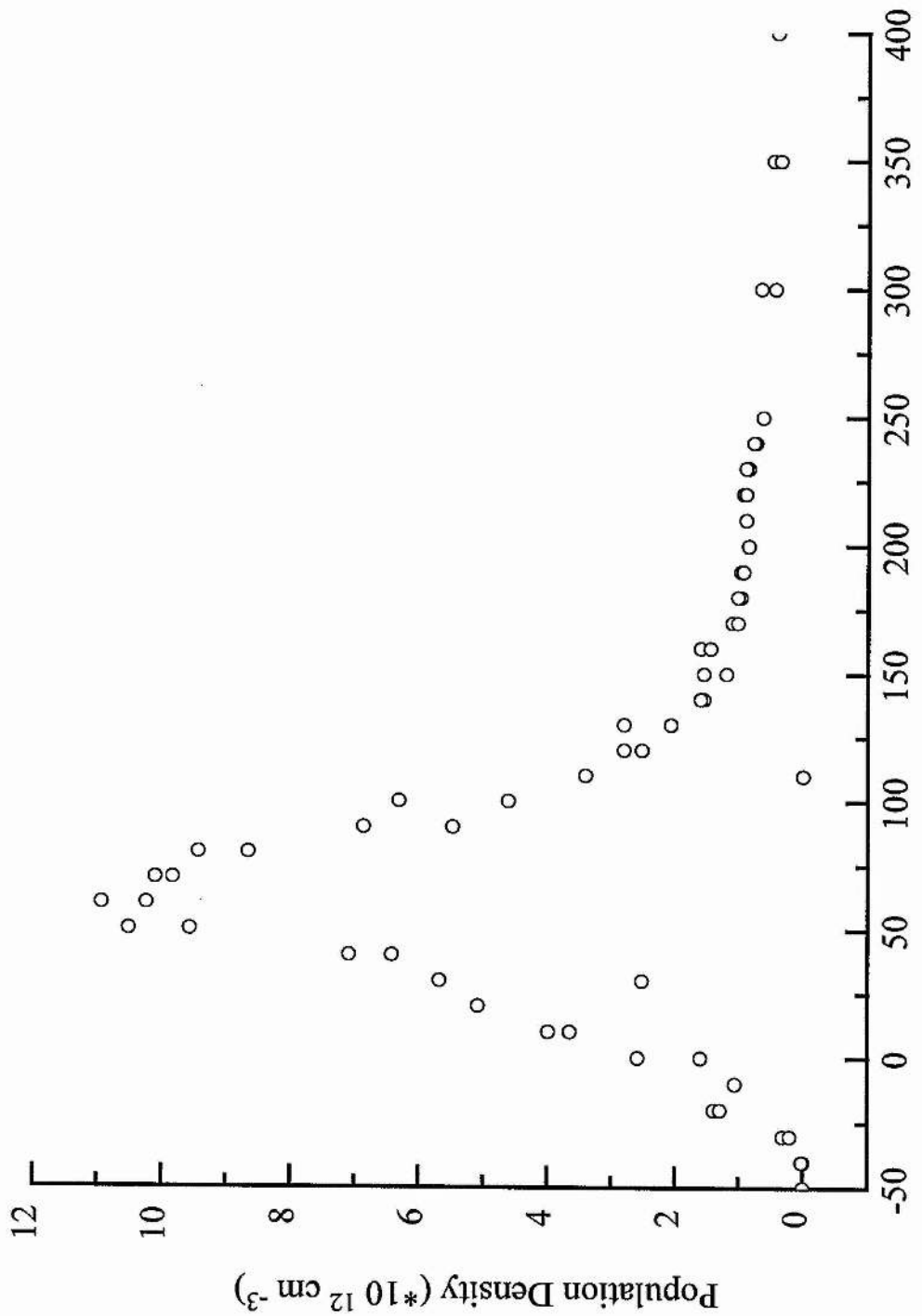


Figure 6.14 Unaveraged yellow upper laser level data

degeneracies in the upper and lower laser levels (1:1.5 & 1:2 in the green and yellow respectively). When the relative populations reach threshold, gain is established. A short time later the gain will exceed the cavity round trip losses and lasing will start. Light emitted near the output coupler end of the tube collinear with the cavity axis will be amplified as it travels towards the high reflector. The seed radiation gains intensity until it depletes the local inversion. As the lost inversion cannot be instantaneously replaced this leads to an area of depleted gain immediately behind the light pulse. Light entering this region will not be amplified and the light intensity behind the pulse will be much lower. In this way saturation of the gain results in a pulse of light travelling through the active medium with very little light behind it. When this light pulse reaches the output coupler 92% of it is coupled out of the cavity as laser output and 8% is fed back to seed the next cavity round trip. The 8% feedback then goes through the same process of amplification and gain saturation during the next round trip and another pulse of light is produced. In this manner a sequence of pulses having performed an even number of passes through the active medium is produced. A similar process happens with light starting in the opposite direction from the high reflector end which exits the resonator after an odd number of traversals through the active medium. In this case the pulses are of lesser intensity due to the fact that 92% is lost after only one pass through the active medium and on the second round trip the gain may not have fully recovered from the depletion due to the light pulse starting at the output coupler. In this manner we obtain an output composed of the sum of a series of light pulses. As the light pulses generated from seed radiation

generated at the high reflector are of lesser intensity, they are often obscured by light pulses which have performed an even number of passes and the output appears to be modulated at the cavity round trip time. The magnitude of the light peaks gives an indication of the gain available in the laser medium during the preceding round trip period.

The laser pulse shown in Figures 6.10 & 6.11 has peaks due to several distinguishable pulses. There are two slight steps on the leading edge which may be attributed to single and double pass emission. There is a further slight step in the leading edge due to the fourth pass. The next peak reaches the maximum intensity of laser emission and corresponds to light which has passed through the active medium six times, the next peak of equal amplitude has performed eight passes and the remaining passes see reduced gain and hence have lower intensity. The tenth pass shows as a slight step on the falling edge.

The circulating laser field changes in time as described above. The yellow upper laser level has a dip in the population coincident with the sixth pass peak of the laser emission. As the ratio of the degeneracies of the upper and lower laser levels for the green transition is 2:1 while that for the yellow transition is only 3:2 and electron collisional cross-sections tend to be similar to optical transition probabilities, the inversion for the yellow transition will take longer to recover after saturation. This explains why there is a pronounced dip in population density in the yellow upper laser level population and not in the green upper laser level population.

### 6.2.3 PEAK POPULATION DENSITY

The peak population density in the upper laser levels is approximately twice that in the CVL. The population peaks slightly (20-30 ns) earlier in the pulse.

The population densities in the two upper laser levels peak at almost the same time. The separation is at most 10 ns which is the same as the time step interval for this period of the discharge. The observed difference in peak timing may therefore be accounted for by error in peak position determination due to the frequency of the measurements and experimental error as discussed in Chapter 5.5.6

The two upper laser levels have very similar energies and we would expect them to be populated in a ratio equivalent to their degeneracies. That is the ratio of the $4p^2P_{3/2}$ population to the $4p^2P_{1/2}$ population should be 2:1. A plot of the two upper state population densities scaled in this ratio is shown in Figure 6.15. The two traces are very similar with only slight variation between the two. It has been shown (Hollins 1980; Lewis 1985) that there is insignificant collisional mixing between the two upper levels on the timescale of the lifetime of an atom in these levels, therefore deviation from the statistical weight ratio of 2:1 is possible. In the case of the CVL the ratio between the upper laser level populations has been variously measured as 1.9:1 (Brown 1988), 1.5:1 - 1.9:1 (Hogan 1993) and 1.6:1 (Lewis 1985)

The relative optical transition probabilities within a multiplet were studied by Woodgate (Woodgate, 1980.) For transitions with $\Delta L = \pm 1$ the strongest transitions are those with $\Delta J$ of the same sign. For the $3d^{10}4p^2P_{1/2}$ level this corresponds to the $3d^{10}4d^2D_{3/2}$ level, for the

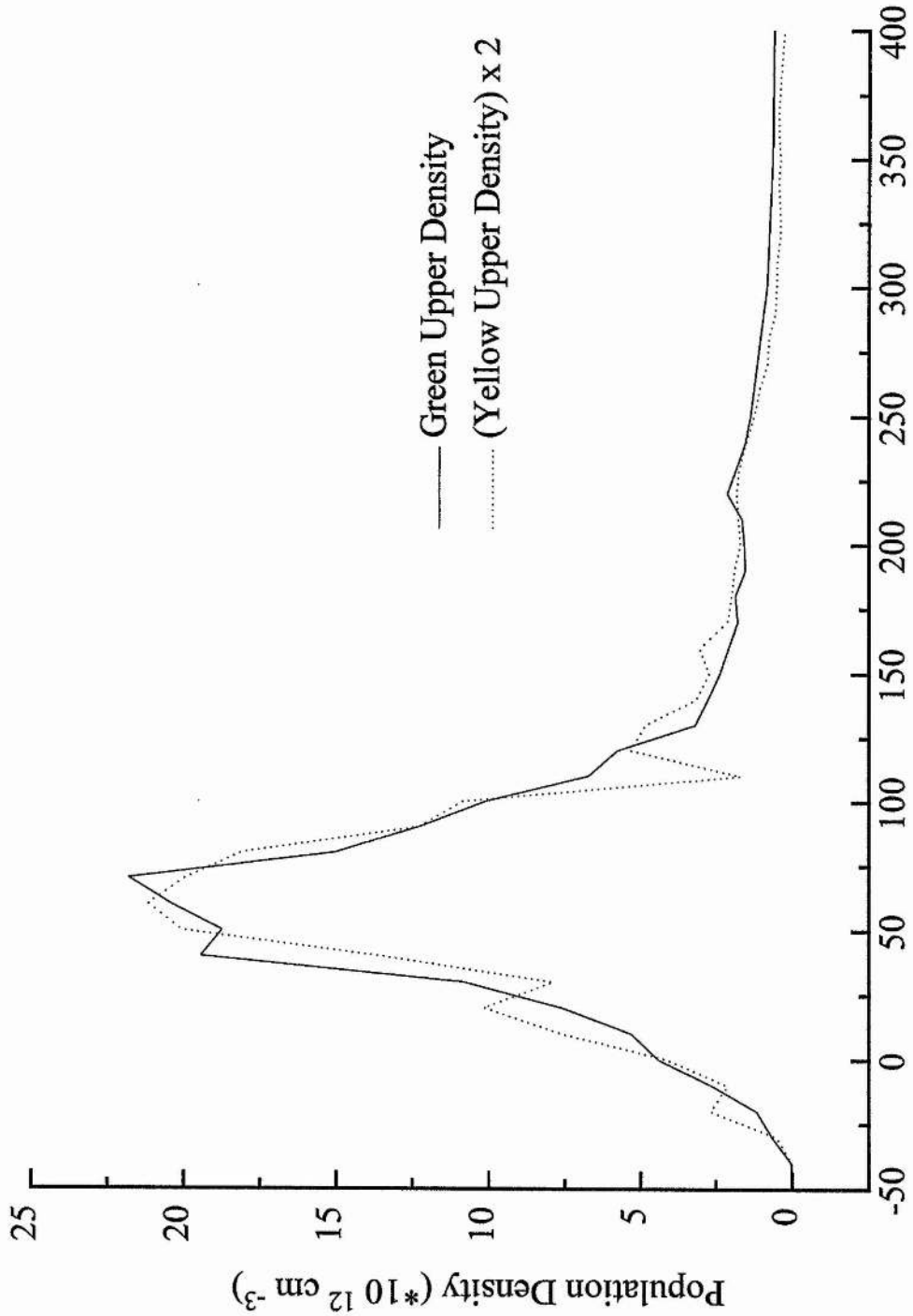


Figure 6.15 Comparison of green and yellow upper laser level population densities

$3d^{10}4p^2P_{3/2}$ the allowed transition is to the $3d^{10}5s^2S_{1/2}$. In addition there are allowed 'cross-over' transitions from the $3d^{10}4p^2P_{3/2}$ to the $3d^{10}4d^2D_{3/2}$ & $3d^{10}4d^2D_{5/2}$. The converse transitions from the $3d^{10}4p^2P_{1/2}$ are entirely optically forbidden. Whilst electron collision cross-sections are not constrained to follow the optical transition possibilities they generally tend to exhibit similar behaviour. This argument shows that there is a relatively larger number of mechanisms influencing the green upper laser level population than the yellow upper laser level and this may result in deviation from the ratio of the statistical weights.

An explanation has been proposed for the difference in leading edge and peak structure (Chapter 6.2.2). The only remaining large difference is a single time point at 110 ns. It is likely that this is due to timing jitter or instability in the measurement of the yellow upper laser level population density as only one of the two data points taken for this time point deviates from the trend of a relatively rapid decay (see Figure 6.14).

### 6.2.4 THE PERIOD OF FALLING POPULATION DENSITY

The populations in both the upper laser levels initially decay very quickly. 120-130 ns after the start of the laser pulse the decay rate changes and subsequently population is removed much more slowly. It is not practical to fit an exponential decay curves to this data as there are two few data points in the initial period of decay to allow a reasonable confidence figure for the fit and the scatter in the results after the change in decay is large due to the low population density at these time points. The population decays more rapidly in the HyBrID

than in the CVL though in both cases the remaining population at time 1 μs is very low. The CVL populations also show a two stage decay which may be due to a change in depopulation mechanism due to falling electron temperature (Hogan 1993).

Population may be removed from the upper laser levels by radiative emission to the ground state, radiative emission to the lower laser levels, excitation to higher lying levels or super-elastic collisional de-excitation. Population may also feed into the upper laser levels from higher lying levels. Emission at the resonance wavelengths will not escape the plasma due to the high density of ground state atoms (radiation trapping), this mechanism is therefore removed. Laser emission has ceased before the upper laser level populations start to decrease, therefore stimulated emission cannot account for the decay in upper laser level population.

Both super-elastic de-excitation and excitation to higher lying levels are dependent on electron temperature. Super-elastic collisions will be of lesser importance when the electron temperature is high and the rate coefficient for excitation to higher lying levels is low for electron energies below 0.5 eV, see Figure 6.12. These two mechanisms will dominate the depopulation of the upper laser levels in different electron energy regimes. There may also be effects due to population cascading into the upper laser levels from higher lying levels, this will be most significant at low electron energies and is discussed in Chapter 6.4, with regard to the quartet levels of copper.

During the laser pulse the electron temperature must be high as pumping of the upper laser levels outstrips pumping of the lower laser levels. At this electron energy the rate coefficient for excitation from

the upper laser levels to the $3d^{10}5s^2S_{1/2}$ and $3d^94d^2D_{5/2}$ & $3d^94d^2D_{3/2}$ levels will be high (Figure 6.12) and significant population is lost from the upper laser levels through this mechanism. The rate coefficient for excitation to higher lying levels remains at least 4 times that for resonance excitation for electron energies below 10 eV (Figure 6.12, curve 5 & curve 11 compared to curve 1). The difference in population density between the ground state and the upper laser levels more than compensates for this imbalance in the rate coefficients early in the excitation pulse when the electron temperature is high. As the electron temperature falls due to the falling tube voltage the rate constant for the resonance transitions falls off more quickly than the rate constant for excitation to higher lying levels. This, in combination with the erosion of the ground state population density causes the rate for excitation to higher levels to become greater than for resonance excitation and net population will be removed from the upper laser levels. In combination with the rising lower laser level population density this erodes the population inversion and optical gain is replaced by absorption, causing the laser pulse to extinguish. At this time the tube voltage has fallen to zero. Calculations of the voltage on the plasma corrected for laser head inductance effects have shown (Chapter 2.3.1) that after this time very little voltage is developed across the plasma. The electron temperature must therefore fall monotonically, though it will be buoyed by recombination heating. The calculated electron temperature on axis (Chapter 4.3.5(ii)) at time 400 ns was approximately 0.5 eV, this indicates that excitation to higher lying levels remains an important process throughout the period of upper laser level population decay.

As the electron temperature falls super-elastic de-excitation will proceed at a higher rate and excitation to higher lying levels will slow. There will be a point at which the dominant mechanism of upper laser level depopulation ceases to be upwards to higher lying levels and becomes downwards de-excitation by super-elastic collisions. It is not clear at what electron energy super-elastic de-excitation will start to dominate the upper laser level depopulation behaviour but there is a definite change in upper laser level depopulation rate at time 120-130 ns. This may be due to a change in depopulation mechanism.

Similar behaviour is seen in the CVL though the change in decay rate occurs at a later time ~500 ns. This is consistent with the suggestion that the electron temperature falls more quickly in the HyBrID laser system due to cooling by hydrogen.

### 6.2.5 RADIAL DEPENDENCE

The radially resolved measurements of the green and yellow upper laser level populations are shown in Figures 6.16 & 6.17. The same results are shown as a family of curves in Figures 6.18 & 6.19. The data is shown for the period from 100 ns before the timing origin to 400 ns after the start of lasing. The population density is low (< 5% of the peak value) at all other times.

The population is strongly axially concentrated, no population is measured outside the central 17.5 mm and more than 90% of the population is created inside the central 10 mm. The populations peak at similar times although there is a slight delay ( < 20 ns) between the peak on axis and 3.5 mm off axis in the yellow upper laser level population. The maximum population in the green upper laser level is

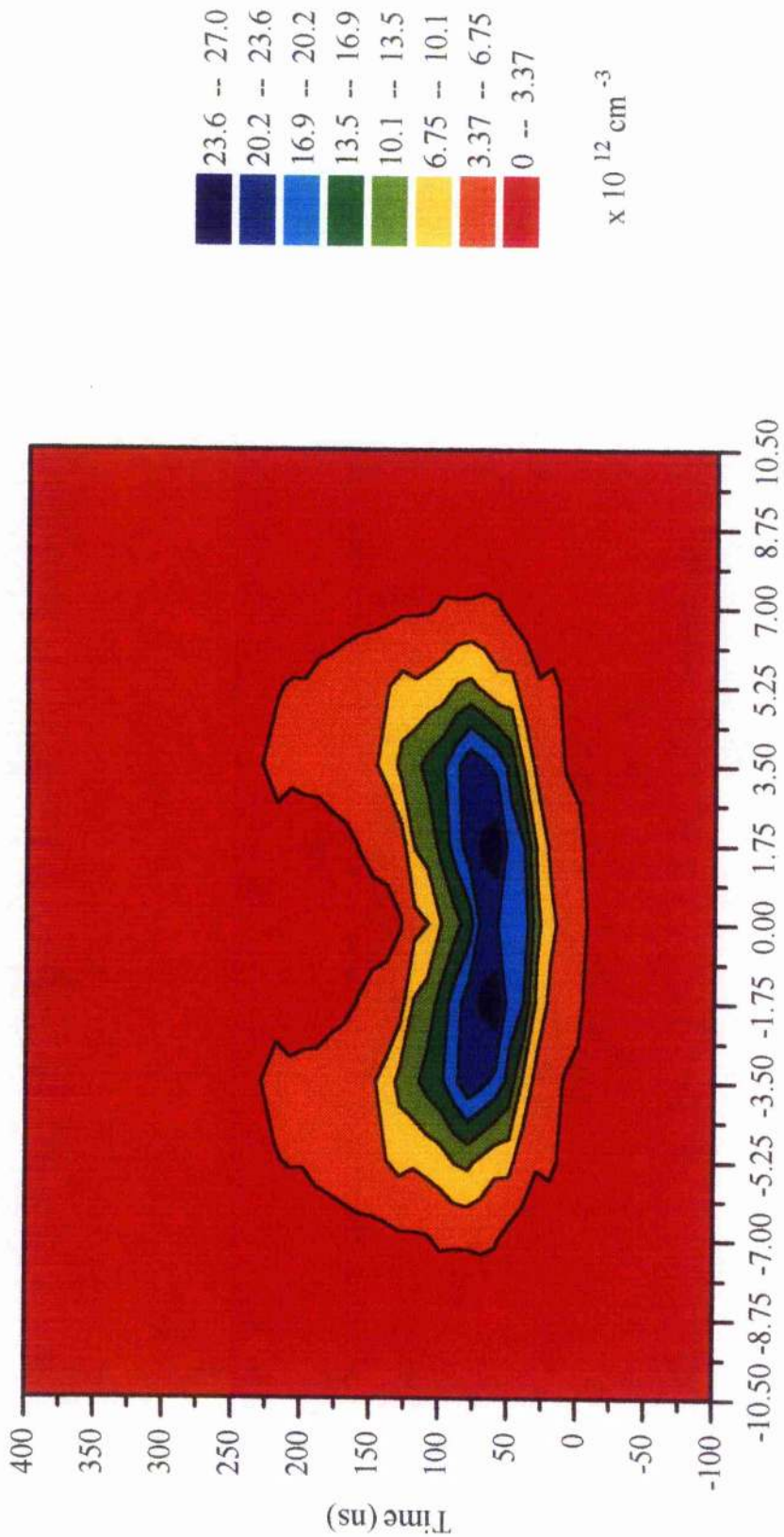


Figure 6.16 Green upper laser level population density

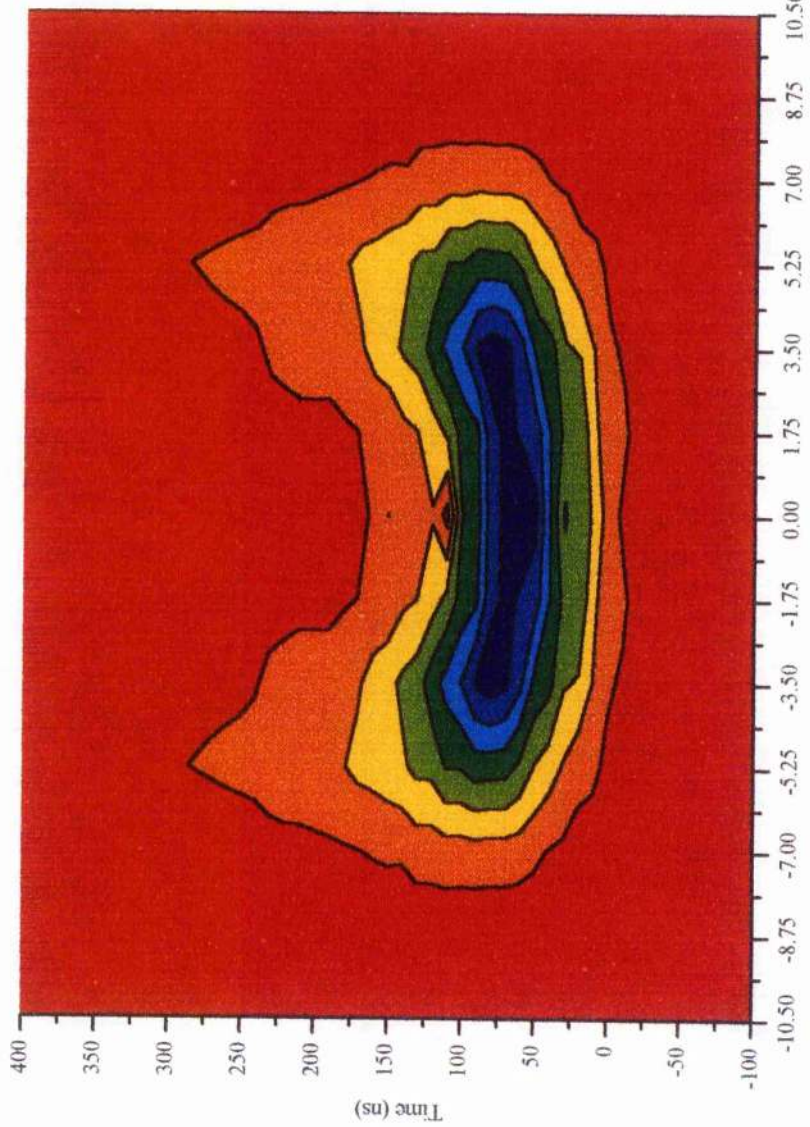


Figure 6.17 Yellow lower laser level population density

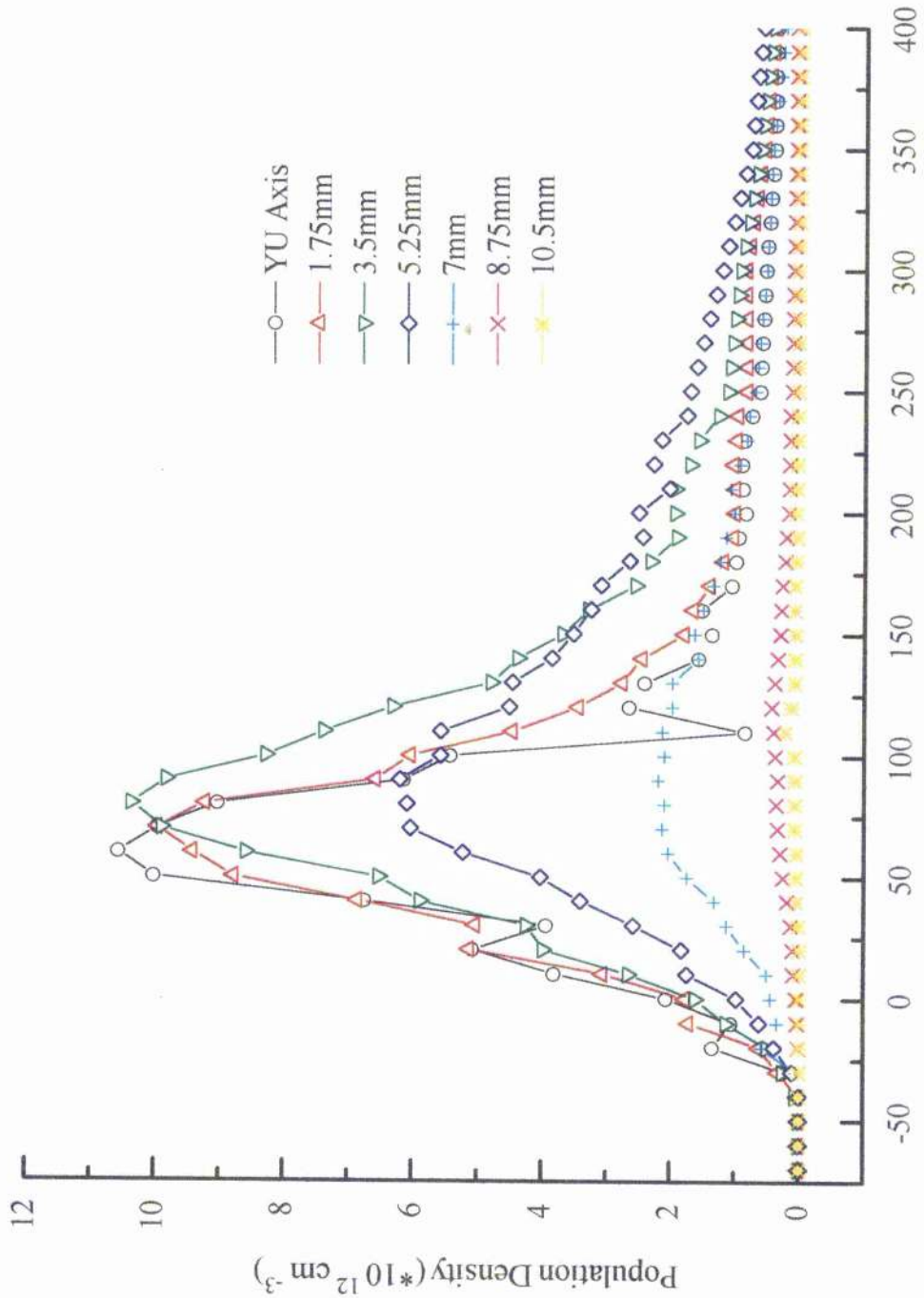


Figure 6.19 Yellow lower laser level population density for various radial positions

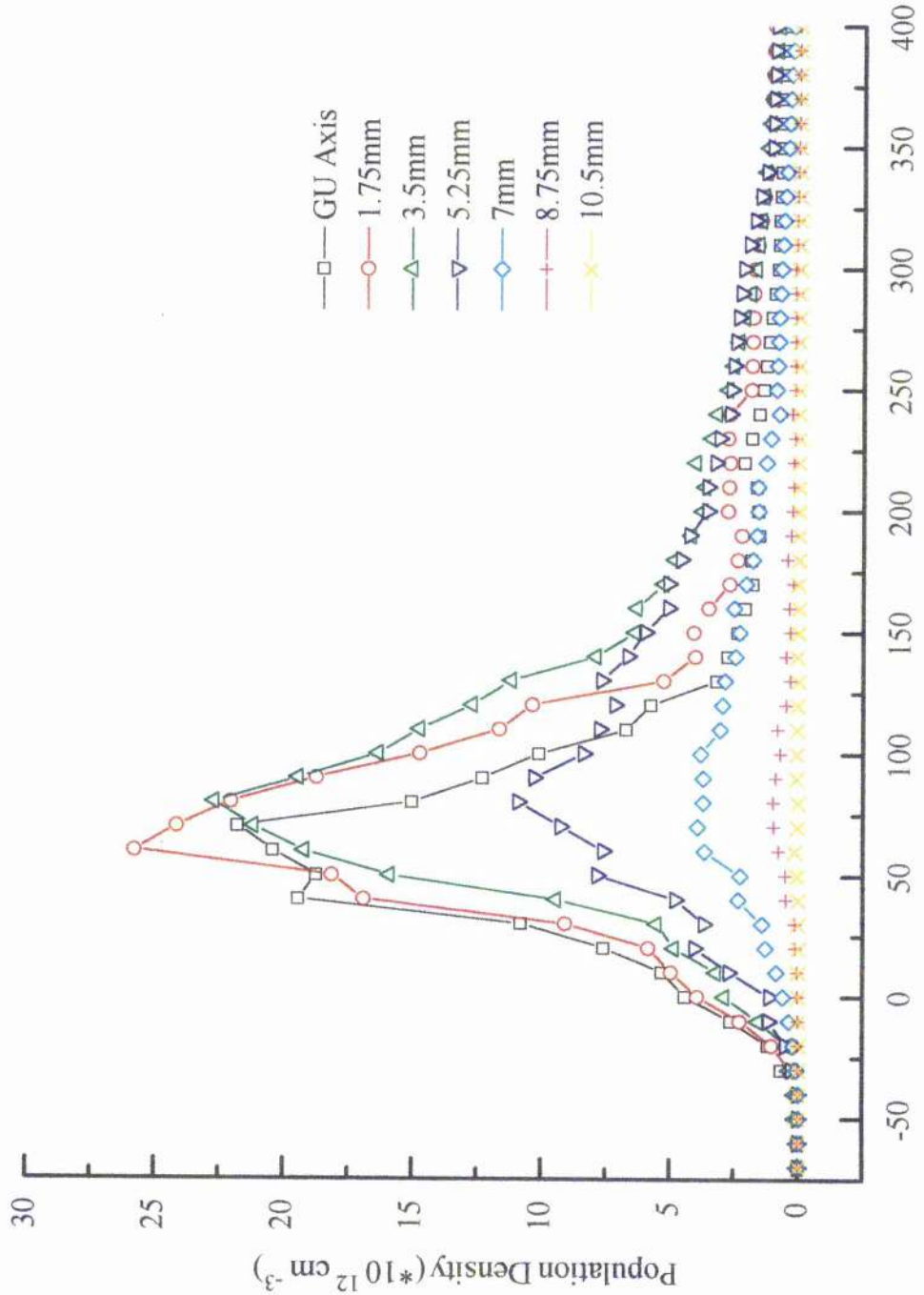


Figure 6.18 Green upper laser level population density for various radial positions

not on axis but 1.75 mm off axis. This may be due to the slightly higher ground state density at this position, the electron density being approximately constant for the axis and the first two radial positions.

The decay rate is not constant across the tube bore, the decay is slower at positions 3.5 and 5.25 mm off axis though the first radial position shows behaviour very similar to the behaviour on axis. This is the case for both upper laser levels. This change in decay rate may be due to a lower electron temperature at these positions which reduces pumping to higher lying levels and thus reduces the decay rate.

The CVL previously investigated (Hogan 1993) shows a much broader radial profile, as does the laser investigated by Brown (Brown 1988). The laser investigated by Brown does however show radial dependence of population decay in the upper laser levels. In both cases the populations persist to near the edge of the tube. Brown attributes the radial dependence of his results to gas temperature effects.

## 6.3. THE LOWER LASER LEVELS

### 6.3.1 INTRODUCTION

The measurement of population in the lower laser levels must be performed with care as the population in the upper level of the transition of interest is not negligible during the first microsecond. In this case the population measured by the hook technique is not the population in the lower level, but the effective population given by

$$N_j^* = N_j - \frac{g_j}{g_i} N_i \qquad [1]$$

the population in the upper laser level is known at all time points, therefore we may calculate the true lower level population density using the above relation.

During the laser pulse population inversion exists, that is the population in the upper laser level is greater than that in the lower laser level. In these conditions no hooks are formed for the conventional interferometer alignment. It is possible to adjust the interferometer alignment such that the fringes in an unperturbed region of the spectrum slope in the opposite direction (Smilanski et al, 1980), hooks would then be formed during population inversion only. Unfortunately time did not allow for this measurement to be made, and there is a period of missing data corresponding to the duration of population inversion.

The lower laser levels are the least suited to measurement by the hook technique as it is desirable to measure the very low population densities in the late afterglow and during the early stages of the excitation pulse with great accuracy. The hook technique is not

the best suited technique for this application but meaningful results for the majority of the period of interest have been made.

The spectrograph is calibrated for wavelengths to a maximum of 1.5 μm. For this reason it was not possible to perform the measurements the of population density in the yellow lower laser level using third order diffraction as in the green lower laser level. Measurements were therefore performed using second order diffraction. This results in a decreased hook separation, and in combination with the weak oscillator strength of the transition and the low population densities involved these measurements are less accurate and have comparatively large scatter.

It would be desirable to perform absorption spectroscopy measurements on the lower laser levels to increase resolution of the critical pre-pulse population density but this is a major undertaking in itself and is best left to a dedicated study.

The population densities in the lower laser levels are shown in Figures 6.20 & 6.21. The population density in the lower laser levels remains below the sensitivity of the apparatus until after the laser pulse, when it increases rapidly to a peak.

The two laser levels show slightly different decay behaviour, the green lower laser level has more pronounced fine structure to the peak which is relatively flat. The population only begins a steady decline 400 ns after the start of the laser pulse. The population then decreases steadily and reaches the noise level after approximately 20 μs. The population appears to follow a 2 stage decay process. The yellow lower laser level starts to decay earlier in the afterglow ( ~ 100 ns). There is some evidence of a two stage decay process though less

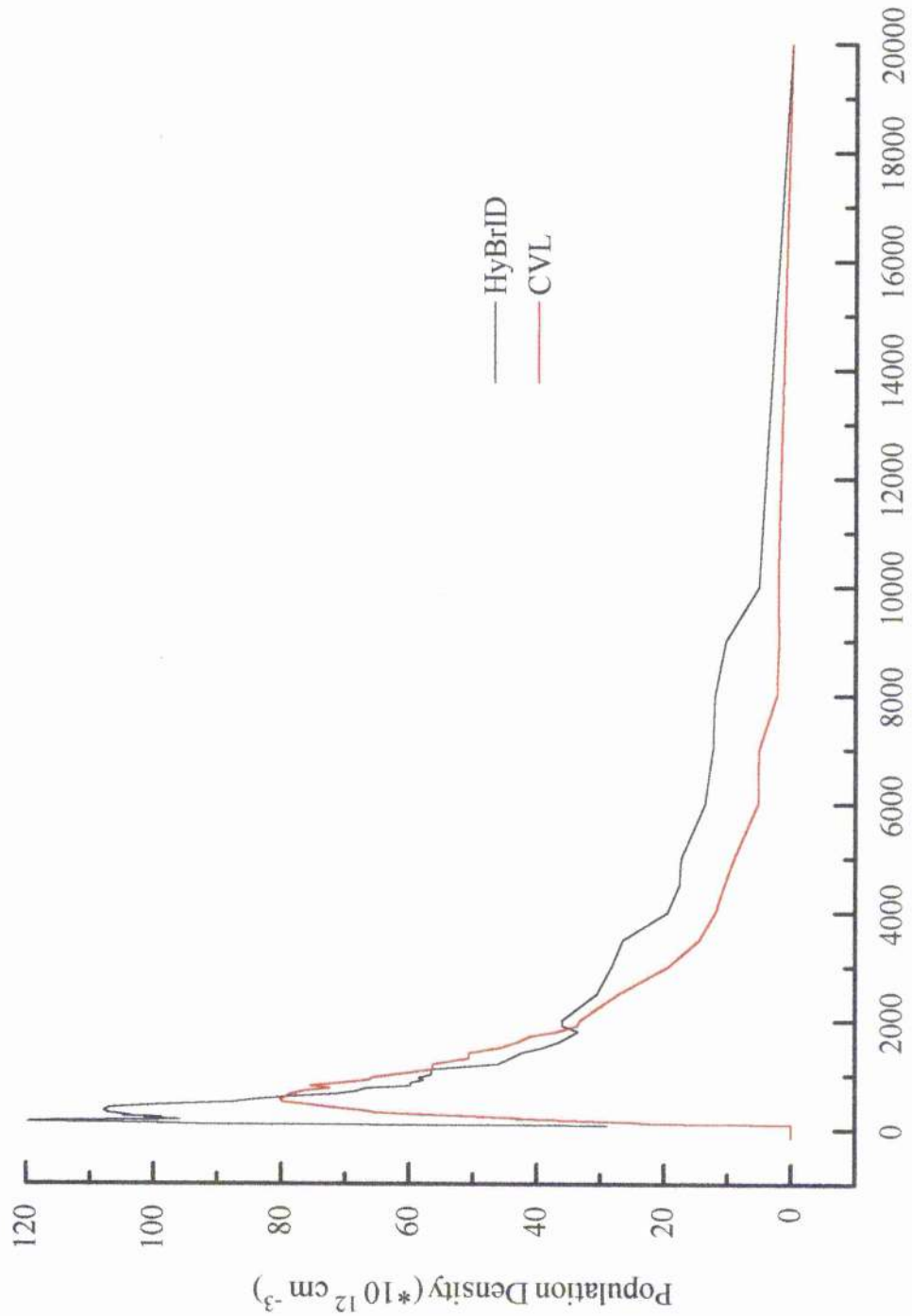


Figure 6.20 Green lower laser level population density

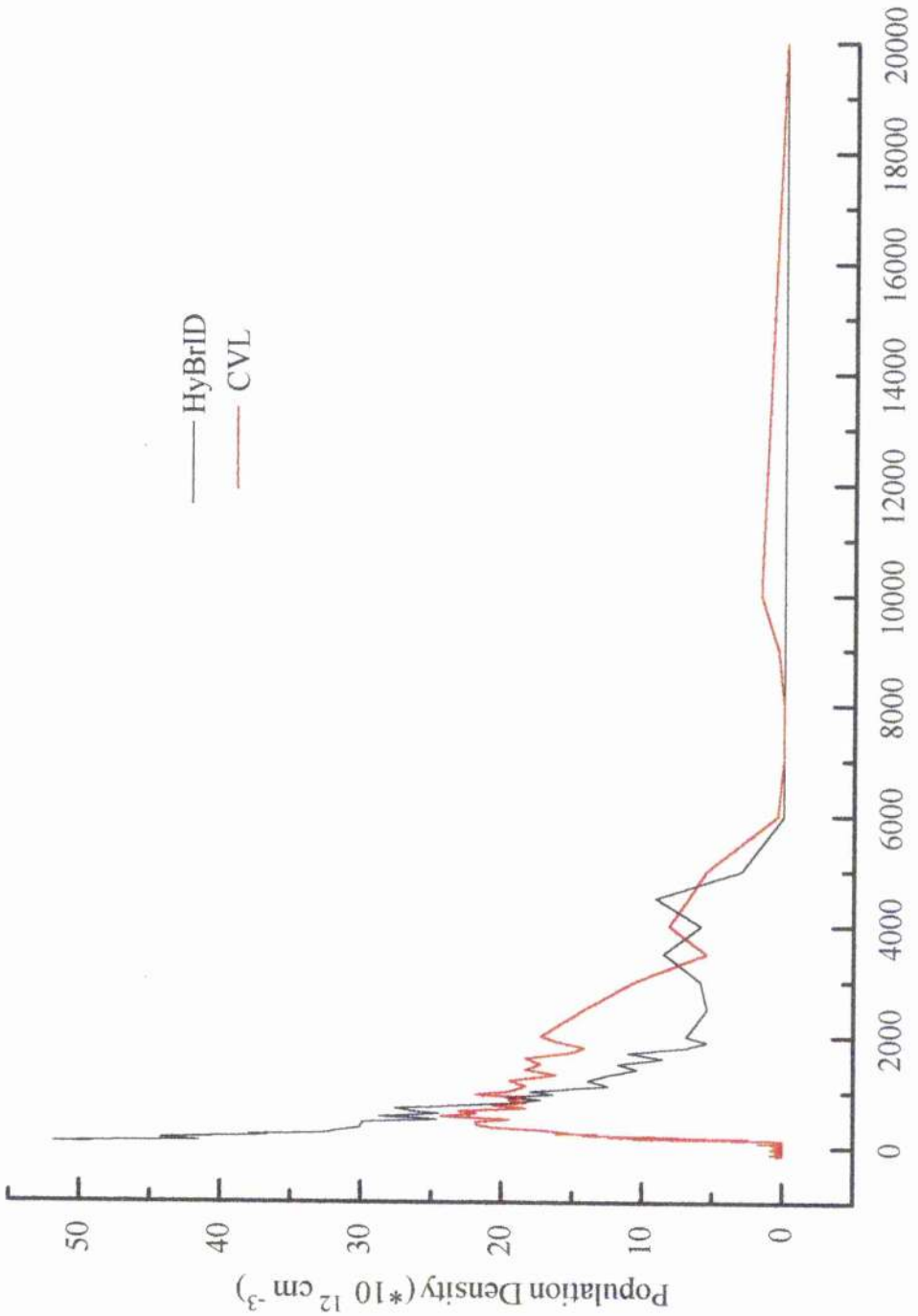


Figure 6.21 Yellow lower laser level population density

convincing than in the case of the green lower laser level. The data scatter in the mid to late afterglow is too large to allow curve fitting to the second part of the population decay.

### 6.3.2 THE PERIOD OF RISING POPULATION DENSITY

The period of rising green lower laser level population density is shown in Figure 6.22. The population density increases rapidly to a peak of $120x10^{12}$ $cm^{-3}$ after the laser pulse. There is then a slight decay to $100x10^{12}$ $cm^{-3}$ followed by a slower rise to $110x10^{12}$ $cm^{-3}$. The population then starts a period of steady decay.

The dip in the peak population may be due to pumping to higher lying levels. Immediately after the laser pulse the electron temperature is high and pumping to the lower laser levels is strong. As the ground state population density is depleted this process slows. The population density in the lower laser levels is now comparable to that in the ground state. The rate coefficient for the transitions from $3d^9 4s^2$ $^2D_{5/2}$ to $3d^9 4s(^3D)4p$ $^4P$, $^4D$, $^4F$ is up to 3 times that for the transitions from $3d^{10}4s$ $^2S_{1/2}$ to $3d^9 4s^2$ $^2D_{5/2}$ for electron energies above 1 eV as can be seen from Figure 6.12. For a short time (10 - 20 ns) pumping from the lower laser levels proceeds faster than pumping from the ground state and population is removed from the lower laser levels. The electron temperature continues to decrease and the rate coefficient for excitation to higher levels falls below that for excitation from the ground state at slightly above 1 eV. Net population is then pumped into the lower laser levels but at a slower rate due to the low electron energy and low ground state density. This ceases when the electron temperature falls to approximately 0.5 eV, at

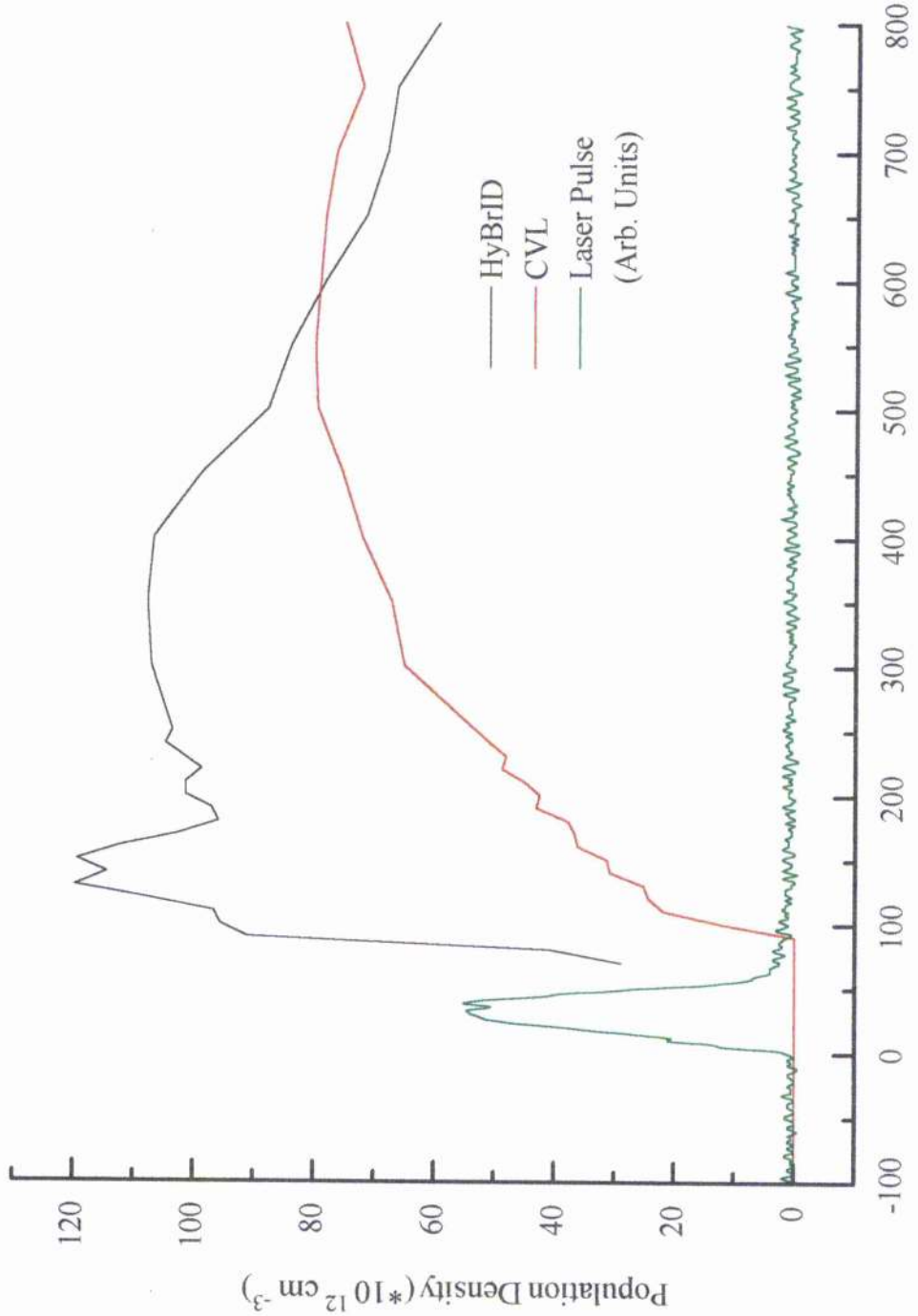


Figure 6.22 Green lower laser level population density

about 350 ns after the timing origin. The predominant mechanism affecting the lower laser level population density is now super-elastic de-excitation to the ground state.

The period of rising yellow lower laser level population density is shown in Figure 6.23. It has some characteristics in common with the green lower laser level but equally there are some differences. The peak population density is much lower, reaching only 52 x $10^{12}$ $cm^{-3}$ and recombination appears to start more quickly. The lower peak population density is not unexpected due to the difference in degeneracies and energies of the two levels. There is evidence of a small dip in the peak population density in the yellow lower laser level. This may be due to pumping to higher lying levels, as in the case of the green lower laser level. The effect will be smaller on the yellow lower laser level because the population is lower and so excitation to higher lying levels will proceed at a slower rate. In order that excitation to higher lying levels should proceed faster than pumping from the ground state for the yellow lower laser level, there must be a larger difference in rate coefficients than in the case of the green lower laser level. The excitation rate to higher lying levels will therefore dominate for a shorter time and less population will be removed. Also super-elastic de-excitation will dominate from a higher electron temperature due to the higher level energy.

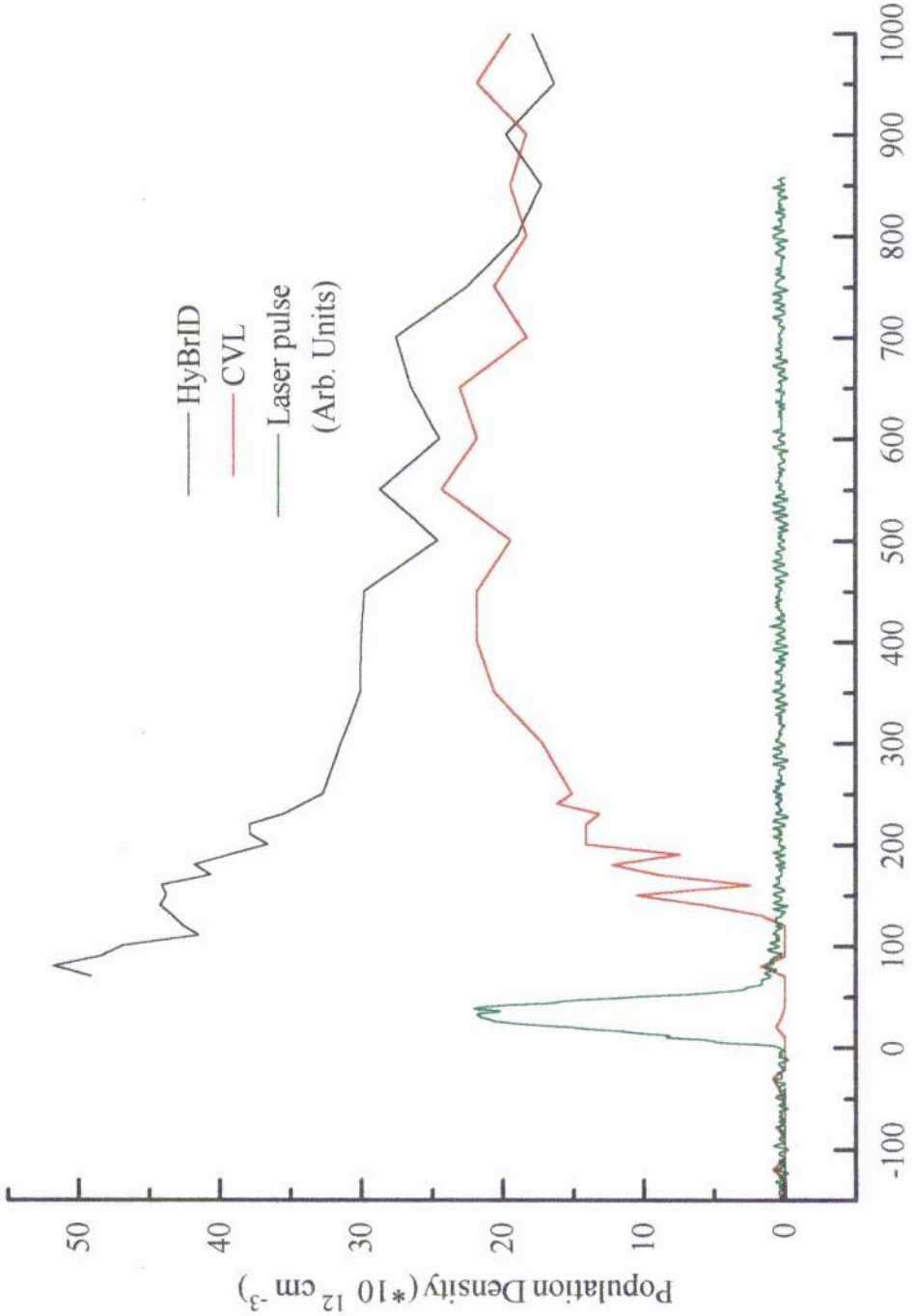


Figure 6.23 Yellow lower laser level population density

### 6.3.3 THE PERIOD OF POPULATION DECAY

The population in the lower laser levels is shown in Figures 6.24 & 6.25 with a two stage exponential decay fitted to the data. Only one part of the exponential decay is fitted for the yellow lower laser levels as the data scatter in the late afterglow is too large for a meaningful data fit. The green lower laser level decays with a time constant of 500 ns from 400 ns to 2 μs and with a time constant of 3 μs from 2 μs onwards. The final decay rate was not fitted to the population to the end of the interpulse period, but rather to the time when the population falls below the sensitivity of the hook method, at approximately 10 ms. The yellow lower laser level decays with a time constant of 670 ns from 200 ns to 2 μs. It would be ill advised to draw too many conclusions from the two stage nature of the decay as the evidence for a bi-exponential decay is less convincing at positions off-axis. Discussion will therefore be limited to consideration of possible causes of a change in decay rate and likely timing of such a change.

There will be a change in population decay rate when Boltzman equilibrium between the states at the prevailing electron temperature is established. If this is the case then Boltzmann equilibrium is established at time 2 μs for both levels. If we assume Boltzmann equilibrium has been established 2 μs after the laser pulse, then we can calculate the lower laser level population density from the calculated electron temperature and the ground state population density using

$$N_{ll} = N_{gs} \frac{g_{ll}}{g_{gs}} e^{-\Delta E / kT_e} \qquad [2]$$

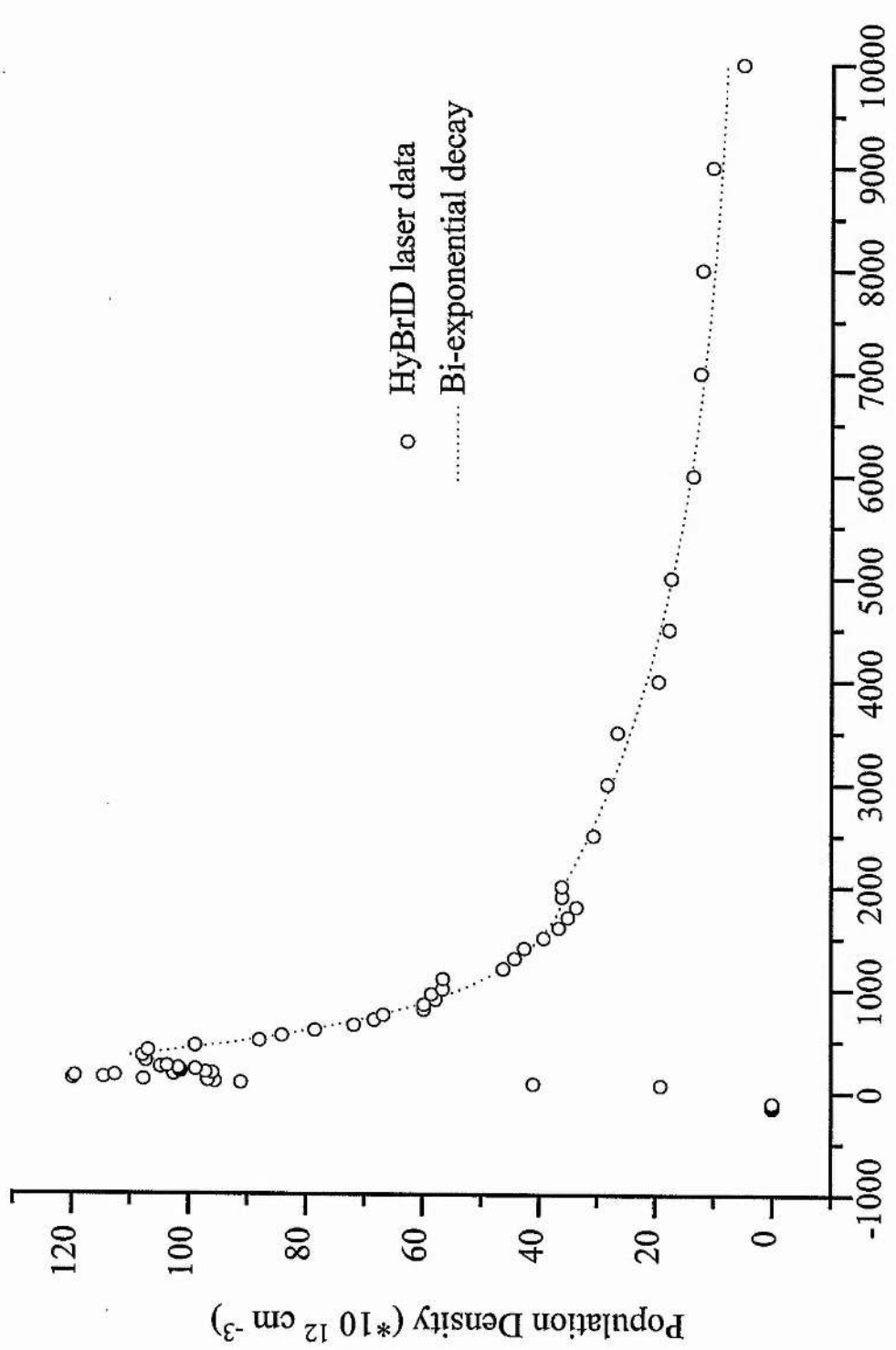


Figure 6.24 Green lower laser level population density with two stage exponential decay fit

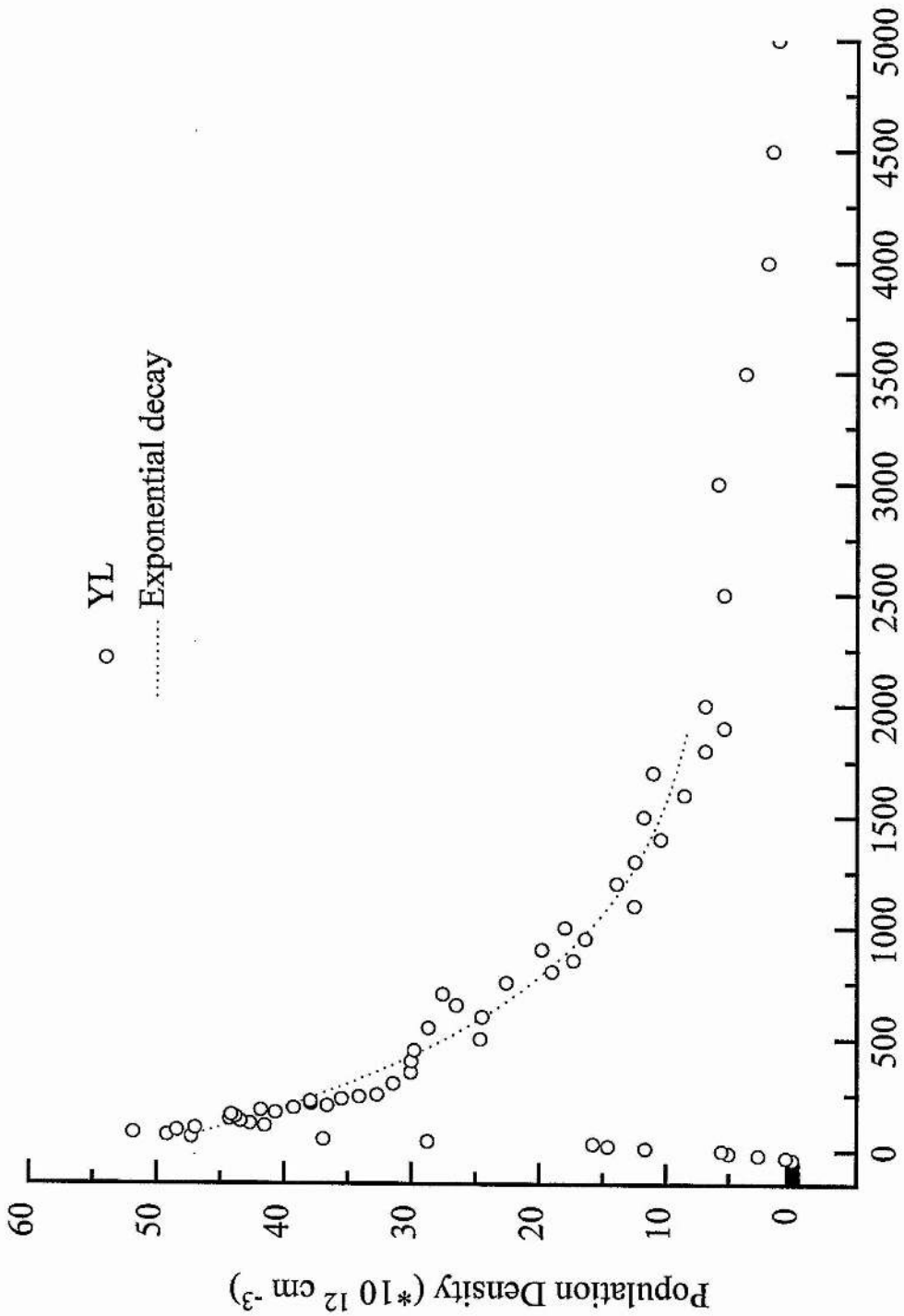


Figure 6.25 Yellow lower laser level population density with exponential decay fit

where $\Delta E$ is the difference in energy between the two levels, in this case the energy gap between the lower laser level and the ground state, $k$ is the Boltzmann constant and the subscripts *ll* and *gs* denote the lower level and the ground state respectively. The results of this calculation are shown in Figure 6.26 with the measured population density shown for comparison. It can be seen that the two curves are markedly different, the calculated decay rate is much faster than that measured and the calculated population is considerably higher than that measured in the early afterglow. From this evidence it is clear that the change in decay rate cannot be due to the establishment of Boltzmann equilibrium.

This conclusion is supported by calculation of the electron temperature from the lower laser level population density, assuming Boltzmann equilibrium, Figure 6.27. The electron temperature calculated from the lower laser level population density is considerably lower and faster falling than that calculated for three body recombination. If the electron temperature did fall as quickly as this calculation suggests three body recombination would proceed at an even more accelerated pace than is measured. The electron temperature calculated assuming pure three body recombination is a minimum estimate of the electron temperature, this calculation therefore shows that Boltzmann equilibrium is not established at this time. The electron temperature calculated from the lower laser level population assuming Boltzmann equilibrium is considerably above that calculated from the three body recombination at times after 15 μs. This indicates that the lower laser level population density is above that calculated from the expected electron temperature at this time and

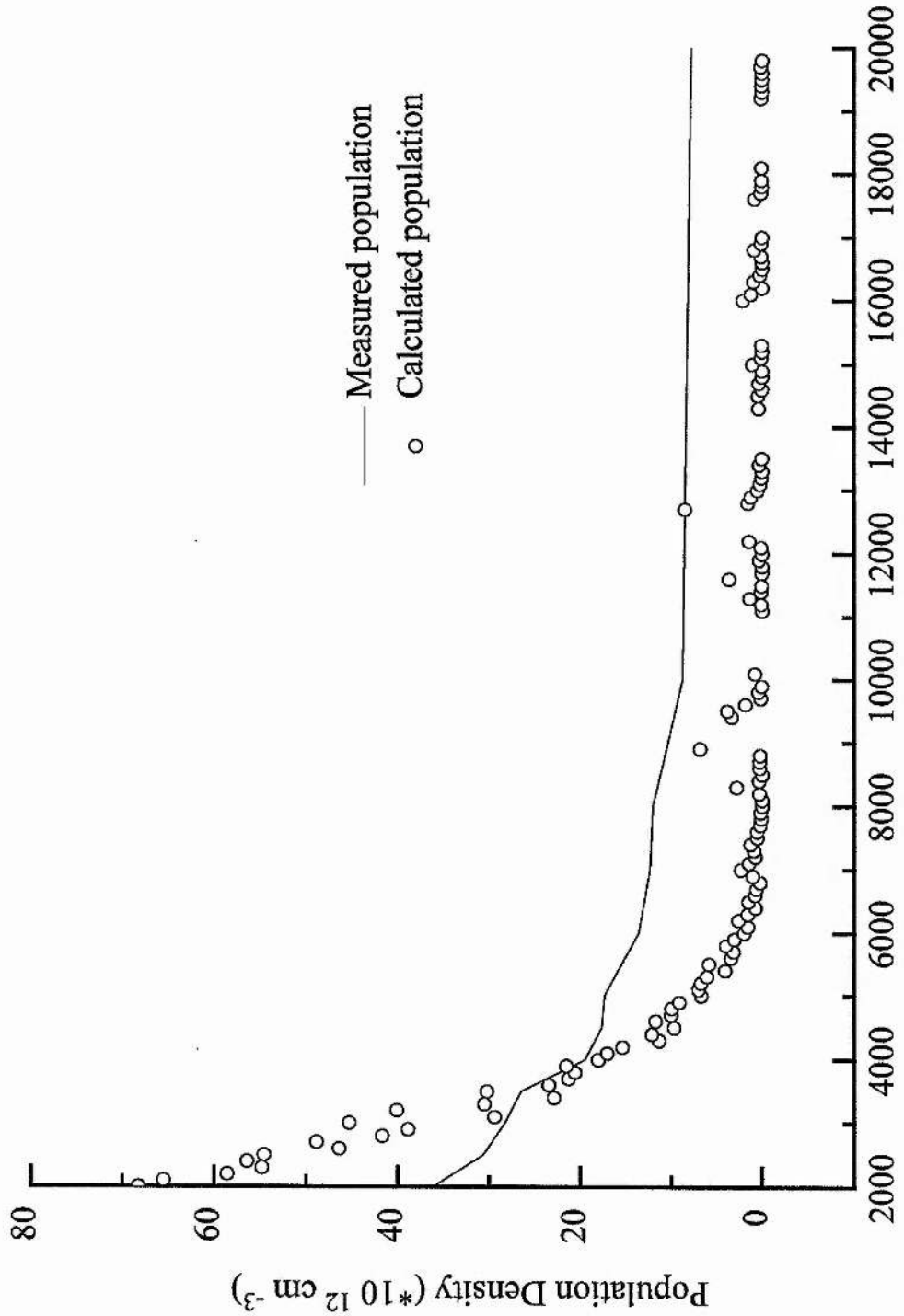


Figure 6.26 Green lower laser level population, measured and calculated from $T_e$

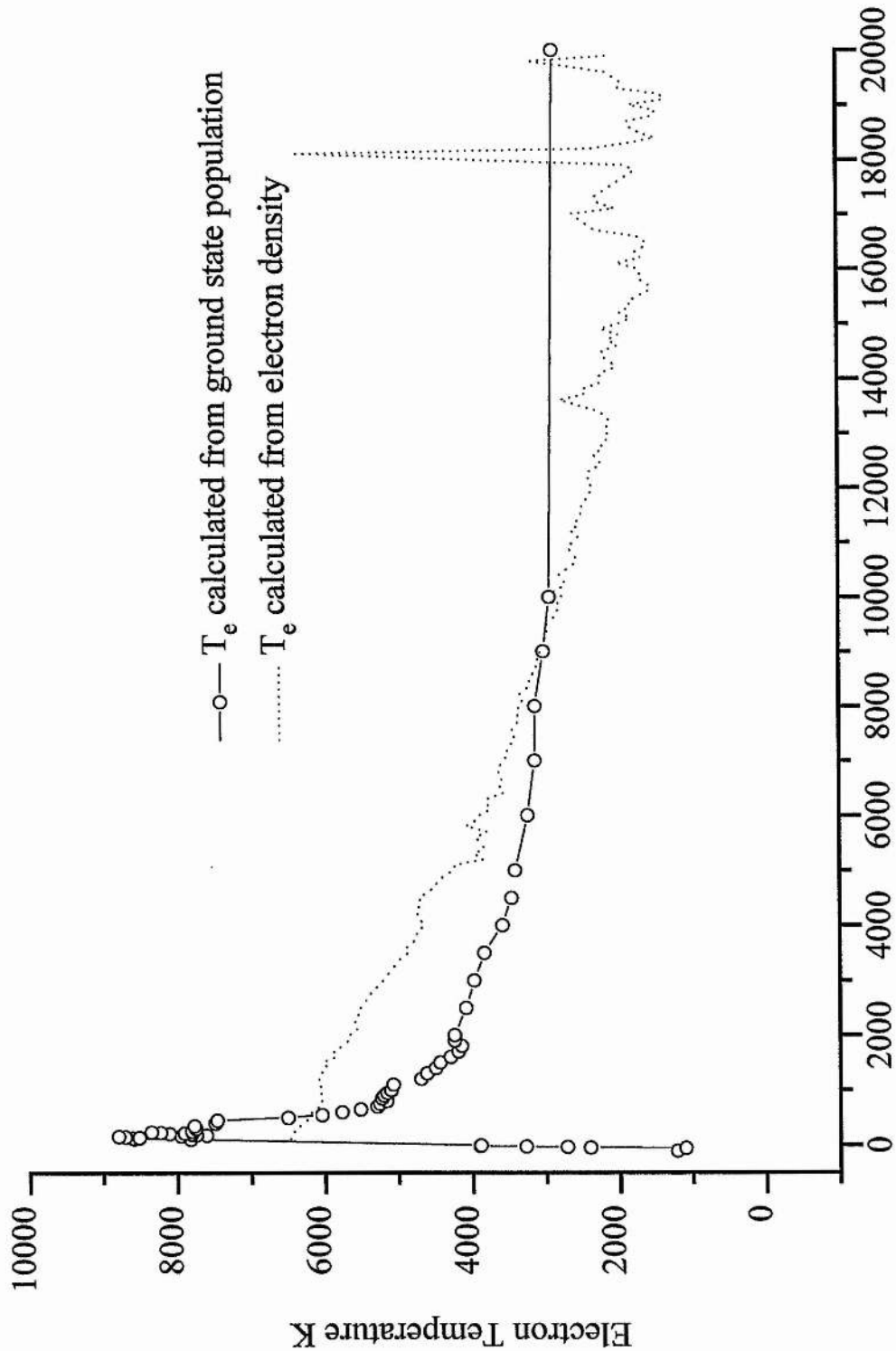


Figure 6.27 Electron temperature as calculated from ground state density and electron density

again supports the contention that the lower laser levels do not reach Boltzmann equilibrium until the late afterglow, if at all.

Further evidence that Boltzmann equilibrium is not established may be drawn from the laser power scaling with PRF. As the PRF is increased above 17 kHz laser power increases, but pulse energy decreases, see Chapter 1.3.2. As the electron density has fallen to a very low level after only 20 μs it is unlikely that this is the cause of the decreased laser pulse energy. A much more likely candidate is increased lower laser level pre-pulse population density. In Chapter 4.3.5(ii) it was argued that the pre-pulse electron temperature was equal to the gas temperature and had been at this level since 20 μs after the timing origin. If this is the case and the lower laser level population density is in Boltzmann equilibrium with the ground state then the lower laser level population density will be constant over the 10 μs preceding the excitation pulse. Laser power would scale linearly with PRF to at least 21 kHz if this was the case and there would be no laser pulse energy decrease with PRF. This argument indicates that Boltzmann equilibrium is not established in the HyBrID system and the lower laser level population density is still falling at the start of the next excitation pulse. It may be the case that due to the very low electron temperature in the late afterglow and the low electron density at times after 20 μs, Boltzmann equilibrium is never established in the HyBrID system.

A higher sensitivity measurement of population density in the late afterglow would enable more accurate decay curve fitting in the afterglow. Accurate measurement of the population density during the 20 μs pre-pulse would enable accurate calculation of the pre-pulse

electron temperature it may then be possible to ascertain whether Boltzmann equilibrium is established or not.

### 6.3.4 RADIAL DEPENDENCE

The radially resolved measurements of the green and yellow lower laser level populations are shown in Figures 6.28 & 6.29. The same results are shown as a family of curves in Figures 6.30 & 6.31. The data is shown for the period from 150 ns before the timing origin to 10 ms after the start of lasing. The population density is low at all other times.

The radial dependence of the lower laser levels is very similar to that of the upper laser levels. The green lower laser level population peaks 3.5 mm off axis, the upper laser level peaks 1.75 mm off axis. The decay rates for the lower laser levels decrease with increasing distance from the tube axis, although the decay rates on axis and at the first radial position are very similar. The change in decay rate may be due to the reduced electron density outside the central 7 mm of the discharge. The dominant depopulation mechanism for the lower laser levels is by super-elastic collision with electrons. This process is dependant on electron density, depopulation may therefore be limited by electron density.

The CVL previously investigated (Hogan 1993) shows a much more uniform radial profile of the lower laser levels. The laser investigated by Brown (Brown 1988) does however show some quite strong radial dependence of population decay lower laser levels, the radial dependence is attributed to gas temperature effects.

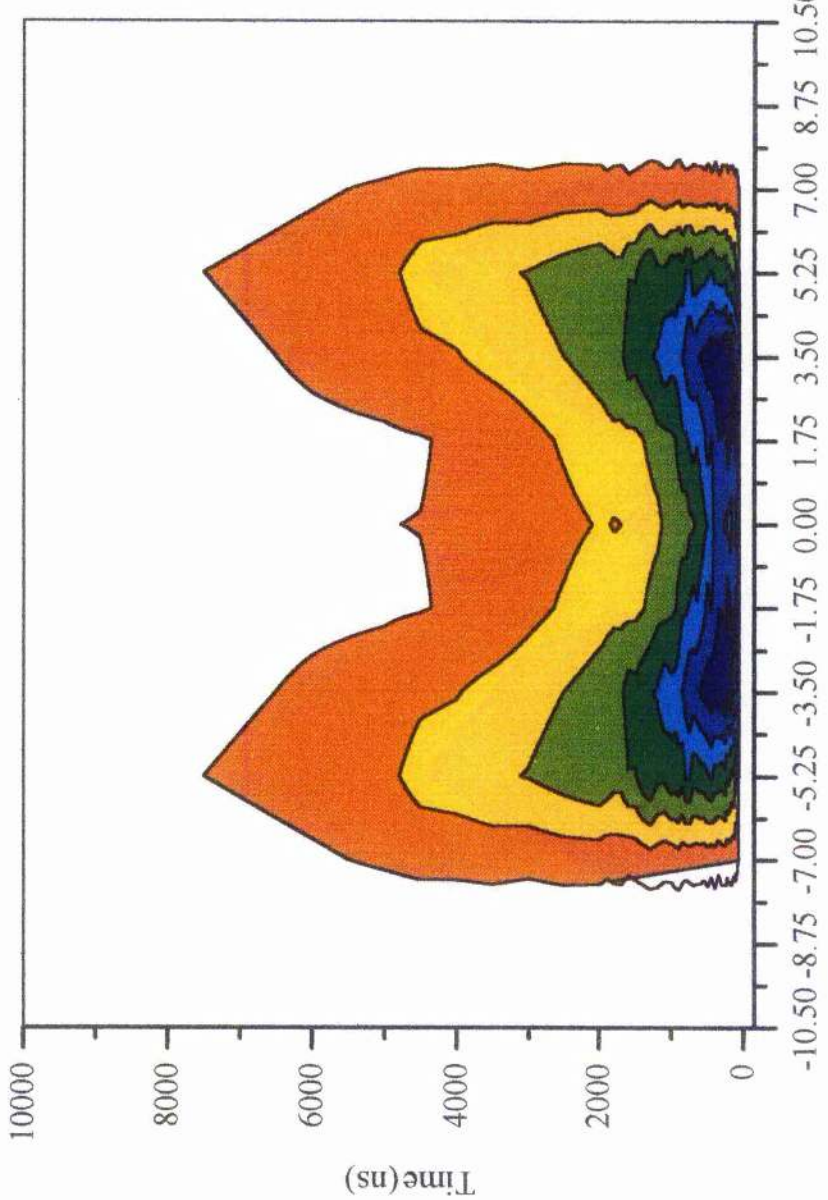


Figure 6.28 Green lower laser level population density

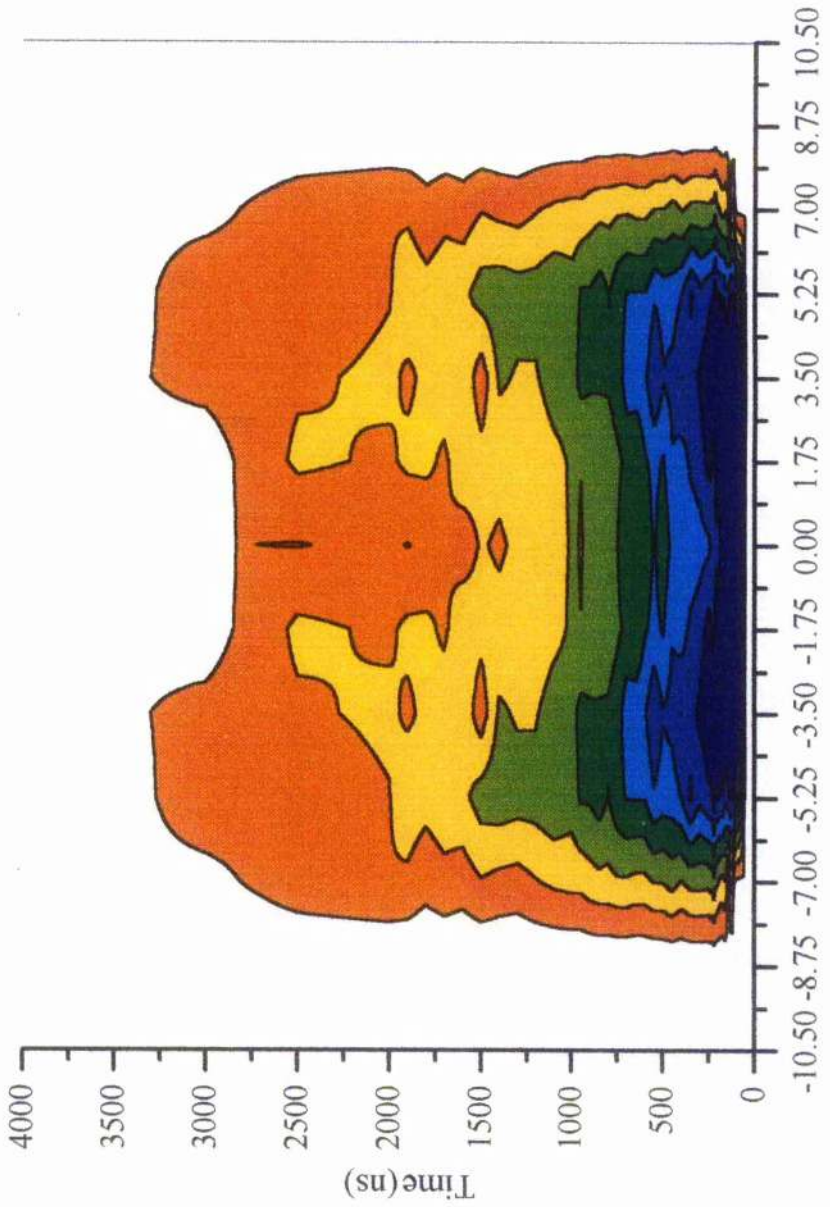


Figure 6.29 Yellow lower laser level population density

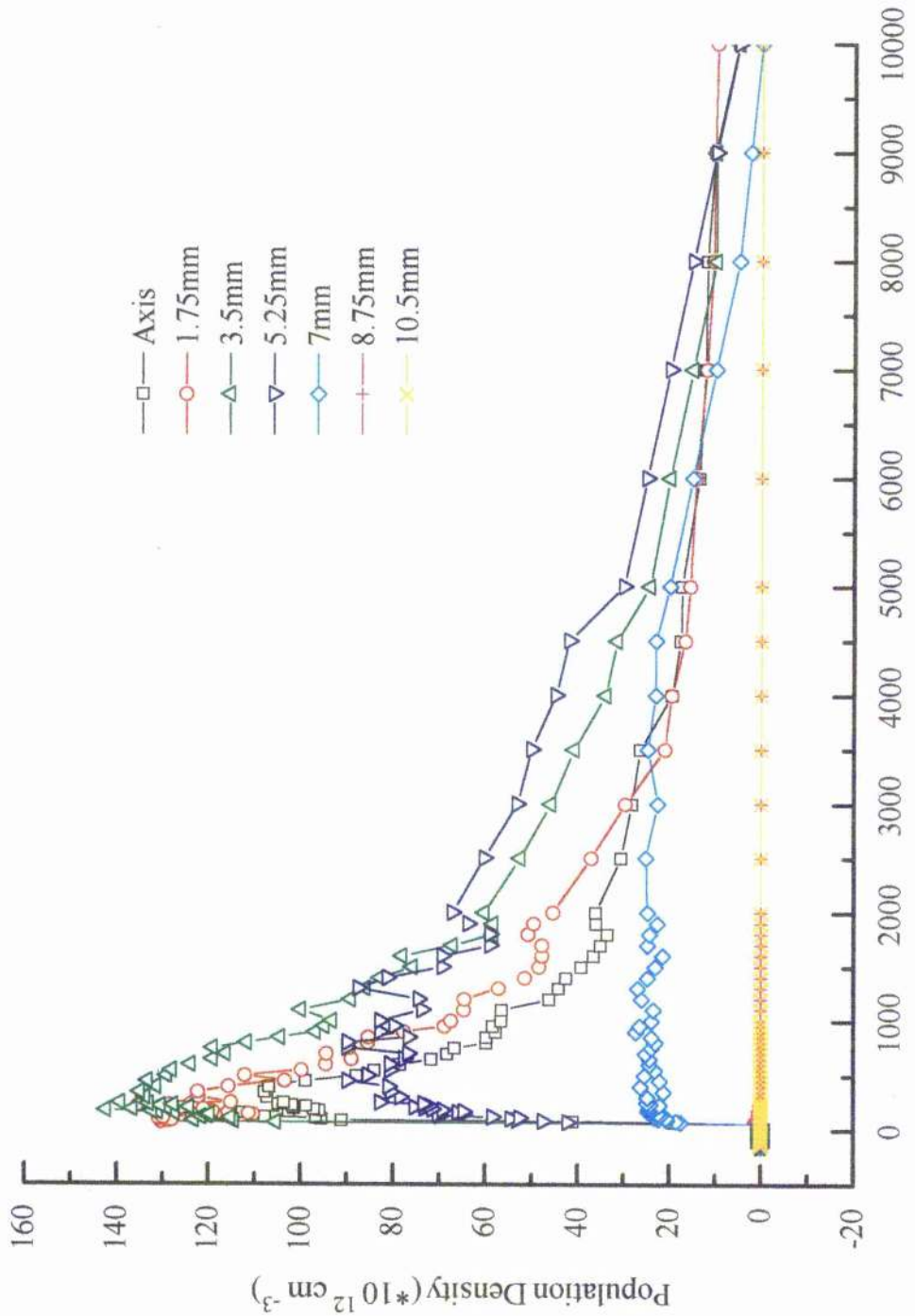


Figure 6.30 Green lower laser level population density for various radial positions

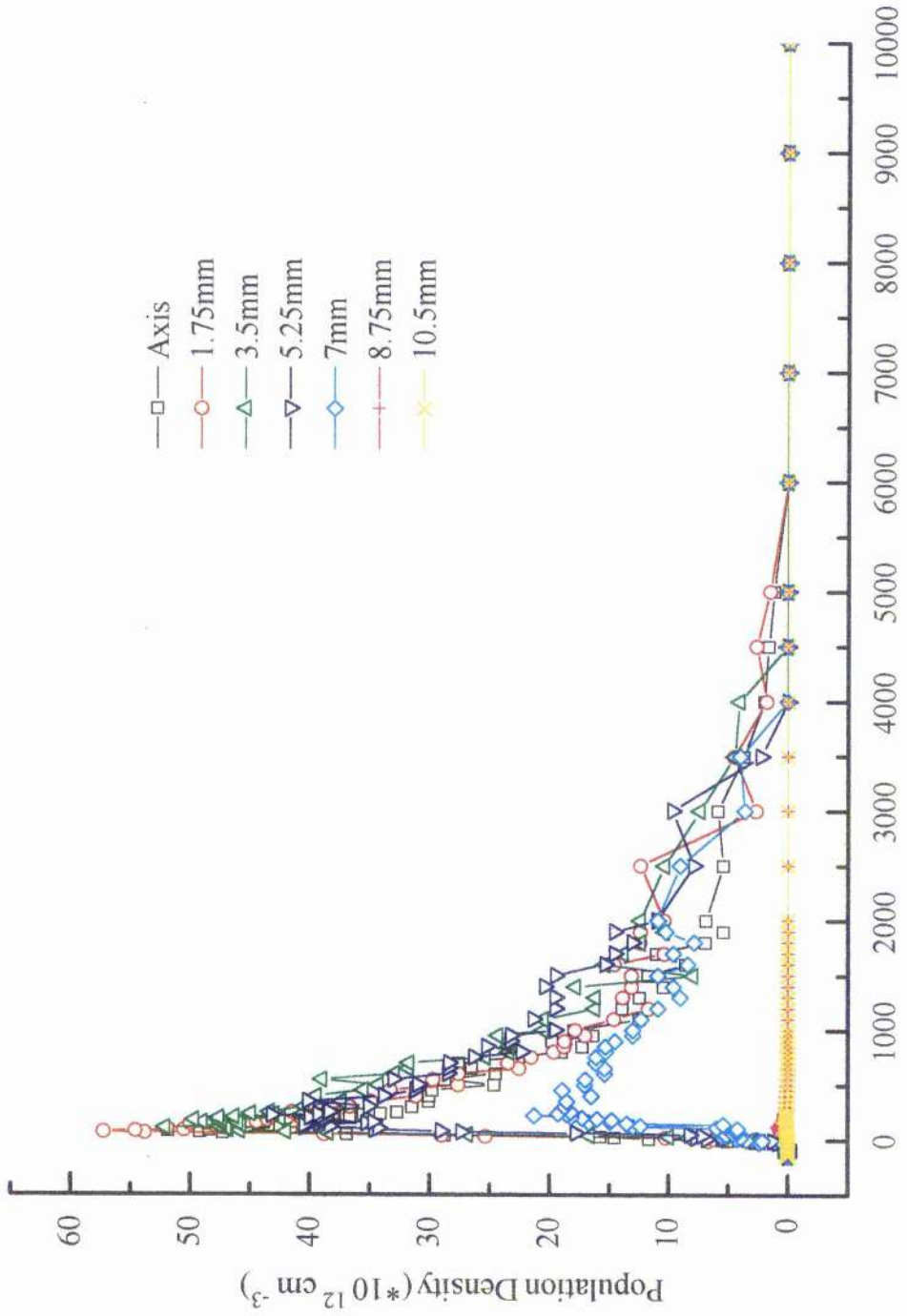


Figure 6.31 Yellow lower laser level population density for various radial positions

# 4 THE QUARTET LEVELS

## 4.1 INTRODUCTION

The populations in the 4s 4p $^4F_{9/2}$ level were measured as they are representative of the quartet levels in copper and typical of the high lying levels not belonging to the main series to which the upper and lower laser levels are strongly connected. The 4s 4p $^4F_{9/2}$ level was chosen as there is an easily accessible transition. The oscillator strength of this transition is relatively weak but measurements are quite feasible.

The population in the 4s 4p $^4F_{9/2}$ level is shown in Figure 6.32, the corresponding result for the CVL investigated previously is shown for comparison. The population density starts to increase before the start of the laser pulse and increases to a peak of $3 \times 10^{12} cm^{-3}$ 60 ns after the timing origin. The population then decays rapidly and reaches the noise level of the apparatus after less than 1 μs. There is some structure evident on both the rising and falling edges of the axial measurement trace, it appears that these are artefacts due to noise in the measurements as they are not repeated at other radial positions.

### 6.4.2 THE PERIOD OF INCREASING POPULATION DENSITY

The population density in the $4s(^3D)4p^4F_{9/2}$ level starts to rise at the same time, increases at a similar rate and peaks at the same time as the population in the upper laser levels. The peak population density is almost a factor of ten less than in the green upper laser level.

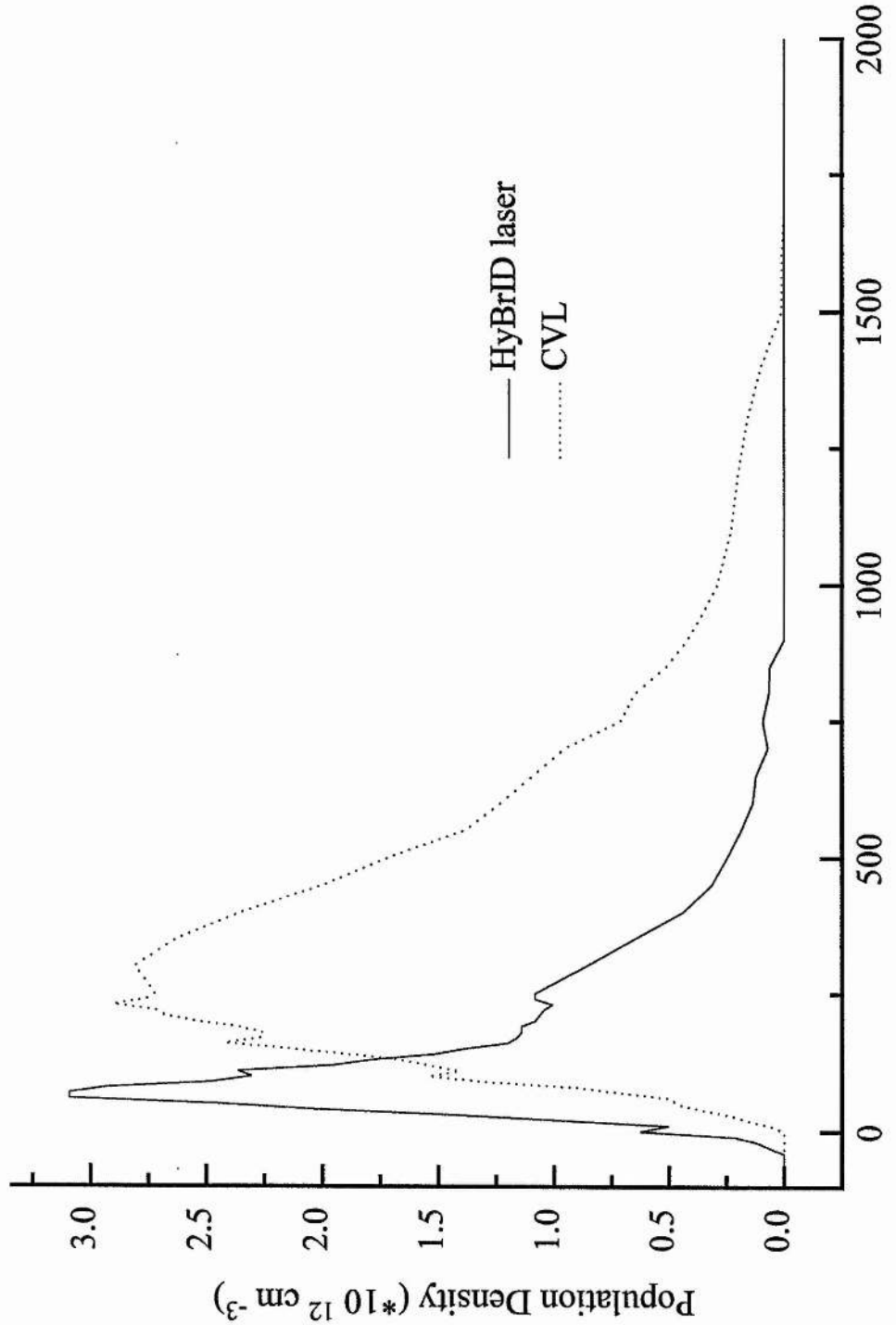


Figure 6.32 Quartet level population density

Figure 6.12 shows that the rate coefficient for excitation from the ground state to the $4s(^3D)4p^4F_{9/2}$ level (curve 9) is a factor of ten to twenty less than the corresponding rate coefficient for the upper laser levels (curve 1) at all electron energies. The $4s(^3D)4p^4F_{9/2}$ level degeneracy is twice that of the green upper laser level. The pumping rate from the ground state to the $4s(^3D)4p^4F_{9/2}$ should therefore be about one tenth of the rate for pumping to the upper laser levels. The similarity in rate of rise and timing of peak population indicates that in the early part of the pulse (0-70 ns) this is the case and the predominant mechanism for population of the $4s(^3D)4p^4F_{9/2}$ level is from the ground state.

### 6.4.3 THE PERIOD OF FALLING POPULATION DENSITY

The population density in the $4s(^3D)4p^4F_{9/2}$ level has a two stage decay. The period from 70 to 180 ns has time constant 95 ns, after this the population decays with time constant 210 ns until 900 ns after the timing origin, when the population has reached the noise level. Bearing in mind that there is significant scatter in the data points due to the low oscillator strength and population density, confirmation of this behaviour was sought from the off axis measurements. The first radial position has a bi-exponential decay as do positions further off-axis. The change in decay rate is less pronounced further off axis as the population is lower and the measurement resolution poorer.

Population transfer to the 4s 4p $^4F_{9/2}$ level from the upper laser levels after 70 ns may be significant as the 4s 4p $^4F_{9/2}$ level population decreases more slowly than the upper laser level population and the

electron temperature at this time is still an appreciable fraction of an electron volt. However from Figure 6.12 we can see that the rate coefficient for excitation from the upper laser levels to the quartet levels (11) is at least a factor of 10 smaller than that for ionisation from the quartet levels (17) until the electron temperature falls below 1 eV. Population of the quartet levels from the upper laser levels will therefore exceed the depopulation due to ionisation, at low electron energies and it is possible that population from the upper laser levels is responsible for the change in 4s 4p $^4F_{9/2}$ level population decay rate. If this is the case then the electron temperature at 150-200 ns should be in the range 0.5-1 eV, this agrees with observations made about electron temperature from the upper and lower laser level population behaviour. The population in the upper laser levels 150-200 ns after the timing origin is low, though it remains larger than the quartet population density at all times.

The two stage nature of the decay may be due to population feeding into the 4s($^3$D)4p$^4F_{9/2}$ level from recombining ions. This would slow the rate of population decrease. The ground state density measurements show population increasing rapidly from approximately 150-200 ns after the start of the laser pulse. This indicates that ion recombination has started and it is likely that population will cascade through the 4s($^3$D)4p$^4F_{9/2}$ level.

### 6.4.4 RADIAL DEPENDENCE

The radially resolved measurements of the 4s 4p $^4F_{9/2}$ level population is shown in Figure 6.33. The same result is shown as a family of curves in Figure 6.34. The data is shown for the period from 150 ns before the timing origin to 1 μs after the start of lasing. The population density is low at all other times.

The population is peaked on axis and the rate of rise and the decay rate are constant across the central 7 mm of the tube bore. This could be explained if the radial electron temperature profile was flat. In Chapter 4.4 the radial electron temperature profile was discussed and it was concluded that the electron temperature should be peaked on axis during the excitation pulse and after 400 ns. From time 150 ns-400ns the electron temperature profile may be flatter though the upper laser levels' behaviour indicates that it is still centrally peaked. This explanation for the observed population behaviour is therefore unlikely to be correct.

At high electron energies the rate coefficients for the processes affecting the quartet level population are not strongly dependant on electron energy, the radially uniform population increase can therefore be explained. However both excitation from the ground state and to higher lying levels is strongly dependant on electron energy for energies in the range 0-1 ev (Figure 6.12). Some variation in decay rate would be expected across the tube if these were the processes controlling the population decay. This is not seen and it may be the case that population from higher lying levels due to de-excitation after recombination of copper ions is important at this time. This process

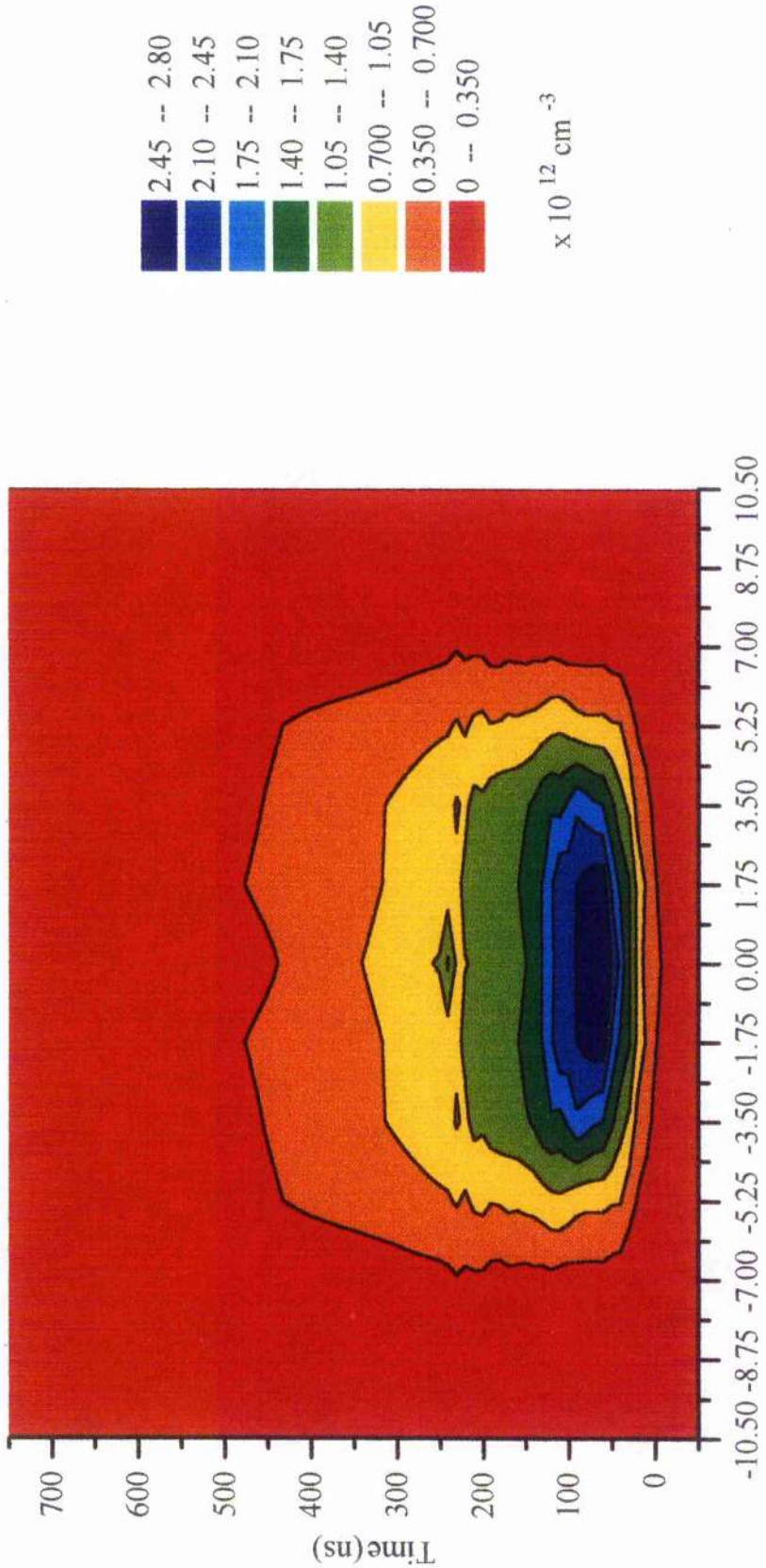


Figure 6.33 Quartet population density

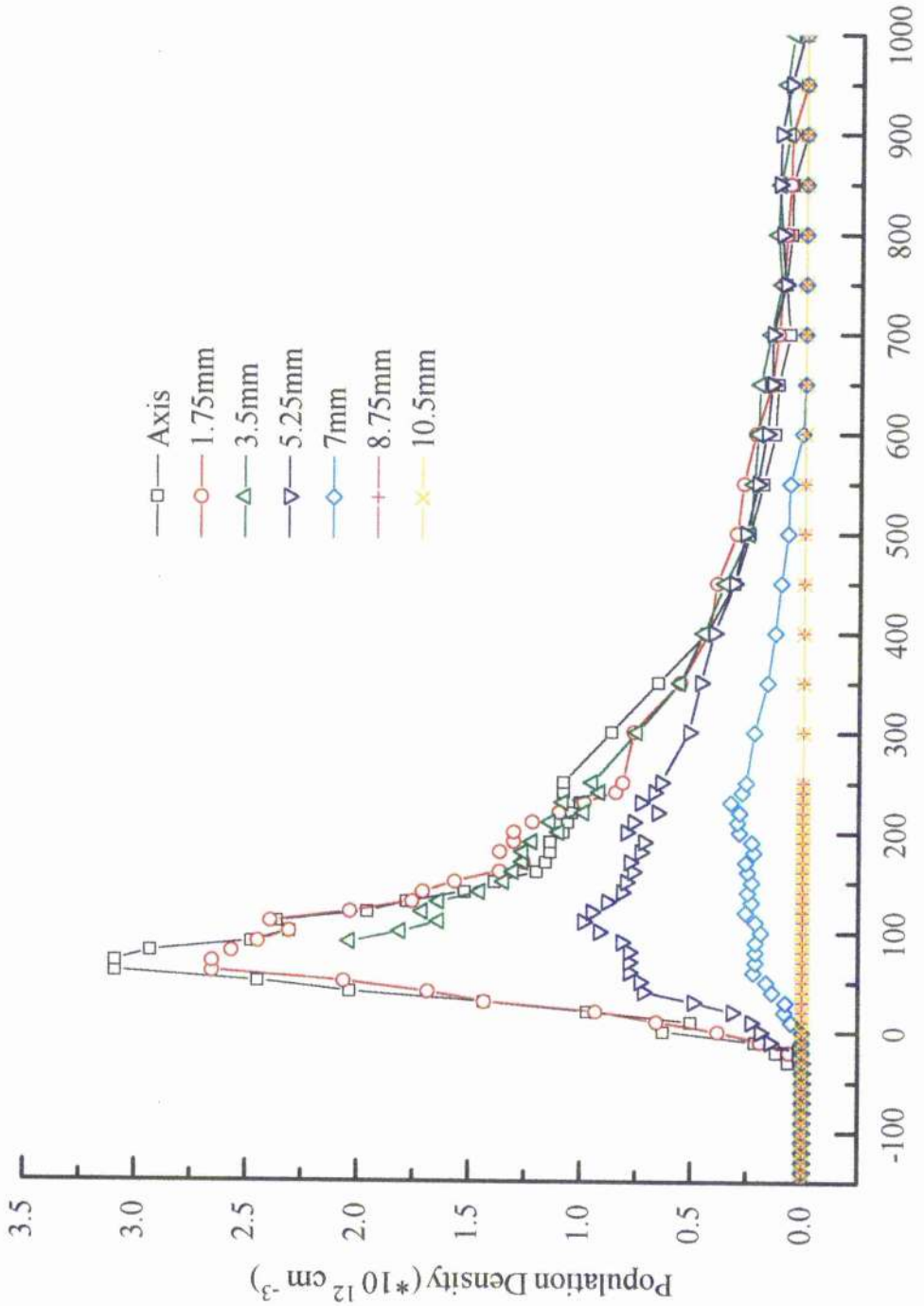


Figure 6.34 Quartet population density for various radial poitions

would be heavily dependant on electron density and so would proceed at an almost uniform rate across the central 7 mm of the tube bore.

The CVL previously investigated (Hogan 1993) shows a much more uniform radial profile, as does the laser investigated by Brown (Brown 1988). The laser investigated by Brown does however show some slight radial dependence of population decay. In this case the populations persist to near the edge of the tube and the radial dependence is attributed to gas temperature effects.

## 6.5. NEON EXCITED STATE POPULATION

### 6.5.1 INTRODUCTION

The population density in the $2p^5 3s$ levels of neon was measured to give an indication of the activity of neon in the discharge. There is strong heavy body and electron collisional excitation between the levels (Parks & Javan 1965; Phelps, 1959) and the levels are populated in the ratio of their degeneracies, the total population can therefore be calculated from measurement of the population in one level.

The population density was calculated using the assumption that a negligible amount of neon is excited in the region where there is an appreciable density of copper. The length of plasma interrogated in this measurement is restricted to the regions near the electrodes where the temperature is too low to support a high vapour density of CuBr. These regions are approximately 1 cm long at each end giving a total plasma length of 2 cm. Determination of this dimension is subjective and the accuracy can be regarded as no better than $\pm$0.5cm or $\pm$25%.

## 5.2 POPULATION BEHAVIOUR

The measured $2p^5 3s$ level population density is shown in Figure 6.35. The corresponding measurement for the CVL is also shown along with the HyBrID current waveform.

The population starts a slow increase 30-40 ns before the laser pulse, 10 ns before the onset of lasing the population starts to increase rapidly. The population peaks at $3 \times 10^{12} cm^{-3}$ 50-60 ns after the timing origin and falls rapidly until time 100-150 ns. The population then undergoes a slow increase until 750 ns when it peaks at $0.6 \times 10^{12} cm^{-3}$.

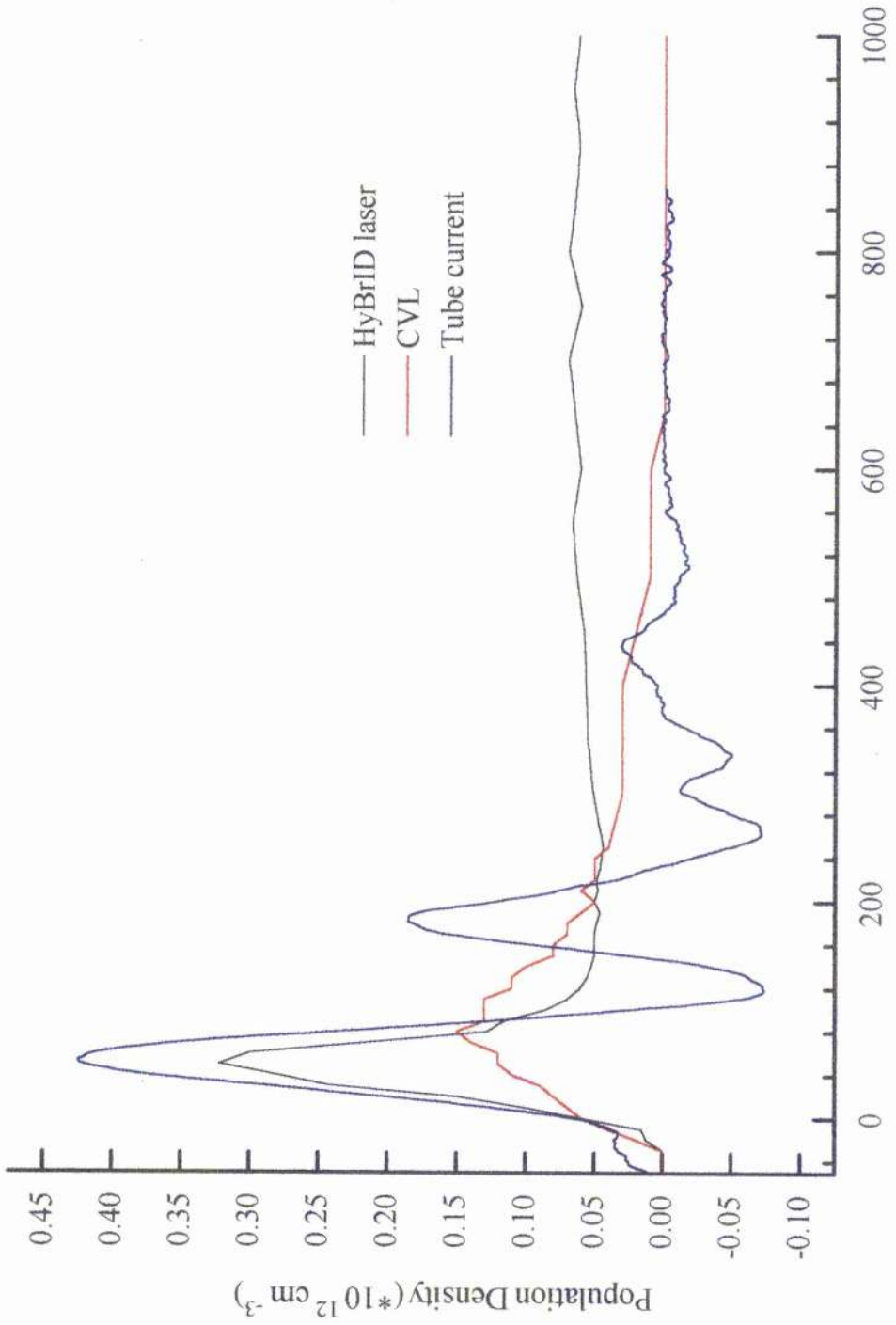


Figure 6.35 Neon metastable level population density

The population then decays to reach zero 6 μs after the timing origin. The secondary peak is only seen on axis, but there is evidence of a change in decay rate at other radial positions.

The populations in the neon $2p^5 3s$ levels follow the first excursion of the current pulse very closely. The subsequent oscillations of the current have no discernible effect on the population density. This supports the evidence presented in Chapter 2.3, that very little voltage is developed across the tube after the first excursion of the tube voltage. The $2p^5 3s$ levels lie 16.7 eV above the ground state, the next higher levels are only 4.9 eV above this, therefore stepwise ionisation will be an important process. As the $2p^5 3s$ levels are so high lying they will only be pumped when the electron temperature in the end regions is very high. The hydrogen concentration will be approximately uniform throughout the laser tube as the gas flow rate is quite slow and hydrogen will rapidly diffuse throughout the volume. Cooling of the electrons by hydrogen will therefore be an important process in the end regions as well as in the 'hot' regions. The electron temperature will fall quickly in the end regions and once the tube voltage has reached zero we may assume that it is too low to cause further population of the $2p^5 3s$ levels. After this time the only mechanism acting to sustain the electron temperature is recombination heating. Calculations of the electron temperature in the end regions of a CVL have shown that in the absence of cooling by hydrogen the electron temperature falls below 5 eV before the tube voltage reaches zero, (Carman et al. 1994). This indicates that further excitation from the $2p^5 3s$ level to higher lying levels will be a slow process at times after the tube voltage first passes through zero. The main mechanisms

of population removal from the $2p^5 3s$ levels must therefore be by super-elastic electron collisions to the ground state and Penning ionisation of copper.

The second peak in the $2p^5 3s$ levels population density is due to population cascading down from higher lying levels as neon ion recombination reaches a peak at 750 ns after the timing origin. This is further evidence that the electron temperature falls quickly in the end regions.

## 5.3 RADIAL DEPENDENCE

The radially resolved measurements of the neon $2p^5 3s$ level population is shown in Figure 6.36. The same result is shown as a family of curves in Figure 6.37. The population is peaked on axis for the first 100 ns and at times after 600 ns. Between 100 ns and 600 ns there is a central minima. This corresponds to the time when population is pumped from the $2p^5 3s$ level to higher levels as discussed previously. Due to discharge constriction in the cold end regions this only occurs on or near the axis where the electron density and temperature are highest. The neon $2p^5 3s$ level in the CVL exhibits behaviour with some similarities though the effects of onward excitation and the consequent recombination are much more marked due to the higher current passed.

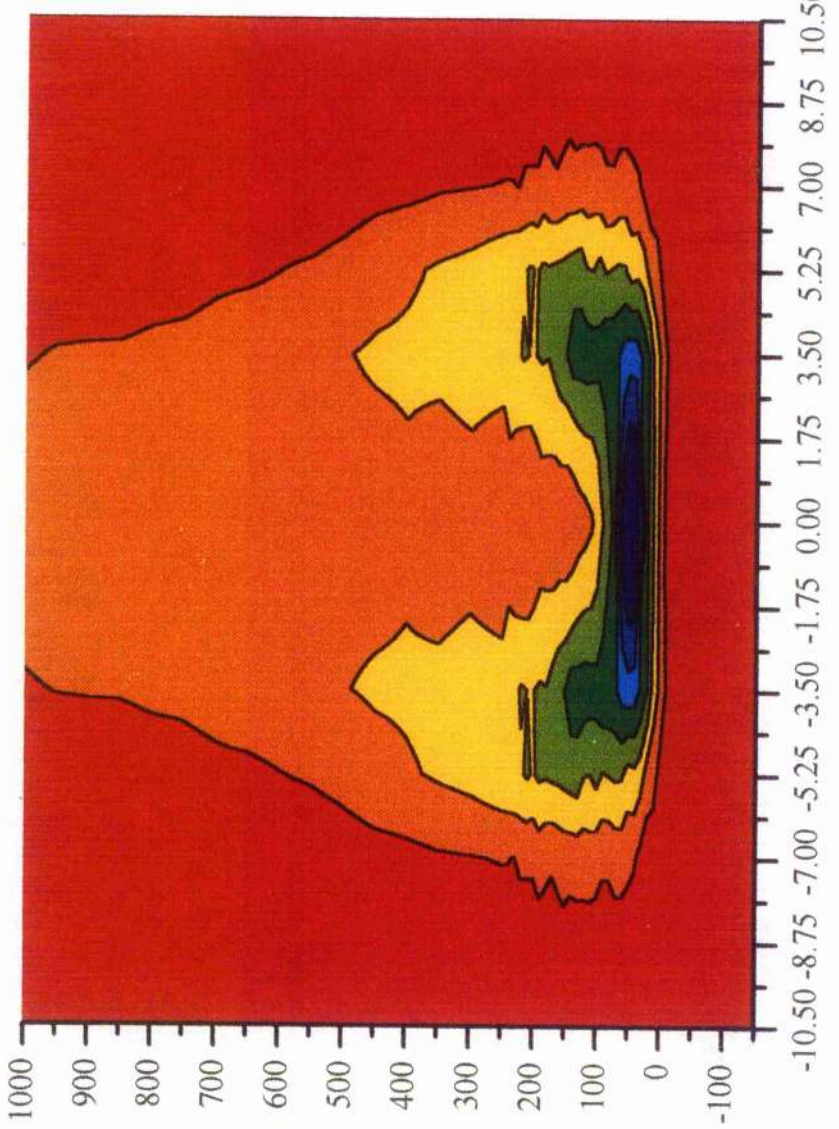


Figure 6.36 Neon metastable level population density

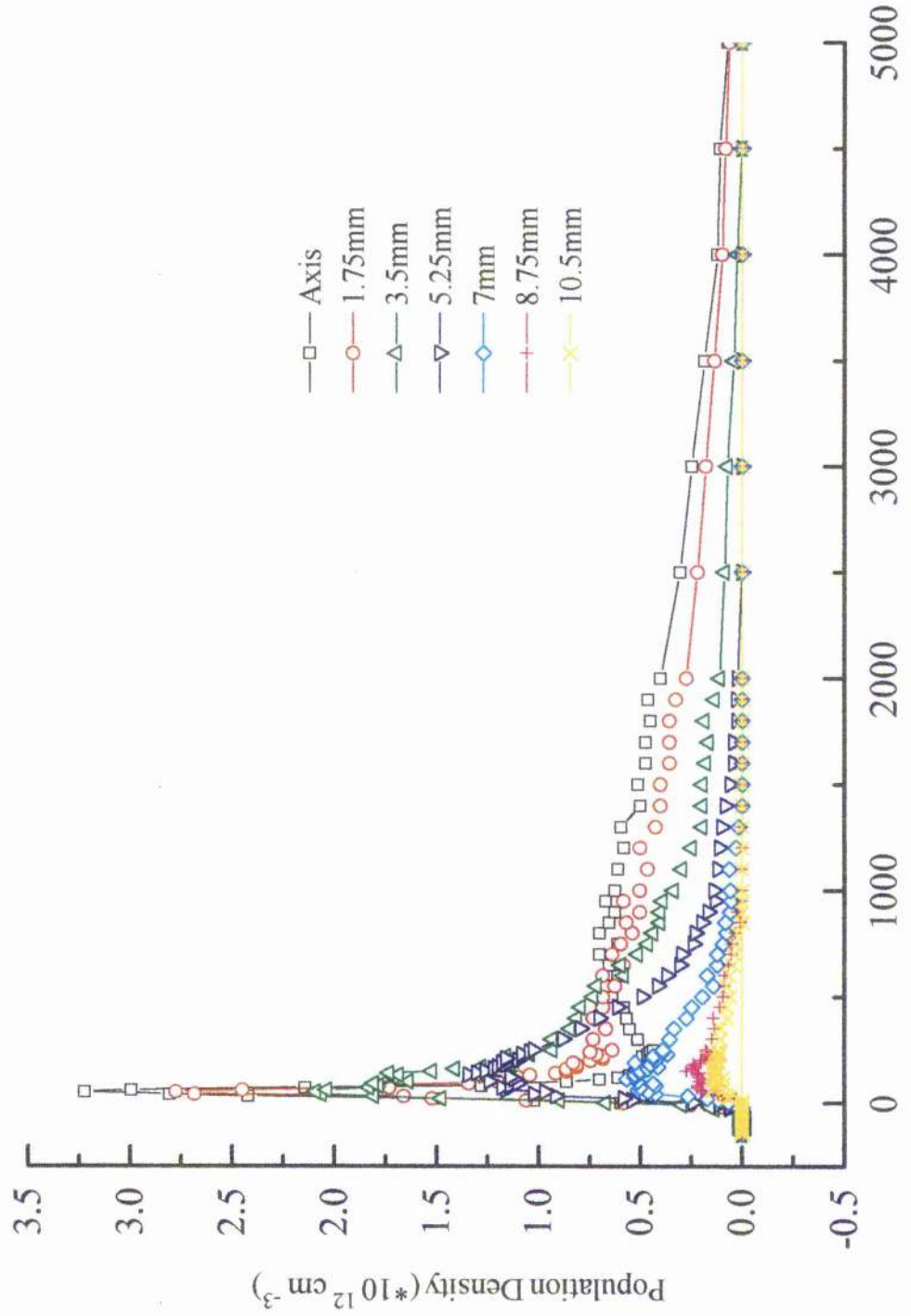


Figure 6.37 Neon metastable population density for various radial positions

## 6.6 ELECTRON TEMPERATURE

Electron temperature is perhaps the most fundamental and important parameter of resonance-metastable cyclic lasers as it is by means of the electrons that energy is coupled from the excitation circuit to the active volume. Its evolution determines the relative excitation rates of the laser upper and lower levels, electron temperature therefore determines the gain characteristics to a large extent and influences active volume and PRF scaling through its effect on the pre-pulse electron density. It is also one of the major differences between HyBrID lasers and CVLs and has been the subject of much comment in this thesis. It was not possible to measure the electron temperature directly during this study but it was possible to calculate certain bounds for the electron temperature at particular times in the pulse inter-pulse period. Estimates of the electron temperature at several other time points can be made if certain assumptions are made

The following discussion applies to the electron temperature in the central 'hot' region of the discharge where the copper density is high and neon ionisation is not significant.

We may assume that the electron temperature immediately before the pulse is equal to the gas temperature. This assumption is justified because the electron density falls to a low level in the early afterglow indicating that three body recombination occurs at a high rate. Three body recombination is strongly dependent on electron temperature ( 3-body recombination rate $\alpha$ $T_e^{-5}$ .)

The electron temperature does not rise with the tube voltage. This can be seen by the delay between the rise of tube voltage and the

start of lasing, as discussed in Chapter 2.3. Population is first seen in the upper laser and higher lying levels only 30-40ns before lasing commences. The rate of population increase is slow at this time and is probably due to electrons in the high energy tail of the electron energy distribution function (EEDF). The rate of population of these levels increases dramatically 0-10ns before the start of lasing. This indicates that the electron temperature has increased to say 3-4eV (quartet levels are populated directly from the ground state at this time.)

The peak electron temperature is a subject for speculation though we may assume that it is not greatly higher than 3.5eV as if this was the case excitation directly to higher lying levels would dominate over excitation to the upper laser levels. The peak electron temperature has been set at 5eV because this is the approximately the peak temperature calculated for CVLs (Kushner & Warner 1983; Carman 1994) Laser emission terminates at 60ns after it begins, the tube voltage also crosses through zero at this time and the rate of population of the upper laser and quartet levels has decreased significantly. This indicates that the electron temperature has fallen to approximately 3-4eV.

At time 120-130ns the rate of depopulation of the upper laser levels changes. This indicates that the dominant mechanism of population removal has changed from excitation to higher lying levels to de-excitation to the lower laser levels by super-elastic collisions with electrons. From the rate coefficients shown in Figure 6.12 we can deduce that this change should occur at approximately 1.5eV

At 200ns after the timing origin, population is removed from the lower laser levels by excitation to higher lying levels,

predominantly the quartet levels. This indicates that this process proceeds faster than direct excitation from the ground state. Again examination of Figure 6.12 shows that this behaviour indicates that the electron temperature has fallen to approximately 1eV.

By the time 350ns, excitation to the lower laser levels from the ground state has ceased, this indicates that the elelctron temperature is no greater than approximately 0.5eV.

Calculation of the electron temperature, assuming only three body recombination removal of the electrons, yields a curve for times between 400ns and 17μs. 17μs after the start of the laser pulse the electron temperature has fallen to the gas temperature (1900K ~ 0.16eV) and remains constant at this level until the next excitation pulse starts. (The gas temperature varies very little during the full excitation cycle as the energy deposited (~0.1J) is small compared with the thermal capacity of the active medium; $\Delta T \sim 25\ ^{o}C$.)

The above information is plotted in Figure 6.38 showing the electron temperature evolution over one discharge period. Comparison of this graph with one produced in a similar fashion for the CVL previously investigated using the same experimental apparatus shows that the graphs have broadly similar behaviour. The results for the CVL differ in that the pre-pulse electron temperature is higher, the electron temperature rises more quickly but falls more slowly. The major difference is the relatively high electron temperature in the CVL at times after 0.5μs. In the HyBrID laser the majority of the electrons recombine during the period between 0.5μs and 20μs. In the CVL very little recombination is seen during this period due to the high electron temperature. After 20μs the electron

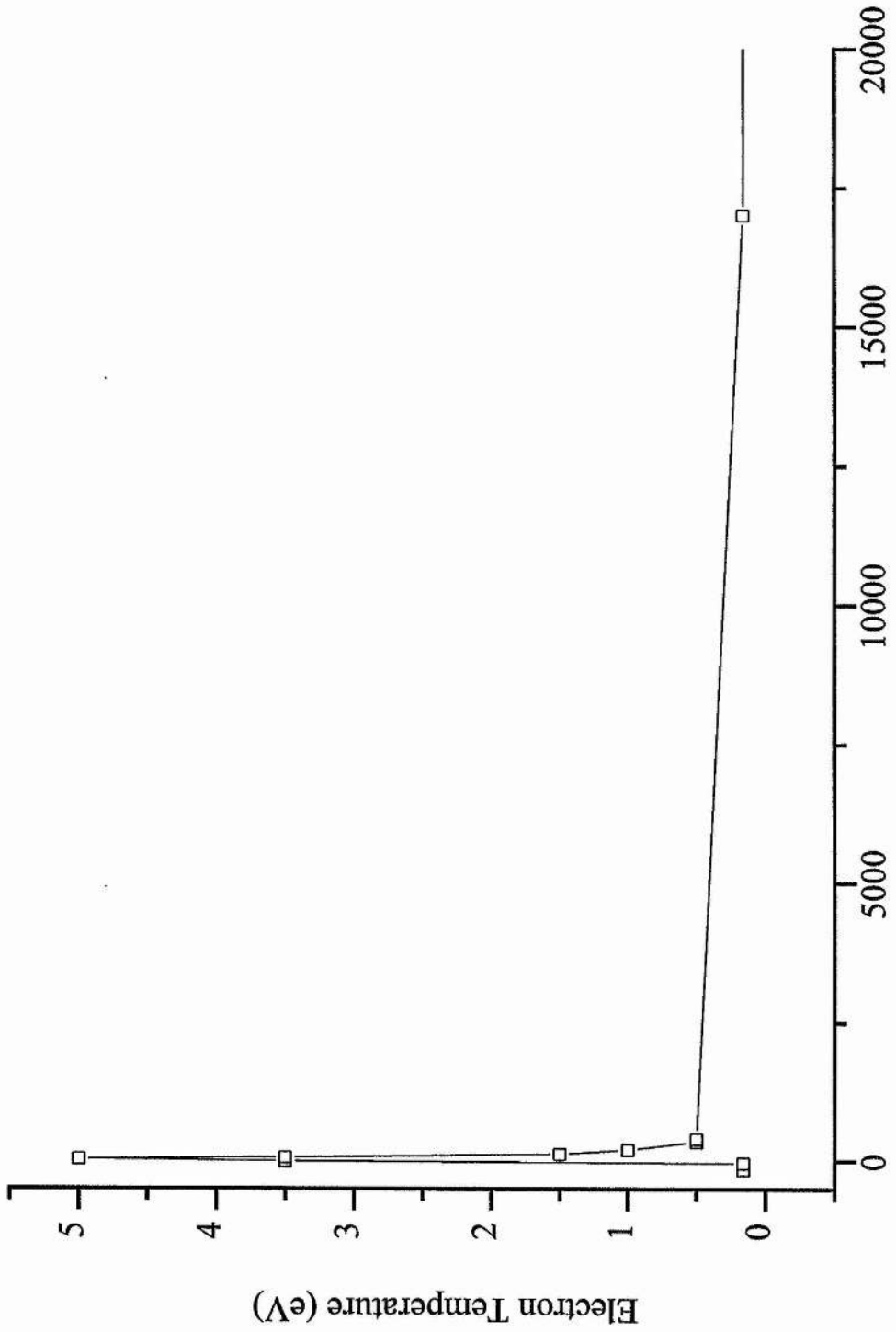


Figure 6.38 Speculative plot of electron temperature

temperature in the CVL still limits the recombination rate and electron removal is so slow that a large fraction of the electron peak density remains when the next excitation pulse is applied. The behaviour differences seen are consistent with a mechanism of strong electron cooling in the HyBrID laser which is not present in the CVL.

The radial dependence of the electron temperature also has important implications for the laser performance. The principal concern is whether the radial distribution is flat or centrally peaked. This question has not been answered for the CVL and, as there are many different device designs and device dimensions, there will be variation from one system to another. Carman (1994) argues that, in a 19mm bore laser, the radial electron temperature profile will be flat at all times except during and immediately after the excitation pulse, this is due to strong inter-electron momentum coupling. Hogan (Hogan 1993), who investigated a device of more than twice the diameter (42mm), concludes from analysis of his electron density measurements that the electron temperature in his device may be peaked on axis.

In the HyBrID laser the system is complicated by the presence of hydrogen which will have a strong effect on the electron cooling, also, the discharge in a HyBrID laser is constricted in comparison to that in a CVL. In Carman's discussion on radial electron temperature profile he states that, as inelastic collisions with copper are the dominant method of electron cooling during the excitation pulse in the CVL the electron temperature is peaked on axis. He then argues that the electron temperature profile is flattened out rapidly by electron to

electron momentum transfer which is strong relative to the electron to gas momentum transfer.

In the HyBrID system it is possible that a similar radial electron temperature profile is created by the centrally dipped copper ground state profile. The hydrogen density will also be dipped on axis due to the gas temperature profile. This will lead to relatively weaker electron cooling on axis and the radial profile may be reinforced by this mechanism. The cooling effect of hydrogen will also depend on the local gas temperature. Hydrogen excited by collision with 'hot' electrons will lose energy by collision with other atoms. As neon has the highest number density in the active region the majority of collisions will be with neon, thus the hydrogen acts to couple the gas and electron temperatures. The hydrogen cannot produce a flat electron temperature profile unless the gas temperature profile is also flat. However, the electron density is very high at this time and the inter-electron momentum coupling will be very strong. As the mass difference between electrons is zero, only one collision is necessary for a complete transfer of momentum, many collisions would be necessary if the collision partner was hydrogen.

Analysis of the measurements of the radial dependance of the electron density show that the electron temperature is peaked on axis. This calculation was performed under the assumption that electron attachment was negligible. This may or may not prove to be valid.

One argument that three body recombination is not responsible for the fast decay in electron density is that the decay is much faster than in the CVL and the difference in behaviour is so great that it is unlikely that the same process is responsible for both. However,

calculations employing the same formulae used sucessfully in a computer model of a high temperature laser (Carman et al. 1994) have shown that, due to the high electron density, three body recombination is very fast even for relatively high electron temperatures. There is considerable evidence from the hook method measurements that the electron temperature in the HyBrID laser is lower than in the CVL and is in the range predicted by calculation from the electron density decay rates. This is certainly justification for the assumption that three body recombination is an important process, though the evidence does not rule out electron attachment as important.

There is not yet conclusive evidence as to the radial dependance of the electron temperature, but the weight of evidence presented leads the author to support the theory that the electron temperature is peaked on axis prior to excitation and remains so during both the excitation and relaxation phases.

# CHAPTER 7 CONCLUSIONS

## 7.1 THE DATA COLLECTED

The temporally and spatially resolved population densities have been measured in the following states: $3d^{10}\ 4s\ ^2S_{1/2}$ , $3d^{10}\ 4s^2\ ^2D_{3/2}$, $3d^9\ 4s^2\ ^2D_{5/2}$, $3d^9\ 4p\ ^2P_{3/2}$, $3d^{10}\ 4p\ ^2P_{1/2}$, $3d^{10}\ 4p\ ^2P_{3/2}$ and $3d^9\ 4s\ 4p\ ^4F_{9/2}$ in copper and the $2p^5\ 3s\ ^3P_0$ in neon. The temporally resolved electron density has also been measured at seven radial positions. Various deductions concerning electron temperature and excitation process rates have been made. The results have been compared with measurements of a CVL made using the same equipment.

## 7.2 THE GROUND STATE

The population density in the ground state on axis is more than twice that seen in the CVL previously investigated by Hogan (1993) using the same apparatus. The percentage depletion of the ground state by the end of the excitation phase is approximately 75% in the HyBrID laser, compared to at most 55% in the CVL. The recovery of the ground state population density in the HyBrID laser is more rapid than in the CVL and starts earlier in the afterglow period. The observed behaviour of the ground state population density on axis is consistant with an electron temperature in the active zone which does not rise with the total tube voltage but only increases shortly before the start of the laser pulse.

The ground state population density is lowest on axis and highest at the tube walls. This is due to the centrally peaked profile. The resultant gas density profile is peaked at the tube walls. The

ground state depletion is highest on axis and at the first two radial positions. There is significant ground state depletion across the central 17mm of the tube. The radial dependance of the ground state depletion is similar to the laser output profile and the peak electron density profile. The radial dependance of the ground state population depletion shows that the entire tube volume is not excited in the HyBrID laser; this contrasts with the situation in the CVL where the entire volume is excited.

## 7.3 THE UPPER LASER LEVELS

The populations in the upper laser level starts to rise some 30-40ns before the start of lasing. The population density when lasing starts is higher than in the CVL previously investigated. The peak population density in the HyBrID laser is approximately twice that seen in the CVL and occurs earlier in the pulse. The ratio of the green to yellow populations in the upper laser levels is 2:1. The populations exhibit a two stage decay; the decay rate changes at time 120-130 ns. The change in decay rate may be due to a change in depopulation mechanism due to the falling electron temperature.

The populations are not peaked on axis, but 1.75mm off axis; 90% of the population is created inside the central 10mm. The off axis peaks may be due to the higher ground state density at these positions. The population decay rate is not constant across the tube bore, but is slower off axis. This may be due to a centrally peaked electron temperature.

## 7.4THE LOWER LASER LEVELS

The population in the lower laser levels is not measured during the laser pulse. After the laser pulse, the population increases rapidly to a peak. In the green lower laser level, the peak displays some structure, the yellow lower laser level results are of poorer resolution due to spectrograph limitations, and the peak shows less structure. The population decays in two stages; the decay rate changes 2μs after the timing origin.

The population density peaks approximately 3.5 mm off axis. The population decay rate decreases with increasing distance from the axis, this may be due to decreased electron density outside the central 7mm of the discharge region.

## 7.5 THE QUARTET LEVELS

The population in the quartet levels of copper rises at the same time as the populations in the upper laser levels. The peak population is a factor of ten less than the population in the upper laser levels. The population decays more slowly than that in the upper laser levels. The population decays in two stages.

The population is peaked on axis and the population decay rates are constant across the central 7mm of the tube bore. This may be due to the relatively flat electron density profile in the central region of the tube during this time.

## 7.6 THE NEON $^3P_0$ LEVEL

The population in the neon $^3P_0$ level on axis has two peaks; the first peak occurs at time 50-60 ns. Stepwise ionisation is an important mechanism depopulating this level. The second peak is at time 750 ns and is due to recombination of ions.

The population in the neon $^3P_0$ level is peaked on axis. Only the axial measurement shows a secondary peak, though a change in decay rate is seen at other radial positions. This may be partly due to discharge constriction in the end regions.

## 7.7 ELECTRON DENSITY

The peak electron densityin the HyBrID laser is approximately four times that in the CVL previously investigated. This may be accounted for by the relative tube bores and the slight discharge constriction seen in the HyBrID laser. The electron density decays much more quickly in the HyBrID laser and has fallen to 2% of the peak value 20μs after the termination of lasing. In the CVL the electron density only falls to approximately 40% of its peak value before the next excitation pulse, despite the much longer interpulse period.

The electron density is peaked on axis. The radial profile is relatively flat over the central 7mm and then falls rapidly to less than 2% of the peak value. The majority (>90%) of the electrons are generated inside the central 10 mm of the tube bore. The high rate of electron density decay may be the result of fast three body recombination due to a low electron temperature. This is supported by deductions concerning the electron temperature drawn from the hook

measurement results. It may be the case that electron attachment is an important process but this study could not ascertain its relative importance.

## 7.8 ELECTRON TEMPERATURE

During the excitation pulse the electron temperature in the HyBrID laser rises more slowly and falls more quickly than in the CVL. Assuming pure three body recombination, the calculated electron temperature during the early after-glow is lower than in the CVL. The electron temperature in the HyBrID laser falls to the gas temperature after 20μs.

Under the assumption that the only mechanism which removes electrons from the active region is three body recombination, the calculated electron temperature is peaked on axis. If this assumption is not valid, then electron attachment to many species, both molecular and atomic must be considered. The radial dependance of electron attachment is not known. If the electron temperature is radially flat, as some authors have suggested, then electron attachment must proceed fastest off axis.

## 7.9 FUTURE WORK

The most important work to be carried out would be a refinement of the electron density measurements described in this thesis. In particular it is desirable to increase the bandwidth of the measurement such that the rising edge of the electron density may be resolved. An increase in sensitivity is also desirable in order to further investigate the pre-pulse electron density. It would also be desirable to measure the electron density at several different HBr concentrations.

Similarly a complete investigation of the parameters investigated in this study for different HBr concentrations would be informative. It would also be interesting to vary the proportion of hydrogen to bromine by addition of either $H_2$ or $Br_2$. There are, of course, limitless possible combinations of HBr partial pressure and input power which could be investigated, but as reliable computer modelling of the HyBrID system is a difficult problem this may be the most productive approach to investigating the effects of hydrogen and the relative importance of electron attachment and three body recombination. This aim would be helped by a direct measurement of electron temperature, using, for instance, the Thomson method.

It was mentioned in the text that the sensitivity of the population density measurement for the lower laser levels was less than that desirable. The hook method is not well suited to this type of measurement and it would be desirable to perform absorption spectroscopy experiments to investigate these levels, particularly in the late afterglow. It would also be productive to measure the population inversion in the laser using the inverse hook method.

# BIBLIOGRAPHY

Allen CW & Asaad AS. 1957 *Mon. Not. R. Astron. Soc.* ***117*** 36.

Alpher RA & White DR. 1959. *Phys. Fluids* ***2*** 162.

Anderson RS, Springer L, Bricks BG & Karras TW. 'A discharge heated copper vapour laser' *IEEE J. Quant. Electron.* **QE-11** 172-3.

Andrews AJ, Webb CE, Tobin RC & Denning RG. 1977 'A copper vapour laser operating at room temperature' *Opt. Comm.* **22** (3) 272-274

Ascoli-Bertoli U, DeAngelis A & Martellucci S. 1962. *Nuovo Cimento* ***18*** 1116.

Astadjov DN, Vuchkov NK & Sabotinov NV. 1988 'Parametric study of the CuBr laser with hydrogen additives' *IEEE J. Quant. Electron.* **QE-24** 9 1927-1935.

Astadjov DN, Vuchkov NK, Sabotinov NV. 1988 'Effect of hydrogen on CuBr laser power and efficiency' *Opt. Comm.* **56** 4 279-282.

Ashby DETF & Jephcoat DF. 1963. 'Measurement of plasma density using a gas laser as an infrared interferometer.' *Appl. Phys. Lett.* **2**(1) 15

Ashby DETF, Jephcoat DF, Malein A & Raynor FA. 1965. "Performance of the He-Ne laser as an interferometer for measuring plasma density." *J. Appl. Phys.* **36**(1) 29-34.

Asmus JF & Moncur NK. 1968 'Pulse broadening in a MHD copper vapour laser' *Appl. Phys. Lett.* **13** (11) 384-5.

Batenin VM, Burmakin VA, Vokhmin PA, Evtyunin AI, Klimovskii II, Lesnoi MA & Selezneva. 1977. 'Time dependance of the electron density in a copper vapour laser.' *Sov. J. Quant. Electron.* 7(7) 891-3.

Bielski A. 1975 'A critical survey of atomic transition probabilities for Cu I'. *J. Quant. Spectrosc. Radiat. Transfer* **15** 463-72

Biondi MA & Brown CS. 1949. 'Measurement of ambipolar diffusion in helium.' *Phys. Rev.* **75** 1700.

Blau P, Simlanski I & Rosenwaks S. 1992. 'Simultaneous time-averaged measurements of gas temperature and electron density in a copper vapour laser using hydrogen emission spectroscopy.' *J. Appl. Phys.* **72**(3) 849-54.

Bokan PA, Nikolaev VN & Solomonov VI. 1975 'Sealed copper vapour laser' *Sov. J. Quant. Electron.* **5** 96-98.

Brown DJW, 1988. 'Experimental study of excited state densities in a copper vapour laser'. PhD. Thesis University of New England, Armidale, NSW

Brown DJW, Kunnemeyer R & McIntosh AI. 1989 'Radial excited state densities in a copper vapour laser' SPIE. **1041** 25-32

Brown DJW, Kunnemeyer R & McIntosh AI. 'Time-resloved measurements of excited state densities in a copper vapour laser' *IEEE J. Quant. Elecron.* **QE-26** 1609-19.

Burmakin VA, Evtyunin AN, Lesnoi MA & Bylkin VI. 1978 'Long-lived sealed copper vapour' *Sov. J. Quant. Electron.* **8** 574-76.

Carman RJ. 1990 'A self-consistent model for a longitudinal discharge excited He-Sr recombination laser' *IEEE J. Quant. Electron.* **QE-26** 9 1588-1608

Carman RJ. 1991 'A time dependant two electron group model for a discharge excited He-Sr recombination laser' *J. Phys. D.* **24** 1803-1810.

Carman RJ, Brown BJW & Piper JA. 1994 'A self-consistent model for the discharge kinetics in a high repitition rate copper-vapout laser' *IEEE J. Quant. Electron.* **QE-30** 8 1876-1895.

Carman R.J. 1995. Private Commumication.

Chen CL, Nerheim NM & Russel GR. 1973 'Double discharge copper vapour laser with copper chloride as a lasant' *Appl. Phys. Lett.* **23** (9) 514-5.

Chen CL & Russel GR. 1975 'High-efficiency multiply pulsed copper vapour laser utilizing copper chloride as a lasant' *Appl. Phys. Lett.* **26** 504-5.

Chen CL, Bhanji AM & Russel GR. 1978 'Long duration high-efficiency operation of a continuously pulsed copper vapour laser utilizing copper bromide as a lasant' *Appl. Phys. Lett.* **33** 146-8.

Corliss CH. 1970. 'A review of oscillator strengths for lines of CuI' *J. Res. Natn. Bur. Stand.* ***74A*** (6) 781-790.

Deguishi H, Hatakeyama T, Murata E, Izawa Y & Yamanak C. 1994. 'Efficient design of multi-stage magnetic pulse compression.' *IEEE J. Quant. Electron.* **QE-30**(12) pp2934-8.

Dyson J, Williams RV & Young KM. 1962. "Interferometric measurement of electron density in Sceptre IV." *Nature* ***195*** pp1291-2.

Fowles GR & Sifvast WT. 1965 'High-gain laser transitions in lead vapour' *Appl. Phys. Lett.* **6** (12) 236-7.

Gerardo JB &Verdeyen JT. 1963. 'Plasma refractive index by a laser phase measurement.' *Appl. Phys. Lett.* ***3*** (7) pp121-3.

Grove RE. 1982 'Copper vapour lasers come of age' *Laser Focus* 45-50 July 1982.

Hogan GP. 1993 'A study of the kinetics of copper vapour lasers' Thesis for D.Phil. University of Oxford.

Hogan GP, Svoboda M & Webb CE. 1993 ' The automation of the hook technique' *Meas. Sci. Technol.* **4** 263-269.

Hogan GP. 1995. Private communication.

Huber MCE & Sandeman RJ. 1986. 'The measurement of oscillator strengths'. *Rep. Prog. Phys.* **49** 397-409

Huber MCE. 1971. 'Interferometric gas diagnostics by the hook method'. *Modern Optical Methods in Gas Dynamic Research* (Ed. DS Dosanjh) 85-112

Huber MCE. & Sandeman RJ. 1986. The measurement of oscillator strengths. *Rep. Prog. Phys.* **49** 397-490.

Isaev AA, Kazaryan MA & Petrash GG. 1972 'Effective pulsed copper-vapour laser with high average generation power' *J.E.T.P. Lett.* **16** (1) 27-9.

Isaev AA & Lemmerman G Yu. 1977 'Investigation of a copper vapour pulsed laser at elevated powers' *Sov. J. Quant. Electron.* **7** 799-801.

Isaev AA, Kazaryan MA, Petrash GG, Rautin SG & Shalagin AM. 1977 'Shaping of the output beam in a pulsed gas laser with an unstable resonator' *Sov. J. Quant. Electron.* **7** 746-52.

Isaev AA, Petrash GG & Pomonarev IV. 1986a. 'Relaxation of metastable states during the afterglow in a copper vapour laser'. *Sov. J. Quant. Electron.* ***16*** (11) 1512-6.

Isaev AA, Kazkov VV, Lesnoi MA, Markova SV & Petrash GG. 1986b 'Decay of metastable states and its influence on the lasing characteristics of a copper vapour laser' *Sov. J. Quant. Electron* ***16*** (11) 1517-21.

Jones DR, Sabotinov NV, Maitland A & Little CE. 1992 'A high power high efficiency Cu-Ne-HBr ($\lambda$=510.6, 578.2nm) laser' *Opt. Comm.* **94** 289-299.

Jones DR, Halliwell SN & Little CE. 1994 'Influence of remanent electron density on performance of copper HyBrID lasers' *Opt. Comm.* **111** 394-402.

Jones DR & Little CE. 1991 'Laser action at 472.2nm in a bismuth halide laser.' *III European and X. Nat. UK quantum Electronics Conf., Heriot-Watt University, Edinburgh 27-30 Aug. 1991,* Technical Digest, 57.

Jones DR & Little CE. 1992a 'A 472.2nm bismuth halide laser' *Opt. Comm.* **91** 223-228.

Jones DR & Little CE. 1992b 'A lead bromide laser operating at 722.9nm and 406.2nm' *IEEE J. Quant. Electron* **QE-28** 590-3

Jones DR & Little CE. 1992c 'A compact, fast start up manganese bromide laser (λ=534-544nm, 1.29-1.40μm)' *Opt. Comm.* **89** 80-7.

Jones DR & Little CE. 1992d 'A self-heated iron bromide (λ=452.9nm) laser with Ne-HBr buffer gas' *Opt. Quant. Electron.* **24** 67-72.

Jones DR, Maitland A and Little CE. 1994. 'A high efficiency 200W average power copper HyBrID laser' *IEEE J. Quant. Electron.* ***QE-30*** *10* pp2385-2390

Jones DR. 1995 . Private communication.

Kan T, Ball D, Schmitt E & Hill J. 1979 'Annular discharge copper vapour laser' *Appl. Phys. Lett.* **35** (12) 676-7.

Kock M, & Richter J. 1968. *Z. Astrophys.* **69** 180

Kunnemeyer R, McLucas CW, Brown DJW & McIntosh AI. 1987 'Time-resolved measurements of population densities in a $Sr^+$ recombination laser' *IEEE J. Quant. Elecron.* **QE-23** 2028-32

Kushner MJ. 1981'A self consistant model for high repetition rate copper vapour lasers' *IEEE J. Quant. Electron.* **17** 8 1555-1565.

Ladenburg R. 1933. 'Dispersion in electrically excited gases'. *Rev. Mod. Phys.* ***5*** (4) 243-256.

Leonard DA. 1967.'A theoretical description of the 510.6nm pulse copper vapour laser' *IEEE. J. Quant. Electron.* **QE-3** 380-1.

Livingstone ES &,Maitland A. 1989 'A low temperature, segmented metal, copper bromide laser'*J.Phys. E.Sci. Instrum.* **22** 63.

Livingstone ES, Jones DR, Maitland A & Little CE. 1991a 'Characteristics of a copper bromide laser with flowing Ne-HBr buffer gas' *Opt. Quant. Electron.* **24** 73-82.

Livingstone ES &,Maitland A. 1991b 'A high power, segmented metal, copper bromide laser' *Meas. Sci. Technol.* **2** 1119-20.

Loveland DG & Webb CE. 1992. 'Measurement of electron density in a strontium vapour laser.' *J. Phys. D.* ***25*** 594-604.

Luck H, Loffhagen W & Botticher W. 1994 'Experimental verification of a zero-dimensional model of the ionisation kinetics of XeCl discharges' *Appl. Phys.* B **58** 123-132.

Marlow WC. 1967. 'Hakenhethode'. *Appl. Optics.* ***6*** 1715-1724.

Meggers WF, Corliss CH & Scribner BF. *Natn. Bur. Stand. Monogr.* ***32***

Miyazaki K, Nakata R, Tomita Y, Seumitsu M, Watanabe S & Fukuda K. 1975. 'Application of dye laser to the hook method on the population measurement of excited He and Ne atoms in the pulsed discharge'. *Japan J. Apple. Phys.* **14** (7) 1075-1076

Miyazaki K & Fukuda K. 1977. 'Time-resolved population measurement with $N_2$-laser-pumped dye lasers'. *J. Phys. D* **10** 1905-1910

Molander WA. 1989 'Measurement of ground state density using hook spectroscopy' SPIE **1041** 11-18.

Naylor GA, Lewis RR & Kearsley AJ. 1988 'Performence of high power copper vapour lasers in an injection controlled oscillator-amplifier configuration' SPIE O/E-LASE'88 Proceedings.

Neger T & Jager H. 1984 'Applicationof the hook method fro the investigation of electrical discharges with rotational symetry'. *J. Appl. Phys. D.* **17** 1983-90.

Nerheim NM, Vetter AA & Russel GR. 1978 'Scaling a double pulsed copper chloride laser to 10mJ' *J. Appl. Phys.* **49** 12-15.

Penkin NP. 1964. 'The determination of the oscillator strength in atomic spectra'. *J. Quant. Spectrosc. Radiat. Transfer* **4** 41.

Piltch M, Walter WT, Solimene N, Gould G & Bennet WR Jr. 1965 'Pulsed laser transitions in manganese vapour' *Appl. Phys. Lett.* **7** (11) 309-310.

Pini R, Salimbeni G, Toci G & Vannini M. 1991 'High-efficiency diffraction limited operation of a copper vapour laser' *Opt. Comm.* **81** 138-44.

Prokofiev VK. 1924. 'Anomalous dispersion. 1. Relations between the dispersion constants in the principal series of potassium'. *Optical Transition Probabilities* **1** 1-33

Prokofiev VK. 1927. 'The rationof the numbers of resonating electrons for the potassium doublets'. *Phil. Mag. S7* **3** (18) 1010-1025

Ramsden SA & McLean EA. 1962. 'Optical refractivity of free electrons.' *Nature* **194** 761-2.

Rozhdestvenskii D. 1912. 'Anomale dispersion im natriumdampf'. *Ann. Phys. Lpz.* **39** 307-45.

Russel GR, Nerheim NM, Pivirotto TJ. 1972 ' Supersonic electrical-discharge copper vapour laser' *Appl. Phys. Lett.* **21** (12) 565-7.

Sandeman RJ. 1979. 'Hook Vernier'. *Appl. Optics* **18** (23) 3873-74

Sandeman RJ & Ebrahim NA. 1977. 'Spatially resolved excitation temperature measurements in a hyper sonic flow using the hook method'. *Appl. Opt.* **16** 1376-79

Shtukin AM, Mishakov VG, Fedotov GA & Ganeev AA. 1975(I) 'Interference method for observing the dissociation of copper halide molecules in a pulsed discharge'. *Opt Spectrosc.* **39** (4) 444

Shtukin AM, Fedotov GA & Mishakov VG. 1975(II). 'Lasing with Cu I lines using copper bromide vapour'. *Opt Spectrosc.* **39** (6) 681

Smilanski I, Kerman A, Levin LA & Erez G, 1978 'Scaling of the discharge heated copper vapour laser' *Opt. Comm.* **25** 79-82.

Smilanski I, Erez G, Kerman A & Levin LA, 1979 'High-power, high-pressure discharge heated copper vapour laser' *Opt. Comm.* **30** 70-74.

Smilanski 1979, 'Copper Hooks - Investigation of the copper vapour laser kinetics' *Proc int. Conf. Lasers '79* 327-334

Smilanski I, Levin LA & Erez G 1980, 'Kinetics of population inversion inverstigated by a modified hook method' *Opt. Lett* **5** (3) 93-95

Smilanski I, Moody SE, Warner B & Flint J. 1981, 'Use of modernised interferometric techniques for laser diagnostics'. *Proc. Int. Conf. Lasers '81*

Tenenbaum J, Smilanski I, Lavi S, Levin LA & Erez G 1981a 'Kinetic investigation of the upper laser levels of the copper vapour laser' *Opt. Comm.* **36** 391-94

Tenenbaum J, Smilanski I, Lavi S, Levin LA & Erez G 1981b 'Investigation of the kinetics of a metal vapour laser by an interferometric method' *Opt. Comm.* **36** 395-98.

Tumakaev GK & Lazovskaya VR. 'Investigation of the state of mercury vapour in a shock tube by the Rozhdestvenskii hook method'. 1965. *Sov.Phys. Tech Phys.***9** 1449-55.

Varnerin LJ. 1951. 'Electron recombination and collision cross-section measurement in hydrogen.' *Phys. Rev.* **84** 56.

Vuchkov NK, Astadjov DN & Saabotinov NV 1991 'A new circuit for CuBr laser excitation'. *Opt Quantum Electron.* **23** S549-53.

Walter WT, Piltch M, Solimene N & Gould G. 1966a 'Pulsed laser action in atomic copper vapour' *Bull. Am. Phys. Soc.* **11** 113.

Walter WT , Solimene N, Piltch M & Gould G. 1966b 'Efficient pulsed gas discharge lasers' *IEEE. J. Quant. Electron.* **QE-2** (9) 474-479.

Walter WT. 1967 '40kW pulsed copper laser' *Bull. Am. Phys. Soc.* **12** 90.

Walter WT. 1968 'Metal vapour lasers' *IEEE. J. Quant. Electron.* **QE-4** 355-6.

Warner BE & Kushner MJ 1981 'Controlling kinetic parameters of 100W large bore copper vapour lasers' *Proc. Int. Conf. Lasers '81* 845-851

Warner BE & Seeley G 1983 'Hook measurements in large copper lasers' *LLNL Report.*

Warner BE 1986 'Injection locking of copper vapour lasers' *Proc. Int. Conf. Lasers '81* 845-51.

Weise WL, Smith MW & Glennon BM. 1966. 'Atomic Transition Probabilities (Vol 1)' *NBS National Standard Reference Data Series.*

Whitmer RF. 1956. 'Microwave studies of the electron loss processes in gaseous discharges.' *Phys. Rev.* **104** (3) 572-5

Withford MJ, Brown DJW & Piper JA. 1994 'Investigation of the effects of hydrogen and deuterium on copper vapour laser performance' *Opt. Comm.* **110** 699-707

Wright JK, Medford RD, Hunt AG & Herbert JD. 1961. 'Interferometric measurements of the electron density in a shock heated Deuterium plasma.' *Proc. Phys. Soc.* **78** 1439.

Zemskov KI, Isaev AA, Kazaryan MA, Petrash GG & Rautin SG. 1974 'Use of unstable resonators in achieving the diffraction divergence of the radiation emitted from high gain pulsed gas lasers' *Sov. J. Quant. Electron.* **4** (4) 474-7.